

# NOTE TO USERS

This reproduction is the best copy available.

**UMI**<sup>®</sup>



UNIVERSITY OF OKLAHOMA

GRADUATE COLLEGE

**WAAS Error, Integrity and Availability Modeling  
for GPS based Aircraft Landing System**

A Dissertation

SUBMITTED TO THE GRADUATE FACULTY

In partial fulfillment of the requirements for the

Degree of

DOCTOR OF PHILOSOPHY

By

**Guangwei Mu**

**Norman, Oklahoma**

**2004**

UMI Number: 3122312

### INFORMATION TO USERS

The quality of this reproduction is dependent upon the quality of the copy submitted. Broken or indistinct print, colored or poor quality illustrations and photographs, print bleed-through, substandard margins, and improper alignment can adversely affect reproduction.

In the unlikely event that the author did not send a complete manuscript and there are missing pages, these will be noted. Also, if unauthorized copyright material had to be removed, a note will indicate the deletion.

**UMI**<sup>®</sup>

---

UMI Microform 3122312

Copyright 2004 by ProQuest Information and Learning Company.

All rights reserved. This microform edition is protected against unauthorized copying under Title 17, United States Code.

ProQuest Information and Learning Company  
300 North Zeeb Road  
P.O. Box 1346  
Ann Arbor, MI 48106-1346

c Copyright by Guangwei Mu 2004  
All Rights Reserved.

# WAAS Error, Integrity and Availability Modeling for GPS based Aircraft Landing System

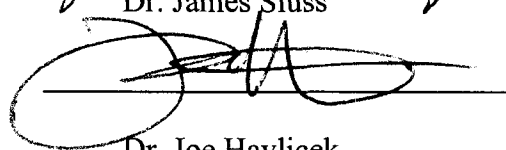
A Dissertation APPROVED FOR THE  
SCHOOL OF ELECTRICAL AND COMPUTER ENGINEERING

By



---

Dr. James Sluss



---

Dr. Joe Havlicek



---

Dr. John Fagan



---

Dr. Monte Tull



---

Dr. J. David Baldwin

## **Acknowledgements**

First and foremost I would like to thank Professor John Fagan. His contributions to this thesis are extensive and pervasive and this work could not have been possible without him. Professor Fagan has an infectious enthusiasm that allows his advice to generate exceptional motivation in his students, including myself. It has been an honor and privilege to work with him over the past few years. His leadership and resourcefulness makes it fun and exciting to work with. My daily interaction with Professor Fagan has allowed this research to develop in ways that I had not originally envisioned. This interaction enabled this dissertation and underlying research to achieve a higher quality and depth.

The Co-Chairs of my advisory committee, Professor Joe Havlicek and Professor James Sluss have also played a major role in this work and my academic development.

Professor Joe Havlicek and Professor Sluss helped steer my early academic career at University of Oklahoma and offered concise criticism of my work during its development to improve the clarity of my research and this thesis. Dr. Joe Havlicek has had a substantial impact on this work. His review and critique of this thesis proved invaluable and timely. His patience, kindness, always being positive and attention to details will always be my model in my future life and work.

The other members of my advisory committee, Professor Monte Tull and Professor J. David Baldwin have also played a major role in this work and my academic development. I appreciate their advice, input and time very much.

The Federal Aviation Administration is the sponsor for this work. Their funding has provided an environment at University of Oklahoma that has enabled true innovation that will contribute to the future of aviation. Without a doubt, this work would not be possible without their support. Also collaboration and discussion with Gerry McCartor of FAA tech center at Oklahoma City proved valuable to the research as well.

This acknowledgement list would not be complete without recognition of my peers. These include my fellow grad students from the OU EVRI and GPS Lab. Most notably HengQing Wen, Walter Ross, Ben Mohr, Scott Graham, Ben Blevins, Andy Archinal, Peter Huang, Charles Thurmann, John Dyer, Chad Sherrel, Brian Birk, Nick Cannon and Brad Taylor. You guys made my study and work here quite an enjoyment. And I can never thank you guys enough for all the help.

I would like to thank my parents, TingYu Mu and QinFen Zhang, who supported my every effort growing up and taught me that nothing is impossible given adequate dedication and time.

Last but certainly not least, the long hours of effort have been bearable only because I have someone special to share my time-off. That someone is Qin, my lovely wife. Her lasting support and understanding has made all of the work worthwhile. Thank you, sweetheart!

# Table of Contents

Acknowledgements .....	iv
Table of Contents .....	vi
List of Tables .....	viii
List of Illustrations.....	x
Abstract .....	xiv
<b>Chapter 1</b>	<b>1</b>
<b>Introduction.....</b>	<b>1</b>
<b>1.1 GPS based navigation system .....</b>	<b>1</b>
<b>1.2 The outline of this thesis and original Contributions .....</b>	<b>4</b>
<b>Chapter 2</b>	<b>7</b>
<b>Background on GPS and Differential GPS (DGPS).....</b>	<b>7</b>
<b>2.1 How GPS works .....</b>	<b>8</b>
<b>2.2 GPS error sources .....</b>	<b>11</b>
<b>2.3 Differential GPS (DGPS).....</b>	<b>19</b>
<b>2.3.1 LAAS.....</b>	<b>20</b>
<b>2.3.2 WAAS.....</b>	<b>21</b>
<b>2.3 GPS measurement equations .....</b>	<b>23</b>
<b>2.3 Error Probability Density Functions (PDFs) .....</b>	<b>27</b>
<b>2.5 Position Solution.....</b>	<b>31</b>
<b>2.6 Confidence Bounds .....</b>	<b>34</b>
<b>Chapter 3</b>	<b>37</b>
<b>WAAS static Error, integrity and availability monitoring and analysis .....</b>	<b>37</b>
<b>3.1 Necessary WAAS Data collection .....</b>	<b>37</b>
<b>3.2 The way the data is classified.....</b>	<b>39</b>
<b>3.3 Define WAAS performance metrics.....</b>	<b>43</b>
<b>3.4 WAAS Signal in Space (SIS) general performance .....</b>	<b>47</b>
<b>3.5 VPL and VPE (Vertical Position Error) performance over time     comparison.....</b>	<b>58</b>
<b>3.6 A new and better metric of VPL and its performance .....</b>	<b>65</b>
<b>Chapter 4</b>	<b>72</b>
<b>Algorithm to improve WAAS based navigation modeling.....</b>	<b>72</b>
<b>4.1 Chaotic nature of WAAS VPL and VPE .....</b>	<b>73</b>
<b>4.2 Rationale for Multiplicative modeling of the VPL.....</b>	<b>76</b>
<b>4.3 Position Domain Approach to improve the WAAS availability     performance.....</b>	<b>83</b>
<b>4.4 Kalman Filter smoothing .....</b>	<b>89</b>
<b>4.4.1 The discret Kalman filter introduction and notation to be used .....</b>	<b>90</b>
<b>4.4.2 Using <math>\alpha - \beta</math> Kalman filter to filter VPL .....</b>	<b>93</b>
<b>4.5 Fault prevention and error correction in this VPL algorithm .....</b>	<b>103</b>

4.6	Fault-proofing the VPE solution.....	104
<b>Chapter 5 106</b>		
	<b>Results and Conclusions.....</b>	<b>106</b>
5.1	<b>Results of the pseudo-VPL algorithm .....</b>	<b>106</b>
	Case 1: 12/01/1999: Before and after filtering.....	107
	Case 2: 04/28/2000: Before and after filtering.....	108
	Case 3: 11/27/2000: Before and after filtering.....	109
	Case 4: 05/01/2001: Before and after filtering.....	110
	Case 5: 11/12/2001: Before and after filtering.....	111
	Case 6: 05/02/2002: Before and after filtering.....	112
	Case 7: 10/12/2002: Before and after filtering.....	113
	Case 8: 10/28/2002: Before and after filtering.....	114
	Case 9: 03/14/2003: Before and after filtering.....	115
	Case 10: 05/29/2003: Before and after filtering.....	116
5.2	<b>Performance of the pseudo-VPL algorithm after altitude smoothing.....</b>	<b>117</b>
	Case 1: Dec. 1 <sup>st</sup> , 1999.....	119
	Case 2: Apr. 28th, 2000.....	123
	Case 3: Nov. 27th, 2000.....	127
	Case 4: May. 1st, 2001 .....	131
	Case 5: Nov. 12th, 2001.....	135
	Case 6: May. 2nd, 2002.....	139
	Case 7: Oct. 12th, 2002 .....	143
	Case 8: Oct. 28th, 2002 .....	147
	Case 9: Mar. 14th, 2003.....	151
	Case 10: May. 29th, 2003.....	155
5.3	<b>Conclusions.....</b>	<b>160</b>
<b>Chapter 6 162</b>		
	<b>Lessons learned and Future Research .....</b>	<b>162</b>
	<b>Appendix A:.....</b>	<b>174</b>
	<b>A new position domain algorithm to improve WAAS availability and continuity while maintaining integrity .....</b>	<b>174</b>
	<b>Appendix B:.....</b>	<b>174</b>
	<b>Acronyms Frequently used in Navigation Research.....</b>	<b>174</b>
	<b>Bibliography .....</b>	<b>183</b>

## List of Tables

Table 2. 1	Standard error model - L1 C/A (no SA) [6].....	16
Table 2. 2	Standard error model - L1 C/A (with SA) [6].....	17
Table 2. 3	Precise error model, dual-frequency, P(Y) code.....	18
Table 2. 4	Confidence bounds for varying Probabilities for the three PDFs. The bounds are on $x/\sigma$ and $a=\sigma$ is set.....	30
Table 4. 1	Satellite elevation and azimuth angles, confidence bounds and projection matrix values both for the all-in-view solution and for a solution without PRN 8... 84	
Table 5. 1	Case 1 Cat I Availability Performance comparison.....	119
Table 5. 2	Case 1 Un-Availability Performance comparison. ....	120
Table 5. 3	Case 1 Misleading Information (MI) Performance comparison.....	121
Table 5. 4	Case 1 Hazardously Misleading Information (HMI) Performance comparison. ....	122
Table 5. 5	Case 2 Cat I Availability Performance comparison.....	123
Table 5. 6	Case 2 Un-Availability Performance comparison. ....	124
Table 5. 7	Case 2 Misleading Information (MI) Performance comparison.....	125
Table 5. 8	Case 2 Hazardously Misleading Information (HMI) Performance comparison. ....	126
Table 5. 9	Case 3 Cat I Availability Performance comparison.....	127
Table 5. 10	Case 3 Un-Availability Performance comparison. ....	128
Table 5. 11	Case 3 Misleading Information (MI) Performance comparison.....	129
Table 5. 12	Case 3 Hazardously Misleading Information (HMI) Performance comparison. ....	130
Table 5. 13	Case 4 Cat I Availability Performance comparison.....	131
Table 5. 14	Case 4 Un-Availability Performance comparison. ....	132
Table 5. 15	Case 4 Misleading Information (MI) Performance comparison.....	133
Table 5. 16	Case 4 Hazardously Misleading Information (HMI) Performance comparison. ....	134
Table 5. 17	Case 5 Cat I Availability Performance comparison.....	135
Table 5. 18	Case 5 Un-Availability Performance comparison. ....	136
Table 5. 19	Case 5 Misleading Information (MI) Performance comparison.....	137
Table 5. 20	Case 5 Hazardously Misleading Information (HMI) Performance comparison. ....	138
Table 5. 21	Case 6 Cat I Availability Performance comparison.....	139
Table 5. 22	Case 6 Un-Availability Performance comparison. ....	140
Table 5. 23	Case 6 Misleading Information (MI) Performance comparison.....	141

Table 5. 24 Case 6 Hazardously Misleading Information (HMI) Performance comparison.	142
Table 5. 25 Case 7 Cat I Availability Performance comparison.....	143
Table 5. 26 Case 7 Un-Availability Performance comparison. ....	144
Table 5. 27 Case 7 Misleading Information (MI) Performance comparison. ....	145
Table 5. 28 Case 7 Hazardously Misleading Information (HMI) Performance comparison.	146
Table 5. 29 Case 8 Cat I Availability Performance comparison.....	147
Table 5. 30 Case 8 Un-Availability Performance comparison. ....	148
Table 5. 31 Case 8 Misleading Information (MI) Performance comparison. ....	149
Table 5. 32 Case 8 Hazardously Misleading Information (HMI) Performance comparison.	150
Table 5. 33 Case 9 Cat I Availability Performance comparison.....	151
Table 5. 34 Case 9 Un-Availability Performance comparison. ....	152
Table 5. 35 Case 9 Misleading Information (MI) Performance comparison. ....	153
Table 5. 36 Case 9 Hazardously Misleading Information (HMI) Performance comparison.	154
Table 5. 37 Case 10 Cat I Availability Performance comparison.....	155
Table 5. 38 Case 10 Un-Availability Performance comparison. ....	156
Table 5. 39 Case 10 Misleading Information (MI) Performance comparison. ....	157
Table 5. 40 Case 10 Hazardously Misleading Information (HMI) Performance comparison.	158
Table 1- 1 Case 1 Cat I Availability Performance comparison for 11/27/2000 Data....	171
Table 1- 2 Case 1 Un-Availability Performance comparison for 11/27/2000 Data. ....	172
Table 2- 1 Case 2 Cat I Availability Performance comparison for 03/14/2003 Data....	172
Table 2- 2 Case 2 Un-Availability Performance comparison for 03/14/2003 Data. ....	172

## List of Illustrations

Figure 2. 1 Standard GPS Triangulation [9].	9
Figure 2. 2 Error Sources [9].	12
Figure 2. 3 LAAS Anatomy [9].	20
Figure 2. 4 WAAS System Overview [18].	21
Figure 2. 5 (a) $i$ th element of Observing Matrix $\vec{G}$ . (b) Pseudorange measurement equation.	25
Figure 2. 6 Three PDFs plotted as functions of $x/\sigma$ .	30
Figure 3. 1 WAAS performance classification, vertical part [27].	40
Figure 3. 2 WAAS performance classification, horizontal part [27].	41
Figure 3. 3 WAAS performance on 12/01/99.	48
Figure 3. 4 WAAS performance on 04/28/00.	50
Figure 3. 5 WAAS performance on 11/27/00.	51
Figure 3. 6 WAAS performance on 05/01/01.	52
Figure 3. 7 WAAS performance on 11/12/01.	53
Figure 3. 8 WAAS performance on 05/02/02.	54
Figure 3. 9 WAAS performance on 10/12/02.	55
Figure 3. 10 WAAS performance on 10/28/02.	56
Figure 3. 11 WAAS performance on 03/14/03.	56
Figure 3. 12 WAAS performance on 05/29/03.	57
Figure 3. 13 VPE and VPL performance over GPS time on 12/01/99.	60
Figure 3. 14 VPE and VPL performance over GPS time on 04/28/00.	60
Figure 3. 15 VPE and VPL performance over GPS time on 11/27/00.	61
Figure 3. 16 VPE and VPL performance over GPS time on 05/01/01.	61
Figure 3. 17 VPE and VPL performance over GPS time on 11/12/01.	62
Figure 3. 18 VPE and VPL performance over GPS time on 05/02/02.	63
Figure 3. 19 VPE and VPL performance over GPS time on 10/12/02.	63
Figure 3. 20 VPE and VPL performance over GPS time on 10/28/02.	64
Figure 3. 21 VPE and VPL performance over GPS time on 03/14/03.	64
Figure 3. 22 VPE and VPL performance over GPS time on 05/29/03.	65
Figure 3. 23 12/01/99 Log(VPE+1) vs. Log(VPL+1).	66
Figure 3. 24 04/28/00 Log(VPE+1) vs. Log(VPL+1).	67
Figure 3. 25 11/27/00 Log(VPE+1) vs. Log(VPL+1).	67
Figure 3. 26 05/01/01 Log(VPE+1) vs. Log(VPL+1).	68
Figure 3. 27 11/12/01 Log(VPE+1) vs. Log(VPL+1).	68
Figure 3. 28 05/02/02 Log(VPE+1) vs. Log(VPL+1).	69
Figure 3. 29 10/12/02 Log(VPE+1) vs. Log(VPL+1).	69
Figure 3. 30 10/28/02 Log(VPE+1) vs. Log(VPL+1).	70
Figure 3. 31 03/14/03 Log(VPE+1) vs. Log(VPL+1).	70
Figure 3. 32 05/29/03 Log(VPE+1) vs. Log(VPL+1).	71

Figure 4. 1 (12/01/99) <i>NonLinearity(VPL - VPE) = 7.43221</i> .....	79
Figure 4. 2 (12/01/99) <i>NonLinearity(LVPL - LVPE) = 0.27741</i> .....	80
Figure 4. 3 (11/27/00) <i>NonLinearity(VPL - VPE) = 9.00821</i> .....	80
Figure 4. 4 (11/27/00) <i>NonLinearity(LVPL - LVPE) = 0.30773</i> .....	81
Figure 4. 5 <i>NonLinearity(VPL - VPE) = 0.46412</i> .....	81
Figure 4. 6 (05/01/01) <i>NonLinearity(LVPL - LVPE) = 0.28392</i> .....	82
Figure 4. 7 Satellite elevation and azimuth values for a standard skyplot. PRN 8 is a low elevation satellite that if not included in the solution dramatically changes the influence of PRN 6.....	85
Figure 4. 8 The triangle plot for all-in-view solutions including one biased satellite in each is shown. Here each bias is de-weighted by the other satellites. No obvious problems are evident in this chart [32]. .....	88
Figure 4. 9 The triangle plot for the subset solutions that expose each biased satellite is shown. Here the biases are exposed as being hazardous for the user. This demonstrates the importance of checking each subset or in the range domain [32]. .....	88
Figure 4. 10 Kalman filter block diagram.....	93
Figure 5. 1 Case 1: 12/01/1999: Before and after filtering.....	107
Figure 5. 2 Case 2: 04/28/2000: Before and after filtering.....	108
Figure 5. 3 Case 3: 11/27/2000: Before and after filtering.....	109
Figure 5. 4 Case 4: 05/01/2001: Before and after the filtering.....	110
Figure 5. 5 Case 5: 11/12/2001: Before and after filtering.....	111
Figure 5. 6 Case 6: 05/02/2002: Before and after filtering.....	112
Figure 5. 7 Case 7: 10/12/2002: Before and after filtering.....	113
Figure 5. 8 Case 8: 10/28/2002: Before and after filtering.....	114
Figure 5. 9 Case 9: 03/14/2003: Before and after filtering.....	115
Figure 5. 10 Case 10: 05/29/2003: Before and after filtering.....	116
Figure 5. 11 Case 1 CAT I PA Availability before (red) and after (green) processing.....	119
Figure 5. 12 Case 1 CAT I PA Un-Availability before (red) and after (green) processing.....	120
Figure 5. 13 Case 1 CAT I PA Misleading Information (MI) before (red) and after (green) processing.....	121
Figure 5. 14 Case 1 CAT I PA Hazardously Misleading Information (HMI) before (red) and after (green) processing.....	122
Figure 5. 15 Case 2 CAT I PA Availability before (red) and after (green) processing.....	123
Figure 5. 16 Case 2 CAT I PA Un-Availability before (red) and after (green) processing.....	124
Figure 5. 17 Case 2 CAT I PA Misleading Information (MI) before (red) and after (green) processing.....	125
Figure 5. 18 Case 2 CAT I PA Hazardously Misleading Information (HMI) before (red) and after (green) processing.....	126
Figure 5. 19 Case 3 CAT I PA Availability before (red) and after (green) processing.....	127
Figure 5. 20 Case 3 CAT I PA Un-Availability before (red) and after (green) processing.....	128

Figure 5. 21 Case 3 CAT I PA Misleading Information (MI) before (red) and after (green) processing. ....	129
Figure 5. 22 Case 3 CAT I PA Hazardously Misleading Information (HMI) before (red) and after (green) processing. ....	130
Figure 5. 23 Case 4 CAT I PA Availability before (red) and after (green) processing. ....	131
Figure 5. 24 Case 4 CAT I PA Un-Availability before (red) and after (green) processing. ....	132
Figure 5. 25 Case 4 CAT I PA Misleading Information (MI) before (red) and after (green) processing. ....	133
Figure 5. 26 Case 4 CAT I PA Hazardously Misleading Information (HMI) before (red) and after (green) processing. ....	134
Figure 5. 27 Case 5 CAT I PA Availability before (red) and after (green) processing. ....	135
Figure 5. 28 Case 5 CAT I PA Un-Availability before (red) and after (green) processing. ....	136
Figure 5. 29 Case 5 CAT I PA Misleading Information (MI) before (red) and after (green) processing. ....	137
Figure 5. 30 Case 5 CAT I PA Hazardously Misleading Information (HMI) before (red) and after (green) processing. ....	138
Figure 5. 31 Case 6 CAT I PA Availability before (red) and after (green) processing. ....	139
Figure 5. 32 Case 6 CAT I PA Un-Availability before (red) and after (green) processing. ....	140
Figure 5. 33 Case 6 CAT I PA Misleading Information (MI) before (red) and after (green) processing. ....	141
Figure 5. 34 Case 6 CAT I PA Hazardously Misleading Information (HMI) before (red) and after (green) processing. ....	142
Figure 5. 35 Case 7 CAT I PA Availability before (red) and after (green) processing. ....	143
Figure 5. 36 Case 7 CAT I PA Un-Availability before (red) and after (green) processing. ....	144
Figure 5. 37 Case 7 CAT I PA Misleading Information (MI) before (red) and after (green) processing. ....	145
Figure 5. 38 Case 7 CAT I PA Hazardously Misleading Information (HMI) before (red) and after (green) processing. ....	146
Figure 5. 39 Case 8 CAT I PA Availability before (red) and after (green) processing. ....	147
Figure 5. 40 Case 8 CAT I PA Un-Availability before (red) and after (green) processing. ....	148
Figure 5. 41 Case 8 CAT I PA Misleading Information (MI) before (red) and after (green) processing. ....	149
Figure 5. 42 Case 8 CAT I PA Hazardously Misleading Information (HMI) before (red) and after (green) processing. ....	150
Figure 5. 43 Case 9 CAT I PA Availability before (red) and after (green) processing. ....	151
Figure 5. 44 Case 9 CAT I PA Un-Availability before (red) and after (green) processing. ....	152
Figure 5. 45 Case 9 CAT I PA Misleading Information (MI) before (red) and after (green) processing. ....	153
Figure 5. 46 Case 9 CAT I PA Hazardously Misleading Information (HMI) before (red) and after (green) processing. ....	154

Figure 5. 47 Case 10 CAT I PA Availability before (red) and after (green) processing.	155
Figure 5. 48 Case 10 CAT I PA Un-Availability before (red) and after (green) processing.	156
Figure 5. 49 Case 10 CAT I PA Misleading Information (MI) before (red) and after (green) processing.	157
Figure 5. 50 Case 10 CAT I PA Hazardously Misleading Information (HMI) before (red) and after (green) processing.	158
Figure 1 WAAS performance classification, vertical part [4].	166
Figure 2 11/27/2000 WAAS performance	166
Figure 3 03/14/03 WAAS performance	166
Figure 4 VPE and VPL performance over GPS time on 11/27/00.	166
Figure 5 11/27/00 LVPE vs. LVPL	167
Figure 6 03/14/03 LVPE vs. LVPL	167
Figure 7 (11/27/00) Nonlinearity of (VPL – VPE):	168
Figure 8 (11/27/00) Nonlinearity of (LVPL – LVPE ):	169
Figure 9 Kalman filtering recursion.	170
Figure 10 11/27/2000: Before and after the filtering	171
Figure 11 03/14/2003: Before and after the filtering	172

## **Abstract**

From its initial conception to deployment, the Wide Area Augmentation System (WAAS) was hailed as revolutionary for the navigation industry. However, the WAAS deployment effort has suffered significant delays and budget overruns. The reason for these misfortunes lies in the demanding mandates on the performance of the WAAS system. The critical performance metrics for WAAS include accuracy, integrity, availability and continuity. In the long process of getting WAAS commissioned, availability has always been the metric that holds the system back from achieving the promised capability. To date WAAS performs well, but not well enough to meet its original objectives. The inherent tradeoff between integrity and availability is the major reason that the VPL and HPL algorithms need to be improved.

The integrity algorithms are well defined in the WAAS Minimum Operational Performance Standards (MOPS). However, our experimental data clearly indicate that the MOPS VPL and HPL algorithms are over-conservative, at least from a practical point of view. As a result, the confidence bounds are sufficiently large to cover the correction error and hence to some extent guarantee the integrity. However, this lack of compactness from the MOPS introduces unnecessary epochs of the system being unavailable. To improve the system performance, the intuitive approach is through the range/correction domain since these factors can be observed, controlled and manipulated to improve the system performance in individual cases. However, we need a better error model and better understanding of the threat model, i.e. we need to know more about the nature of all error sources and the threats the WAAS faces, which is very difficult to

accomplish due to the stochastic natures of these sources. Therefore, it is unlikely that a range/correction domain solution can be applied to a wide range of applications while having significant improvement for the system performance. Besides, it is still subject to the hindrance that the WAAS message structure might need to be changed or adjusted to take advantage of the new development.

In this dissertation, a new position domain algorithm is presented to improve the MOPS integrity methodology in hopes of improving the overall system performance. The information needed to do this is already in the WAAS messages. Therefore, this new algorithm will not require any change of the existing correction messaging.

The new VPL and HPL measure developed in this dissertation is based on the MOPS algorithms and improves upon them. The new VPL and HPL algorithms are developed by taking advantage of the WAAS correction error's stochastic characteristics and Kalman filtering. The algorithm has been tested using real static and dynamic data collected by our Enhanced Miniature Advanced GPS Receiver (EMAGR) used in conjunction with the OU flight test program. This methodology shows significant improvement over the standardized MOPS algorithms. It improves the system availability and continuity without penalizing integrity.

# Chapter 1

## Introduction

### 1.1 GPS based navigation system

The Wide Area Augmentation System (WAAS) is a very attractive solution for various stages of air flight. One of the major setbacks for the WAAS project has been a lack of system availability suitable for aviation use. This dissertation will demonstrate this is mostly due to the fact that the WAAS Protection Level (PL) algorithm is unnecessarily over-conservative. This dissertation will present the results of research done on the nature of this problem, a new algorithm for PL will be presented, and its promises of improved system performance, including integrity and availability will be shown. This will help promote the use of WAAS as a landing aid by improving the WAAS SIS performance significantly. The new PL algorithm takes advantage of the intrinsic looseness of the current VPL and HPL algorithm and uses Kalman filtering to reduce the false alarm rate of the PL. Linearization transformation was used to better model the PL.

Landing has always being the most challenging stage of commercial flight. Weather often prevents timely and safe landing, which is the foremost reason for common airline delays. Any means to improve this would improve airport efficiency and airline quality of service. To achieve these improvements, a Global Navigation Satellite System (GNSS) was developed. The backbone of GNSS is the Global Positioning System (GPS) in the United States. Since GPS was first commissioned, improvements have been researched to make the system more accurate and safer. Differential GPS

systems are the main projects that have offered the possibility of benefiting most users. Of possible candidates, the Local Area Augmentation System (LAAS) and the Wide Area Augmentation System (WAAS) are the options best suited for takeoffs and landings [1]. This report of research will study WAAS as the choice for Category I aircraft landing.

WAAS is a GPS based navigation system developed and being tested in the United States by the Federal Aviation Administration (FAA). WAAS provides correction signals to aviation users equipped with a WAAS-capable GPS receiver. The correction signal improves the positioning solution by supplying more accurate GPS clock, satellite ephemeris, and delay times for the GPS in its correction signal as it passes through the ionosphere and troposphere. These corrections are broadcast for use by virtually all users with WAAS capability in North America via geostationary satellites. A master station and a network of monitoring ground stations are needed to collect information, generate these correction messages and upload them to the geo-synchronized WAAS satellite. WAAS provides improvements in four metrics over standard GPS: accuracy, integrity, availability and continuity [2].

In the FAA's Minimum Operational Performance Standards (MOPS) for phase I WAAS, it was required that WAAS provide an aviation signal with sufficient accuracy, integrity, availability and continuity to safely guide category I landing through instrument aid. The specific accuracy requirement was for a vertical error of less than 12 meters and a horizontal error of less than 30 meters. In addition, the system integrity requirement specified that the probability of errors in the GPS solution falling below the Vertical Protection Limit (*VPL*) and the Horizontal Protection Limit (*HPL*) must be more than

99.99999% (in other words the rate of occurrence of hazardously misleading information must be less than  $10^{-7}$  every approach), while the availability requirement specified that the system must be available at least 99.9% of the time [3].

While these numbers seems unreachably stringent, the concepts will later be clarified, and these numbers will be shown to be based on a stochastic process instead of averaging of real collected data. The definition will be used to show the result of the new algorithm developed as a result of the dissertation effort on the system availability and integrity.

One interesting point that needs to be stressed is that the Selective Availability (SA) has been disabled per presidential order on May 2<sup>nd</sup>, 2000 [4]. However, in this research SA is treated as if it is still a factor. This is for two reasons:

1. Although the SA has been turned off, there is still chance that the SA could be turned back on in the future if national security considerations motivate this action.
2. A substantial amount of the data collected and analyzed in the proposed research was acquired prior to the SA being turned off. This put us in a great position to study how the SA contributes to the total error of WAAS system.

In Section 4.1 some primary results on integrity and availability will be shown. What the system can achieve in a static configuration will be calculated and compared to the requirements from the MOPS. Suggestions will be made to improve the performance of the system.

The research presented here is based on the recognition that high quality error, integrity, and availability models are crucial factors that will determine the success of differential GPS as a viable aircraft instrument landing system.

An accepted integrity model has been previously developed [3], [5]. Evaluating its performance is one of the research tasks addressed in this dissertation. Availability modeling is less mature, depends on environmental conditions, and doesn't seem to have a clear pattern from which to draw conclusions. However, it is informative to study integrity and availability together in order to gain useful insights into the expected performance of differential GPS landing systems. Continuity is of relatively less concern. This is due to the fact that a differential GPS system can only coast for a limited period of time when signal integrity is absent in hope of quick recovery when signal integrity returns. Any long lasting absence of a "good" signal will result in a flag of "NOT TO USE" being issued. Therefore, continuity doesn't concern us as much as integrity and availability. However, continuity is an important parameter indicating how well the differential GPS system is performing.

One of the major setbacks for the WAAS project has been a lack of system availability suitable for aviation use. This dissertation will demonstrate that most of this is due to the WAAS Protection Level (PL) algorithm being unnecessarily over-conservative. This dissertation will present the results of research done on the nature of this problem. A new algorithm for PL will be presented and its promises for improved system performance, including integrity and availability, will be shown.

## **1.2 The outline of this thesis and original Contributions**

In this dissertation a number of issues about the position domain solution to the WAAS SIS availability are addressed. Among them the following contributions are original and significant:

Chapter 2 provides the theoretical background for the GPS and WAAS error performance analysis. It builds the foundation for the later chapters.

In Chapter 3, real WAAS data collected through the lifetime of WAAS is analyzed and the results show *that WAAS SIS has consistent problem of not reaching the required availability performance criteria. The conclusion that the VPL algorithm has a problem with over-conservative nature is established.* By observing *VPL – VPE* performance over GPS time, I conclude that a new metric about VPL and VPE needs to be devised. Then in 3.6 *the new and better LVPL and LVPE are devised and the transformations between VPL and LVPL, VPE and LVPE are proposed and defined.* Preliminary analysis and observation indicate that the new LVPL and LVPE are better metrics to study the WAAS performance.

Chapter 4 establishes the new WAAS integrity-availability algorithm. *The multiplicative modeling of the VPL is justified, i.e. the superior linearity of the LVPL-LVPE is verified.* The VPE false alert situations are discussed and an approach to solve them is proposed. In Section 4.4, the Kalman filter is introduced and applied to the WAAS integrity and availability modeling. *The LVPL is modeled as a one-dimensional tracking problem and the  $\alpha - \beta$  Kalman filter is applied to it.* Fault prevention and error correction in the VPL algorithm are discussed. Then, in 4.6, fault proofing of the VPE is discussed. Without leaving the position-domain solution, a simple lowpass filter is recommended for fault proofing.

In Chapter 5 the results of the pseudo-*VPL* algorithm are studied. The conclusion that emerges is that the *new algorithm developed in this dissertation tightens up the VPL in a desirable way by removing unnecessary over-conservatism in the previously existing algorithm. In ordinary cases the pseudo-VPL reduces the VPL magnitude by 3dB.* This helps tremendously to increase the system availability.

This pseudo-*VPL* algorithm has different effects on the system integrity. For good WAAS data it improves the availability without harming the integrity. For lower quality data sets the effects vary. *The performance of the pseudo-VPL algorithm depends on the data type to which it is applied. But for ordinary WAAS data it achieves the research goal, i.e. it significantly improves the system availability and continuity without penalizing the system integrity.*

Chapter 6 discusses the future research possibilities on this topic and some candidate approaches are proposed.

## Chapter 2

### Background on GPS and Differential GPS (DGPS)

The ordinary GPS system was developed by the Department of Defense and has gradually become a civil-military dual use system. The objective of the GPS system is to provide an omnipresent positioning mechanism for those who need accurate positioning. One of the most important applications of GPS is aviation. Unfortunately, aviation requires more precise positioning information than many other GPS applications such as consumer automobile navigation and route selection. For example, in an automotive navigation service, performance is acceptable as long as the right moving map shows up and vehicle position is determined within a reasonable time and error bound, usually in tens of meters. By contrast, aviation applications depend on the system working in almost real time when the aviator needs it. Moreover, the error has to be very small so that the plane doesn't crash or fail to find the airport.

The accuracy of standard GPS alone is not sufficient to guarantee successful landings for category I approaches. When one talks about accuracy, it must be remembered that there is always a stochastic element present because this positioning operation is such a complex procedure with all elements involved considered. Before SA was turned off, the range of vertical accuracy was only about 100 meters with a probability of 95%, which means that for no less than 95% of the time users could expect a range error of less than 100 meters. After the SA was off, the vertical accuracy improved to within 10 meters, which is comparable to that of WAAS [6]. Despite this fact, WAAS rather than standard GPS is still preferred for takeoff and landing navigation

because WAAS generally provides better position estimates and also provides continuous monitoring of the signal quality, thereby providing integrity and availability of the aviation system as well as the position information.

In the following sections, I will briefly introduce the basic concepts of GPS and differential GPS systems, with the emphasis being placed on WAAS.

## **2.1 How GPS works**

GPS is a Satellite Navigation System, funded by and controlled by the U.S. Department of Defense (D.O.D). The system is made up of 27 space-borne satellites (Space Vehicles, or SVs) that orbit the earth in 12 hours and a number of ground stations that monitor the SVs. While there are thousands of civil users of GPS worldwide, the system was designed for and is operated by the United States D.O.D. [7].

GPS provides specially coded satellite signals that can be processed in a GPS receiver, enabling the receiver to compute its position, velocity and the time. Signals from at least four GPS satellites are used to compute positions in three dimensions as well as the time offset in the receiver clock.

Essentially GPS uses the known positions of the satellites to locate the precise position of the working GPS receiver. Following is a step-by-step description of how GPS works:

1. To use the satellites as the reference, one needs to know exactly where the satellites are in space. Relative high orbits and careful monitoring of the satellites provides the solution. Orbits are high and hence are not affected significantly by lower atmosphere and earth bound phenomena. The orbits are well modeled and can be predetermined to a close degree of approximation [8], with the master station monitoring and

controlling the orbits. User receivers get clock, ephemeris and almanac information through decoding pseudocode broadcast of the SVs.

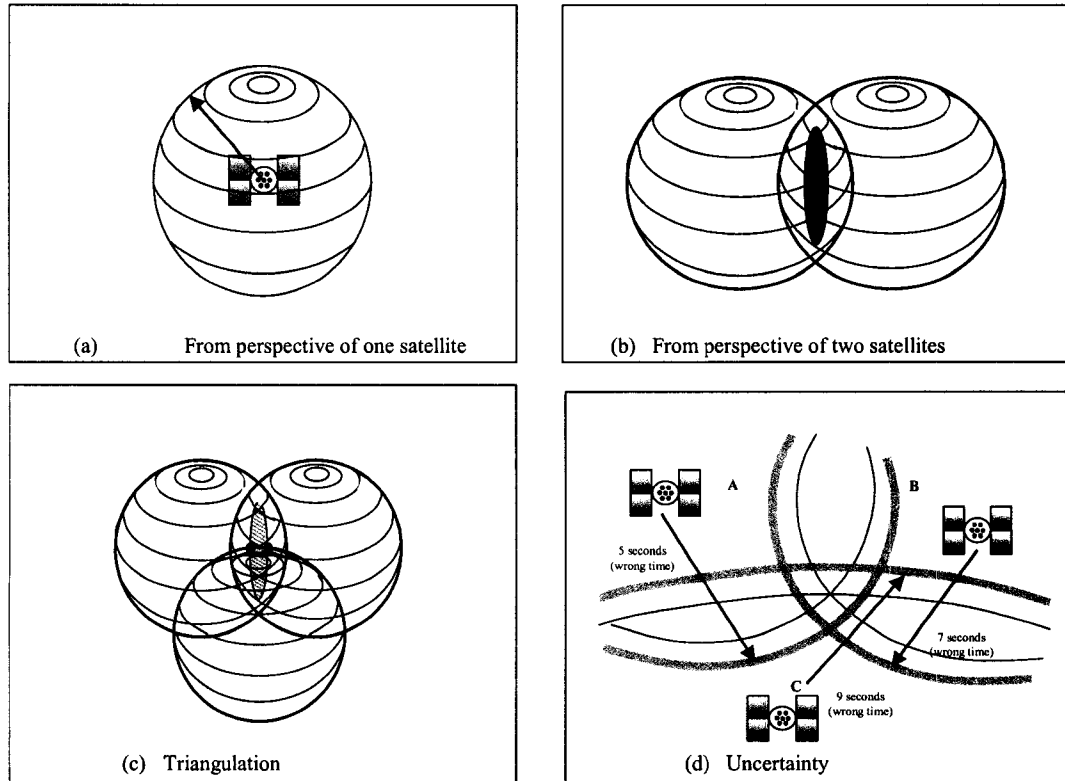


Figure 2. 1 Standard GPS Triangulation [9].

A GPS receiver measures distance using the travel time of radio signals. The signals transmitted from the satellites are pseudo-noise codes that are unique to the GPS system. The receivers are able to pick these signals out of the background noise and calculate the travel time by measuring the phase shift of the carrier of the pseudo-noise codes between when they are sent and when they are received. Note that the clock error of the receiver is included in this step, and thus the range estimate of this measurement is called pseudorange. Now the positioning process is equivalent to

solving a system of three equations for longitude, latitude and altitude. The three equations are determined by measuring the distances from three different satellites to the receiver. Fig. 2.1(a) to Fig. 2.1(c) demonstrates the process by which the position of the user is determined.

Travel time of the GPS signal from one specific satellite is illustrated in Fig. 2.1(a). The distance between the receiver in space and this specific GPS satellite is determined as the product of the speed of light and the travel time of the GPS signal. One can be sure that the receiver is located somewhere on the surface of a sphere centered at the GPS satellite and with a radius equal to the distance that the signal traversed (Fig. 2.1(a)). Once the distances to two satellites have been determined, then the position is known to be somewhere on the circle that forms the intersection of the two corresponding spheres. This is shown in Fig. 2.1(b). Once the distance to a third satellite is also determined, the locus of the possible solutions for the position is reduced to just two points, as shown in Fig. 2.1(c). This process is called “Triangulation”. The question of which one of those two points is the correct solution can be answered easily. Usually one solution is so absurd that it is negative or thousands of miles away from the expected position, and thus is excluded.

3. In step 2, the clock error of the receiver was introduced into the pseudorange. Satellites keep precise timing by using ultra-accurate atomic clocks, which cost a few hundred thousand dollars each. Individual receivers would not be able to afford such clocks. To precisely measure travel time, GPS needs very accurate timing, which it achieves by incorporating a fourth satellite to generate precise timing. By using four satellites the original problem of three equations in three unknowns is transformed

into a system of four equations in four unknowns, where the receiver clock error is the fourth unknown. Therefore, an atomic clock is not needed in the user receiver.

Only a fourth visible satellite is needed, whose atomic clock can be utilized.

4. Finally, any delays the radio signals experience as they travel through the atmosphere must be corrected for. By studying these signals, the errors may be reduced to acceptable magnitude. Fig. 2.1(d) shows how the actual position of the receiver is blurred by the uncertainty of the of travel delays of the satellite signals. The nature of these delays is of interest since it can provide insight to reduce delay and hence improve the GPS performance. The following section gives an overview of the major contributing sources of the GPS errors.

## **2.2 GPS error sources**

Ranging errors are grouped into the six following classes: satellite clocks, selective availability, ephemeris, atmospheric delays, multipath and receiver clock errors. Each class is briefly discussed in the following sections. Representative values for these errors are shown in Table 2.1 and 2.2. Fig. 2.2 illustrates how the error sources are grouped into six sources according to when they occur in the process of computing the GPS position solution. For civilian users, there used to be intentional errors added to degrade the quality of position solution that could be obtained without using special military equipment. This policy of injecting intentional errors was known as Selective-Availability or SA. SA is limited by DOD to within 100 meters 2-D RMS [10], and is considered mostly a clock perturbation [11], [12]. For reasons to be stated later, the SA will be treated like it is still part of the GPS signal in this dissertation. The atmospheric

delays are divided into ionospheric and tropospheric errors since each of these are modeled differently and contribute differently to the overall error of the final GPS position solution.

Ephemeris errors result when the GPS message does not convey the correct satellite location. Kalman filtering has to be implemented in the receiver to reduce this error. Because satellite errors reflect a position prediction, they tend to grow with time from the last control station upload. It is also possible that a portion of the deliberate SA error is added to the ephemeris data [11]. However, the predictions are long smooth arcs, so all errors in the ephemeris tend to be slow with time. Therefore, their utility in SA is quite limited and rarely used. The contribution of ephemeris error to the ranging error is believed to be within a few meters [12].

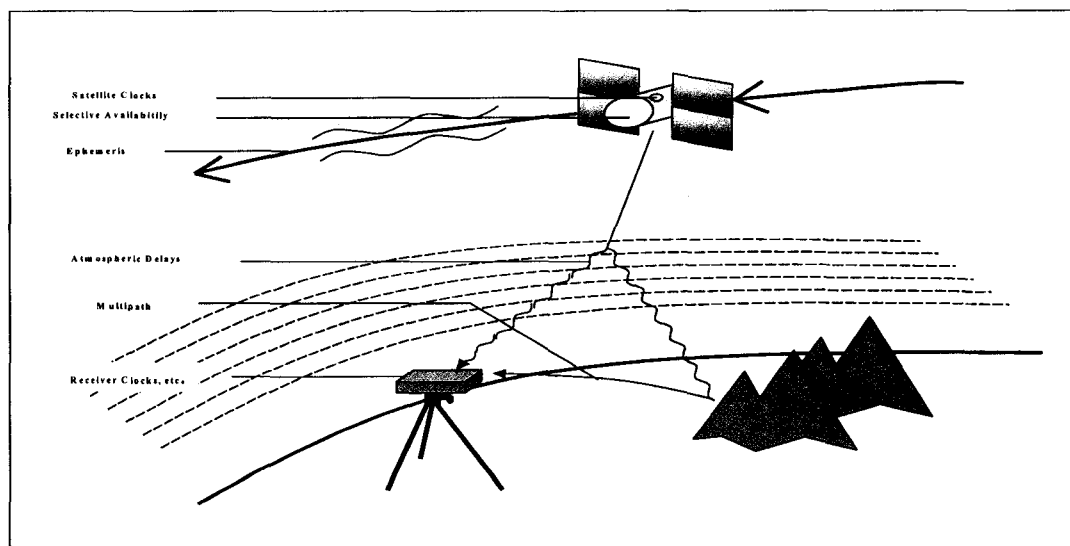


**Figure 2.2 Error Sources [9].**

Satellite clock--Errors in the transmitted clock, including SA, are fundamental since GPS is a one-way ranging that ultimately depends on satellite clock predictability.

Satellite clock errors affect both civilian C/A and military P-code users in the same way. This effect is also independent of satellite direction, which is important when the technique of differential corrections is used. All differential stations and users measure an identical satellite clock error. A major source of apparent clock error is SA, which is varied so as to be unpredictable over periods longer than about 10 minutes [10]-[12]. The root mean square value of SA is typically about 20 meters. More interesting is the underlying accuracy of the system with SA off. The ability to predict clock behavior is a measure of clock quality. GPS uses atomic clocks (cesium and rubidium oscillators), which have stabilities of about 1 part in  $10^{13}$  over a day. If a clock can be predicted to this accuracy, its error in a day ( $\sim 10^5$  seconds) will be about  $10^{-8}$  seconds or about 3.5 m [6].

Errors in the corrections of pseudorange caused by ionospheric effects are another source of position error. Because of free electrons in the ionosphere, GPS signals do not travel at the vacuum speed of light as they transit to the receiver. The modulation on the signal is delayed in proportion to the number of free electrons encountered and is also (to first order) proportional to the inverse of the carrier frequency squared ( $1/f^2$ ). The phase of the radio frequency carrier is advanced by the same amount because of these effects. Carrier-smoothed receivers take this into account in the design of their filters [13], [14]. The ionosphere is usually reasonably well behaved and stable in the temperate zones; however, near the equator or magnetic poles it can fluctuate considerably. As will be later shown, the differential GPS is a very good solution to reduce this error factor.

All users correct the raw pseudoranges for the ionospheric delay. The simplest correction is the use of an internal diurnal model of these delays. The parameters can be updated using information in the GPS communications message. The effective accuracy

of this modeling is about two to five meters for users in the temperate zones. A second technique is the use of dual-frequency P-code receivers to measure the signal at both frequencies and directly solve for the delay. The difference between the L1 frequency band and the L2 frequency band arrival times allows a direct algebraic solution of the delay. This dual-frequency technique provides one to two meters accuracy, due to the ionosphere, for a well-calibrated receiver [15]. Although this P-code is usually only available to military users, since this technique only requires carrier measuring, some civil user also have utilized this dual carrier method.

A third technique is to rely on a near real-time update. An example would be the Wide Area Augmentation System (WAAS). This should produce corrections with accuracies of one to two meters or better in the temperate zones of the world. This is the subject of this research.

Errors in the correction of the raw pseudoranges are also caused by tropospheric effects. Deviation from the vacuum speed of light in the troposphere causes these effects. Variations in temperature, pressure, and humidity all contribute to variations in the propagation speed of radio waves [14]. Both the code and carrier will have the same delays. For most users and circumstances, a simple model is accurate to about 1 meter or better [15].

Multipath--Errors caused by reflected signals entering the receiver antenna is the most prominent form of surface error. Multipath is the error caused by reflected signals entering the front end of the receiver and masking a real correlation peak. These effects tend to be more pronounced in a static receiver near large reflecting surfaces, where 15 m of error can be found in some extreme cases [16]. The first line of defense against

multipath is the use of antenna cut-off angle and antenna location that minimizes this problem. A second approach is to use a "narrow correlator" receiver which tends to minimize the impact of multipath on range tracking accuracies. With proper antenna selection and positioning, the net impact to a moving user should be less than 1 m under most circumstances.

Errors in the receiver's measurement of range caused by thermal noise, software accuracy, and interchannel biases represent additional sources of position error.

Initially most GPS commercial receivers were sequential in that one or two tracking channels shared the burden of locking on to four or more satellites. With advances in modern chip technology, it is common today to place three or more tracking channels on a single inexpensive chip. As the size and cost have diminished, techniques have improved and five- or six-channel receivers are becoming common. Most modern receivers use a reconstructed carrier to aid the code tracking loops. This produces a precision of better than 0.3 m. Interchannel bias is minimized with digital sampling in all-digital designs. Table 2.1 - 2.3 have been generated from actual measurements made by NOAA [6]. The error sources have been broken down into the six classes enumerated above. These three tables describe how each error source contributes to the total error. In this dissertation, it was assumed that all the error sources are independent of one another. Therefore, the total error is the mean square root of the contributing factors.

Table 2.1 assumes that SA is not operating. Consequently, the residual satellite clock error, at 2.1 m, is not the dominant error; in fact, the largest error is expected to be the mismodeling of the ionosphere, at 4.0 m. Thus, the worldwide civilian positioning error for GPS is potentially about 10 m (horizontal), as shown in Table 1.1. The data in

Table 2.1 - 2.3 are from actual measurements. The bias and random components are analogous to the AC and DC components of common electrical signals and are assumed to be statistically orthogonal to each other, which is reasonable since their sources are independent to one another. Therefore, the expected total error is the mean square root of the bias and random components. DGPS represents the differential GPS data under the same circumstance. Similarly, different contributions of these components are considered independent and thus the User Equivalent Range Error (UERE) is the mean square root of the contributions. The filtered UERE is a smoothed version of the UERE [6]. The Vertical Dilution Of Precision (VDOP) and Horizontal Dilution Of Precision (HDOP) are the vertical and horizontal components for Geometric

**Table 2.1 Standard error model - L1 C/A (no SA) [6]**

Error source	One-sigma error, m			DGPS
	Bias	Random	Total	
Ephemeris data	2.1	0.0	2.1	0.0
Satellite clock	2.0	0.7	2.1	0.0
Ionosphere	4.0	0.5	4.0	0.4
Troposphere	0.5	0.5	0.7	0.2
Multipath	1.0	1.0	1.4	1.4
Receiver measurement	0.5	0.2	0.5	0.5
-----				
User equivalent range error (UERE), rms	5.1	1.4	5.3	1.6
Filtered UERE, rms	5.1	0.4	5.1	1.5
-----				
<b>Vertical one-sigma errors</b> --VDOP= 2.5			<b>12.8</b>	<b>3.9</b>
<b>Horizontal one-sigma errors</b> --HDOP= 2.0			<b>10.2</b>	<b>3.1</b>

Dilution Of Precision (GDOP), a quantity that describes the quality of the visible satellite constellation from the receiver. GDOP is computed from the geometric relationships between the receiver position and the positions of the visible satellites that the receiver is

using for navigation. GDOP is often computed from almanacs and an estimated receiver position. Estimated GDOP does not take into account obstacles that block the line-of-sight from the position to the satellites. The products of the Filtered UERE and VDOP and HDOP represent the total estimated vertical and horizontal error.

**Table 2.2 Standard error model - L1 C/A (with SA) [6]**

Error source	One-sigma error, m			DGPS
	Bias	Random	Total	
Ephemeris data	2.1	0.0	2.1	0.0
Satellite clock (dither)	20.0	0.7	20.0	0.0
Ionosphere	4.0	0.5	4.0	0.4
Troposphere	0.5	0.5	0.7	0.2
Multipath	1.0	1.0	1.4	1.4
Receiver measurement	0.5	0.2	0.5	0.5
-----				
User equivalent range error (UERE), rms	20.5	1.4	20.6	1.6
Filtered UERE, rms	20.5	0.4	20.5	1.5
-----				
<b>Vertical one-sigma errors</b> --VDOP= 2.5			<b>51.4</b>	<b>3.9</b>
<b>Horizontal one-sigma errors</b> --HDOP= 2.0			<b>41.1</b>	<b>3.1</b>

A second example shows the impact of SA on these errors. Because the deliberately mismodeled clock so dominates the ranging error, all other effects can be safely ignored in the error budget. The results of Table 2.2 have been repeatedly corroborated by actual measurements. Note that SA is listed as a bias because it cannot be averaged to zero with a one second (or less) filter. Selective Availability (SA) is expected to be zero mean, but only when averaged over many hours or perhaps days. Of course, such averaging is not practical for a dynamic user who only sees the satellite for a portion of the orbit. If differential corrections are used, they will eliminate the SA error entirely (if corrections are passed to the navigation receivers at a sufficiently high data rate).

**Table 2.3      Precise error model, dual-frequency, P(Y) code**

Error source	One-sigma error, m			DGPS
	Bias	Random	Total	
Ephemeris data	2.1	0.0	2.1	0.0
Satellite clock	2.0	0.7	2.1	0.0
Ionosphere	1.0	0.5	1.2	0.1
Troposphere	0.5	0.5	0.7	0.1
Multipath	1.0	1.0	1.4	1.4
Receiver measurement	0.5	0.2	0.5	0.5
-----				
User equivalent range error (UERE), rms	3.3	1.5	3.6	1.5
Filtered UERE, rms	3.3	0.4	3.3	1.4
-----				
<b>Vertical one-sigma errors</b> --VDOP= 2.5			<b>8.3</b>	<b>3.7</b>
<b>Horizontal one-sigma errors</b> --HDOP= 2.0			<b>6.6</b>	<b>3.0</b>

The errors for dual-frequency PN code are similar to those already presented except that SA errors are eliminated because the authorized user can decode the nature of the induced error as part of a classified message. The expected horizontal error is less than 10 m. The ionosphere error is reduced to a 1-m bias and about 0.7 m of noise by the dual-frequency measurement. The dominant error sources are the satellite ephemeris and clock errors. This is illustrated in Table 2.3.

From this discussion, it is seen that standard GPS is subject to many error sources, and DGPS is able to improve on the error performance. All data presented here is from a NOAA source of measurements taken at one of the Continuously Operating Reference Stations (CORS) operated by the NCAD Corp. at Erlanger, Kentucky. On May 2, 2000, SA was set to zero [4]. The measurements show that SA causes 95% of the points to fall within a radius of 45.0 meters. Without SA, 95% of the points fall within a radius of 6.3 meters [6].

As an illustration, consider a football stadium. With SA on, you only know if you are on the field or in the stands at that football stadium; with SA switched off, you know around which yard marker you are standing on.

Even though standard non-SA GPS alone can be quite accurate, there are inherent problems with it. The error can vary over a wide range. Standard GPS doesn't have the capability of continuous monitoring of the signal quality. This can result in considerable danger to the aviation user in the rare case that hazardously misleading information is provided by the system without warning the user. This could lead to serious misfortune. Therefore, differential GPS was introduced.

### **2.3 Differential GPS (DGPS)**

Although GPS generally provides good resolution (since the removal of SA), standard GPS suffers from at least one limitation: it provides no performance guarantee, and hence no protection against transient losses in accuracy that could prove catastrophic in aviation applications. It would have been prohibitively expensive to resolve this limitation by starting over from scratch with a new system. Instead, differential GPS (DGPS) was developed to address the problem.

What DGPS does is establish well-surveyed positions as reference stations that are able to receive a GPS signal and to transmit a correction signal. Within a reasonable range of distance from a given reference station, the corrections are almost constant and this is the basis of differential GPS.

### 2.3.1 LAAS

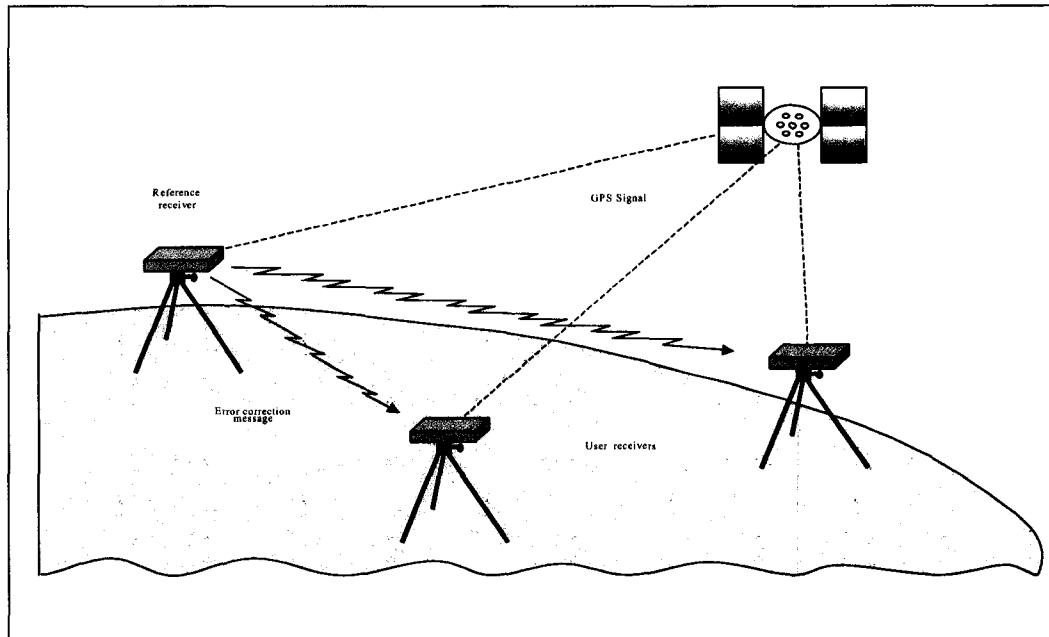
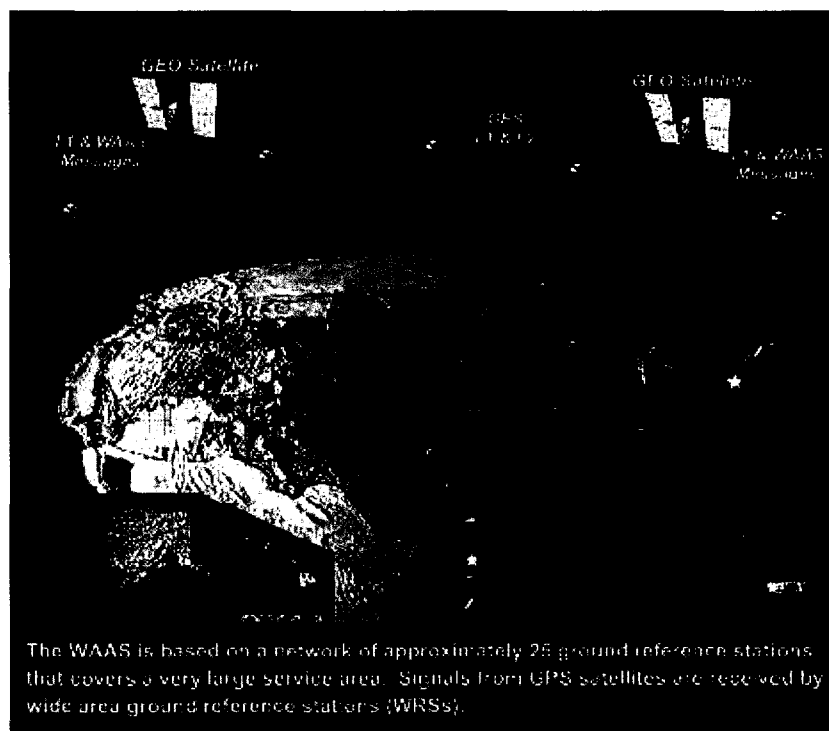


Figure 2. 3 LAAS Anatomy [9].

When the reference station for a DGPS application is established in a local area, it is called LAAS (Local Area Augmentation System). Fig. 2.3 illustrates how the local DGPS is implemented. The reference station receives standard GPS signals and calculates the correction, then broadcasts it. LAAS users receive both standard GPS signals from GPS satellites and the correction signal from a reference station. By combining results from the decoded standard GPS signals with the correction signal from a reference station, the user receivers obtain an improved position solution. LAAS is capable of providing accurate corrections to users at ranges of up to a few tens of miles from the reference station. On top of that, LAAS provides the signal integrity monitoring capability. Therefore, a pilot within the valid area using the LAAS signal will be able to tell how good the signal quality is and to what degree the error of positioning solution is

bounded [17]. However, LAAS only covers an area with a radius of about 25 to 50 miles with reasonable accuracy. Beyond that, the accuracy can no longer be guaranteed. Thus, if highly accurate positioning is needed in an area that is not within 25 to 50 miles radius of an existing LAAS reference station, then one must be constructed and maintained. This effort can cost a few hundred thousand dollars.

### 2.3.2 WAAS



**Figure 2. 4 WAAS System Overview [18].**

Fig. 2.4 demonstrates the overview of the Wide Area Augmentation System (WAAS). To serve a wider area, for instance the continental U.S., without having to set up countless LAAS base stations, the FAA sponsored development of a new augmentation system called the “Wide Area Augmentation System”, or WAAS, to improve upon LAAS system. The basic idea was the same as for LAAS, but with ‘base’

stations that could broadcast a correction signal that would work better and cover bigger area. One approach for WAAS is to build a more powerful base station and put it at a high elevation, so that it covers a larger area. How big this area should be and how high the station should be put is a real engineering problem. Experience suggested that the best solution would be the use of a Geo-Synchronous satellite that is powerful enough to broadcast accurate correction signals to as many users as possible and sensitive enough to know its exact position. To design and launch a new special Geo-Synchronous GPS satellite is a complicated and expensive undertaking. The geostationary satellites provide correction signals over a wide area; hence they are called Wide Area Augmentation System (WAAS) satellites. A minimum of three WAAS satellites is required to cover the whole globe and achieve universal coverage. In addition to broadcasting GPS correction signals, these satellites are also able to broadcast the ordinary GPS pseudorange signal, which improves the availability of the normal GPS system, since one of these WAAS satellites will always be over at least one third of the earth's surface and hence can provide a pseudorange signal for that area.

The issues of WAAS are more complex than those of LAAS since Geo-Synchronous satellites are involved. In LAAS, the base station is built at a well-surveyed position on the surface of the earth, while in WAAS, the base station is located in geostationary orbit above the earth and it is difficult to know the spacecraft locations with high accuracy at all times. Any unexpected force could affect the satellite position. Other incidents can influence the WAAS service as well. For example, when solar spot activity became too active during late April 2001, the WAAS signal was occasionally lost. Although this represents an extreme, at any given moment solar wind, gravity of some

celestial body passing by or a host of other factors can change the position of the WAAS satellite and hence affect the performance of the whole WAAS system. It is normal to see the WAAS satellite's altitude varying by as much as 50 to 100 kilometers [8]. Various techniques have been used to model as many of the geostationary satellite factors as possible [8].

WAAS provides a signal integrity monitoring capability [2]. Unlike LAAS, where one base station serves only the limited surrounding area, hence guaranteeing the integrity information validity for the served community, WAAS has to serve a huge area, which can vary significantly in geography, weather and ionospheric conditions [19], [5]. To make the correction and integrity information available to receivers all around the continental US, the broadcasting must have all the local flavors included. The 25 ground stations serve as the providers of the signal integrity monitor in addition to the correction generator. It then is the task of the individual WAAS receivers to take the needed information out of the broadcast signal to produce the positioning solution and integrity implementation.

All these elements, together with the standard GPS and WAAS satellite orbiting above, are ready to work. What still needs to be done is to determine the math behind the system to make sure it will function as desired. The next section describes the error modeling and integrity modeling for the GPS and WAAS system.

### **2.3 GPS measurement equations**

The objective of WAAS error modeling is to determine the Probability Distribution Functions (PDFs) for the position and time errors through analysis of

pseudorange errors, which is the only data source available to users. The pseudorange has to be connected to the actual position in order for the user to relate the pseudorange errors to the actual position and time errors.

Assuming there are N satellites (or as they are usually called, Space Vehicles, or SVs), clearly the only thing one has a hand on is the measurement. It is not clear at this point how exactly the measurements will work into positioning. Neither are the stochastic characteristics of the measurement and how they behave under various circumstances well understood. To form the reverse relation from measurement of pseudorange errors to position errors, a localized reference system is established.

Usually, in GPS applications the Earth Centered Earth Fixed (ECEF) coordinate frame is used. But when a receiver is involved, a localized reference frame with (North, East and Elevation) is preferred. The “North” axis is directed from the receiver to the North Pole, tangent to the earth surface; the “Elevation” axis is normal to the surface of the earth; the “East” axis is directed to form orthogonal RHS with the “North” and “Elevation” axes.

Define an observing matrix  $\vec{G}$ , which consists of the unit vectors from SVs in view to the receiver. Fig. 2.5(a) shows the  $i$ th row of the observing matrix  $\vec{G}$ , which corresponds to the unit vector from the  $i$ th SV,  $SV_i$  in view to the receiver. In terms of elevation angle  $El_i$  and azimuth angle  $Am_i$ , the  $i$ th row of the observing matrix  $\vec{G}$  is written as:

$$\vec{G}_i = -[\cos El_i \cos Am_i \quad \cos El_i \sin Am_i \quad \sin El_i \quad -1] \quad (2.1)$$

And this is the unit vector in the direction from the  $SV_i$  to the receiver.

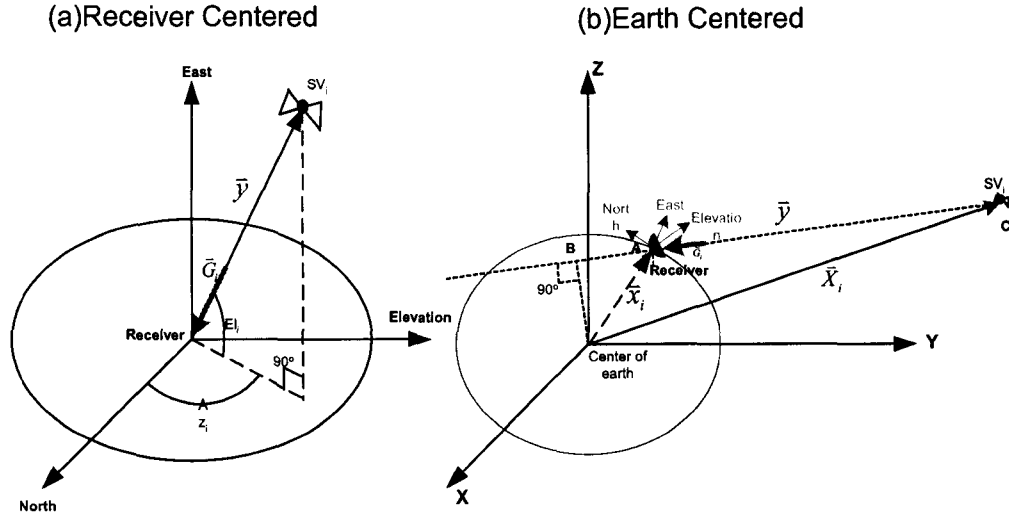


Figure 2.5 (a)  $i$ th element of Observing Matrix  $\bar{G}$ . (b) Pseudorange measurement equation.

The true 4-dimensional position of SV <sub>$i$</sub>  is denoted by  $\bar{X}_i$ , which is the vector from the center of earth to the  $i$ th SV in view, as shown in Fig. 2.5(b).  $\bar{X}_i$  is known from the GPS ephemeris data, which specify the SV in the ECEF coordinate frame. Therefore, it needs to be translated into the localized coordinate frame, based on the receiver, as  $\bar{x}$ .

$\bar{S}$  is the N-dimensional vector that tells about the position and clock state of each SV in use. The elements in vector  $\bar{S}$  are given by

$$S_i = -\bar{G}_i \cdot \bar{X}_i \quad (2.2)$$

The measurement pseudorange  $\bar{y}$ , an N x 1 vector, the true 4-dimensional position vector  $\bar{x}$  (North, East, Elevation and Time), the observing matrix  $\bar{G}$ , an N x 4 matrix containing information about 4-dimensional position for each of the SVs, and the N-dimensional noise term  $\bar{\eta}$  telling measurement error are related through the linearized equation

$$\bar{y} = \bar{S} + \bar{G} \cdot \bar{x} + \bar{\eta} . \quad (2.3)$$

Fig. 2.5(b) illustrates the mechanics of equation (2.3).

Since  $\bar{G}$  depends on  $\bar{x}$ , this problem is nonlinear and is complicated to solve. Fortunately, it is possible to do some linearization that is sufficiently accurate. One wishes to represent the error of this estimate in terms of observation error. With estimates for the user's and the satellites' positions and the time, one can generate estimates for  $\bar{G}$ ,  $\bar{y}$  and  $\bar{S}$ , denoted as  $\hat{G}$ ,  $\hat{y}$  and  $\hat{S}$ . Then, by subtracting the estimate of  $\bar{y}$  from the actual measurements, assuming  $\hat{x}$ , the estimate of  $\bar{x}$  is sufficiently accurate such that  $\hat{G} = \bar{G}$ , one has

$$\Delta\bar{y} = \bar{G} \cdot \Delta\bar{x} + \bar{\varepsilon} , \quad (2.4)$$

where  $\Delta\bar{y} = \bar{y} - \hat{y}$ ,  $\Delta\bar{x} = \bar{x} - \hat{x}$ , and  $\bar{\varepsilon}$  is the observation error including measurement, satellite position, and clock errors:

$$\bar{\varepsilon} \equiv \bar{S} - \hat{S} + \bar{\eta} . \quad (2.5)$$

Equation (2.4) defines the linear transformation of PDFs for  $\Delta\bar{x}$  into PDFs for  $\Delta\bar{y}$ . However, what is needed is the inverse of this. The PDFs of  $\Delta\bar{x}$  need to be derived from the PDFs of  $\Delta\bar{y}$ . In general, the number of measurements  $N$  exceeds 4, since the GPS constellation guarantees there are more than 4 SVs in view over continental US at any moment. Hence, the solution is over determined and optimal inversion depends on the PDFs of  $\bar{\varepsilon}$ .

## 2.3 Error Probability Density Functions (PDFs)

As previously mentioned, the PDFs for  $\bar{\epsilon}$  cannot take arbitrary form if there is to be even a slim hope of solving this problem. Fortunately, past experience suggests that GPS measurement errors are generally well behaved [19], which means they have a greater likelihood of being small than of being large. Errors can be traced from measurements made at the reference stations, through the various algorithms, all the way to the pseudorange observation. Along the way many different error sources are combined and averaged, biases are calibrated or estimated and removed, and outliers are detected and removed. The central limit theorem says that as a large number of independent error sources are combined, the PDF of the resulting error tends to become more and more Gaussian [20]. Thus, it is not unreasonable to assume that the PDF for  $\bar{\epsilon}$  is approximately Gaussian. In fact, since the master station also implements fault detection and exclusion algorithms, which discard overly large errors, it is quite likely that the tail of the actual error distribution will be clipped. Therefore, it is likely that a Gaussian distribution is already over-conservative compared to the true error. An ideal approach is to consider distributions other than Gaussian so that the model doesn't rely too heavily on the Gaussian assumption. What one desires is a model that is robust for a wide class of PDFs. However, since human lives are at stake, being conservative is essential. In Chapter 4, an algorithm to improved performance over that based on the Gaussian assumption will be provided.

The approach outlined so far relies on covariance propagation, making use of the central limit theorem to predict the Gaussian distribution. Another means for reducing errors is the threshold method [21]. This method exploits independent redundant

measurements. If the measurements agree with one another to within a pre-specified threshold, the data is treated as if it is accurate to a level on the same order as the threshold. Otherwise, it is treated as less accurate or invalid. Provided the measurements are independent and the occurrence of bad data is sufficiently infrequent, this method should constrain the errors within an upper and lower bound.

Another error source worth investigation is that introduced by the constraint of the correction data link. The master station is not able to convey all of its knowledge to the users due to the limited bandwidth. This requires that the proposed error model and algorithm be sufficiently adaptive to minimize the average errors and provide confidence levels that reflect errors a user might experience along with model uncertainty.

Several possible PDFs for observation errors have been investigated [21]. All of these PDFs have zero mean, which is appropriate because biases in individual measurements and corrections usually can be estimated and removed. Thus, the covariance propagation method favors a zero mean Gaussian distribution given by

$$n(x) \equiv \frac{1}{\sigma\sqrt{2\pi}} e^{-\frac{x^2}{2\sigma^2}} \quad , \quad (2.6)$$

where  $\sigma^2$  is the variance of the distribution.

The threshold approach favors either a clipped Gaussian or a uniformly distributed variable whose PDF is given by

$$u(x) \equiv \begin{cases} \frac{1}{2a} & |x| < a \\ 0 & \text{Otherwise} \end{cases} \quad , \quad (2.7)$$

where  $a$  is the resulting bound on the error. A more conservative view of the threshold approach is that since the error can take any value up to  $a$ , it must be assumed that the

user has the worst case error. This view is particularly applicable for the errors induced by the bandwidth constraint, which is due to the fact the WAAS Geo-synchronous satellite can broadcast correction data only to grid points with spatial distance of no finer than 5 degrees. Since some users will have errors as large as the bound, for the sake of safety, even though the uniform distribution more accurately describes the PDF for users scattered within the service area, for modeling integrity the more conservative distribution given by

$$d(x) \equiv \frac{1}{2} \{ \delta(x+a) + \delta(x-a) \} \quad (2.8)$$

must be used to ensure there is zero chance of integrity breach, where  $\delta(x)$  is the Dirac distribution. This density function places all of the probability mass right at the thresholds.

There are many other approaches that could be taken in describing the PDFs of the measurement errors. However, for any fault free measurement with no equipment or human fault, errors can be combined to create a reasonable bounding PDF. For modeling integrity, consider each element of  $\bar{\epsilon}$  to be composed of the sum of two independent random errors, one with the conservative distribution (2.8) and one with the normal distribution. This new random variable has the distribution

$$f_1(x) \equiv \frac{1}{2\sigma\sqrt{2\pi}} \left\{ e^{-\frac{(x+a)^2}{2\sigma^2}} + e^{-\frac{(x-a)^2}{2\sigma^2}} \right\} . \quad (2.9)$$

The expected distribution for the ensemble airspace would be the sum of the Gaussian with the uniform in place of the conservative distribution. Its PDF takes the form

$$f_2(x) \equiv \frac{1}{4a} \left\{ \operatorname{erf}\left(\frac{x+a}{\sigma\sqrt{2}}\right) - \operatorname{erf}\left(\frac{x-a}{\sigma\sqrt{2}}\right) \right\} . \quad (2.10)$$

These two distributions that will be considered in this research are shown for similar conditions in Fig. 2.6, where  $erf(x)$  is defined as

$$erf(x) = \frac{2}{\sqrt{\pi}} \int_0^x e^{-t^2} dt \quad (2.11)$$

and the parameters are set as  $\sigma = 1$ ,  $a = 3\sigma$ .

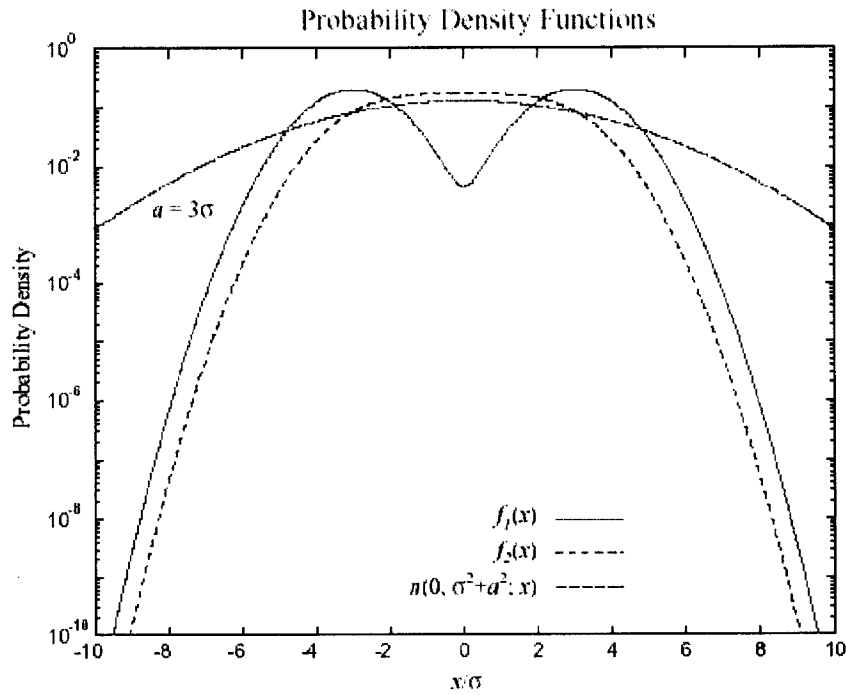


Figure 2. 6 Three PDFs plotted as functions of  $x/\sigma$ .

Table 2. 4 Confidence bounds for varying Probabilities for the three PDFs. The bounds are on  $x/\sigma$  and  $a = \sigma$  is set.

Dist/Pr	1.000E-02	1.000E-03	1.000E-04	1.000E-05	1.000E-06	1.000E-07	1.000E-08	1.000E-09
$n(x)$	2.576	3.291	3.891	4.417	4.892	5.327	5.731	6.109
$f_1(x)$	3.327	4.090	4.719	5.265	5.795	6.199	6.612	6.998
$f_2(x)$	2.938	3.718	4.363	4.924	5.425	5.882	6.305	6.699

Knowing the full PDFs for the errors allows us to specify containment bounds for arbitrary error probabilities. The bounds are found by integrating the PDFs from minus to plus corresponding bound, which integrates to the desired confidence level. Table 2.4 lists some confidence bounds of  $x/\sigma$  for various probabilities. For the distributions given by  $f_1$  and  $f_2$ ,  $a = \sigma$  is set. For example, to reach integrity of  $10^{-7}$ , which is the requirement for WAAS based landing system, the  $x/\sigma$  value is 5.327 for  $n$ , 6.199 for  $f_1$  and 5.882 for  $f_2$ , respectively. It shows in these three distributions  $f_1$  is the most conservative one while  $n$  is the least conservative one. However, even the difference between  $f_1$  and  $n$  is not too significant, meaning  $n$  can be a close replacement for the approximating  $f_1$ . Of course, one has less confidence in the knowledge of the true PDF for the lower probabilities. However, one can still hope the fault detection and isolation mechanism, which discards overly large errors, works to remove outliers. This would result in a true PDF which is bounded by (2.9) and (2.10). Notice that  $f_1(x/\sigma)$  is the most conservative distribution for large  $x$ . Despite this fact, the zero mean constraint creates smaller confidence bounds than would be expected from a biased Gaussian. The latter case results in bounds given by  $b = a + \kappa(\text{Pr})\sigma$ , where  $\kappa(\text{Pr})$  corresponds to the values listed in Table 2.4 for the Gaussian distribution.

## 2.5 Position Solution

The next step towards finding the confidence bounds in the position domain is to determine the best method to estimate the position. If the errors were Gaussian in nature, then the maximum likelihood estimate would coincide with weighted least squares

solution. Given (2.9) and (2.10), it is possible to devise a maximum likelihood estimator specific to each distribution. However, provided  $a$  is not much greater than  $\sigma$ , neither of these distributions is significantly distinct from Gaussian. An estimator optimized to one of these bounding functions would not yield a large improvement over weighted least squares, even if the errors truly were distributed according to (2.9) or (2.10). An advantage of the weighted least squares method is that it is easily solved. Other estimators require non-linear techniques, which are not necessarily guaranteed to converge. Weighted least squares is simple, fast and sufficiently accurate [22]. The weighted least squares solution requires only the variances of the measurement errors. The variance of  $\varepsilon_i$ , the error element due to the  $i$ th SV, are defined as:

$$\sigma_{\varepsilon_i}^2 \equiv \langle (\varepsilon_i - \langle \varepsilon_i \rangle)^2 \rangle , \quad (2.12)$$

and the covariance  $\varepsilon_{i,j}$  between the measurement errors associated with  $SV_i$  and  $SV_j$

$$\sigma_{\varepsilon_{i,j}}^2 \equiv \langle (\varepsilon_i - \langle \varepsilon_i \rangle)(\varepsilon_j - \langle \varepsilon_j \rangle) \rangle , \quad (2.13)$$

where the angle brackets  $\langle \rangle$  about an object denote its expected value. All the PDFs considered are zero mean, which again is a necessary result of well designed correction algorithms and receivers. The equivalent variances for the conservative and expected distributions  $f_1$  and  $f_2$  are given in terms of a Gaussian distribution parameter  $\sigma$  by [19]

$$\sigma_{f_1}^2 = \sigma^2 + a^2 , \quad (2.14)$$

$$\sigma_{f_2}^2 = \sigma^2 + \frac{a^2}{3} . \quad (2.15)$$

The weighted least squares estimator minimizes the cost function given by

$$\Delta \hat{y}^T \cdot W \cdot \Delta \hat{y} , \quad (2.16)$$

where the weighting matrix  $W$  is the inverse of the measurement error covariance matrix

$$W^{-1} = \langle \tilde{\epsilon} \cdot \tilde{\epsilon}^T \rangle = \begin{bmatrix} \sigma_{\epsilon_1}^2 & \sigma_{\epsilon_{1,2}}^2 & \sigma_{\epsilon_{1,3}}^2 & \cdot & \cdot & \cdot & \sigma_{\epsilon_{1,N}}^2 \\ \sigma_{\epsilon_{1,2}}^2 & \sigma_{\epsilon_2}^2 & \sigma_{\epsilon_{2,3}}^2 & \cdot & \cdot & \cdot & \sigma_{\epsilon_{2,N}}^2 \\ \sigma_{\epsilon_{1,3}}^2 & \sigma_{\epsilon_{2,3}}^2 & \sigma_{\epsilon_3}^2 & \cdot & \cdot & \cdot & \sigma_{\epsilon_{3,N}}^2 \\ \cdot & \cdot & \cdot & \cdot & \cdot & \cdot & \cdot \\ \cdot & \cdot & \cdot & \cdot & \cdot & \cdot & \cdot \\ \cdot & \cdot & \cdot & \cdot & \cdot & \cdot & \cdot \\ \sigma_{\epsilon_{1,N}}^2 & \sigma_{\epsilon_{2,N}}^2 & \sigma_{\epsilon_{3,N}}^2 & \cdot & \cdot & \cdot & \sigma_{\epsilon_N}^2 \end{bmatrix} . \quad (2.17)$$

If one had no knowledge about correlation between measurement errors, then the off-diagonal elements of the covariance matrix would be zero in order to form a position solution. Of course, the off-diagonal elements would be helpful in improving the position solution. However, it is unlikely that they would be available to an aircraft receiver or pilot in real time. A naive solution is to let them all be zero and hope that this works. In [5], this assumption was made and tested by Monte-Carlo simulation and proved to work reasonably well. Therefore, the cross-correlation terms will be set to zero, simplifying the procedure for finding the position estimate. It has been shown that further simplification can be obtained by setting the covariance matrix to a constant multiplying the identity matrix. This approach still delivers a reasonable non-weighted position solution [23].

Given an initial estimate for position and an estimate for the weighting matrix, the weighted least squares inverse of (2.4) can be performed to improve the position estimate. The solution is given by [22], [24]

$$\Delta \hat{x} = (G^T \cdot W \cdot G)^{-1} \cdot G^T \cdot W \cdot \Delta \hat{y} \equiv K \cdot \Delta \hat{y} , \quad (2.18)$$

where  $K$  is defined as

$$K \equiv (G^T \cdot W \cdot G)^{-1} \cdot G^T \cdot W . \quad (2.19)$$

As mentioned above, the solution may need to be iterated, updating  $\hat{x}$ ,  $\hat{G}$ ,  $\hat{S}$  and  $\hat{y}$  at each step. The best estimate for position  $\hat{x}$  is obtained when  $\Delta\hat{x}$  is driven to 0 and the cost function (2. 16) is at a minimum.

Notice that the definition for  $K$  has the weighting in both its denominator and numerator. If all variance estimates were uniformly scaled up or down, it would have no impact on the position solution. The best estimate of  $\bar{x}$  depends only on the relative confidence between the measurements and not on their absolute values. The same is not true for the confidence bounds on the position estimate. In fact, the bounds have been shown to be very dependent on the overall scaling of the measurement variances [19].

## 2.6 Confidence Bounds

Finding the confidence bound is not as simple as finding the position estimate. Since there are human lives at stake, extra care must be taken. One way to formulate a bound is to find worst-case bounds in each step of the position calculation and sum them up. This approach works for any distribution and is always safe. However, it is so safe that it practically kills any application based on it since the individual errors will never be available in a practical system.

Luckily, the stochastic nature of these error sources dictates that the worst cases don't happen all the time. In fact, the worst cases are low-probability cases, therefore, their contribution to the overall PDF is very limited. And, even if they do, the errors don't come in a worst possible combination, i.e. they usually cancel each other instead of building up through positive reinforcement, which is an extremely low probability situation. The covariance propagation method makes better sense for providing high integrity while maintaining availability most of the time. The final PDF for position error

would be given by the convolution of the elements  $K_{3,i} \cdot \varepsilon_i$ , where  $K_{3,i}$  is the  $i$ th element along the third row of  $K$  in (2.19). The resulting distribution approaches a Gaussian as  $N$  becomes sufficiently large [25]. The mean and variance of this distribution are determined respectively by the sums of the means and variances of original variables,  $K_{3,i} \cdot \varepsilon_i$ . Thus, *e.g.*, the second moment of the vertical estimate can be written as

$$\sigma_{\hat{x}_3} = \sqrt{\sum_{i=1}^N (K_{3,i} \cdot \sigma_{\varepsilon_i})^2} . \quad (2.20)$$

We can define the Vertical Protection Limit ( $VPL$ ) by using (2.20). The assumption that the position error is bounded by a Gaussian with variance (2.20) and confidence bounds from Table 2.4 results in a less conservative  $VPL$  :

$$VPL_{\sigma} \equiv \kappa(\text{Pr}) \cdot \sigma_{\hat{x}_3} . \quad (2.21)$$

Still there is space to improve. It has been shown in [19] that it is reasonable to further simplify (2.21) as

$$VPL_{\sigma_V} \equiv \kappa(\text{Pr}) \cdot \sigma_V , \quad (2.22)$$

where the variance of the vertical position estimate is given by the third diagonal element of the position estimate covariance matrix

$$\sigma_V \equiv \sqrt{\left[ (G^T \cdot W \cdot G)^{-1} \right]_{3,3}} . \quad (2.23)$$

For integrity purposes,  $W$  could either be the same diagonal weighting matrix used to form the position estimate, or it can include bounds on cross-correlation terms. While these bounds are unlikely to improve our position estimate, they will most likely make the expected integrity bounds more conservative, by properly accounting for

correlations between measurement errors. These off-diagonal elements should be applied only when they are actually known.

All of the Integrity and availability modeling in this dissertation will be based on the above equations and assumptions.

## **Chapter 3**

### **WAAS static Error, integrity and availability monitoring and analysis**

In the preceding chapters, the theoretical fundamentals about GPS and WAAS have been presented. The WAAS integrity algorithm is overly conservative. This is good and bad at the same time. It is good because being conservative guarantees to keep the system safe, which is the main concern when airplanes and aviation are involved. However, as will be shown in this chapter, being overly conservative generates the problem of low availability. It is okay to lose the service of the system for seconds here and there during the En Route stage of flight. At the final landing stage, however, this can mean a missed approach, which is just the opposite of what the WAAS based landing system was developed for.

In order to develop a practical algorithm regarding WAAS protection level, the actual data has to be analyzed while appropriately incorporating aviation concerns.

#### **3.1 Necessary WAAS Data collection**

In order to validate the new *VPL* algorithm, all of the system software was tested with actual WAAS data to show the improvement over the old algorithm. In this section, the equipment and tools used in the data collection and processing are listed.

The GPS research group at the University of Oklahoma has been taking observations of the WAAS signal in both static and dynamic settings. The devices used include the Rockwell EMAGR (Enhanced Miniature Aviation GPS Receiver) WAAS

capable GPS receiver, the Ashtech Z12 GPS receiver, Rockwell BBCOM software and post processing software, and the Ashtech Prism post processing software. In addition, we use two personal computers for these tasks, one for data acquisition running BBCOM version K (formerly version J) and one for Ashtech data post processing and other data processing and analysis. Additional tools used in the research include Matlab and Microsoft Visual C++.

The analysis here focuses on WAAS static data, which is used to formulate new Error, Integrity, and Availability algorithm. WAAS static data is the major object of study, upon which most analysis and discussion will be performed. Static Data is a good starting point for the ease of getting the ground truth. For moving aircraft, only small adjustments need to be made.

In order to carry out these tasks, ground truth was required. In this regard, the project team has performed a series of surveys to determine the true positions of a few stable sites that have good satellite visibility and relatively easy access for installation of antennae. Two antennae were installed on the roofs of buildings at the University of Oklahoma (OU). One is on building 210 of the OU north research campus, located coincidentally with Max Westheimer Airport. The other is on the Carson Engineering Center building on the main OU campus. Both antenna sites were accurately surveyed in longitude, latitude and altitude. In addition, both are maintained to ensure quality of satellite signal reception.

The research effort uses a second redundant EMAGR WAAS receiver to make sure that any unexpected results are not due to malfunctioning on the part of the WAAS receiver. Preliminary results indicate that the Rockwell EMAGR works reliably and

doesn't seem to be an error source [9]. It was concluded that the observed errors originate from the quality of the Signal In Space (SIS), which is maintained by Raytheon. For the proposed research, it will be assumed that the receiver is working to specification, and only an analysis of the signal in space is required.

### **3.2 The way the data is classified**

This research project is specifically designed to improve the navigation system performance. Therefore, the navigation requirements have to be understood to do a good job of upgrading the system integrity and availability. The definitions of some concepts that are to be used extensively are [3]:

**Accuracy:** The difference between the measured position and the actual (or the true) position is referred to as accuracy.

**Integrity:** The capability of the system to broadcast timely warnings to all its users that the SIS is not fit for navigation or to shut itself down when it should not be used for navigation is the Integrity.

**Availability:** The fraction or percentage of time that the system service is capable of providing SIS with integrity is the availability.

**Continuity:** If the system supports the required accuracy and integrity throughout a maneuver, then the continuity is achieved.

For a navigation system to provide some specific capability, which is usually set by a government agency after extensive research on safety and economy, some system performance metrics are to be set as the standard. Minimum system performance has to be at least on par with the standards, i.e. the accuracy, integrity, availability and

continuity needs to perform at or above a set standard. For precision landing, the requirements are as follows:

1. A severe bandwidth limitation of 250 bits per second.
2. Stringent user integrity: less than  $10^{-7}$  chance of receiving Hazardously Misleading Information (HMI) per approach.
3. Six second time to alarm for any failure that could lead to HMI.
4. High availability: the system should be usable in more than 99.9% of the time.
5. Support for global or near global coverage.
6. Flexibility to support different service providers [26].

The standard can be devised in different ways, according to different agencies and different purposes. Most notable in the list above are the integrity requirement of less than  $10^{-7}$  chance of receiving HMI per approach and the availability requirement that the system should be usable more than 99.9% of the time. For the requirement in Category I airplane Precision Landing, the standard for classification of the data points are shown in Fig. 3.1 and 3.2.

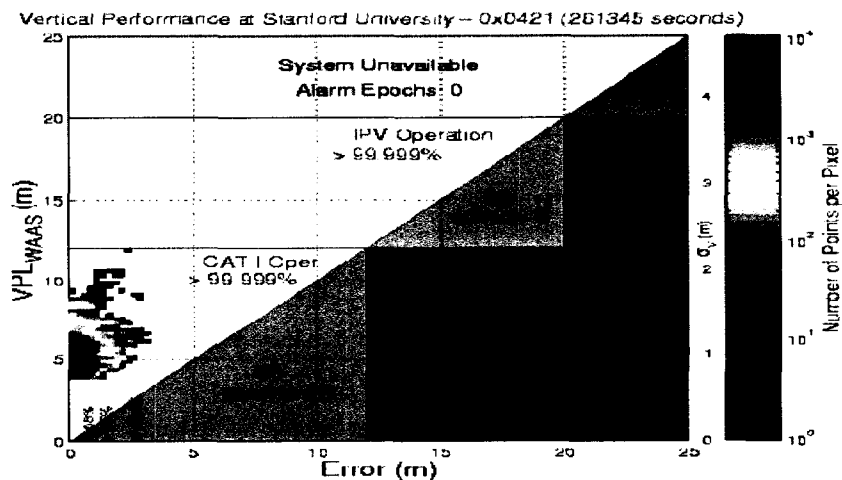


Figure 3.1 WAAS performance classification, vertical part [27].

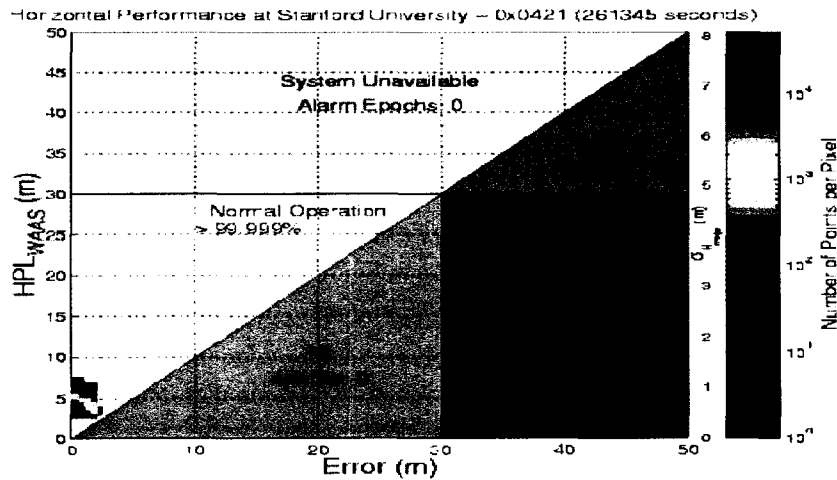


Figure 3. 2 WAAS performance classification, horizontal part [27].

These diagrams, Fig. 3.1 and 3.2, use triangle charts with real data on a better day for the WAAS signal in space (SIS) to demonstrate the division of the sample space of the performance classification. Both vertical and horizontal charts are shown. In the original specifications, the above triangle charts were used. However, the updated technical target and corresponding new procedure for Lateral Navigation/Vertical Navigation (LNAV/VNAV) is a bit different and will be addressed later. This dissertation will address only the vertical performance because it is the most important. This is not to minimize the importance of horizontal integrity. The horizontal integrity and vertical integrity are independent of each other and exhibit similar behaviors and characteristics.

The most stringent applications for WAAS will be Category 1 precision approach (CAT I) and the instrument approach with vertical guidance (IPV). These operations have a Vertical Alert Limit (VAL) of 12 and 20 meters, respectively. Thus, based on the navigation requirements, the whole absolute  $VPL - VPE$  space will be broken into the seven color-coded parts so that it's easier to track historical performance [28]. From the lower-left corner and going clockwise, the whole  $VPL - VPE$  plane is divided into 7 areas:

1.  $VPL > VPE$ ;  $VPL \leq 12$ ; Available, for CAT I operation.
2.  $VPL > VPE$ ;  $VPL \leq 19$ ; Available, for instrument approach with vertical guidance (IPV) operation.
3.  $VPL > VPE$ ;  $VPL > 19$ ; System Unavailable.
4.  $VPL < VPE$ ;  $VPL > 19$ ; Misleading Information (MI-1).
5.  $VPL < VPE$ ;  $12 < VPL < 19$ ,  $12 < VPE < 19$ ; Misleading Information (MI-2).
6.  $VPL < VPE$ ;  $VPL < 12$ ,  $VPE < 12$ ; Misleading Information (MI-3).
7.  $VPL < VPE$ ; all the remaining area; Hazardously Misleading Information (HMI).

Of these sections in the triangle charts, case 1 represents the requirement for CAT I precision approach, with the Vertical Alert Limit (VAL) as 12 meters.

Case 2 represents the requirement for IPV precision approach, with the Vertical Alert Limit (VAL) as 19 meters.

Case 3 is the unavailable area where VPL is too large to support the desired navigation procedure.

Case 4, 5 and 6 are the cases when the error exceeds the VPL and provides Misleading Information (MI). Operationally, these regions are not necessarily hazardous. However, it should be remembered that in normal operation mobile users do not have access to the actual error. They are entirely dependent on the accuracy of the VPL estimate. Therefore, this definition only makes sense in post analysis of altitude data.

Case 7 is an unsafe region where the VPL supports the operation but the error is large enough to create Hazardously Misleading Information (HMI). It is the part of the VPL-VPE space that we are most concerned about, since it indicates the system's failure

to inform users of a breach of integrity and, therefore, can potentially cause fatal consequence.

In the unavailable region, the procedure will not be flown since the VPL exceeds the VAL, while in the usable region the error is small enough to keep the aircraft within the obstacle clearance region. Despite these operational considerations, from a systems standpoint, the master station and/or integrity equation have failed to protect the navigation solution if the error becomes larger than the VPL. Thus, all points should be above the diagonal line.

### **3.3 Define WAAS performance metrics**

The objective of SIS integrity monitoring is to ensure that the probability of Hazardously Misleading Information (HMI), both vertical and horizontal, being provided to the aircraft by the navigation system is sufficiently low. The original definition of the WAAS performance metrics and how they are used in this dissertation is listed as followed:

**Accuracy:** The difference between the measured position and the actual (or the true) position is referred to as accuracy. In this dissertation only vertical error is researched. When Vertical Position Error (VPE) is within a pre-set bound, called the Vertical Alarm Limit (VAL) for a specific application, the system achieves sufficient accuracy.

**Integrity:** The capability of the system to broadcast timely warnings to all its users that the SIS is not fit for navigation or to shut itself down when it should not be used for navigation is the Integrity. In our case, as long as the VPL and HPL are large enough to bound vertical and lateral errors, integrity is achieved.

**Availability:** The fraction or percentage of time that the system service is capable of providing SIS with integrity is the availability. In our triangle charts, this means the percentage of time that the data fall into the available region of a specific application, which means VPL must be greater than the vertical limit and VPL must be less than the respective Vertical Alarm Limit (VAL).

**Continuity:** If the system supports the required accuracy and integrity throughout a maneuver then continuity is achieved.

In the latest update to the WAAS specification, the FAA replaced the original technical target of Category 1 capability (Decision height of 200 feet with visibility of one-half mile) with a certified Lateral Navigation/Vertical Navigation (LNAV/VNAV) capability (decision height of 350 feet with visibility of one-half mile). It is expected in late 2003 that the FAA will publish a new procedure for the full capability of WAAS, resulting in approaches down to 250 feet above the runway in  $\frac{3}{4}$ -mile visibility. These changes are partially due to the difficulty of achieving the original requirements [29]. Regardless of the updates, the classification of performance in Fig. 3.1 and 3.2 still makes a lot of sense.

The calculation of availability is special and needs some explanation before proceeding. As proposed in [2], [26] and defined in the MOPS [3], the WAAS integrity requirement for precision approach is  $10^{-7}$  HMI per approach. This means the probability of an instance when the system error surpasses the system protection level is less than  $10^{-7}$  over the time of final approach, which lasts around 3 minutes. This makes sense since the average yearly number of landings in the US is about  $10^7$ . Most of these landings are visual flight rule (VFR) landings. This stringent requirement guarantees that

WAAS would be at least comparable, if not much better than, the current existing aviation infrastructure.

This creates a dilemma. On one hand, this stringent standard requires averaging the data over a large sample. To reach the required integrity level, at least  $10^7$  samples are needed, provided that the system performs up to the standard. For the WAAS signal with 5 samples a second, that means at least  $2 \times 10^6$  seconds are needed at the minimum. That is more than 555 hours and dilutes the approach, which lasts only minutes. On the other hand, if we choose to compute the availability over the final approach, which makes sense, the integrity will not be achieved within the precision demanded by the MOPS. The best precision for a 3-minute final approach integrity computation is  $1.1 \times 10^{-3}$  per approach, which is not of sufficient precision for the MOPS.

Today, availability is a concept that ideally needs to be calculated over an infinite number of samples. It is misleading that this quantity needs to be computed over an infinitely long period of time since this is the only way that a large number of samples can be accumulated. Instead, availability at any moment needs to be calculated based on an infinitesimal time interval over an infinitely large ensemble of data points with equivalent circumstance. In other words, this requirement is hypothetical and applies to a hypothetical collection of users who are all under equivalently identical conditions. By using equivalence, we stress the overall conditions that might affect the outcome of the system. For instance, the whole ensemble needs to be under identical ionospheric and tropospheric conditions, needs to have identical satellite constellation and configuration, needs to have the same clock error, needs to have identical noise features and multipath, and so on. This is practically impossible due to the fact that satellite navigation systems

and their associated errors are inherently non-stationary. Any true ensemble would average over unlimited different conditions, combining users with high and low risk. Thus, an ensemble of users must be imagined, for each point in space and time, whose errors follow probability distributions specific to that point. For an aircraft on approach, there is only one actual user at a given point in space and time. That user will experience a specific set of errors that combine to create the position error. These errors can be broken into deterministic and stochastic components. The distinction is that if we could replicate the conditions and environment for the user, the deterministic components would be completely repeatable. Thus, these errors would be common mode; all users in our ensemble would suffer them to the same degree. On the other hand, stochastic errors such as thermal noise would be different for each user in the ensemble. Overall, these components combine to form a range of possible errors whose magnitudes have differing probabilities. When we look at a very large number (approaching infinity) of hypothetical users in the ensemble, some will have errors that exceed the protection level while most will not. The fraction of users that exceed the Protection Level (PL) can be used to determine the probability of an integrity failure under those conditions.

The aviation integrity requirement of  $1-2 \times 10^{-7}$  per approach applies in principle to each and every approach. It is not an ensemble average over all conditions. This integrity requirement has to be met at every point in the Continental United States (CONUS) at any given moment, instead of being averaged out through time or space. This makes computing the performance metrics, the availability and integrity, a little tricky. As previously discussed, the availability is a concept that in principle needs to be calculated over an infinite ensemble of data. Since that is practically impossible, this

study uses a circular buffer with a buffer size of 900 (3 minutes) to calculate a moving-averaging availability. This is not the availability in the true definition. However, one can agree that if the true availability is high enough, this Moving-Averaged Availability (MAA) certainly will hold high enough as well. The choice of 3 minutes is due to the mean time a typical final approach takes. MAA is an indicator of how the true availability performs and is diluted as the averaging window widens. Since MAA is the only way we can measure real system performance, we will simply call it WAAS SIS availability.

### **3.4 WAAS Signal in Space (SIS) general performance**

To attack the problem of lower-than-needed-availability that is currently faced by the WAAS system, it is best to start by characterizing as many as possible of the contributing factors. We need to understand how the WAAS SIS performs, what seems to be the root of the problem, and what could be the best way to solve, or at least improve it. Fig. 3.3 - 3.13 below illustrate performances from data files containing 11 days of WAAS data picked from the data collection we have accumulated from 1999 to 2003. These figures demonstrate the consistency of the stochastic features of the WAAS system over time, and specifically, over the entire lifetime of WAAS. These specific days were picked to represent the overall data we have collected. Indeed they include basically all types of days we can expect. These days include the ordinary days when the performance falls into the expected type; or better days when the performance is more ideal than WAAS was designed for. And there are worse days when the system performs poorly. The data sets are picked from different years to demonstrate the consistency of the WAAS performance over time. Although these days weren't picked randomly, they still represent

all data types in the data collection. We have chosen to investigate these specific days as they are representative of most of the characteristics of the data archive. They don't, however, represent the data types evenly.

It is of interest to look into the performance over time to be sure of the statistical consistency over time. Therefore, a quick look at the GPS-time versus Altitude, Latitude and Longitude errors will help us learn about the WAAS SIS behavior in each selected sample. The VPL-versus-VPE (Vertical Position Error) curve shows how the integrity monitoring system works in each selected day.

A few observations on how the overall characteristic behavior of the WAAS Signal in Space (SIS) looks and on classification of data type are presented next.

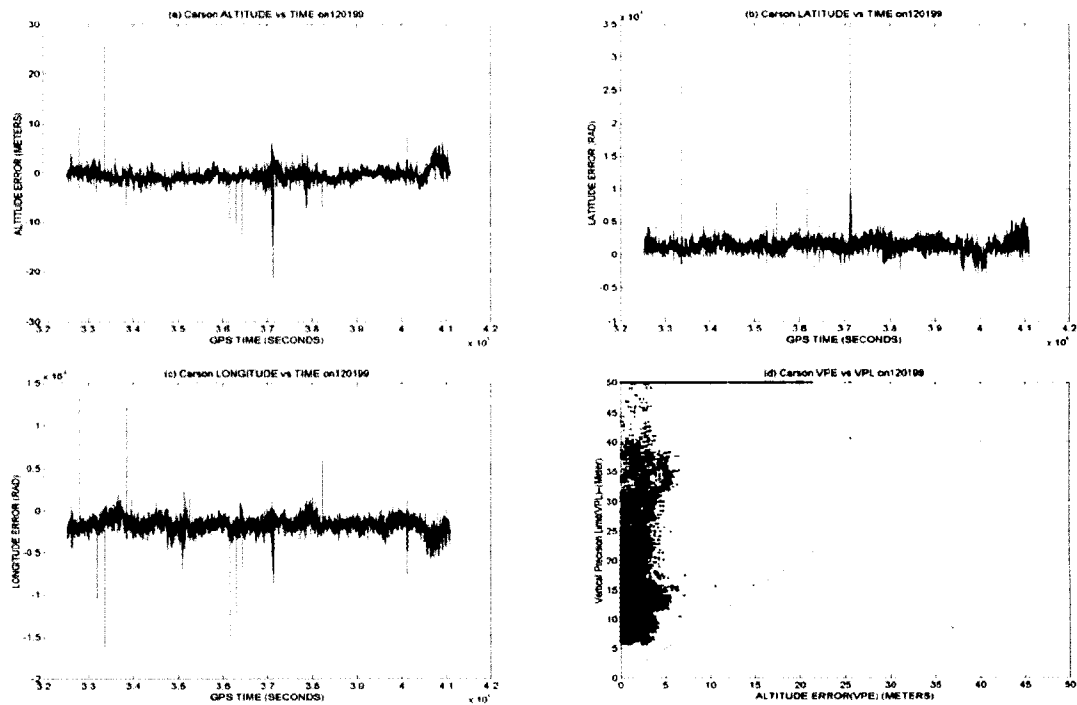


**Figure 3.3 WAAS performance on 12/01/99.**

Better days are when the data points all fall into the upper left part in the triangle chart Fig. 3.3 d and 3.3 d, i.e. VPL is always greater than or equal to VPE. At the same

time, both VPE and VPL are well bounded within the Vertical Alarm Limit (VAL), such as 12 meters for CAT I precision approach and 20 meters for IPV operation. VPL should mimic VPE closely and therefore in an ideal day the VPL-VPE triangle chart will have all the data points located above the  $VPL = VPE$  diagonal line and cramped into the lower part of the up triangle (preferably under the VAL line of the application, such as the 12 meter for CAT I precision approach).

On Dec. 1<sup>st</sup>, 1999 WAAS recorded one of the common days. It can be considered a good day. As shown in Fig. 3.3 all of the altitude, latitude and longitude data behaved fairly well except some spikes, i.e. excessively large errors. The width of each spike varies from a single data point to minutes, mostly in tens of seconds. We need to keep in mind that the data spans over 24 hours and that there are 5 samples every second. These bad spikes are not frequent compared to the better part of the data. The frequency and reason that these spikes occur need further investigation. The integrity monitoring system works perfectly since there is not one single HMI case. However, as can be seen from the altitude-time chart and the VPL-VPE triangle chart, the VPE is within the five meter limit most of the time, while the VPL is spread over 6 to 50 meters and beyond. The congregated dots along  $VPL = 50$  meters only indicate there are points with VPL greater than 50 meters, which is understandable considering the spikes. The statistics needs further analysis and will be presented in the chapter 4.

This day is typical of what WAAS users can expect. The system performs reasonably well. The errors are limited to reasonable values. The integrity-monitoring works. The only concern is that the VPL is not mimicking the VPE very well since VPL is spread too wide while VPE is not. For category I precision landing purpose, which has

a VAL of 12 meters, there is a significant amount of data falling out of the available area. The number or percentage of cases that are not within the CAT I or IPV operation requirement needs additional analysis. The original WAAS project performance of more than 99.9% availability for CAT I precision landing is not met. The over-conservativeness of current WAAS integrity algorithm is to blame for at least part of this.

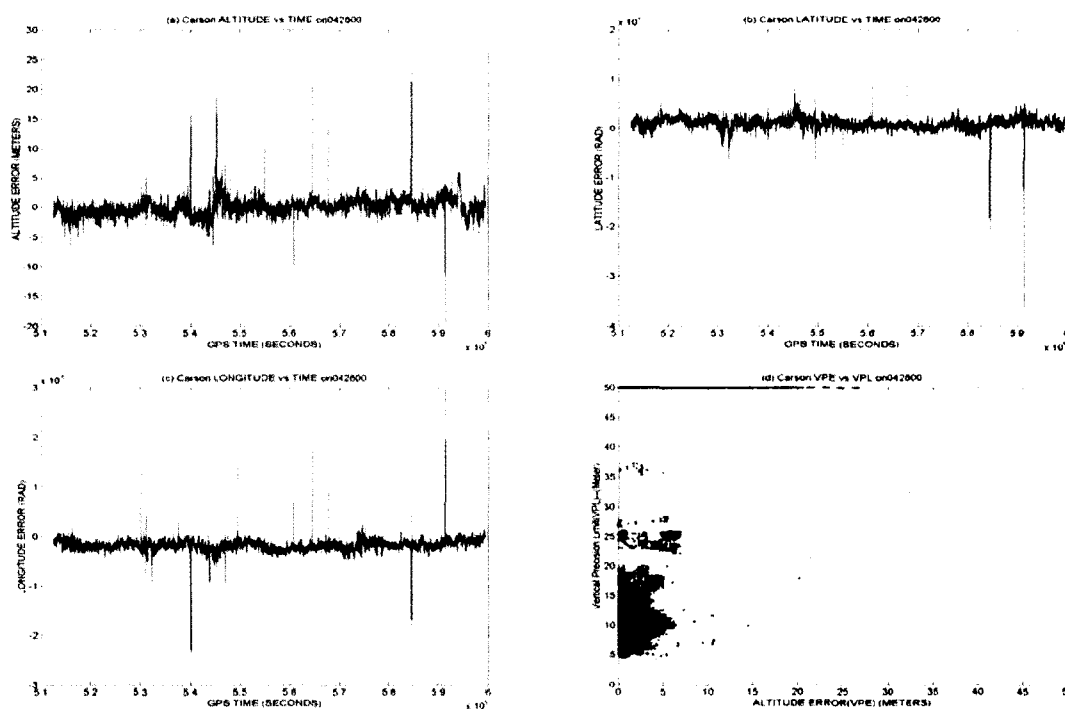


**Figure 3. 4 WAAS performance on 04/28/00.**

A similar day is April 28<sup>th</sup>, 2000, as shown in Fig. 3.4, which incidentally was a couple of days before Selective Availability (SA) was turned off per president Clinton's presidential order [4]. Again the WAAS SIS works well, limiting errors to meters. As in the 12/01/1999 case in Fig. 3.3, spikes again appear, which was expected. This day shows better data than those of 12/01/1999, since the majority of data points falls below a VPL of 20 meters, which is the VAL for IPV operation. This shows that the VPL algorithm is doing a better job this day relating to the VPE. However, there are integrity breaches

which are not allowed by the WAAS system design. These are data points with vertical error larger than their bounding limit, VPL. Since a pilot has no access to the real time error information, he can only depend on the system-provided VPL as the upper bound of the estimate of VPE. Since the VPL is less than according VPE, the pilot can make an incorrect assessment of the altitude of the airplane.

It was not a good performance day for WAAS SIS due to these integrity breaches. However the number of these HMIs is limited and very small compared to the quantity of acquired data in a 24-hour span. These breaches also appear to be independent and isolated cases. Further research needs to be done to determine the causes of these integrity breaches.

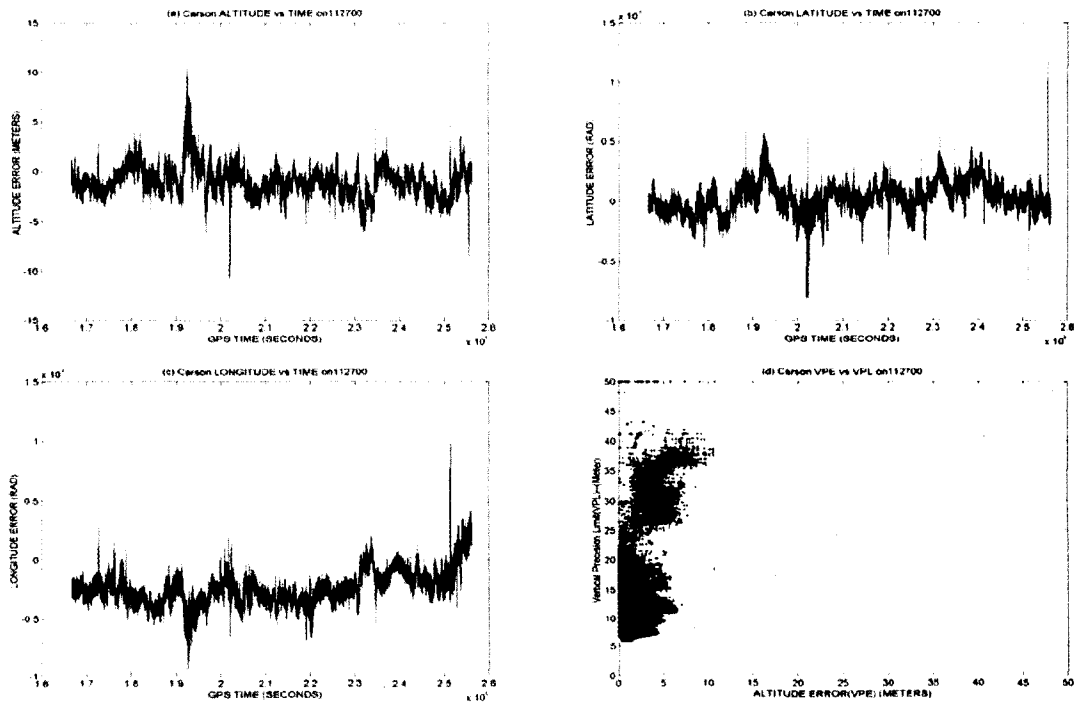
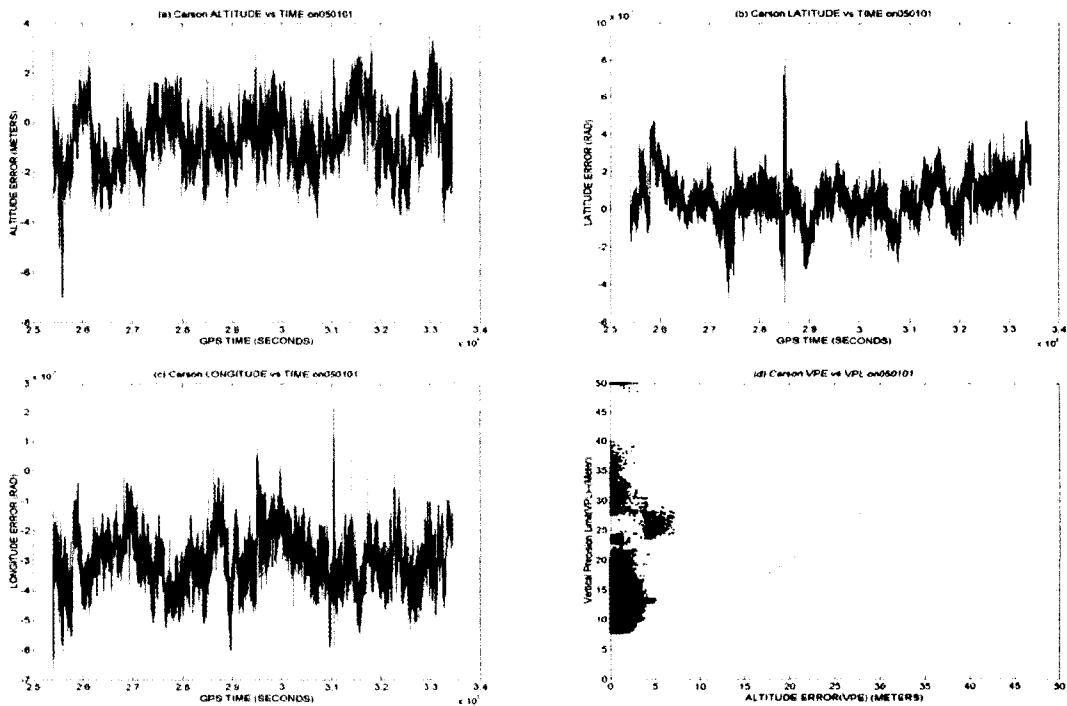


Figure 3.5 WAAS performance on 11/27/00.

The 11/27/2000 data in Fig. 3.5 is after the SA was turned off. It can be easily seen that the error performance gets better since the errors are smaller. Other than that, on this day WAAS SIS performs a lot like 12/01/1999 in Fig. 3.3. This data day represents a good solid day with integrity monitoring working well, but the availability is not up to the WAAS initial project requirement.



**Figure 3. 6 WAAS performance on 05/01/01.**

The data for day 05/01/2001, shown in Fig. 3.6, shows again that after SA was switched off, the overall error performance improved. There are fewer spikes and the spike values are less significant. By now the benefit of switching off SA can be seen. WAAS is capable of removing the positioning error introduced by SA, which can be attested by noticing overall smaller errors all around, and also by noticing the smaller number and lower magnitude of spikes. In the VPL-VPE chart, we notice a higher

concentration of data points in below the VPL 20 meter line. This says that the integrity monitoring system is doing a better job without the interference of SA. Therefore, this can be classified as a better day in the data collection.

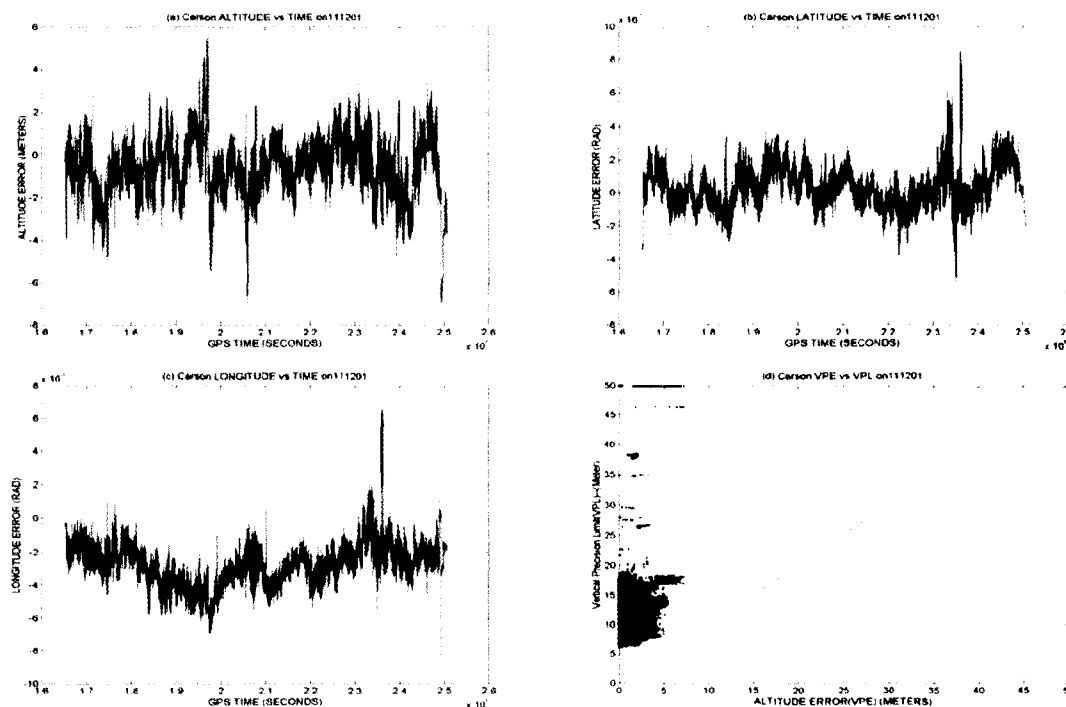


**Figure 3. 7 WAAS performance on 11/12/01.**

Data from 11/12/2001 is shown in Fig. 3.7. Statistically, this is a repeat of 05/01/2001 as shown in Fig. 3.6. No major change occurred in any meaningful category. Errors are limited and spikes did not occur as frequently. The system integrity monitoring mechanism worked very well. This also can be treated as a better day.

WAAS data for 05/02/2002, as given in Fig. 3.8, shows major WAAS problems. Not much information can be gained by checking the error performance charts due to the fact that the overly large magnitude of the spikes overwhelms the baseline error values. Also, instead of the spikes usually expected, the sustained high value of errors raises

concern. A closer look is needed to evaluate the error performance. The large magnitude of the errors is a bad problem, indicating that the WAAS failed to provide a timely and accurate positioning solution to the users. On the other hand, it is a blessing in disguise since the overly large magnitude of errors makes them easy to pick out from normal data due to their nature. It is relatively straightforward for the users to threshold and identify the problem data points. And then these problem data points can be separated, and the system performance integrity can be protected.

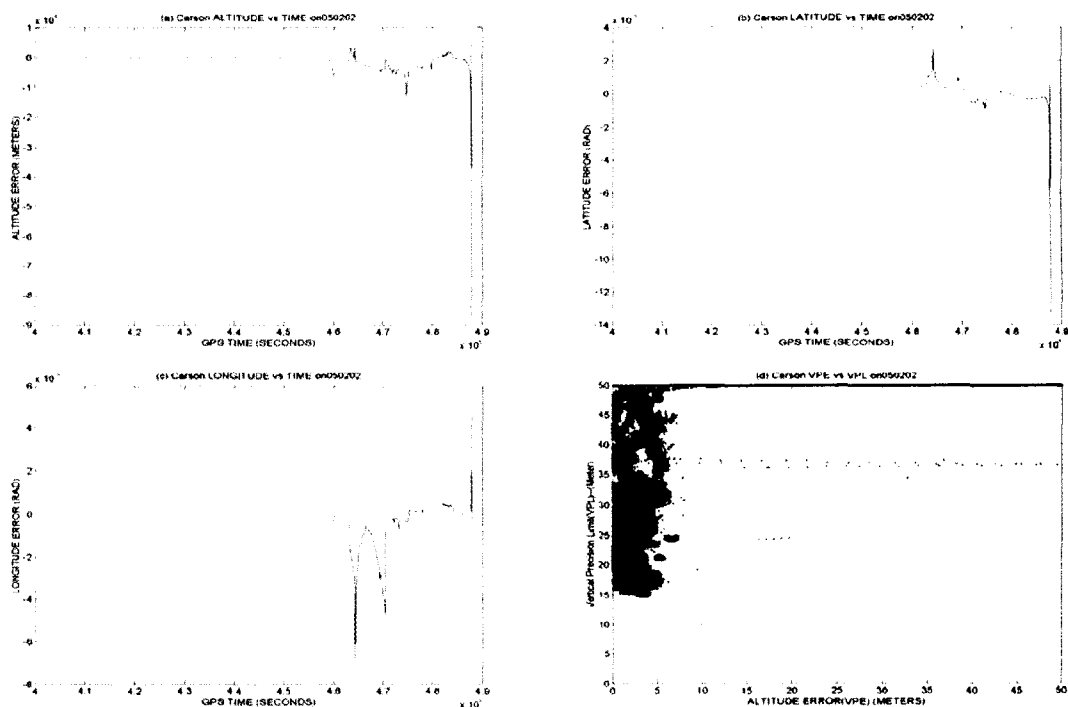


**Figure 3. 8 WAAS performance on 05/02/02.**

In Fig. 3.8 (d), the VPE-VPL triangle chart shows a series of HMIs that seem to be time-correlated. Considering the error performance we have on that day this is not surprising. The small number of HMIs make this day a suitable day to study the cause of them happening. More discussions on this will be done in Section 4.5.

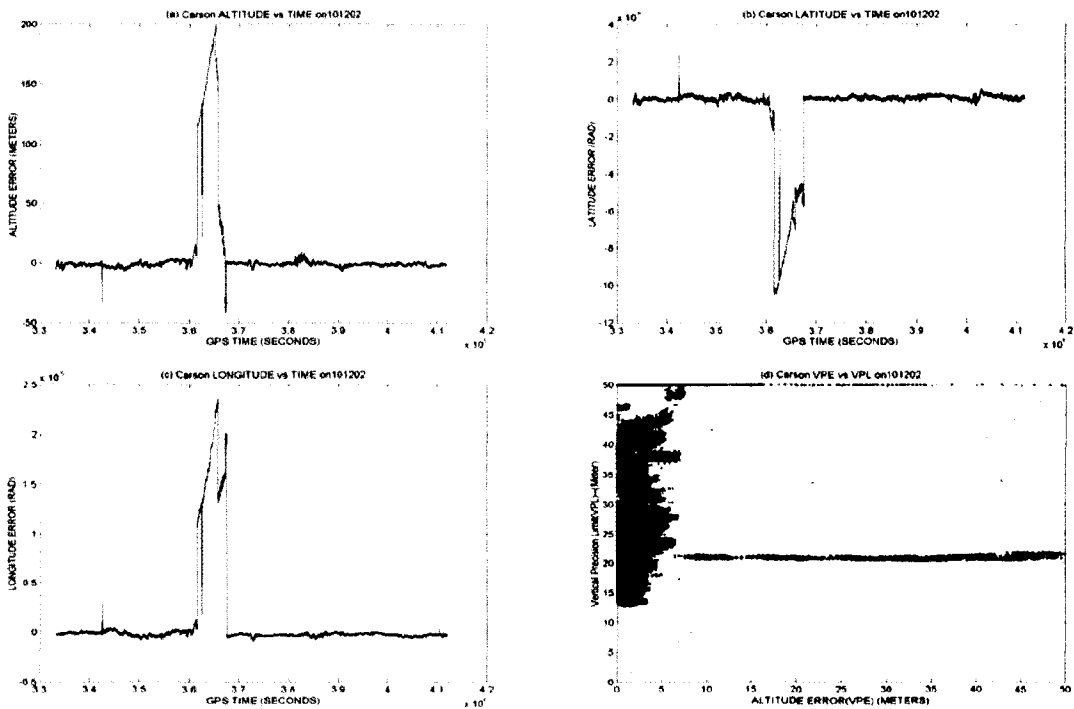


**Figure 3.9 WAAS performance on 10/12/02.**

Data for 10/12/2002 is shown in Fig.3.9, and this is a similar day to 05/02/2002 as shown in Fig. 3.8, except that the number of HMIs is far more than that of 05/02/2002 (Fig. 3.8). The error performance is better than the integrity breach and seems more severe with a higher number of HMIs. This is a very bad WAAS day.

The first glimpse of 12/28/2002 given in Fig. 3.10 shows promise without the sustained high towers of error values. Only isolated spikes are present. The overall error performance is not too bad. But, observing the VPL-VPE chart, we seem to have a problem with a large number of HMI incidents. This is a very bad WAAS day.

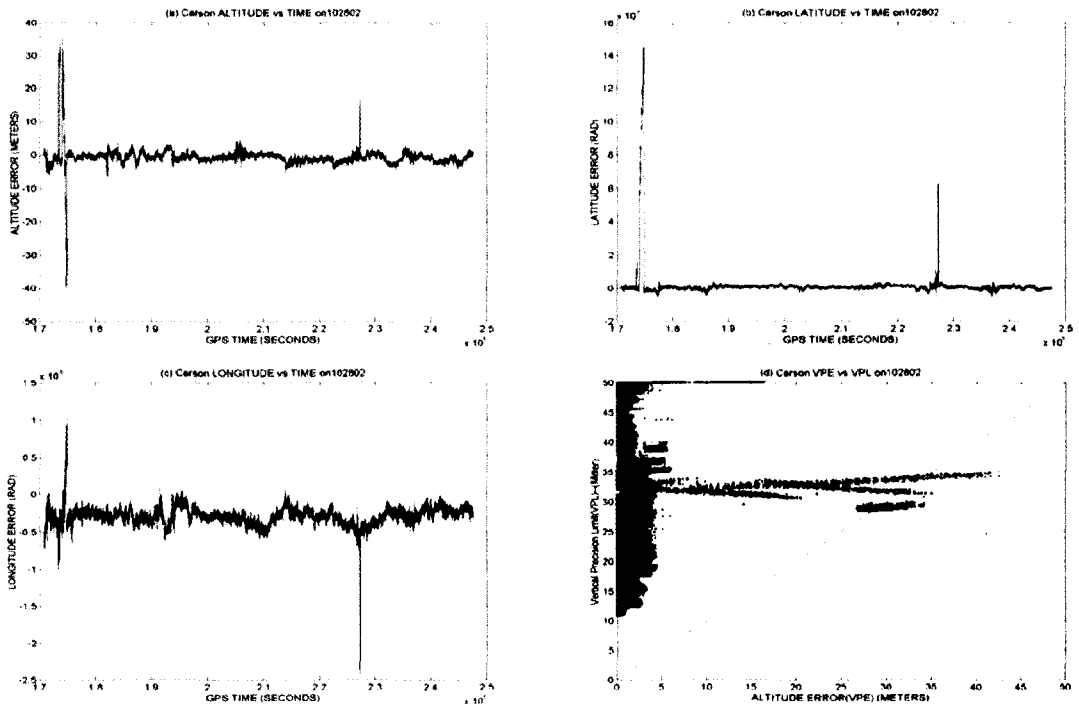


Figure 3.10 WAAS performance on 10/28/02.

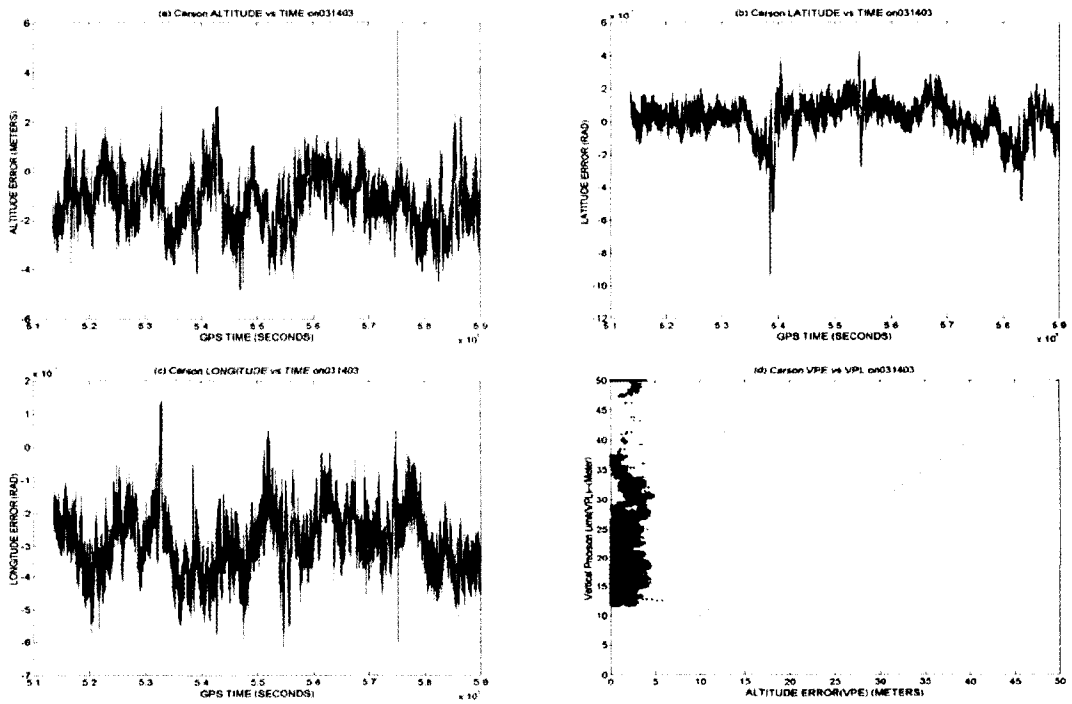
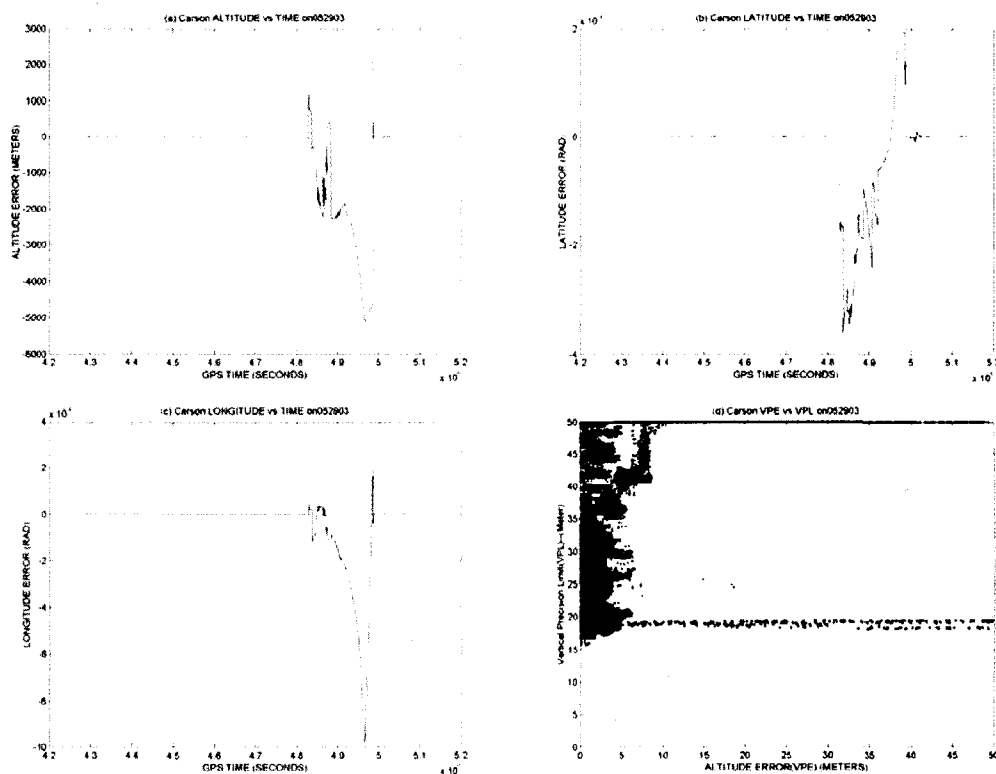


Figure 3.11 WAAS performance on 03/14/03.

Data from 03/14/2003 shown in Fig. 3.11 demonstrates that this is an exceptional day for WAAS performance. All data fall into the expected performance standards. Data clusters in the VPL-VPE chart are compact and not spread all over. Still, this day is not good enough for the original specification for CAT I precision approach. It is a very good WAAS day.



**Figure 3.12 WAAS performance on 05/29/03.**

Data from 05/28/2003 shown in Fig. 3.12 represents another bad day due to the sustained high towers of errors and the HMIs.

I have chosen more than a fair share of bad WAAS days for WAAS SIS. The reason behind this is to have sufficient data types to gauge how the new VPL algorithm will behave. When the current integrity monitoring mechanism is working great it might

be hard to appreciate the improvement the new algorithm makes. When the system is not working as it is supposed to, is when the new algorithm shines.

### **3.5 VPL and VPE (Vertical Position Error) performance over time comparison**

I have presented the general performance charts on the days I have chosen to be representative of all the data over time since WAAS was established. From good days and bad days we can see the validity of the integrity algorithm. Most of the time the system performs well and the protection level (PL) guards against bad data being used in the aviation system. I have identified the problem with current HPL and VPL algorithm, specifically the over-conservative nature of the current integrity algorithm. There still could be false alarms since, from the figures in Section 3.4, we have no way to determine the nature of the malfunction of the integrity monitoring system. This could be caused by insufficient number of GPS satellites or just because the Sun Spot activity is very high. Therefore, we don't know for sure that these problems actually exist, nor do we know how serious they are, if they do exist, since in the triangle charts Fig. 3.3 (d) through Fig. 3.12 (d) all the data points are cut off at VAL = 50 meters. To investigate more thoroughly we have to look at a group of charts of VPE and VPL performance over time. This dissertation only concerns itself with the vertical part of the system performance, i.e. the VPL versus VPE (vertical position error). This is not to underplay the importance of the horizontal facet of the WAAS system. It is only because the horizontal and vertical parts of WAAS are independent of each other [14] and behave very similar to one

another. Therefore, once the VPL is understood and improved, the horizontal counterpart HPL versus horizontal error can be similarly improved.

In Section 3.4, inter-relation performance of VPL-VPE was demonstrated. The next logical question to ask is how they behave over time and what the temporal correlation is between excessively large errors and VPLs. Again, the same data files chosen in 3.4 are used to show how VPL and VPE vary over the course of a day. Consistency of the stochastic features of the WAAS system over this period of time was confirmed. And since WAAS was officially commissioned early in 2003 [29], it is unlikely to change very much in the near future. This means the statistic measures of WAAS will, more than likely, stay where they are unless major changes are to be made in the system.

In a quick look at the VPL-versus-VPE (Vertical Position Error) characteristics given in Fig. 3.13 through Fig. 3.22 I observe the following:

1. The VPE (Represented as the Red dots) is bounded by the VPL (Green dots) for the majority of time;
2. When there are sustained bad data with excessive large value of VPE the VPL algorithm usually gets into trouble.
3. There is an upper bound of how high the VPL can go, around 3500 meter, probably assigned by system for unavailable situations.
4. HMIs happen occasionally and need to be further studied.
5. The VPL behaves like an amplified version of VPE, with distortion.
6. When the VPL algorithm is working there is a consistent bias between VPL and VPE that can be taken advantage of to improve the system availability.

7. More information is needed to help VPL mimic VPE better, i.e. a better model for the VPE with less chance of HMIs is needed. The information needed could be range/correction information, or satellites in view information, or a wide variety of physical limitation to receiving the signal.

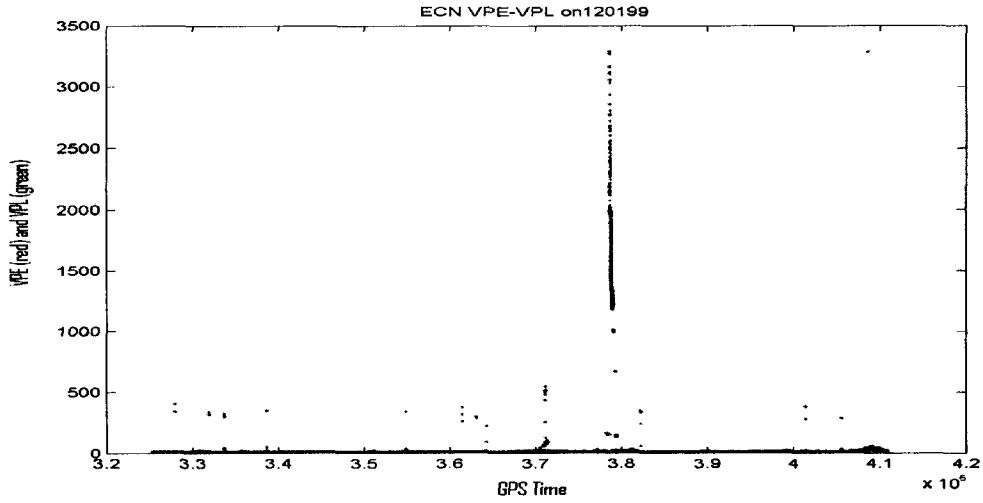


Figure 3. 13 VPE and VPL performance over GPS time on 12/01/99.

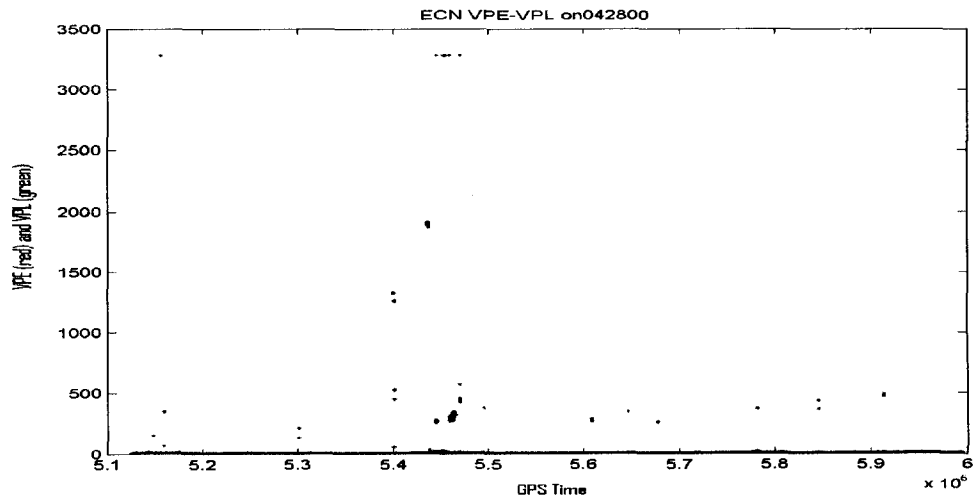


Figure 3. 14 VPE and VPL performance over GPS time on 04/28/00.

In Fig. 3.13 and 3.14 the baseline VPEs are overwhelmed by the large value of the VPLs. It is hard to tell if the VPE actually jumped the VPL, which happens when HMI appears, due to the afore-mentioned fact. One can zoom in along the baseline to see or simply return to Fig. 3.3 to know that in the Fig. 3.13 some VPEs do jump VPLs.

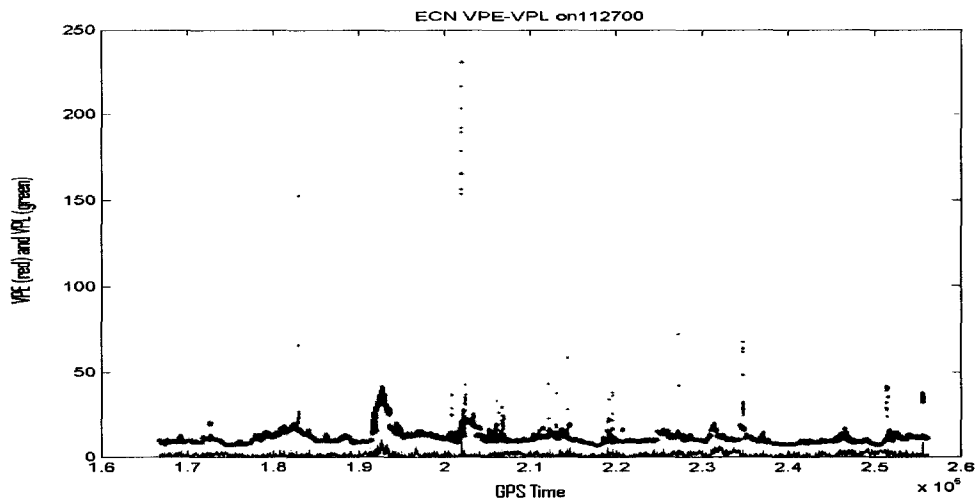


Figure 3. 15 VPE and VPL performance over GPS time on 11/27/00.

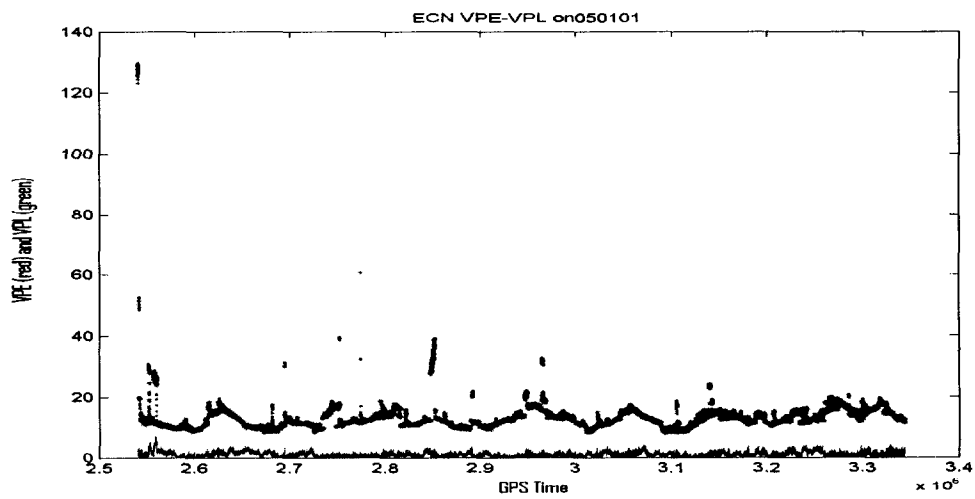
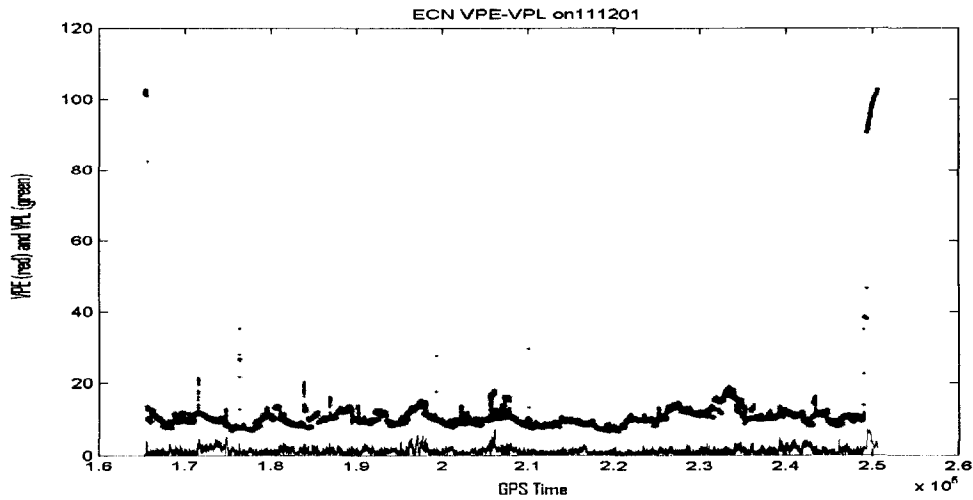


Figure 3. 16 VPE and VPL performance over GPS time on 05/01/01.



**Figure 3. 17 VPE and VPL performance over GPS time on 11/12/01.**

Fig. 3.15 to 3.17 look better due to the lower spike rate making the baseline features more observable. These are three good days for WAAS integrity monitoring since there is no occurrence of VPE crossing VPL to generate HMI. Also we can easily identify the action VPL takes when VPE has a significant upward turn, which shows how well the VPL algorithm is mimicking the vertical error. The consistent gap between VPL and VPE also catches our eye. This is the potential space we can tap into to improve the tightness of the VPL algorithm.

From Fig. 3.18 to 3.22, a wide range of performance shows up. More sustained spans of VPE are present. During those spans the integrity monitoring system has a hard time to contain the VPE and thus large portion of data are either unavailable or HMIs. Closer investigation will prove it can be improved by implementing fault detection in our new VPL algorithm.

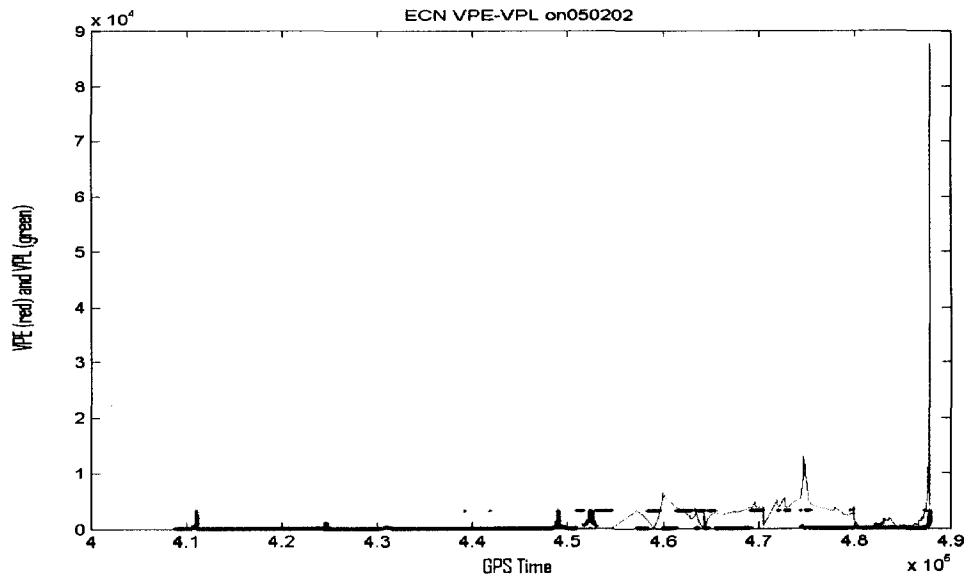


Figure 3. 18 VPE and VPL performance over GPS time on 05/02/02.

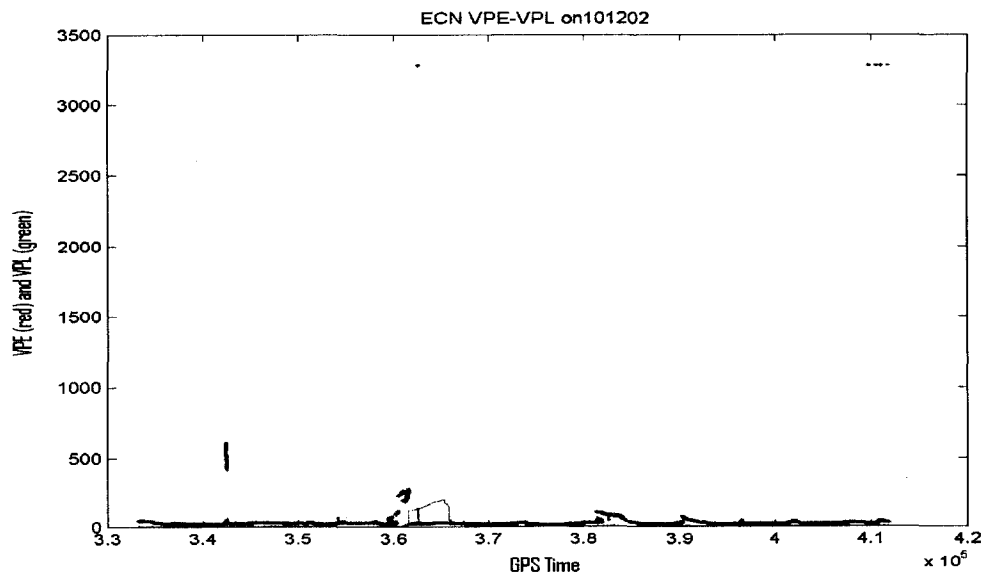


Figure 3. 19 VPE and VPL performance over GPS time on 10/12/02.

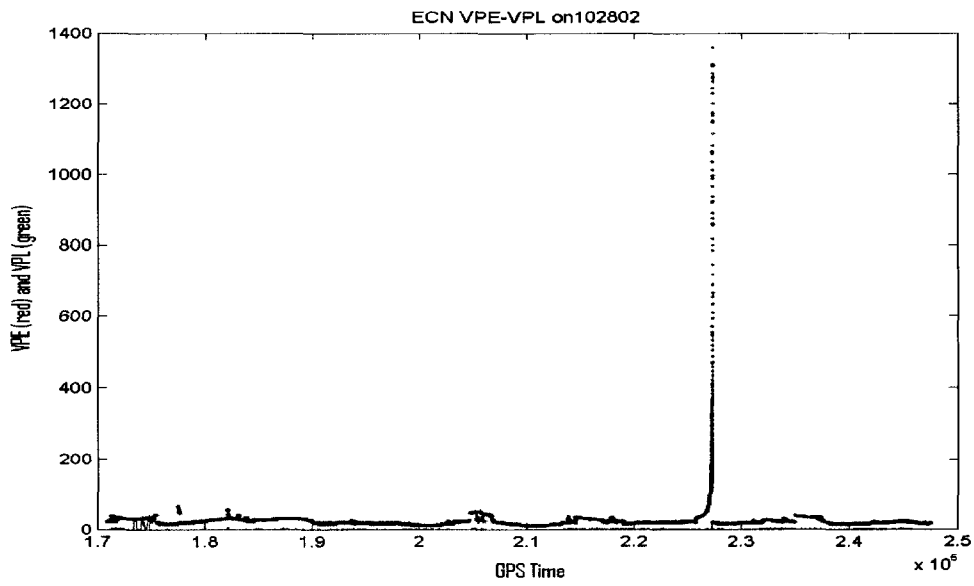


Figure 3. 20 VPE and VPL performance over GPS time on 10/28/02.

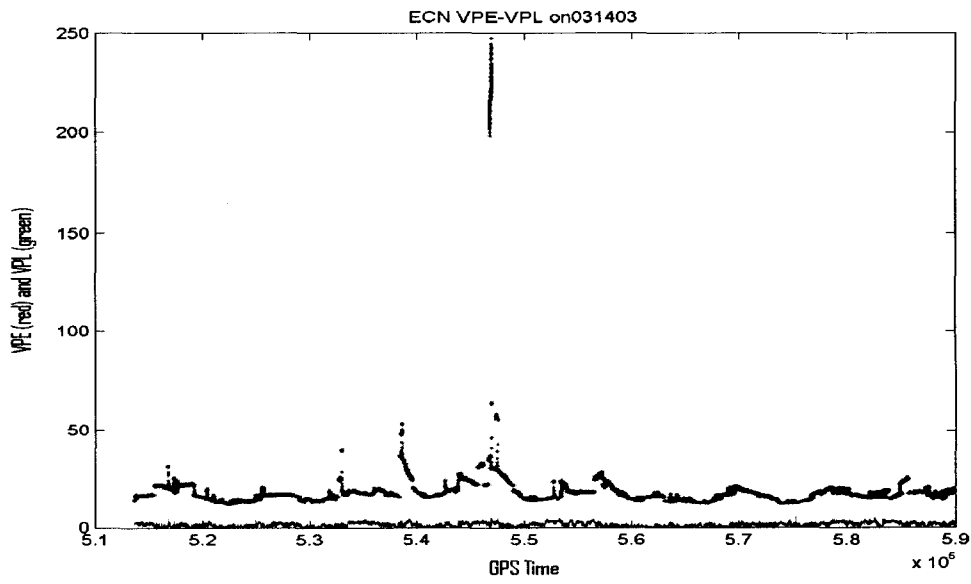


Figure 3. 21 VPE and VPL performance over GPS time on 03/14/03.

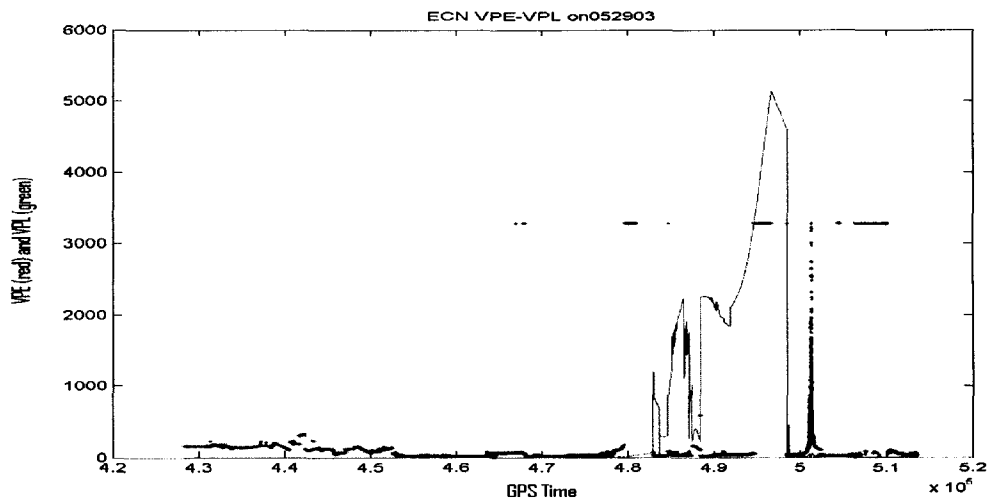


Figure 3. 22 VPE and VPL performance over GPS time on 05/29/03.

These graphs help us understand the performance of VPE and VPL better.

However, as seen from Fig. 3.13 to 3.22, there is still more to be desired. This kind of graphing doesn't help us at coming into the new VPL algorithm too much. To have a more intuitively perceptive way of reading information from data, a new metric of VPL and VPE can be introduced. That will be in Section 3.6.

### 3.6 A new and better metric of VPL and its performance

By looking at Fig. 3.13 through 3.22, it is hard to draw any clear-cut conclusion on how VPL and VPE relate. VPLs are usually much larger than the VPE and thus make VPE look like background noise. To see more details of the comparison one needs a better way to look at them. One easy way is to zoom in around the baseline, but that leaves the bigger picture out. Noticing that the VPL and VPE have peaks of no more than tens of thousand, one wonders if using logarithmic scale would be beneficial. In the following graphs from Fig. 3.23 to 3.32,  $\text{Log}(VPL + 1)$  vs.  $\text{Log}(VPE + 1)$  are shown. The

new scale transformation converts even the highest VPL and VPE into more modest values. The constant number 1 is for avoiding the singularity at 0 which could happen for VPE, and still not being a factor for VPL since it is relatively small. The difference between these charts and those in Section 3.5 are very noticeable. Now we can view the details of the VPE and VPL performance. The striking point of the observation is the resemblance between the two envelopes. The VPL envelope follows the VPE envelope quite closely with a comfortable cushion in majority of “UP” time. There are exceptions when the whole picture look like totally messed up, such as in Fig. 3.28, 3.29, 3.32, where the sustained span of excessively large value of VPE present problems to the system.

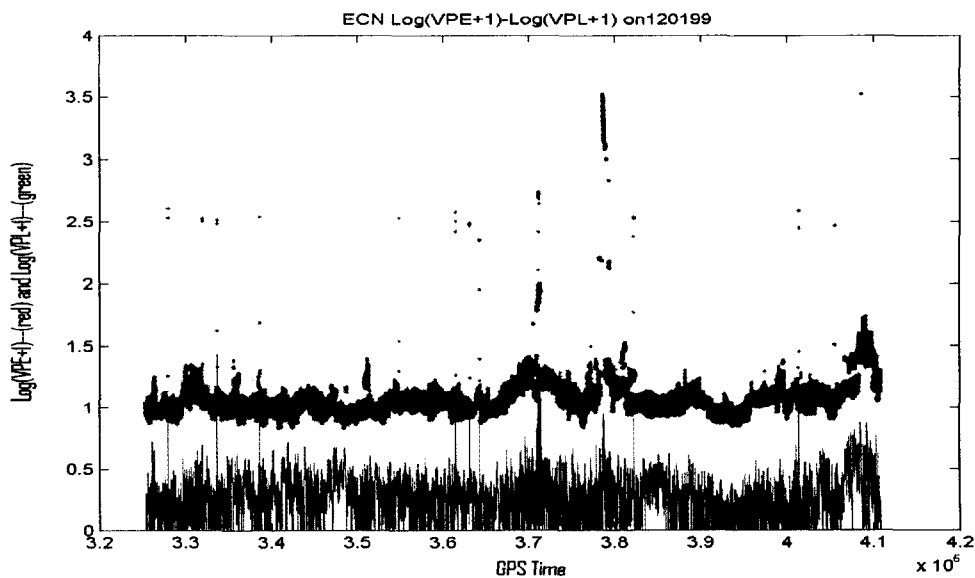


Figure 3. 23 12/01/99 Log(VPE+1) vs. Log(VPL+1).

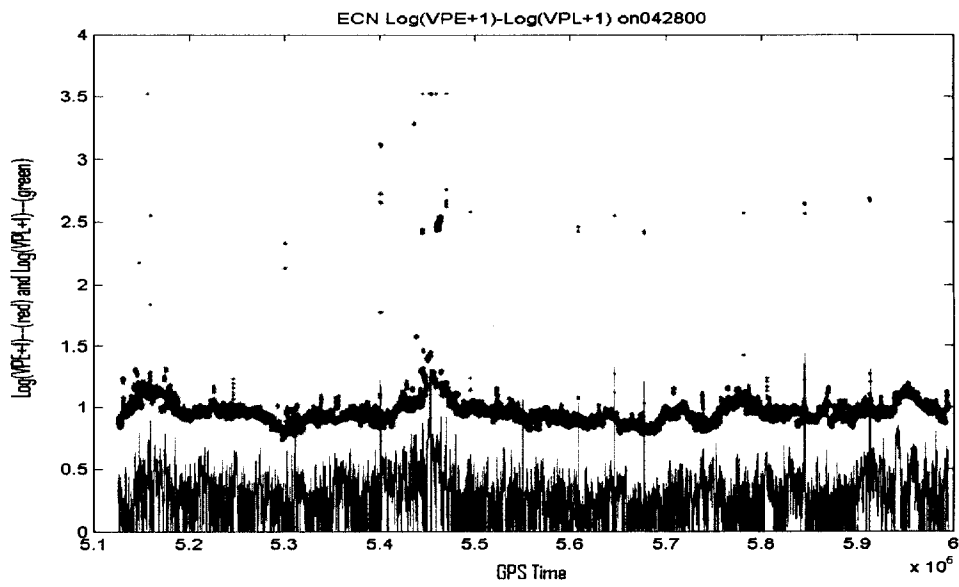


Figure 3. 24 04/28/00 Log(VPE+1) vs. Log(VPL+1).

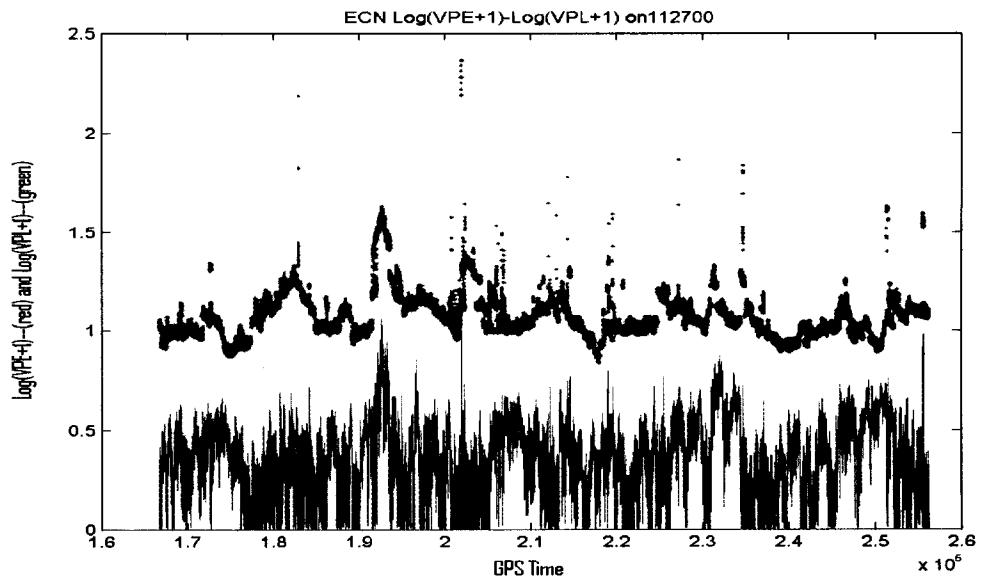


Figure 3. 25 11/27/00 Log(VPE+1) vs. Log(VPL+1).

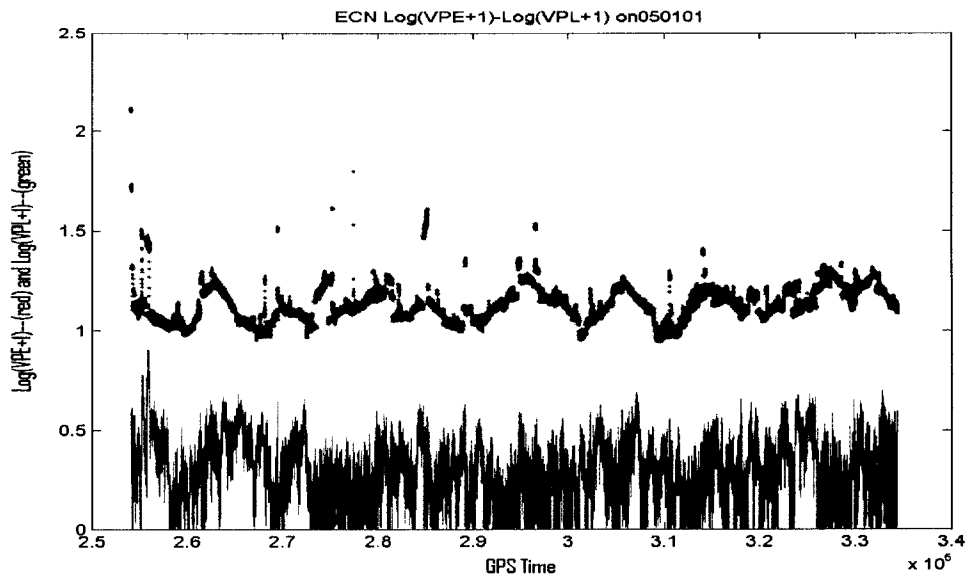


Figure 3. 26 05/01/01 Log(VPE+1) vs. Log(VPL+1).

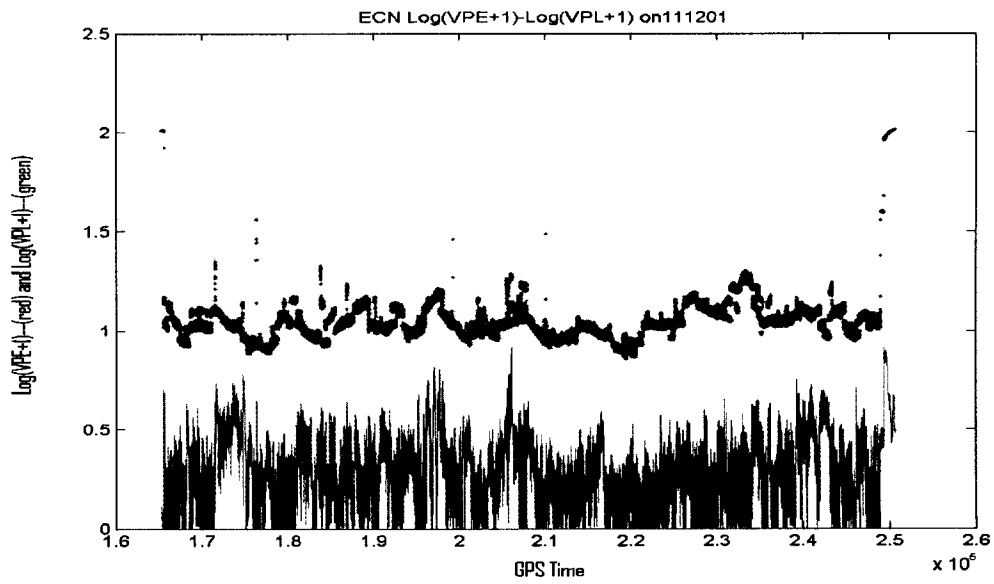


Figure 3. 27 11/12/01 Log(VPE+1) vs. Log(VPL+1).

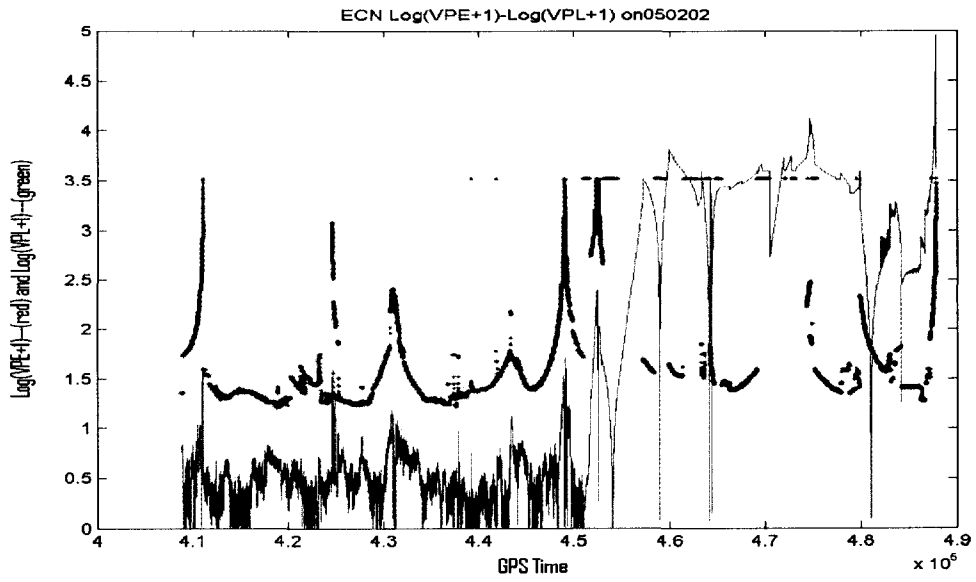


Figure 3. 28 05/02/02 Log(VPE+1) vs. Log(VPL+1).

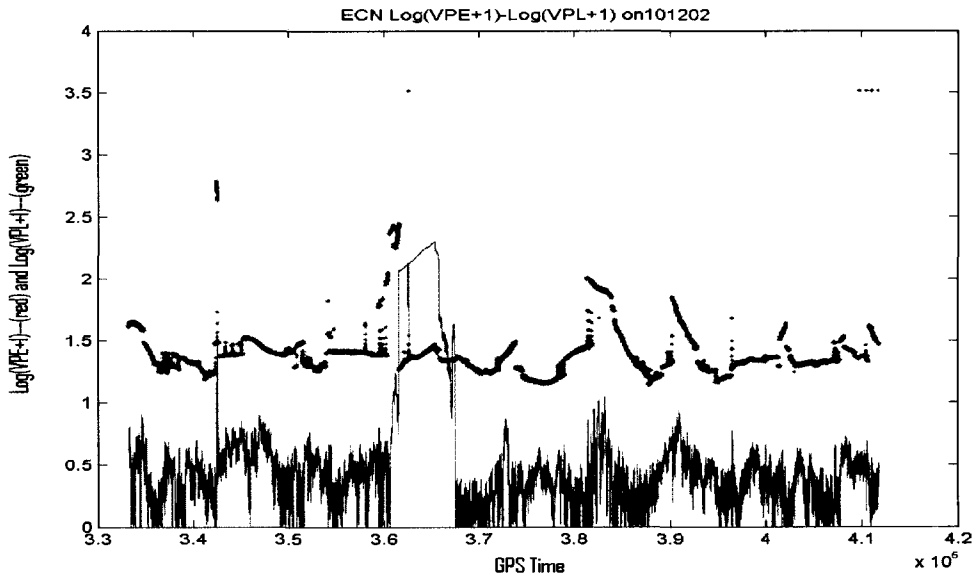


Figure 3. 29 10/12/02 Log(VPE+1) vs. Log(VPL+1).

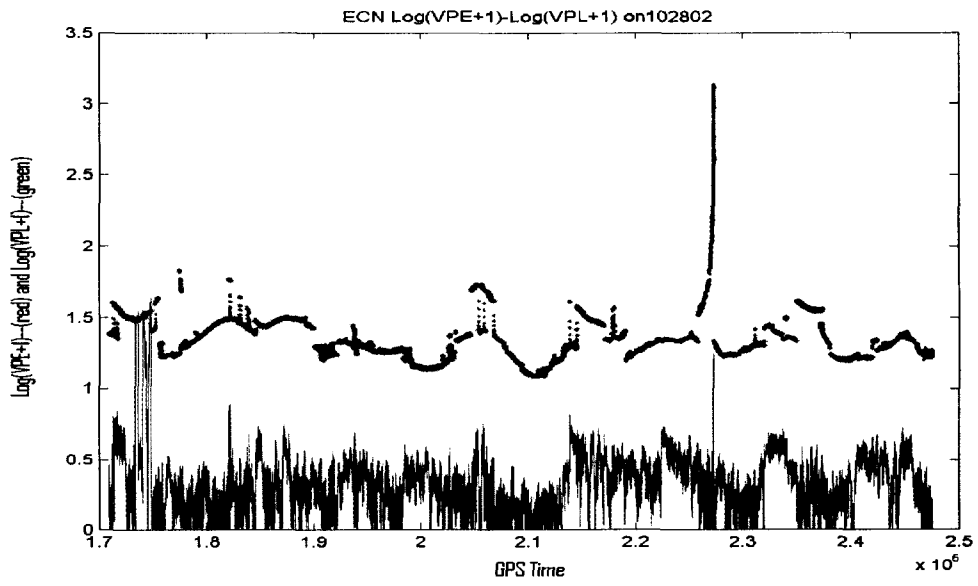


Figure 3. 30 10/28/02 Log(VPE+1) vs. Log(VPL+1).

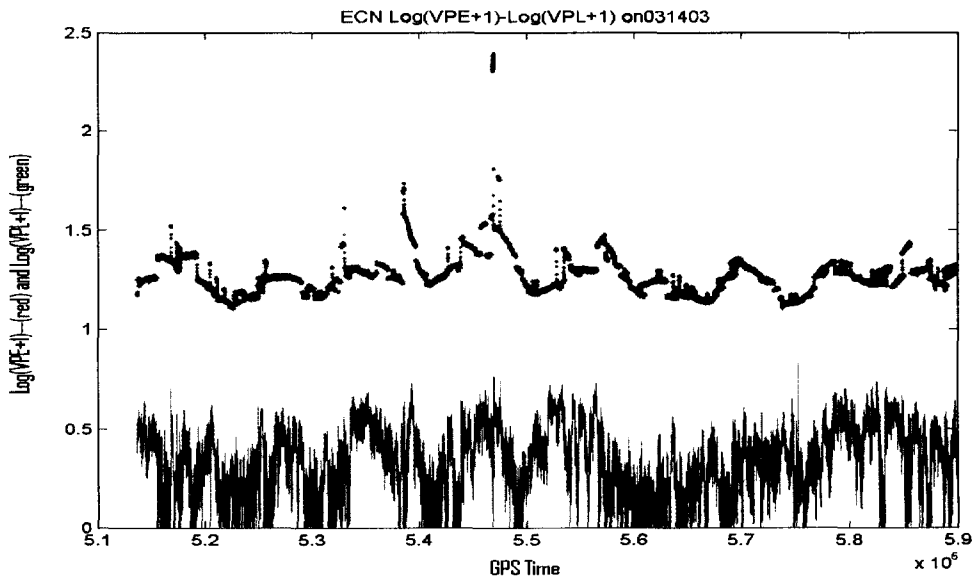


Figure 3. 31 03/14/03 Log(VPE+1) vs. Log(VPL+1).

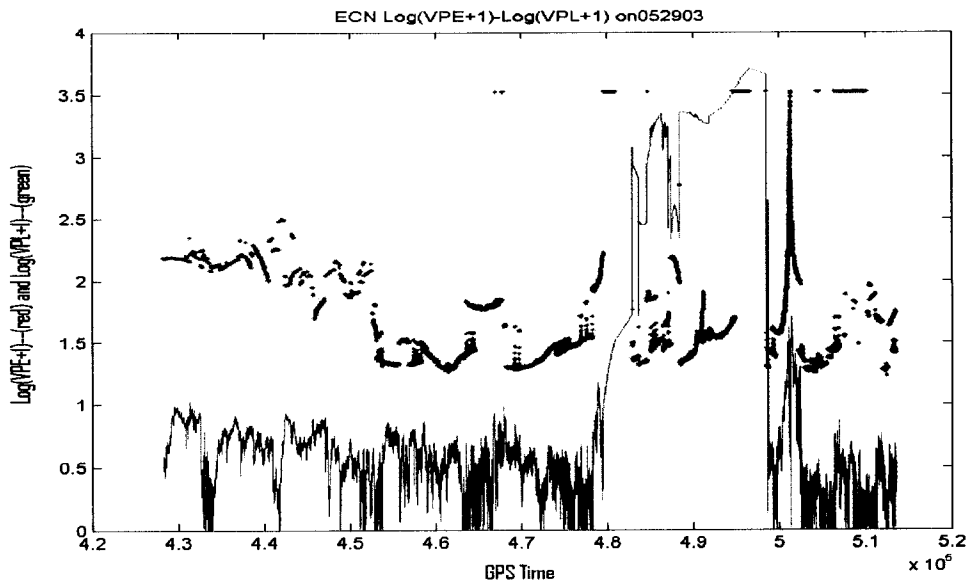


Figure 3.32 05/29/03 Log(VPE+1) vs. Log(VPL+1).

In all, we can agree that the logarithmic scale represents the inter-correlation between VPL and VPE better and give more insight to the solution to improve the WAAS VPL's lack of availability through the Fig. 3.23 to Fig. 3.32. The reverse process is trivial. We might need to pay attention to the attrition during processing due to limited storage precision while computing is carried on. It turned out it is of non-major concern in this regard.

The new VPL algorithm can now be developed in the following chapter.

## Chapter 4

### Algorithm to improve WAAS based navigation modeling

This chapter presents a new algorithm to improve the HPL and VPL. The algorithm will be developed and it will be performance tested to show its effectiveness compared to present methods.

From its concept, the Wide Area Augmentation System (WAAS) was hailed to be a revolution to navigation industry. Since then WAAS deployment has suffered more than its fair share of delays and budget overruns. The reason for these deployment misfortunes lies in the demanding mandates on the performance of the WAAS system. The critical performance metrics for WAAS include accuracy, integrity, availability and continuity, from which, in the long process of getting the WAAS commissioned, the availability has always been the feature that holds back the system from its promised capability. To date, WAAS performs well, but not well enough to meet its original objectives. The inherent contradiction between integrity and availability is the major reason that the VPL and HPL algorithms need to be improved.

The integrity algorithms are well defined in WAAS Minimum Operational Performance Standards (MOPS). However, through our study, it is clear that the MOPS VPL and HPL algorithms are over-conservative. This, on one hand, makes confidence bounds sufficiently large to cover the correction error and hence to some extent guarantees the integrity. On the other hand, however, this lack of compactness from the MOPS introduces the unnecessary epochs of system being unavailable. Methods to improve upon this setback are proposed by different authors. Mainly and intuitively all

are trying to solve this in range/correction domain [30], [31]. In this dissertation, an alternative algorithm in position domain is presented to improve the MOPS integrity algorithms in hope of improving the overall system performance. All the information that is needed is already in the WAAS messages. Therefore, this alternative algorithm will not require any change of existing correction messaging.

A pseudo-VPL, (similarly a pseudo-HPL algorithm can be devised) is presented in this dissertation. It is based on the MOPS algorithms and improves upon them. The pseudo-VPL and pseudo-HPL algorithms are developed by taking advantage of the WAAS correction error's stochastic characteristics and Kalman filtering. The algorithm is tested by real static data collected by Enhanced Miniature Advanced GPS Receiver (EMAGR) and shows improvement over the MOPS algorithms. It improves the system availability and continuity while, to a satisfactory extent, keeping the integrity from suffering.

The following sections describe in detail the progression of the development of this new VPL algorithm.

#### **4.1 Chaotic nature of WAAS VPL and VPE**

According to the WAAS Minimum Operational Performance Standards (MOPS) [3], the formation of WAAS integrity monitoring systems is quite definitive. The MOPS specifies how users combine error confidences from the different sources to form a position bound. The service provider guarantees that the error at any user location is smaller than the respective bound with a sufficiently high confidence.

Simple as it seems, it is naive to think the system is definitive, since WAAS is inherently a non-stationary system. WAAS relies on satellites that are constantly in motion and that may change their characteristics. Additionally, the propagation of the satellite signals varies with local conditions; thus, the system has differing properties over time and space. By now it is very clear that the WAAS SIS integrity is by no means simple. The WAAS integrity algorithm currently in use is well defined in Chapter 2 of the published MOPS [3]. In Section 4.2 below, I will analyze the formulas given in [3] for calculating the VPL and HPL. One has to wonder though, for two or more locations in a relatively large area, if the integrity will be almost the same as long as the locations are within the same grid zone defined in MOPS. This is an important question to examine even in the absence of obviously localized effects such as weather and multipath.

If one wishes to solve the VPL in closed form, which would have been the best thing for this space based augmentation system, he or she finds out it will cost an enormous amount of energy and computing time to even get close. It quickly becomes clear that the Navigation error and VPL system can be likened to a chaotic system, as described in [33]. Chaos theory studies the interdependence of things in a far-from-equilibrium state. Every open nonlinear dissipative system has some relationship to another open system and their operations will intersect, overlap and converge. If the state trajectories are sensitive to the initial conditions, then these systems are potentially chaotic. Even for systems that are not, strictly speaking, chaotic, imperfections in the system model or incomplete knowledge of the dynamics generally leads to uncertainty in the state trajectories. If such systems are perturbed either internally or externally, they can display chaotic behavior and this behavior will be amplified microscopically and

macroscopically. The WAAS system resembles a chaotic system, to a high degree. By nature we shouldn't try to solve the integrity in closed form because that can't be done for a chaotic system. We can, however, try to understand how the system behaves under different condition and circumstance of which to take advantage and improve the overall system performance.

In [28], the validation of the MOPS integrity equation is described. Actual data from the National Satellite Test Bed (NSTB), a prototype for WAAS, is compared side-by-side to simulated data. The difference between actual and expected performance is investigated in detail. It was shown that compared to the real data, the assumptions used in the integrity equation are conservative. Integrity is maintained both in the simulated data and in the live data. The comparison of the two data sets provides insights into the actual probability distribution of the errors in the live data and into the correlations between different error components. This knowledge helps to ensure that the full integrity requirements are always met. It may also be possible to utilize this information to increase the availability of the system.

My objective is to take advantage of the overly-conservative nature of the MOPS integrity algorithm. The integrity performance of the WAAS system was studied by collecting and analyzing real WAAS data. Out of these observations, insight was developed to improve the integrity algorithm. As stated in the [28], stringent requirements are already met by the MOPS integrity algorithm. We need to improve the availability to improve the overall system performance.

From VPL and VPE performance graphs in Section 3.6, there is certainly some inter-correlation between the two functions of VPL and VPE. For the sake of simplicity,

the functions of VPL and VPE will be called LVPL and LVPE, the added L in front indicating logarithmic function relation between them:

$$LVPL = f(LVPE) \quad . \quad (4.1)$$

With the chaos background in mind and the observations made in the figures of Sections 3.5 and 3.6, we can linearly model the LVPL as LVPE with certain stochastic noise characteristics, plus a bias, which was introduced intentionally to safe guard the integrity:

$$LVPL = LVPE + n_{vpe} + bias \quad , \quad (4.2)$$

where  $n_{vpe}$  is the central focus of this dissertation. Once one understands the way this noise characteristic works, one can easily establish an algorithm to de-noise VPL so that it will better track the VPE, and thereby reduce the conservativeness of the MOPS VPL algorithm. This in turn increases the system availability.

## 4.2 Rationale for Multiplicative modeling of the VPL

The most widely used noise model is Additive White Gaussian Noise (AWGN). AWGN models are commonly used in virtually all branches of signal processing. In the LVPL VPL modeling problem, however, I will argue that a multiplicative noise model is more appropriate. It should be noted that multiplicative models can be transformed into additive models by applying a homomorphic approach.

From all the articles regarding the WAAS error sources up to today, it has always been assumed that the different noise sources are combined additively [4, appendix J]. It has also been assumed that the additive model leads to the most conservative bound and therefore satisfies the requirement of the integrity algorithm. This is intuitive and simple. Even though it is unlikely that worst case errors and different error sources combining

constructively to cause a failure of the WAAS system, it has been proved by simulation and real WAAS test bed that the bounds based on MOPS are almost always too conservative [28]. Without progress on the fundamental understanding of each and every error threat model, this situation cannot be changed with the current approach. This makes a new alternative approach desirable.

The essential point of the new algorithm is that of modeling VPL as a noise stained version of VPE. The threat model for VPE is an additive model with clock error, ephemeris error, ionospheric error and tropospheric error all combining additively. But that doesn't address the second-order relationship between the VPL and VPE, which still needs to be investigated. In the development of the MOPS VPL algorithm, there are different error source estimates contributing to the total error bound, which is the VPL [3], [26], [28]. The upper bounds as these estimates are combined in a worst case scenario that is very unlikely to occur in practice. After that, the VPL has to be large enough to ensure that the probability of VPE exceeding VPL is extremely small. Therefore, assuming a Gaussian distribution, one can use a constant K to generate a 3-Sigma bound, which ensures a probability of less than  $10^{-3}$ . This constant K is inherently over-designed due to the steps taken before its evaluation and the use of the assumption of Gaussian Noise.

Given an initial estimate for position and an estimate for the weighting matrix, the weighted least squares inverse of (2.18) improves our position estimate. The solution is

$$\Delta \hat{x} = (G^T \cdot W \cdot G)^{-1} \cdot G^T \cdot W \cdot \Delta \hat{y} \equiv K \cdot \Delta \hat{y} \quad , \quad (4.3)$$

where K is defined as

$$K \equiv (G^T \cdot W \cdot G)^{-1} \cdot G^T \cdot W \quad . \quad (4.4)$$

The VPL equation

$$VPL_{\sigma} \equiv \kappa(\text{Pr}) \cdot \sigma_{\hat{x}_3} \quad (4.5)$$

was also given in Chapter 2. Along the vertical direction,

$$VPL_{\sigma_v} \equiv \kappa(\text{Pr}) \cdot \sigma_v \quad (4.6)$$

where

$$\sigma_v \equiv \sqrt{\left[ (G^T \cdot W \cdot G)^{-1} \right]_{33}} \quad (4.7)$$

Equations (4.3) to (4.7) have already appeared in Chapter 2. For instance, the VPL equation (2.22) is repeated here as (4.6) for convenience.  $\kappa(\text{Pr})$  is a PDF and integrity requirement dependant constant.  $\kappa(\text{Pr})$  can be determined by the PDF integration over the tails. For instance, in the current WAAS integrity model, with the Gaussian distribution and the requirement of the integrity of better than  $10^{-7}$ , the constant  $\kappa(\text{Pr})$  is determined to be 5.33, the point from which integrating the PDF to infinity produces  $10^{-7}$ . As mentioned before, the tails are cut off to some degree due to the fault detection and error correction mechanism implemented in the integrity algorithm. This alone certifies the over-conservativeness of the MOPS algorithm.

The worst case combination rarely happens. Also, the individual error models are loosely established and therefore conservative in the first place. The Gaussian Noise assumption is not accurate at least due to the implementation of the error correction and fault detection mechanism, which clips off the tails of the Gaussian curve. Therefore, there is room for the MOPS VPL algorithm to be relaxed. An improved algorithm can be established through the use of real world data. After testing the new algorithm in

sufficiently diversified data types and getting satisfactory results, it can be claimed this real-data-based algorithm will work in general cases.

From the figures in Section 3.6, it is apparent that  $(LVPL - LVPE)$  is more linear than  $(VPL - VPE)$ . Indeed, a few simple tests based on the data sets that have been chosen below will show that this observation is valid. In Fig. 4.1 through 4.6 below, it can be seen that, with the nonlinearity criteria defined in equation (4.8),  $(LVPL - LVPE)$  does indeed have a better linearity than the  $(VPL - VPE)$  relation. In these figures the nonlinearity of random variable X is defined as the standard deviation of X divided by the expected value of X:

$$NonLinearity(X) = \frac{Std(X)}{\langle X \rangle} . \quad (4.8)$$

This makes it a fair metric for comparing different random variables since it is unified, as long as the expected value of X is non-zero, which is true in my proposed algorithm.

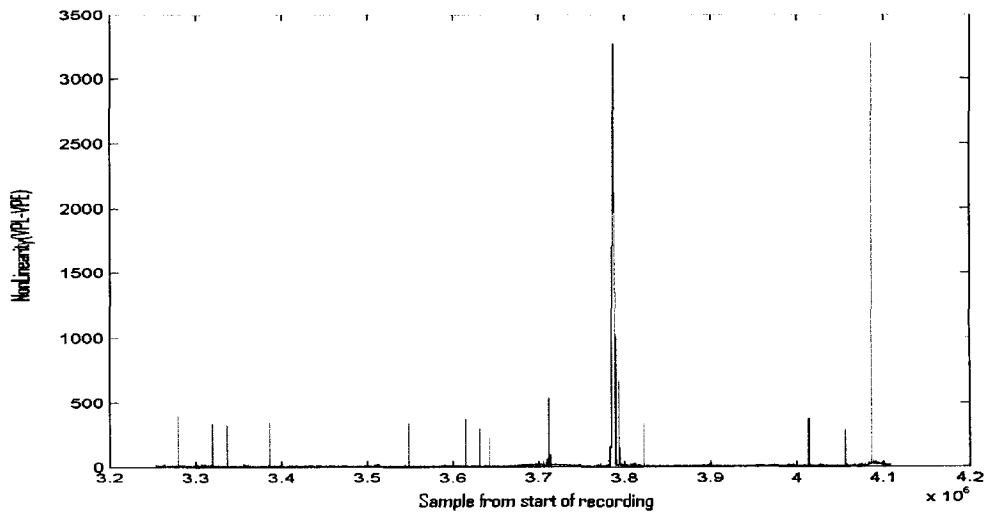


**Figure 4. 1 (12/01/99)  $NonLinearity(VPL - VPE) = 7.43221$ .**

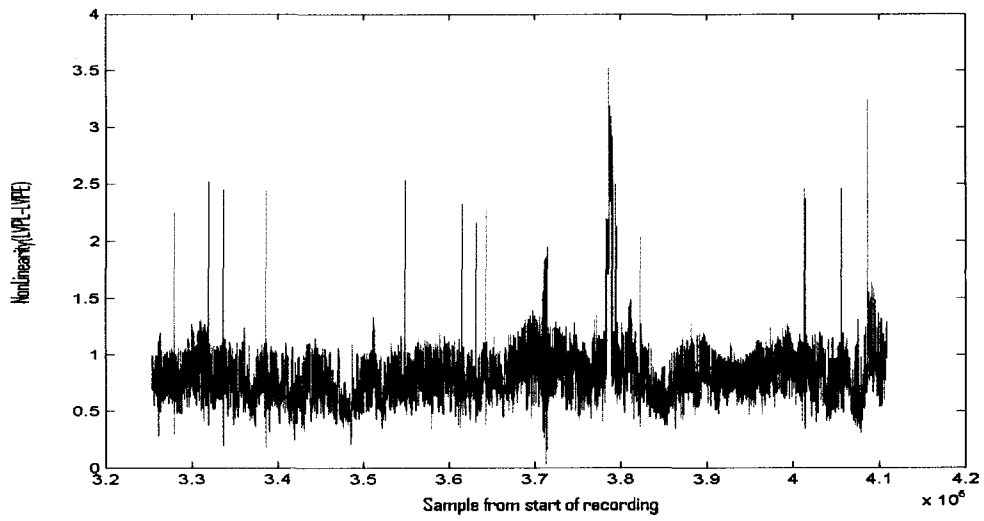


**Figure 4. 2 (12/01/99)  $NonLinearity(LVPL - LVPE) = 0.27741$ .**

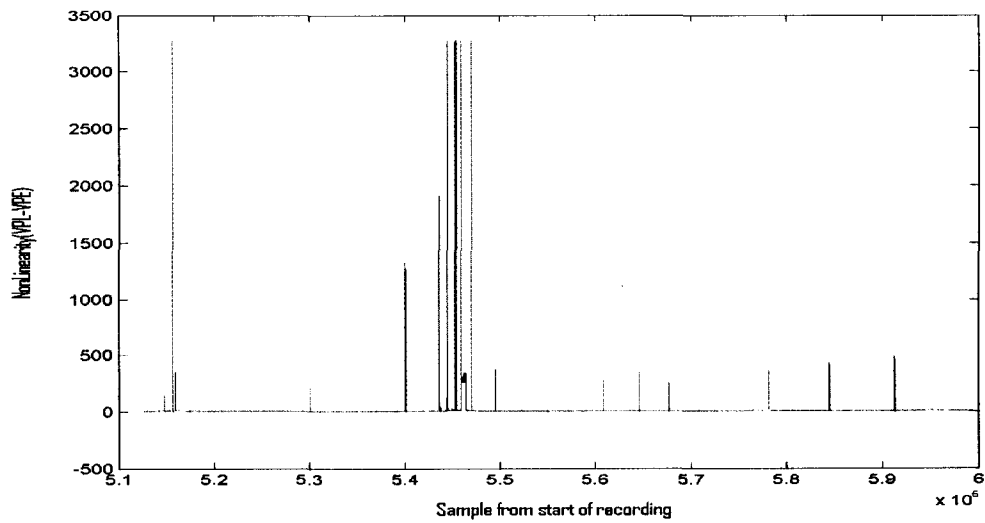


**Figure 4. 3 (11/27/00)  $NonLinearity(VPL - VPE) = 9.00821$ .**

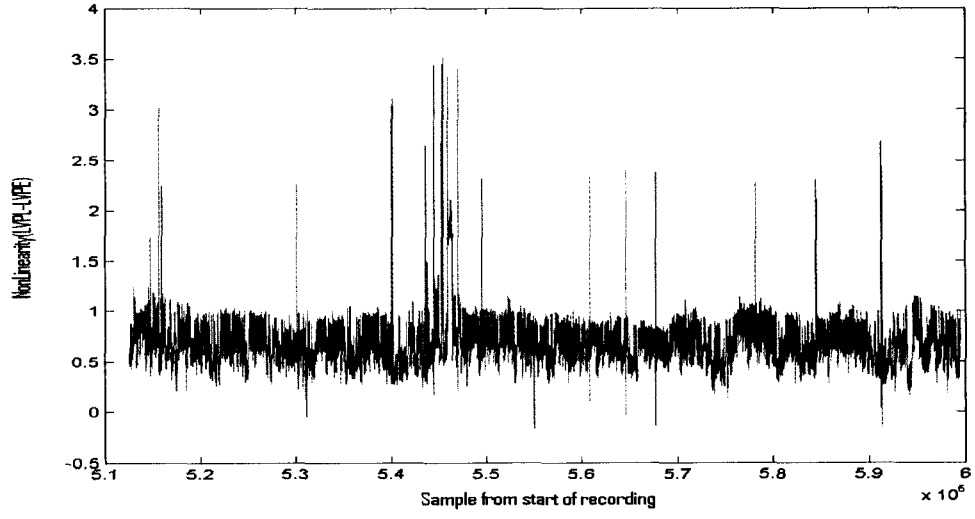


**Figure 4. 4 (11/27/00)  $NonLinearity(LVPL - LVPE) = 0.30773$ .**

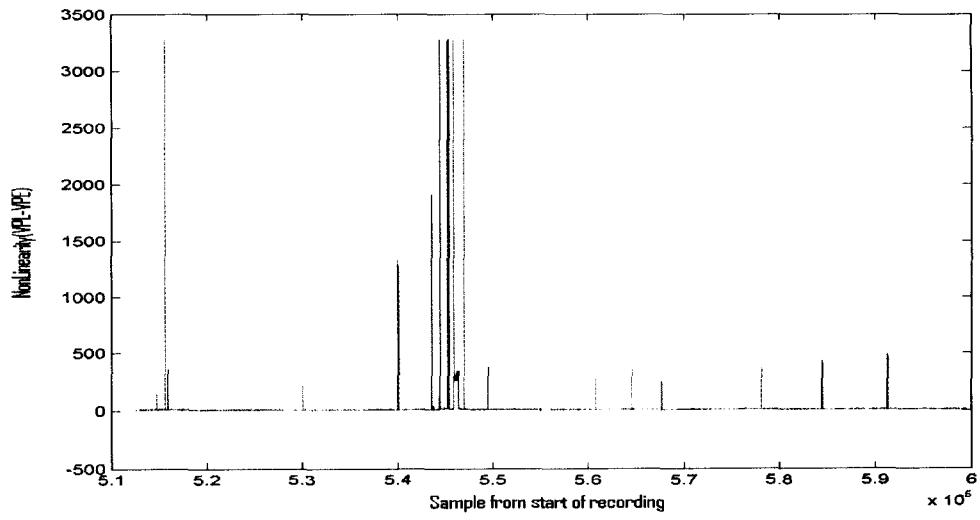


**Figure 4. 5  $NonLinearity(VPL - VPE) = 0.46412$ .**

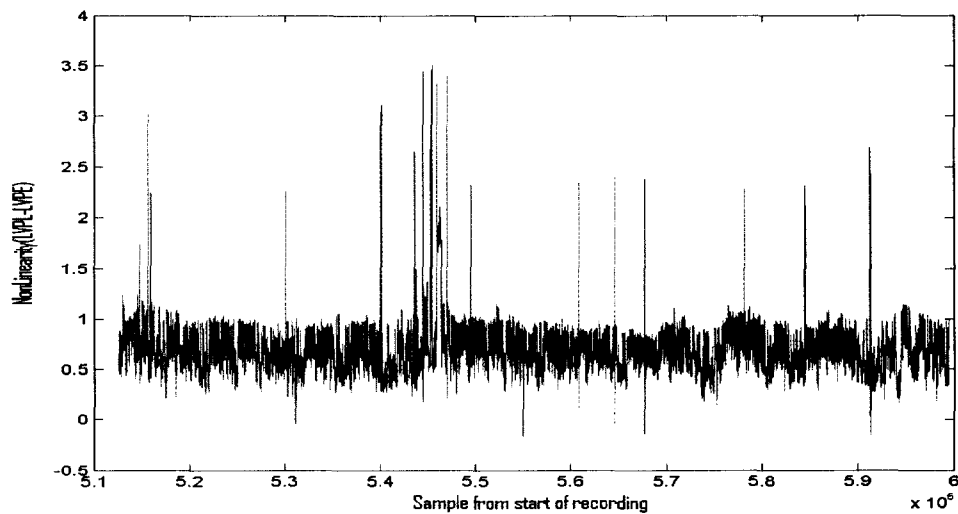


**Figure 4. 6 (05/01/01)  $NonLinearity(LVPL - LVPE) = 0.28392$ .**

These illustrations are just some examples to show that the logarithmic based function of VPL and VPE is a better fit to use as the basis to improve the WAAS SIS performance. We now can utilize the LVPL-LVPE linearity to simplify the filtering process in the De-Noiseing process in the new methodology. This makes good sense in view of the inherent overdesign of the overvalued 3-Sigma bound. By assuming a bias between LVPL and LVPE, we can rid the VPL of the averaging factor in the over-estimated error sources combination. This has the added benefit of simultaneously reducing the bias and thereby the 3-Sigma constant bound.

From analysis of the actual WAAS data that have been collected since year 1999, it becomes clear that the current algorithm used by the integrity model to calculate the VPL and HPL is over-conservative. Using the LVPL-LVPE it is straightforward to estimate the bias between the current model and the real data. The actual number used to reduce the bias will be determined experimentally to a satisfactory degree. The reduction of the bias between VPL and VPE results in higher availability, fewer constraints on

structures around the airports, higher availability for a pilot in flight, and therefore higher success rates of on-time arrival and safer landings.

Considering the path that GPS signal takes from the GPS SVs to the receiver, one can see that there is uncertainty along the way. Errors are added in sequentially and result in the inaccuracy of the final GPS solution. If one can better model the process by which the errors accumulate, then one can be better equipped to remove them automatically in the augmentation system. It then becomes a tremendously complicated system due to the complex nature the signal interactions with the medium along its path of travel. It is reminiscent of the AM-FM modulation in wireless communication. The AM part can be neglected for our purpose, since we don't care too much here about the receiver sensitivity. The FM part is what needs investigation. How the signal is changed due to the FM modulation can shed some light on the error generating process in the GPS system.

### **4.3 Position Domain Approach to improve the WAAS availability performance**

It has been suggested that the improvement of WAAS integrity, availability and continuity needs to be done in the range/correction domain [30]. This suggestion has merit. In order to improve the system performance, a better error model and better understanding of the threat model is needed, i.e. there is a need for more information about the nature of all error sources and the threats that WAAS faces. This is very difficult due to the stochastic nature of these error and threat sources. It can be argued that it is impossible to convince a real skeptic of the feasibility of an effective integrity algorithm [28]. On the other hand, it is obvious that improvement in the range/correction

domain alone is not sufficient. For the receiver, a position domain solution can alternatively be used to improve the system performance to some extent. It is known that the HMI requirement is specified in the position domain, yet WAAS broadcasts values in the range/correction domain. WAAS receivers combine the corrections and confidences with their geometry to form the position solution and protection level. Depending on individual circumstances, each receiver determines which corrections and satellites are used. The WAAS SIS is not directly used as input in these decisions. Therefore, how the position error builds up for one specific receiver depends on the residual errors, and is known only to this receiver. A combination of position domain and range/correction domain monitoring should be more effective. This is most clearly demonstrated by a real example. As shown in [33], a close-to-real example can be set up for specific user geometry by using Stanford's Matlab Algorithm Availability Simulation Tool (MAAST) [34], which can be used to simulate WAAS performance. In this example, the eight satellites are in view as shown in Table 4.3.1. The standard skyplot of the satellites are shown in Fig. 4.7 with their elevation and azimuth values and PRN numbers listed.

**Table 4. 1 Satellite elevation and azimuth angles, confidence bounds and projection matrix values both for the all-in-view solution and for a solution without PRN 8.**

PRN	EL	AZ	$\sigma_i$	$K_{3i}$	$K_{3i}$ without PRN 8
2	45.8°	-32.3°	2.34 m	0.595	0.451
5	11.2°	-76.8°	10.1 m	0.258	0.437
6	36.6°	48.4°	2.32 m	0.162	2.005
8	9.98°	73.0°	3.74 m	1.000	N/A
9	61.4°	28.5°	2.03 m	-1.928	-3.087
15	32.8°	151.0°	6.89 m	-0.015	0.174
21	42.3°	-136.0°	4.83 m	0.066	-0.003

Table 4.1 also shows the PRN, elevation, azimuth, and one-sigma confidence bound ( $\sigma_1$ ). In addition, the fifth column  $K_{3i}$  shows the dependence of the vertical error on a pseudorange error associated with each SV.  $K$  is the projection matrix and is defined as equation (2.18),  $K = (G^T W G)^{-1} G^T W$ , where  $K$  is the geometry matrix and  $W$  is the weighting matrix, [4 Appendix]. The term  $K_{3i}$  multiplying the pseudorange error determines the contribution of this error to the overall vertical error. Thus a 1 m ranging error on PRN 2 would create a positive 59.5 cm vertical error for the user with this combination of satellites and weights. The last column in Table 4.3.1 is the case when the most-likely-to-lose satellite, which in this setup is the SV with the lowest elevation angle, is dropped from view sight.

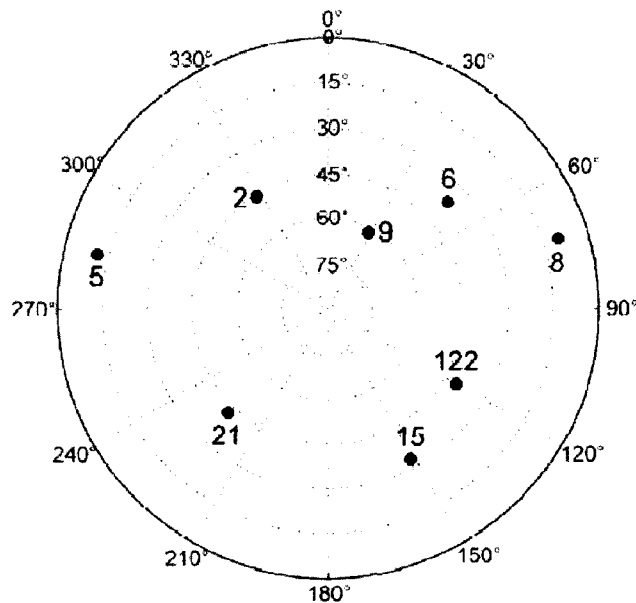


**Figure 4. 7 Satellite elevation and azimuth values for a standard skyplot. PRN 8 is a low elevation satellite that if not included in the solution dramatically changes the influence of PRN 6.**

After PRN 8 no longer contributes to the solution, the projection matrix values change accordingly. Note that the value of  $K_{3i}$  changes significantly after PRN 8 is

dropped. Most noticeably, the  $K_{3i}$  of PRN 6 changes from 0.162 to 2.005, an increase of more than 1000%. What does this mean? In a perfect world, this may not matter too much. In real world, however, as could be simulated in MAASR, with the all-in-view solution, the user has a VPL of 33.3 m (HPL = 20.4 m). When PRN 8 is dropped, the VPL increases to 48.6 m (HPL = 20.5 m). This seems acceptable since both values are below the 50 m Vertical Alert Limit (VAL) for LPV [35]. Either solution could be used for vertical guidance. However, if the ephemeris data for the SV positions contain errors, the relative minor change of constellation has an immediate impact on the WAAS solution. Notice that the vertical error dependency changes dramatically with the loss of PRN 8. In particular, PRN 6 had little influence over the all-SVs-included solution. After PRN 8's drop from view, PRN 6 has a very strong impact on the new solution. Also notice that the other values change as well. PRNs 2, 21, and 122 lose influence while PRNs 5, 6, 9 and 15 become more important. More surprisingly, the influences of PRNs 15, 21, and 122 change sign; therefore, what was a positive error for the all-in-view solution becomes a negative error for this particular subset.

The changes in the  $K_{3i}$  values with subset or superset position solutions limit the ability to verify performance exclusively in the position domain. For example, if PRN 6 had a 25 m bias on its pseudorange, it would lead to a vertical error of greater than 50 m with PRN 8 missing, but just over 4 m for the all-in-view solution. A position domain check with all satellites would not be concerned with a 4 m bias compared to a 33.3 m VPL. Thus, one would be inclined to think that all was well. However, the user unfortunate enough to lose PRN 8 would suffer a 50 m bias, large enough to cause harm. A 25 m bias would be more than a ten-sigma error in the range domain and thus would be

easily detectable. Therefore, it is the combination of range and position domain checks that protects users with different combinations of satellites.

There is nothing unique about this particular geometry. In fact, by setting MAAST to look for subset solutions that had very different  $K_{3i}$  values in its subset solutions, one finds that similar situations are not rare [32]. For instance, a search restricted to geometries that had VPLs below 40 m for all-in-view and investigated subsets with VPLs below 50 m showed that, of the 3726 geometries investigated, the  $K_{3i}$  values changed by more than 40% or less in only two cases. To better illustrate this effect, biases were placed on the satellite with the largest change for the remaining 3724 geometries. Each bias was chosen such that it would lead to a 50 m positioning bias in the subset solution (a 25 m bias on PRN 6 in the example above). Each pseudorange was also assigned a zero-mean Gaussian error with a standard deviation of one half of its one-sigma confidence bound (column four of Table 4.3.1). The broadcast WAAS confidence bounds are approximately three times larger than the nominal no-fault values (this inflation is necessary to protect against fault modes). Calculated position errors and VPLs for both the all-in-view and subset solutions are needed. The results are plotted in standard triangle charts, Fig. 4.8 and 4.9. Fig. 4.8 is similar in appearance to a nominal triangle chart except the VPLs are clipped at 40 m due to the special geometry selection process and the position errors are worse than normal due to the injected error on the single satellite. However, the position errors are all below the VPL and the aggregate is not obviously biased. An observer might be inclined to declare that the system is functioning safely based on this chart. However, Fig. 4.9 shows that with the same errors and biases, but a slightly different geometry, this is not true. The subset solution removes

satellites that were masking the bias for each case. The result is an obviously faulted triangle chart. Thus, a triangle chart without obvious faults, such as the one shown in Fig. 4.8, is no guarantee of a safe system, as evidenced by Fig. 4.9.

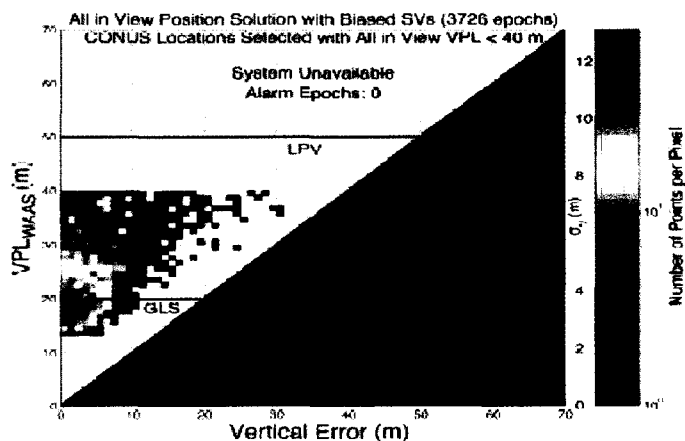


Figure 4.8 The triangle plot for all-in-view solutions including one biased satellite in each is shown. Here each bias is de-weighted by the other satellites. No obvious problems are evident in this chart [32].

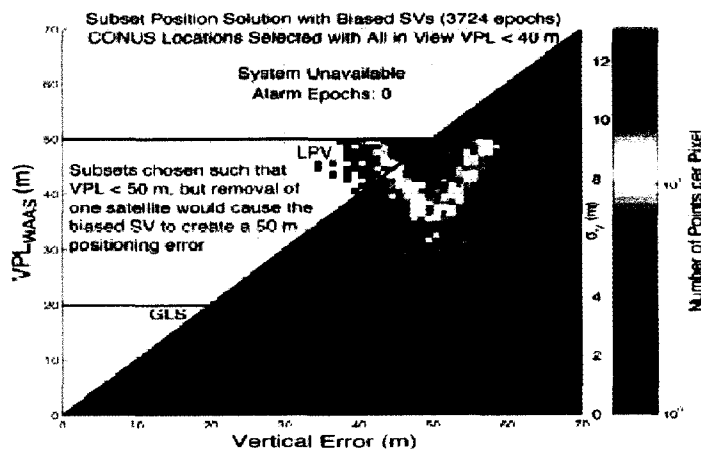


Figure 4.9 The triangle plot for the subset solutions that expose each biased satellite is shown. Here the biases are exposed as being hazardous for the user. This demonstrates the importance of checking each subset or in the range domain [32].

This simulation was pessimistic in its construction since the minimum unacceptable error was placed on the most sensitive satellite, which is PRN 6 in the example. Here the minimum unacceptable error means this intentionally introduced error doesn't change system performance so much in the all-in-view solution that the WAAS system becomes unavailable. This introduced error only becomes unacceptable after the constellation change and the most sensitive satellite contributes heavily to the subset solution. On the other hand, the geometries were chosen at random and do not have any unique subset characteristics. It is quite disenchanting that such radically different triangle charts can be created from the same pseudorange errors and one biased satellite simply by looking at subsets. Making the situation even worse is the fact that two or more pseudoranges can be corrupted to create arbitrarily large errors in the subset solution and zero error for the all-in-view solution. It has not previously been realized how well single errors could be hidden. The lesson is that it is not sufficient to observe a particular set of position solutions. The most effective method is to combine position domain monitoring with range domain monitoring.

#### **4.4 Kalman Filter smoothing**

It would be desirable to "smooth out" the LVPL so that it doesn't have the choppiness demonstrated by much of the data set, e.g. in Fig. 3.28 and 3.30. Also, using Kalman filtering retains the localized flavor of the WAAS performance to a certain degree. During a span of time without violent thunderstorms, sunspot activity, or other adverse conditions, one expects the WAAS solution to be virtually continuous. However, as was demonstrated in the time-VPL-VPE charts of sections 3.5 and 3.6, due to various

reasons choppy gaps do exist and generate HMIs. Since these gaps represent faulty solutions of the WAAS, they can be deemed as gaps in the valid data that could be disoccluded (filled in) by appropriate interpolation or smoothing.

#### 4.4.1 The discret Kalman filter introduction and notation to be used

From the historical 1960 work of R. E. Kalman [36] describing a recursive solution of the discrete-data linear filtering problem, advances in technology and computer science have made Kalman Filter widespread in many real-time applications, including GPS signal processing. In this section I will introduce the discrete kalman Filter and clarify the notation that will be used.

In order to apply the Kalman Filtering framework, it is necessary to assume that the ransom process to be estimated can be adqutely described by a finite dimensional state space model Assuming a random process to be estimated can be modeled in the form:

$$x_{k+1} = \phi_k x_k + w_k , \quad (4.8)$$

and the observation or measurement, must be an affine function of the state with additive uncorrelated noise known as the measurement noise. The measurement noise must also be uncorrelated with the input process. The measurement equation is given by

$$z_k = H_k x_k + n_k , \quad (4.9)$$

where

- 1)  $x_k$  is the  $n \times 1$  state vector at time  $t_k$  ;
- 2)  $\phi_k$  is the  $n \times n$  state transition matric relating  $x_{k+1}$  and  $x_k$  in the absence of any forcing function;

- 3)  $w_k$  is the  $n \times 1$  input signal which must be an uncorrelated stochastic process (white noise) with known covariance structure;
- 4)  $z_k$  is the  $m \times 1$  measurement vector at time  $t_k$ ;
- 5)  $H_k$  is the  $m \times m$  observation matrix connecting measurement and state vector at time  $t_k$ ;
- 6)  $n_k$  is the  $m \times 1$  measurement error vector, assumed to be a white noise sequence with known covariance structure and zero crosscorrelation with  $w_k$ .

The covariance structures for  $w_k$  and  $n_k$  are given by

$$E[w_k w_i^T] = \begin{cases} Q_k, & i = k \\ 0, & i \neq k \end{cases} = Q_k \delta[k], \quad (4.10)$$

$$E[n_k n_i^T] = \begin{cases} R_k, & i = k \\ 0, & i \neq k \end{cases} = R_k \delta[k], \quad (4.11)$$

where  $\delta[k]$  is the Kronecker delta. The crosscorrelation between  $w_k$  and  $n_k$  must be zero:

$$E[w_k n_i^T] = 0, \quad (\text{for all } k \text{ and } i). \quad (4.12)$$

The *a priori* estimate of the state vector at time  $t_k$  given measurements only up through time  $t_{k-1}$  will be denoted  $\hat{x}_k^-$ . The error on this estimate is given by  $e_k^- = x_k - \hat{x}_k^-$ , and has associated error covariance matrix

$$P_k^- = E[e_k^- e_k^{-T}] = E[(x_k - \hat{x}_k^-)(x_k - \hat{x}_k^-)^T]. \quad (4.13)$$

The new information provided by the measurement  $z_k$  is used to update the *a priori* estimate  $\hat{x}_k^-$  according to

$$\hat{x}_k = \hat{x}_k^- + K_k(z_k - H_k \hat{x}_k^-) , \quad (4.14)$$

where  $K_k$  is the Kalman gain sequence which will be developed below.

Similar to  $P_k^-$  we can define  $P_k$ , the error covariance matrix associated with the updated (or *a posteriori*) estimate:

$$\begin{aligned} P_k &= E[e_k e_k^T] = E[(x_k - \hat{x}_k)(x_k - \hat{x}_k)^T] \\ &= E[\{x_k - \hat{x}_k^- + K_k(z_k - H_k \hat{x}_k^-)\} \{x_k - \hat{x}_k^- + K_k(z_k - H_k \hat{x}_k^-)\}^T] \\ &= (I - K_k H_k) P_k^- (I - K_k H_k)^T + K_k R_k K_k^T . \end{aligned} \quad (4.15)$$

To obtain for the minimum mean square error the Kalman gain  $K_k$  can be solved as [3]

$$K_k = P_k^- H_k^T (H_k P_k^- H_k^T + R_k)^{-1} . \quad (4.16)$$

The error covariance matrix associated with the optimal *a posteriori* state vector estimate is then given by

$$P_k = (I - K_k H_k) P_k^- . \quad (4.17)$$

The updated state vector estimate can then be projected ahead to obtain a now *a priori* estimate for the state vector at time  $t_{k+1}$ :

$$\hat{x}_{k+1}^- = \phi_k \hat{x}_k . \quad (4.18)$$

The error covariance matrix associated with  $\hat{x}_{k+1}^-$  is

$$\begin{aligned} P_{k+1}^- &= E[e_{k+1}^- e_{k+1}^-^T] = E[(x_{k+1} - \hat{x}_{k+1}^-)(x_{k+1} - \hat{x}_{k+1}^-)^T] \\ &= E[(\phi_k e_k + w_k)(\phi_k e_k + w_k)^T] \\ &= \phi_k P_k \phi_k^T + Q_k . \end{aligned} \quad (4.19)$$

The whole recursion can be summarized as shown in Fig. 4.10.

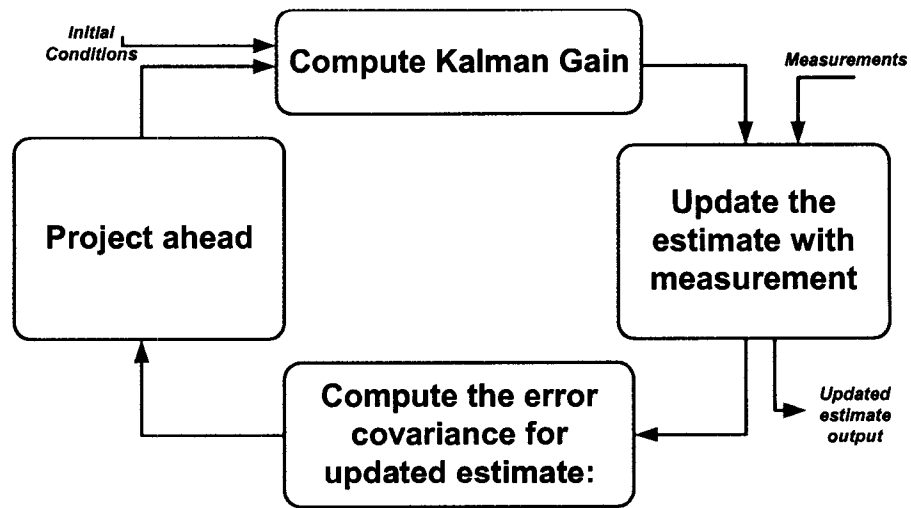


Figure 4. 10 Kalman filter block diagram.

#### 4.4.2 Using $\alpha - \beta$ Kalman filter to filter VPL

In this research project WAAS static data is the object of study and all the algorithm development was done on this data. In essence the VPL is a modeled version of VPE, which in turn is the result of numerous contributing error sources. By central limit theorem VPE is a Gaussian like random process. In [37] how WAAS combines all different message types to arrive to the correction information is described in details. This demonstrates that the VPE can be modeled as a Brownian Motion process,

$$\frac{d}{dt} LVPL(t) \equiv \dot{y}(t) = u(t) \quad , \quad (4.20)$$

Its discrete state model is

$$\begin{bmatrix} \dot{y} \\ \dot{v} \end{bmatrix} = \begin{bmatrix} 1 & \Delta \\ 0 & 1 \end{bmatrix} \begin{bmatrix} y \\ v \end{bmatrix} + \begin{bmatrix} 0 \\ 1 \end{bmatrix} u, \quad (4.21)$$

$$x = \begin{bmatrix} y \\ v \end{bmatrix} . \quad (4.22)$$

Recall that from Section 3.6 and 4.2 it is concluded that  $LVPL$  is a better metric than  $VPL$ , and can be modeled as a random process. Therefore define

$$LVPL_k \equiv y_k = \log_{10}(1 + VPL_k) , \quad (4.23)$$

where  $y_k$  is a random process as well. From analysis and data presented in Chapter 3, it seems reasonable to cast the problem of smoothing/interpolating  $y_k$  as a 1-D target problem with noisy measurements. A simple yet fitting model would be the  $\alpha - \beta$  tracking filter.

An  $\alpha - \beta$  tracking filter is a two-state version of the Kalman filter, i.e. a special case of Kalman Filter. Basically, it is a minimum mean-square error (MMSE) solution of the problem given the statistical measurements.

In this solution, it is assumed that the quantity of interest ( $y_k$  in this case) has a first derivative (or “velocity”) that changes only slightly from one measurement time to the next. Thus it is assumed that the first derivative may be modeled as a constant plus a small additive noise or “drift”. For this reason, the  $\alpha - \beta$  filter is also sometimes called a “constant velocity” tracker. As can be seen from the VPL data presented in Section 3.4 the constant velocity model is applicable to  $y_k$  as given in (4.23). There are 5 samples per second in the WAAS signal. The position of target at the time of the  $(k + 1)th$  measurement can be written as

$$y_{k+1} = y_k + \Delta v_k , \quad (4.24)$$

where  $\Delta$  is the time between successive measurements, which is 0.2 seconds in this case.

As stated above, it is unlikely that over a long period of time the velocity remains truly constant. A small “velocity drift” from measurement to measurement will now be allowed

$$v_{k+1} = v_k + w_k \quad (4.25)$$

where  $w_k$  is modeled as a white “velocity drift” noise with the statistics of

$$\begin{aligned} E[w_k] &= 0, \\ E[w_k w_i] &= \sigma_v^2 \delta_{k-i}, \end{aligned} \quad (4.26)$$

where  $\delta_{k-i}$  is defines as

$$\delta_{k-i} = \begin{cases} 1 & \text{when } k = i \\ 0 & \text{other} \end{cases}. \quad (4.27)$$

For the measurement noise the symbol  $n_k$  will be used and  $n_k$  is also a white noise process, with

$$\begin{aligned} E[n_k] &= 0, \\ E[n_k n_i] &= \sigma_n^2 \delta_{k-i}, \end{aligned} \quad (4.28)$$

and  $E[w_k n_i] = 0$ . The observation is then given by

$$z_k = y_k + n_k \quad (4.29)$$

By combining the above equations the system model can be written in matrix form:

$$\begin{pmatrix} y_{k+1} \\ v_{k+1} \end{pmatrix} = \begin{pmatrix} 1 & \Delta \\ 0 & 1 \end{pmatrix} \begin{pmatrix} y_k \\ v_k \end{pmatrix} + \begin{pmatrix} 0 \\ 1 \end{pmatrix} w_k \quad (4.30)$$

$$z_k = (0 \quad 1) \begin{pmatrix} y_k \\ v_k \end{pmatrix} + n_k \quad (4.31)$$

Compare these equations to the equations (4.8) through (4.19), we have

$$\phi_k = \begin{pmatrix} 1 & \Delta \\ 0 & 1 \end{pmatrix}, \quad x_k = \begin{pmatrix} y_k \\ v_k \end{pmatrix}, \quad (4.32)$$

$$w_k = \begin{pmatrix} 0 \\ w_k \end{pmatrix}, \quad (4.33)$$

$$H_k = (0 \quad 1), \quad (4.34)$$

$$n_k = n_k. \quad (4.35)$$

And covariance structures

$$Q_k = E \left\{ \begin{pmatrix} 0 \\ w_k \end{pmatrix} \begin{pmatrix} 0 & w_k \end{pmatrix} \right\} = \begin{pmatrix} 0 & 0 \\ 0 & \sigma_v^2 \delta_{i-k} \end{pmatrix}, \quad (4.36)$$

$$R_k = E[n_k n_i] = \sigma_n^2 \delta_{i-k}. \quad (4.37)$$

To initialize this recursion, at  $k = -2$ , the measurement is

$$z_{-2} = y_{-2} + n_{-2}, \quad (4.38)$$

and at  $k = -1$ , the measurement is

$$z_{-1} = y_{-1} + n_{-1}. \quad (4.39)$$

Take  $\hat{y}_{-1} = z_{-1}$ , and  $\hat{v}_{-1} = \frac{z_{-1} - z_{-2}}{\Delta}$ . It is worth pointing out that the averaging reduces the

effects of the measurement noise  $n_k$ .

This leads to

$$x_{-1} = \begin{pmatrix} \hat{y}_{-1} \\ \hat{v}_{-1} \end{pmatrix} = \begin{pmatrix} z_{-1} \\ \frac{z_{-1} - z_{-2}}{\Delta} \end{pmatrix}. \quad (4.40)$$

Then

$$\begin{aligned}
P_{-1} &= E[e_{-1}e_{-1}^T] = E\{[(x_{-1} - \hat{x}_{-1})(x_{-1} - \hat{x}_{-1})^T]\} \\
&= E\left\{\left(\begin{pmatrix} y_{-1} \\ v_{-1} \end{pmatrix} - \begin{pmatrix} \hat{y}_{-1} \\ \hat{v}_{-1} \end{pmatrix}\right)\left(\begin{pmatrix} y_{-1} \\ v_{-1} \end{pmatrix} - \begin{pmatrix} \hat{y}_{-1} \\ \hat{v}_{-1} \end{pmatrix}\right)^T\right\} = E\left\{\begin{pmatrix} y_{-1} - \hat{y}_{-1} \\ v_{-1} - \hat{v}_{-1} \end{pmatrix}\begin{pmatrix} y_{-1} - \hat{y}_{-1} \\ v_{-1} - \hat{v}_{-1} \end{pmatrix}^T\right\}. \quad (4.41)
\end{aligned}$$

Now,

$$y_{-1} - \hat{y}_{-1} = y_{-1} - z_{-1} = y_{-1} - (y_{-1} + n_{-1}) = -n_{-1}, \quad (4.42)$$

$$\begin{aligned}
v_{-1} - \hat{v}_{-1} &= v_{-1} - \frac{z_{-1} - z_{-2}}{\Delta} = v_{-1} - \frac{(y_{-1} + n_{-1}) - (y_{-2} + n_{-2})}{\Delta} \\
&= v_{-1} - \frac{(y_{-1} - y_{-2}) + (n_{-1} - n_{-2})}{\Delta} = v_{-1} - \frac{[(y_{-2} + \Delta v_{-2}) - y_{-2}] + (n_{-1} - n_{-2})}{\Delta} \\
&= (v_{-2} + w_{-2}) - \frac{\Delta v_{-2} + (n_{-1} - n_{-2})}{\Delta} = w_{-2} - \frac{n_{-1} - n_{-2}}{\Delta}. \quad (4.43)
\end{aligned}$$

To compute  $P_{-1}$  the following quantities are needed:

$$E[(y_{-1} - \hat{y}_{-1})^2] = E[(-n_{-1})^2] = \sigma_n^2, \quad (4.44)$$

and

$$\begin{aligned}
E[(y_{-1} - \hat{y}_{-1})(v_{-1} - \hat{v}_{-1})] &= E[(-n_{-1})(w_{-2} - \frac{n_{-1} - n_{-2}}{\Delta})] \\
&= E[(-n_{-1}w_{-2} + \frac{(n_{-1} - n_{-2})n_{-1}}{\Delta})] = E[(-n_{-1}w_{-2} + \frac{n_{-1}^2}{\Delta} - \frac{n_{-2}n_{-1}}{\Delta})] \\
&= -E[n_{-1}w_{-2}] + E[\frac{n_{-1}^2}{\Delta}] - E[\frac{n_{-2}n_{-1}}{\Delta}] = E[\frac{n_{-1}^2}{\Delta}] = \frac{\sigma_n^2}{\Delta}. \quad (4.45)
\end{aligned}$$

Using symmetry the following is shown:

$$E[(v_{-1} - \hat{v}_{-1})(y_{-1} - \hat{y}_{-1})] = E[(y_{-1} - \hat{y}_{-1})(v_{-1} - \hat{v}_{-1})] = \frac{\sigma_n^2}{\Delta}. \quad (4.46)$$

The last term in  $P_{-1}$  is

$$\begin{aligned}
E[(v_{-1} - \hat{v}_{-1})^2] &= E[(w_{-2} - \frac{n_{-1} - n_{-2}}{\Delta})^2] \\
&= E[(w_{-2}^2 - \frac{2}{\Delta}(w_{-2}n_{-1} - w_{-2}n_{-2}) + \frac{(n_{-1} - n_{-2})^2}{\Delta^2})] \\
&= E[w_{-2}^2] - \frac{2}{\Delta}E[w_{-2}n_{-1}] + \frac{2}{\Delta}E[w_{-2}n_{-2}] + \frac{1}{\Delta^2}E[n_{-1}^2] - \frac{2}{\Delta^2}E[n_{-1}n_{-2}] + \frac{1}{\Delta^2}E[n_{-2}^2] \\
&= \sigma_v^2 + \frac{1}{\Delta^2}\sigma_v^2 + \frac{1}{\Delta^2}\sigma_v^2 = (1 + \frac{2}{\Delta^2})\sigma_v^2 .
\end{aligned} \tag{4.47}$$

Combine all four components,

$$P_{-1} = \begin{pmatrix} \sigma_n^2 & \frac{\sigma_n^2}{\Delta} \\ \frac{\sigma_n^2}{\Delta} & (1 + \frac{2}{\Delta^2})\sigma_v^2 \end{pmatrix} . \tag{4.48}$$

The initial *a priori* estimate may now be developed according to

$$\hat{x}_0^- = \phi_{-1}\hat{x}_{-1} = \begin{pmatrix} 1 & \Delta \\ 0 & 1 \end{pmatrix} \begin{pmatrix} \hat{y}_{-1} \\ \hat{v}_{-1} \end{pmatrix} = \begin{pmatrix} 2z_{-1} + z_{-2} \\ \frac{z_{-1} - z_{-2}}{\Delta} \end{pmatrix} \tag{4.49}$$

and

$$\begin{aligned}
P_0^- &= \phi_{-1}P_{-1}\phi_{-1}^T + Q_{-1} = \begin{pmatrix} 1 & \Delta \\ 0 & 1 \end{pmatrix} \begin{pmatrix} \sigma_n^2 & \frac{\sigma_n^2}{\Delta} \\ \frac{\sigma_n^2}{\Delta} & (1 + \frac{2}{\Delta^2})\sigma_v^2 \end{pmatrix} \begin{pmatrix} 1 & 0 \\ \Delta & 1 \end{pmatrix} + \begin{pmatrix} 0 & 0 \\ 0 & \sigma_v^2 \end{pmatrix} \\
&= \begin{pmatrix} 5\sigma_n^2 + \Delta^2\sigma_v^2 & \frac{3\sigma_n^2}{\Delta} + \Delta\sigma_v^2 \\ \frac{3\sigma_n^2}{\Delta} + \Delta\sigma_v^2 & 2(\frac{\sigma_n^2}{\Delta^2} + \sigma_v^2) \end{pmatrix} .
\end{aligned} \tag{4.50}$$

With these initial conditions one can enter the Kalman filtering loop shown in Fig. 4.10

and see how the general Kalman filter reduces to the  $\alpha - \beta$  filter. Begin with

$$\hat{x}_k = \hat{x}_k^- + K_k(z_k - H_k\hat{x}_k^-) . \tag{4.51}$$

For the  $\alpha - \beta$  filter, this becomes

$$\begin{pmatrix} \hat{y}_k \\ \hat{v}_k \end{pmatrix} = \begin{pmatrix} \hat{y}_k^- \\ \hat{v}_k^- \end{pmatrix} + K_k (z_k - [1 \quad 0] \begin{pmatrix} \hat{y}_k^- \\ \hat{v}_k^- \end{pmatrix}) = \begin{pmatrix} \hat{y}_k^- \\ \hat{v}_k^- \end{pmatrix} + K_k (z_k - \hat{y}_k^-) . \quad (4.52)$$

Denote  $K_k = \begin{pmatrix} \alpha \\ \beta \end{pmatrix}$  to obtain scalar equations for the updated estimates of the state vector entries:

$$\begin{cases} \hat{y}_k = \hat{y}_k^- + \alpha_k (z_k - \hat{y}_k^-) \\ \hat{v}_k = \hat{v}_k^- + \beta_k (z_k - \hat{y}_k^-) \end{cases} . \quad (4.53)$$

The update equation for the predicted state vector is

$$\hat{x}_{k+1}^- = \phi_k \hat{x}_k . \quad (4.54)$$

For our “constant velocity” model this gives

$$\begin{pmatrix} \hat{y}_{k+1}^- \\ \hat{v}_{k+1}^- \end{pmatrix} = \begin{pmatrix} 1 & \Delta \\ 0 & 1 \end{pmatrix} \begin{pmatrix} \hat{y}_k \\ \hat{v}_k \end{pmatrix} = \begin{pmatrix} \hat{y}_k + \Delta \hat{v}_k \\ \hat{v}_k \end{pmatrix} . \quad (4.55)$$

In scalar form, we have that

$$\begin{cases} \hat{y}_{k+1}^- = \hat{y}_k + \Delta \hat{v}_k \\ \hat{v}_{k+1}^- = \hat{v}_k \end{cases} . \quad (4.56)$$

Combinng these results we arrive in the classical  $\alpha - \beta$  filter equations:

$$\begin{cases} \hat{y}_k = \hat{y}_k^- + \alpha_k (z_k - \hat{y}_k^-) \\ \hat{v}_k = \hat{v}_k^- + \beta_k (z_k - \hat{y}_k^-) \\ \hat{y}_{k+1}^- = \hat{y}_k + \Delta \hat{v}_k \\ \hat{v}_{k+1}^- = \hat{v}_k \end{cases} . \quad (4.57)$$

So far everything is available except the so-called “Kalman Gain”  $\alpha_k$  and  $\beta_k$ .

From the derivation above:

- 1) The Kalman gains  $K_k$  depend on the predicted state vector error covariance matrix, but not directly on the observations.

- 2) The predicted state vector error covariance matrix  $P_k$  depends on the filtered state vector error covariance matrix, but not directly on the observations.
- 3) The filtered state vector error covariance matrix  $P_{k+1}^-$  depends on the predicted state vector error covariance matrix and on the Kalman gains, but not directly on the observations.
- 4) The starting “seed”  $P_0^-$  doesn't depend on observation  $z_k$ .

Therefore, all the Kalman gains can be pre-computed and stored in a file.

Implementation of the Kalman filter is then reduced to processing the measurements  $z_k$ , which in my research comes with the observed VPL over time. The initial conditions are given by:

$$\hat{y}_{-1} = z_{-1}, \quad \hat{v}_{-1} = \frac{z_{-1} - z_{-2}}{\Delta}, \quad \hat{x}_{-1} = \begin{pmatrix} z_{-1} \\ \frac{z_{-1} - z_{-2}}{\Delta} \end{pmatrix}, \quad \hat{x}_0^- = \begin{pmatrix} 1 & \Delta \\ 0 & 1 \end{pmatrix} \begin{pmatrix} \hat{y}_{-1} \\ \hat{v}_{-1} \end{pmatrix}. \quad (4.58)$$

To pre-compute the Kalman gains  $\alpha_k$  and  $\beta_k$ , let

$$P_k = \begin{pmatrix} P_k(1,1) & P_k(1,2) \\ P_k(2,1) & P_k(2,2) \end{pmatrix}, \quad (4.59)$$

and

$$P_k^- = \begin{pmatrix} P_k^-(1,1) & P_k^-(1,2) \\ P_k^-(2,1) & P_k^-(2,2) \end{pmatrix}. \quad (4.60)$$

Then (4.16) can be rewritten as

$$\begin{aligned}
\begin{pmatrix} \alpha_k \\ \beta_k \end{pmatrix} &= \begin{pmatrix} P_k(1,1) & P_k(1,2) \\ P_k(2,1) & P_k(2,2) \end{pmatrix} \begin{pmatrix} 1 \\ 0 \end{pmatrix} \left( (1 \ 0) \begin{pmatrix} P_k^-(1,1) & P_k^-(1,2) \\ P_k^-(2,1) & P_k^-(2,2) \end{pmatrix} \begin{pmatrix} 1 \\ 0 \end{pmatrix} + \sigma_n^2 \right)^{-1} \\
&= \begin{pmatrix} \frac{P_k^-(1,1)}{P_k^-(1,1) + \sigma_n^2} \\ \frac{P_k^-(2,1)}{P_k^-(1,1) + \sigma_n^2} \end{pmatrix} \tag{4.61}
\end{aligned}$$

i.e.

$$\begin{aligned}
\alpha_k &= \frac{P_k^-(1,1)}{P_k^-(1,1) + \sigma_n^2} \ , \\
\beta_k &= \frac{P_k^-(2,1)}{P_k^-(1,1) + \sigma_n^2} \ . \tag{4.62}
\end{aligned}$$

The filtered state vector error covariance matrix in (4.17) is then given by

$$\begin{aligned}
P_k &= \left( \begin{pmatrix} 1 & 0 \\ 0 & 1 \end{pmatrix} - \begin{pmatrix} \alpha_k \\ \beta_k \end{pmatrix} \begin{pmatrix} 1 & 0 \end{pmatrix} \right) \begin{pmatrix} P_k^-(1,1) & P_k^-(1,2) \\ P_k^-(2,1) & P_k^-(2,2) \end{pmatrix} \\
&= \begin{pmatrix} (1 - \alpha_k)P_k^-(1,1) & (1 - \alpha_k)P_k^-(1,2) \\ (1 - \alpha_k)P_k^-(1,2) & P_k^-(2,2) - \beta_k P_k^-(1,2) \end{pmatrix} \ . \tag{4.63}
\end{aligned}$$

The *a priori* state vector error covariance matrix in (4.19) can be written as

$$P_{k+1}^- = \begin{pmatrix} 1 & \Delta \\ 0 & 1 \end{pmatrix} \begin{pmatrix} P_k(1,1) & P_k(1,2) \\ P_k(2,1) & P_k(2,2) \end{pmatrix} \begin{pmatrix} 1 & 0 \\ \Delta & 1 \end{pmatrix} + \begin{pmatrix} 0 & 0 \\ 0 & \sigma_v^2 \end{pmatrix} \ . \tag{4.64}$$

In other words, we have the scalar relations:

$$\begin{aligned}
P_{k+1}^-(1,1) &= P_k(1,1) + 2\Delta P_k(1,2) + \Delta^2 P_k(2,2) \ , \\
P_{k+1}^-(1,2) &= P_k(1,2) + \Delta P_k(2,2) \ , \\
P_{k+1}^-(2,1) &= P_k(2,1) + \Delta P_k(2,2) = P_k(1,2) + \Delta P_k(2,2) \ , \\
P_{k+1}^-(2,2) &= P_k(2,2) + \sigma_v^2 \ . \tag{4.65}
\end{aligned}$$

The pre-computation of the Kalman Gains ( $\alpha_k$  and  $\beta_k$ ) is summarized in the following

steps:

- 1) Begin with  $P_0^-$  as given;

- 2)  $k = 0$ ;
- 3) Compute  $\alpha_k$  and  $\beta_k$  using (4.58) and (4.59);
- 4) Compute  $P_k$  using (4.60);
- 5) Compute  $P_{k+1}^-$  using (4.62)
- 6) Let  $k = k+1$
- 7) Go loop back to step 3.

Typically the Kalman gains converge to asymptotic values. From what has been observed about my Kalman Filter implementation on the pseudo-VPL, this is certainly true. The overall Kalman iteration is now:

- 1) Initialize  $(P_0^-)^{-1}$  and  $\hat{x}_0^-$ ;
- 2)  $k = 0$ ;
- 3)  $P_k = (P_k^-)^{-1} + H_k^T R_k^{-1} H_k$
- 4)  $K_k = \begin{pmatrix} \alpha_k \\ \beta_k \end{pmatrix}$  -----has been computed and stored in a file
- 5)  $\hat{x}_k = \hat{x}_k^- + K_k(z_k - H_k \hat{x}_k^-)$
- 6)  $\hat{x}_{k+1}^- = \phi_k \hat{x}_k$
- 7)  $P_{k+1}^- = \phi_k P_k \phi_k^T + Q_k$
- 8) Let  $k = k+1$
- 9) Loop back to step 3.

Now all that is needed is to specify the initialization and some parameters. From the graphs in Chapter 3 it can be easily estimated the range for these parameters. It turned out that the filtering process converged fairly quick, making this a moot point. Assume

the Noise\_to\_VPL and VPL itself are pseudo random processes. They are independent and are covariance stationary. Fig. 4.11 below is the initialization section of the filter written in MatLab for the  $\alpha - \beta$  filter in this dissertation. As mentioned above, the initial sigma\_vpl\_2 and sigma\_measure\_2 turned out to be not very sensitive.

```

delta=0.2;    % Frame seperation, which in WAAS is 0.2 second

delta2 = delta * delta; % (Frame seperation) squared

I = [1 0
     0 1];

Phi_k = [1 delta
         0 1 ]; % Conversion Matrix

H_k = [1 0]; %Measurement matrix

%The initialization: Determine the stochastic properties of the random process: L_VPL

sigma_vpl_2 = 0.8; % 2 at the end stands for --Squared, sigma_vpl_2 is the auto covariance of L_VPL,

% Another thing that has to be taken into account is the VPL is studied through L_vpl=log10(1+VPL)

sigma_measure_2 = 0.4; % 2 at the end stands --Squared,

```

**Figure 4.11 Initialization of the  $\alpha - \beta$  Kalman filter.**

## 4.5 Fault prevention and error correction in this VPL algorithm

The basic idea behind fault prevention and error correction is that the GPS and WAAS system is a physical system. This means that the observations concerning GPS and WAAS have to follow physics rules. An easy example is that there will not be things flying faster than the speed of light. Closer to reality, if the system indicates that speed of the user changes at a rate beyond reasonable possibility, for instance, at a rate exceeding

what is possible even for the best fighter jets, then it can be safely concluded that a fault is present. From the historical data archive, the following conclusions could be drawn.

1. When there are only 4 SVs, the HPL and VPL tend to suffer the most and are often significantly degraded.
2. The more SVs are in sight, the better are the HPL and VPL that can be expected.
3. To calibrate the VPL performance, Metrics  $L\_VPL = \text{Log}10(1+VPL)$  and  $L\_VPE = \text{Log}10(1+VPE)$  are used to transform the possible multiplicative noise factors into additive ones, in which the bias 1 was added to remove singularity of logarithmic function at zero since VPE and VPL can reach this magnitude.

#### **4.6 Fault-proofing the VPE solution**

Merely dealing with VPL, which is what has been done thus far, will not help the integrity. If anything, it can hurt the VPL since the pseudo-VPL generally reduces the value of the VPL and doesn't affect the error performance. Ideally one wants to move the HMI points in the lower-right part of the upper triangle charts to the available part of the triangle charts, which is in the upper-left area. Therefore, to increase the integrity performance, the VPE has to be processed accordingly to be reduced.

From the Section 4.3 example one can see a bogus bias caused by change of SVs. When one low satellite moves out of view it may cause all the bias in the remaining satellites be magnified under certain circumstances. This could cause otherwise perfectly good data points to fall into the dangerous HMI region and would hence degrade the performance of the WAAS system. By using post analysis one can assess the seriousness of this problem and hopefully formulate a way to compensate for it.

In Section 4.5, by modeling  $VPL$  as a function of  $VPE$  with multiplicative noise and using Kalman Filtering to smooth abrupt changes (which don't make physical sense), one is able to move the data cluster downward, i.e. to increase the system availability under a specific  $VAL$ . This algorithm doesn't affect the  $VPE$  and therefore will not improve the integrity performance. The best scenario is when all the Kalman Filtering and following processing doesn't make the  $VPL$  envelope cross the  $VPE$  spikes, i.e. doesn't create new hazards. In that case this unchanged integrity performance is the best one can wish for. From the triangle charts shown in Section 4.3 example, data cluster will only move downward but not leftward, which is our ideal WAAS performance.

Because the  $VPE$  moves around zero and doesn't have a large envelope one is better off to filter the altitude directly and not some function of the altitude, as was done for the  $VPL$ . Other than these differences the whole problem is identical to that of the  $VPL$  problem. This time only a windowed low pass filter to de-spike the  $VPE$  solution is used. After that, a similar fault prevention as used in  $VPL$  case is implemented.

## Chapter 5

### Results and Conclusions

#### 5.1 Results of the pseudo-VPL algorithm

After the respective filtering processes of VPL and VPE a straightforward result comparison is shown. Again, plots of the triangle charts before and after the filtering processes to see obvious result of the algorithm. Take notice that this is only a qualitative assessment of the performance of the new algorithm since it is impossible to tell the density of data points at certain position by just looking at the triangle charts. These charts do give us some useful information about how the majority of data points behave after the new algorithm is carried out. Triangle charts of all 10 cases we have selected from our data archive will be presented to show how the algorithm performs under different situations.

As discussed in Section 4. 6, merely dealing with *VPL* will not help the integrity. If anything it can hurt the *VPL* since the pseudo-*VPL* generally reduces the value of *VPL* and doesn't affect the error performance. To improve the integrity performance it is necessary to reduce. The error needs to be reduced while maintaining *VPL* . Altitude solution filtering helps this cause, as mentioned in Section 4.6. The improvement this action brings into the WAAS system is also shown in the following triangle charts.

### Case 1: 12/01/1999: Before and after filtering

WAAS data collected on December 1, 1999 is shown in Fig. 5.1. Vertical performance using the MOPS specified algorithm is shown in the upper plot. The result after using the new pseudo-*VPL* algorithm is shown in the lower plot. Here we see that the entire locus of data points is translated down as a result of filtering, providing an obvious improvement in the availability. This improvement comes at the price of additional MI and HMI occurrences being generated. In the next section I will investigate the implications and seriousness of these extra MI and HMI events.

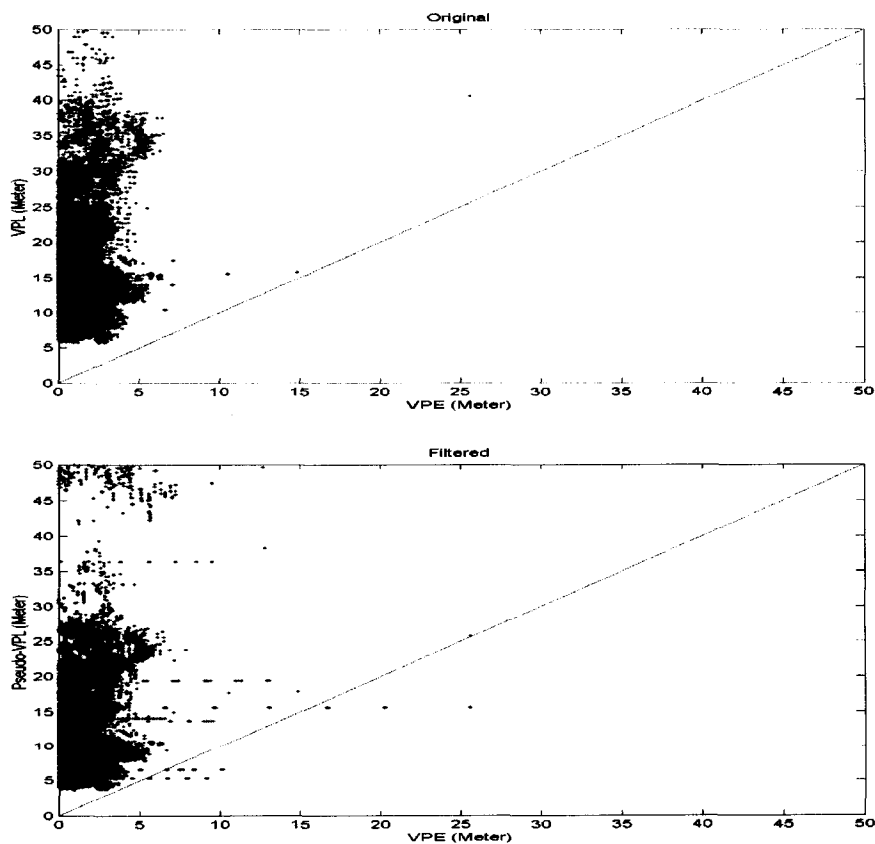


Figure 5. 1 Case 1: 12/01/1999: Before and after filtering.

### Case 2: 04/28/2000: Before and after filtering

In case 2 WAAS data collected on April 28, 2000 is shown in Fig. 5.2. Vertical performance using the MOPS specified algorithm is shown in the upper plot. The result after using the new pseudo-*VPL* algorithm is shown in the lower plot. Here we see the performance of the WAAS SIS is not very good due to the MI and HMI occurrences. After applying the pseudo-*VPL* algorithm, the entire locus of data points is translated down and the availability is improved. At the same time, however, additional MI and HMI occurrences are generated. The implications and seriousness of these extra MI and HMI events are to be investigated in the next section.

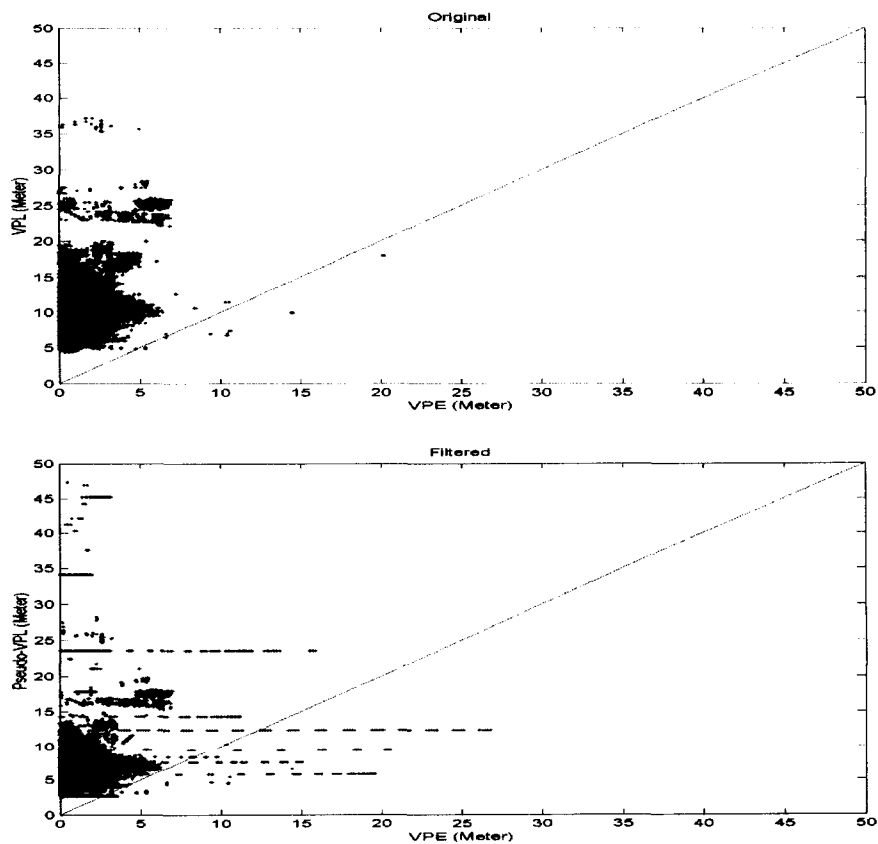


Figure 5.2 Case 2: 04/28/2000: Before and after filtering.

### Case 3: 11/27/2000: Before and after filtering

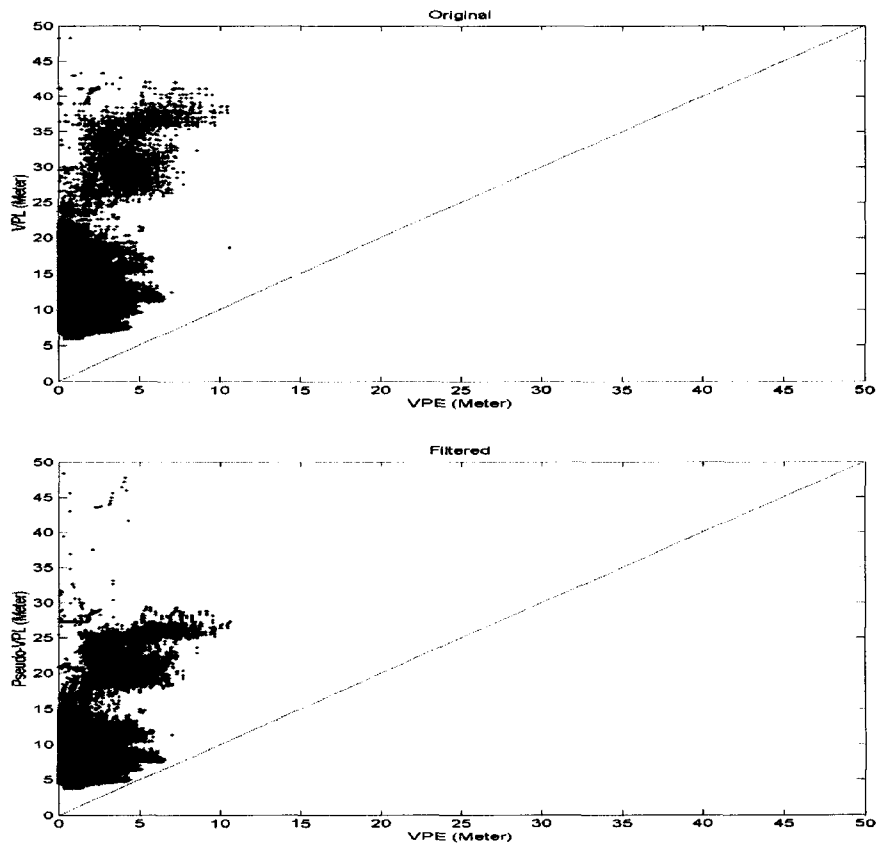


Figure 5.3 Case 3: 11/27/2000: Before and after filtering.

On November 27<sup>th</sup>, 2000, WAAS SIS performance is good as shown in upper part of Fig. 5.3. There is no NI or HMI in the original triangle chart. An excellent performance improvement is achieved after the pseudo-*VPL* algorithm is applied. The system availability is improved without generating additional MI or HMI event as demonstrated in the lower part of Fig. 5.3. Most data points are squeezed into the lower part of the upper half of the triangle chart and there is no HMI present before and after the algorithm is applied. The system availability is improved and yet the integrity is not compromised. Thus, the research goal has clearly been achieved in this case.

#### Case 4: 05/01/2001: Before and after filtering

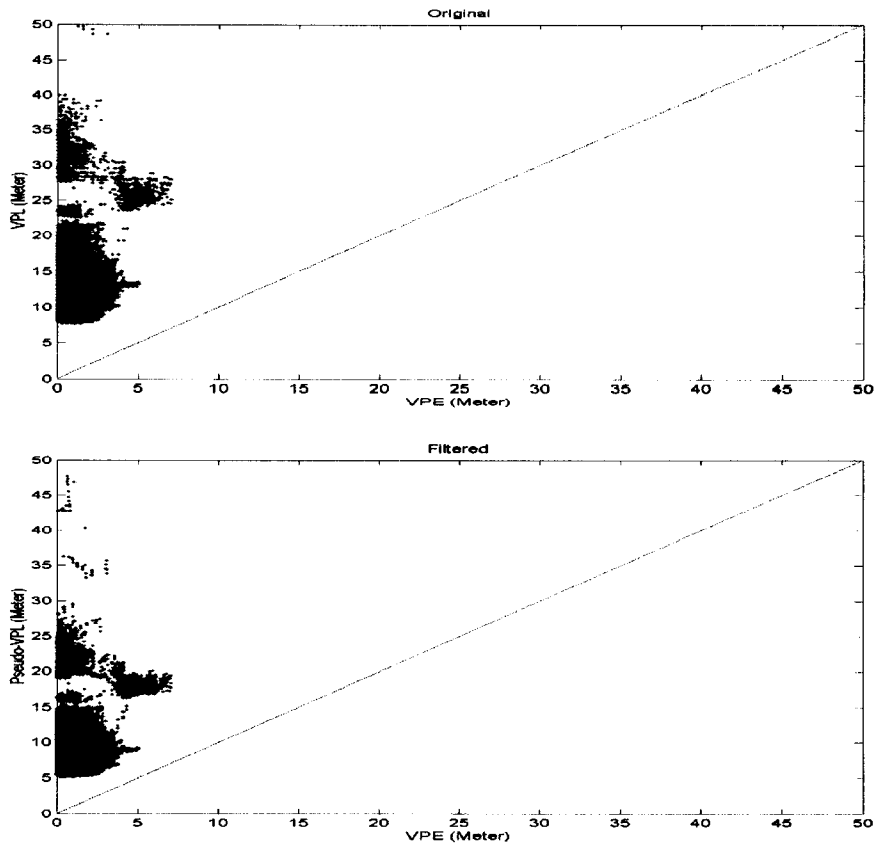


Figure 5.4 Case 4: 05/01/2001: Before and after the filtering.

May 1<sup>st</sup>, 2001 recorded an excellent data set as shown in upper part of Fig. 5.4. The pseudo-*VPL* algorithm shows that it works perfectly as shown in the lower half of Fig. 5.4. From case 1 to case 4 it can be observed that there is a possible pattern that the pseudo-*VPL* algorithm works well on good data sets, while less perfectly on days with significant MI and HMI occurrences.

### Case 5: 11/12/2001: Before and after filtering

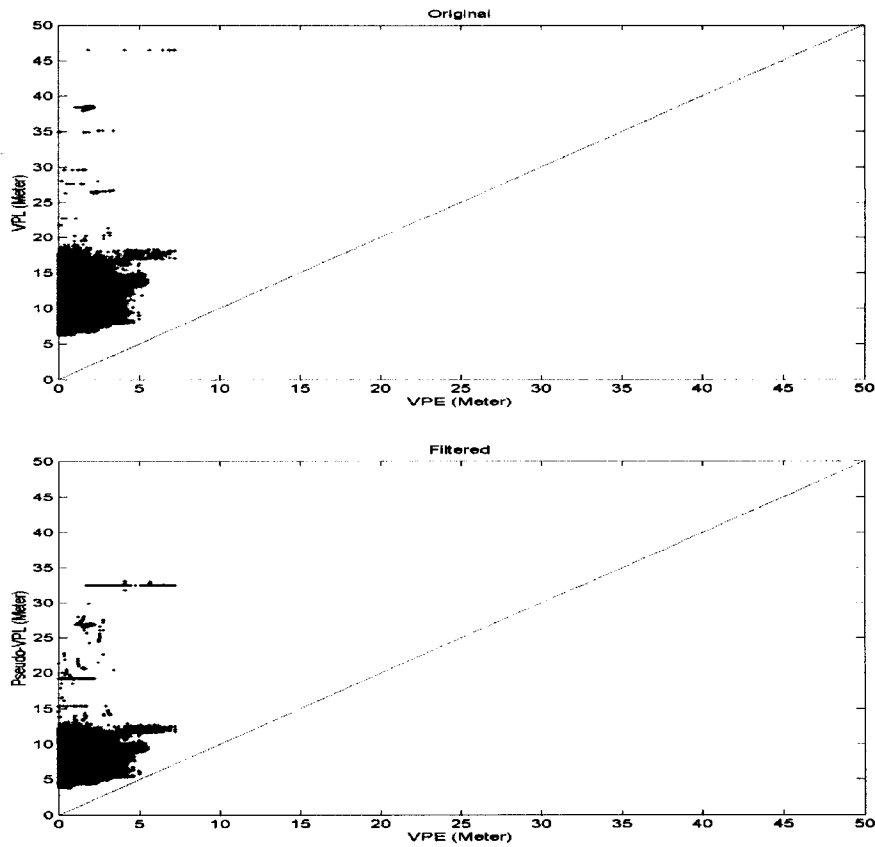


Figure 5.5 Case 5: 11/12/2001: Before and after filtering.

A good WAAS data set was recorded on November 12<sup>th</sup>, 2001 as shown in upper half of Fig. 5.5. The pseudo-*VPL* algorithm works very well to improve the system availability while without generating extra MI or HMI event as illustrated in the lower half of Fig. 5.5. This confirms the observation made in case 4 about how the pseudo-*VPL* algorithm works better on good data sets.

### Case 6: 05/02/2002: Before and after filtering

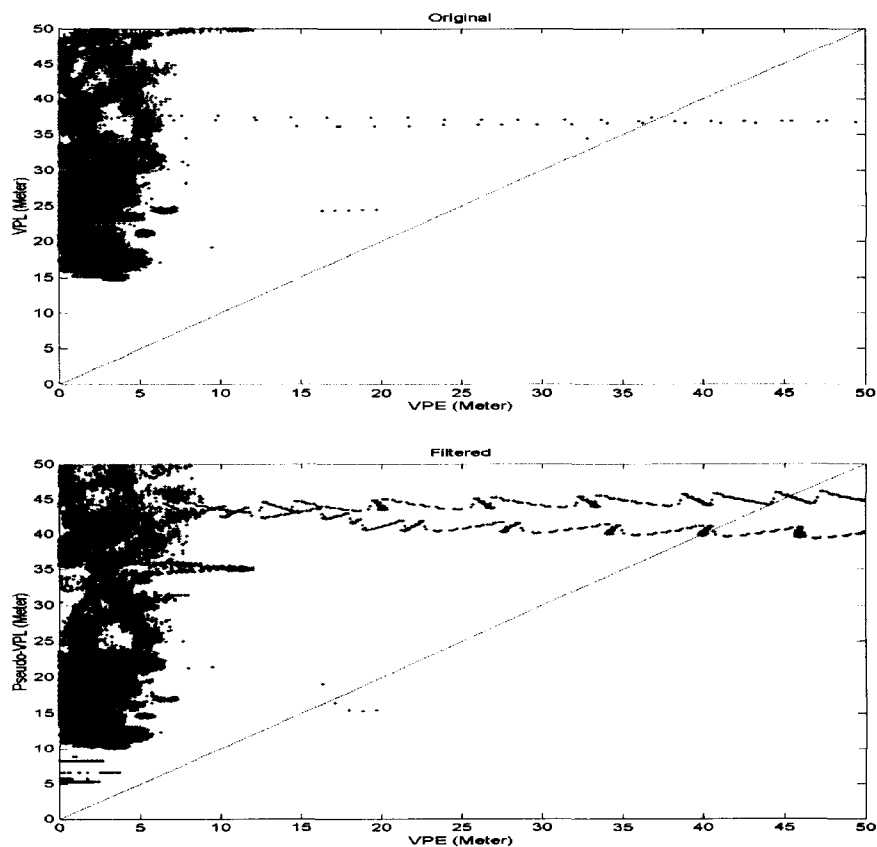


Figure 5. 6 Case 6: 05/02/2002: Before and after filtering.

On May 2<sup>nd</sup>, 2002 a less-than-desired WAAS data set is observed as shown in the upper part of Fig. 5.6. There are MI events and some data points close to the borderline. The pseudo-*VPL* algorithm performs with mixed results. The system availability is improved as the locus of data points are translated downwards as shown in the lower half of Fig. 5.6. At the same time, the system integrity performance is mixed as well. Some previously non-existent MI was generated while some previously existed MI events are removed.

### Case 7: 10/12/2002: Before and after filtering

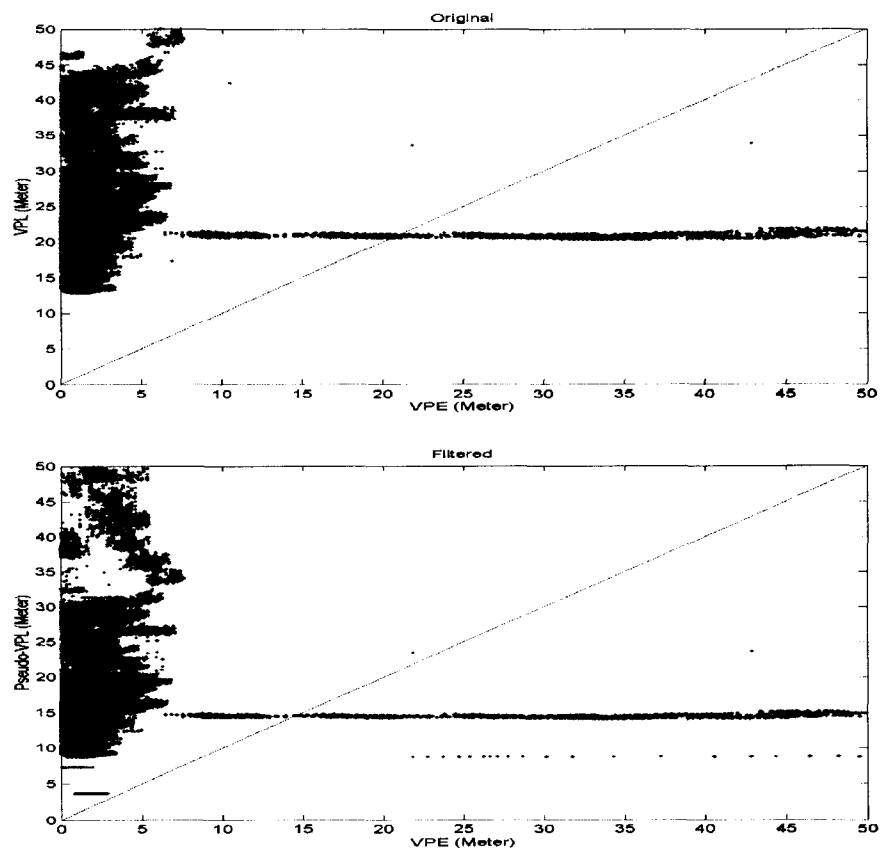


Figure 5.7 Case 7: 10/12/2002: Before and after filtering.

On October 12<sup>th</sup>, 2002 the WAAS performance is again very poor as shown in the upper part of Fig. 5.7. Consistent MI and HMI events are present. The pseudo-*VPL* algorithm doesn't help in term of integrity although the system availability seems to be improved as shown in the lower part of Fig. 5.7. Details about the tradeoff between the Integrity and Availability performance will be investigated in the next section.

### Case 8: 10/28/2002: Before and after filtering

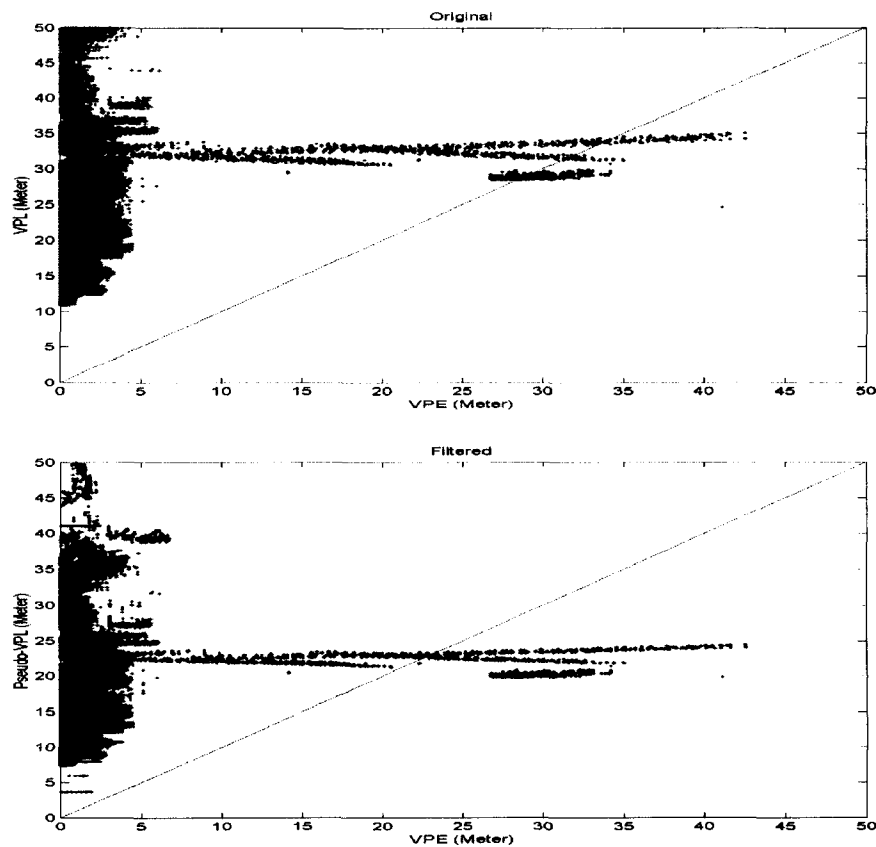


Figure 5.8 Case 8: 10/28/2002: Before and after filtering.

WAAS data recorded on 10/28/2002 shown in upper Fig. 5.8 is an example of poor WAAS performance. As the lower part of Fig. 5.8 shows, the performance of the pseudo-*VPL* algorithm is not very good. Although the system availability seems to be improved, the integrity of the system is sacrificed since there seem to be more MI and HMI occurrences as shown in the lower Fig. 5.8. As in Fig. 5.6 and 5.7, the seriousness of the integrity sacrifice needs further study in the next section.

### Case 9: 03/14/2003: Before and after filtering

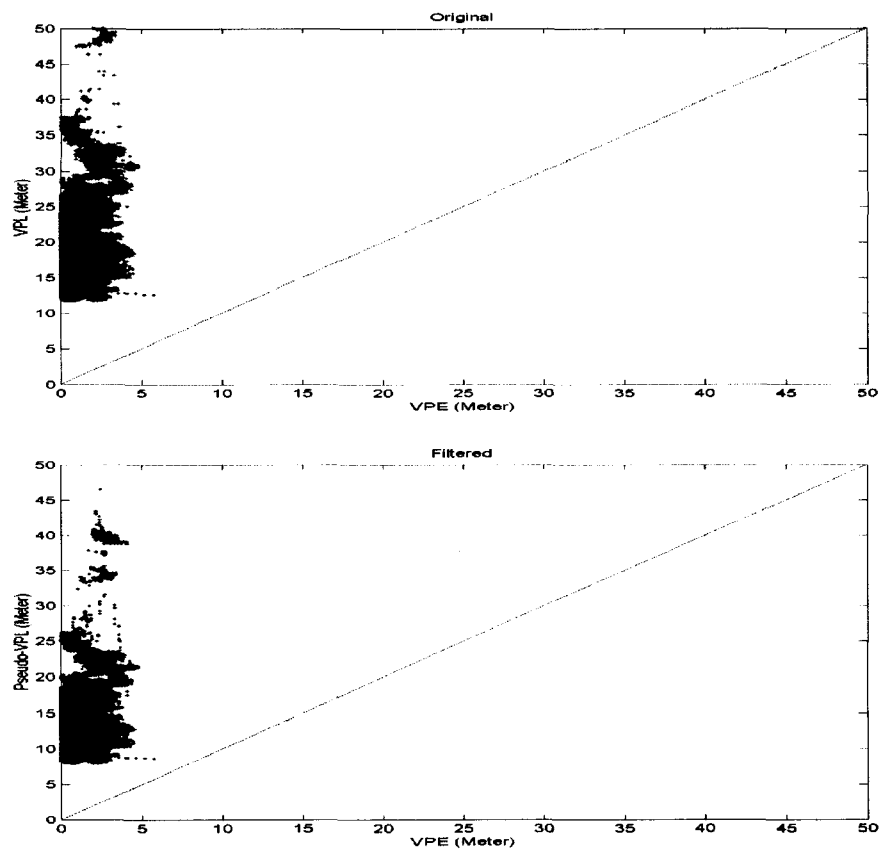


Figure 5.9 Case 9: 03/14/2003: Before and after filtering.

March 14<sup>th</sup>, 2003 witnessed a day of quality WAAS data as illustrated in upper part of Fig. 5.9. There is no MI or HMI and the data cluster is away from the borderline  $VPL = VPE$ , which is desired of the system integrity monitoring algorithm. In the lower part of Fig. 5.9, the pseudo- $VPL$  algorithm performs consistently well like the cases presented previously on days with good WAAS data. The locus of data is translated downwards and compressed. Therefore, the system availability is improved while the integrity is kept intact.

### Case 10: 05/29/2003: Before and after filtering

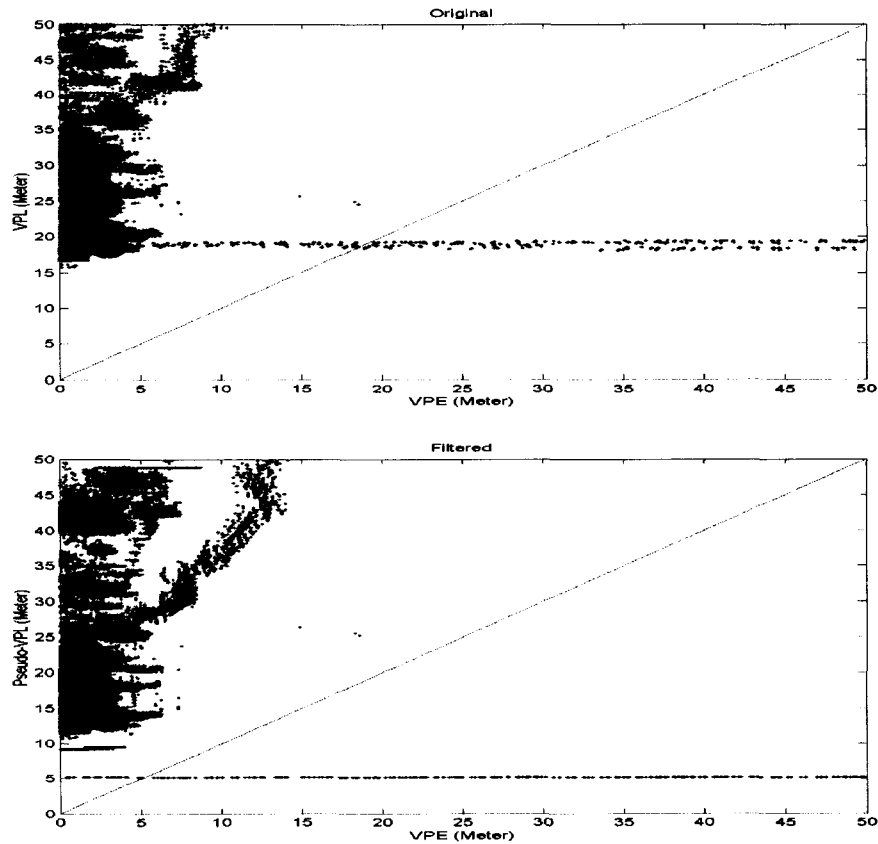


Figure 5.10 Case 10: 05/29/2003: Before and after filtering.

May 29<sup>th</sup>, 2003 is yet another example of bad WAAS performance. Considerable amount of MI and HMI occurrences results as shown in the triangle chart in upper Fig. 5.10. The pseudo-*VPL* algorithm again seems to improve the system availability. However, the change on system integrity is inconclusive from the lower half of Fig. 5.10. More investigation in the next section is needed to gauge how the integrity in this case performs under the pseudo-*VPL* algorithm.

Using the pseudo-*VPL* algorithm proposed in this dissertation and demonstrated in the previous examples, one can see the improvements in system availability by simply

looking at Fig. 5.1 through 5.10. Even without quantitative analysis to back up yet, it can be concluded that the system availability performance is improved.

Understandably, with the Kalman filtering and bias reduction one can lower the *VPL* significantly and therefore increase the system availability. This process essentially translates the whole data set cluster downward by a bias-reduction size, which is a trial-and-readjustment process. For *LVPL*, this bias-reduction size is determined, by experiment, to be 0.15, which is a compromise value to maximize the pseudo-*VPL* algorithm's ability of increasing system availability and to minimize the chance of generating additional MI or HMI occurrences. This improvement corresponds to a 3dB decrease in *VPL* magnitude. For the bias reduction, however, it seems the pseudo-*VPL* algorithm does not work well. Some VPE filtering and/or range-correction domain solution is needed for improvement of the bogus bias reducing demonstrated in Section 4.3.

## **5.2 Performance of the pseudo-*VPL* algorithm after altitude smoothing**

In the Section 5.1 only *VPL* is filtered. The results have shown promise. Improvement on availability has been observed. However, the algorithm can still be improved, as evidenced in Section 4.3. Efforts to remove the bogus bias in the WAAS SIS will be presented in this section. To ensure consistency throughout this dissertation, the same cases presented in Section 5.1 will be treated in this section. I have generated tables based on these same data sets to demonstrate the performance improvement of the

pseudo-*VPL* algorithm over the present algorithm. Each table lists the averaged system performance after the combined *VPL* and *VPE* filtering is applied.

As mentioned in Section 3.3, the performance metrics are defined in a statistical sense. Since it is impossible to have the performance metrics as strictly defined in the WAAS MOPS, the averaging-over-certain-period-of-time performance is used. For each case there is about 24 hours worth of data. I used a time interval of 30 minutes to do the averaging. This 30-minute interval was chosen so that for each case reasonable-sized tables could be generated and the reported performance could remain close to the strictly defined one. There are 9000 data samples for each interval. Thus, these data sets are large enough to ensure that the calculated performance is close to the actual performance.

For every case there are four tables that present the following performance metrics: CAT I Availability, CAT I Un-Availability, CAT I Misleading Information (MI) and CAT I Hazardously Misleading Information (HMI). These metrics are defined in the seven-section triangle chart in Fig. 3.1 as area 1 (CAT I Availability), area 3 (Un-Availability), area 4+5+6 (Misleading Information (MI)), and area 7 (Hazardously Misleading Information (HMI)). Area 2 is not directly related to CAT I precision approach thus is not listed here. Each table contains three columns that present:

1. Performance before the pseudo-*VPL* algorithm is applied;
2. Performance after the pseudo-*VPL* algorithm is applied;
3. Relative change between the before and after performance. Defined as

$$Column\ 3 = \frac{Column\ 2 - Column\ 1}{Column\ 1} \quad (5.1)$$

In certain cases, column three has no physical meanings because datum in column one is nearly zero. When this happens, column three has a value of NaN, which stands for

“Not a Number” and is the result of zero divided by zero or infinity divided by infinity. Although this NaN doesn’t provide much information for us except that there is not much change before and after the pseudo-*VPL* algorithm is applied, I kept them in for the reason of keeping the tables in each case to appear consistent. In the majority of the cases from our WAAS data archive, this problem does not occur and one can get some insight into the averaged system performance.

**Case 1: Dec. 1<sup>st</sup>, 1999**

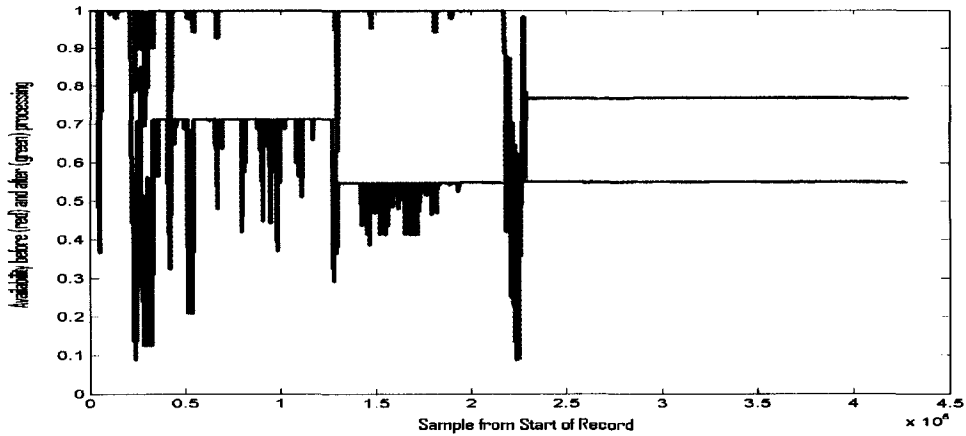


**Figure 5.11 Case 1 CAT I PA Availability before (red) and after (green) processing.**

**Table 5.1 Case 1 Cat I Availability Performance comparison.**

CAT I Avai Before	CAT I Avai After	Rela. Change	CAT I Avai Before	CAT I Avai After	Rela. Change
0.996256705	1	0.00375736	0.547908025	0.88982716	0.624044767
0.921588889	0.999559259	0.084604286	0.548482716	0.547012222	-0.002681021
0.957779012	0.998216049	0.04221959	0.550003086	0.768648025	0.397534021
0.354298148	0.91470679	1.581743074	0.550437654	0.768872222	0.396837982
0.615676543	0.987851728	0.604497913	0.55102284	0.768888889	0.395384789
0.67725	0.93260321	0.377044238	0.54931358	0.768742593	0.399460382
0.582081481	0.991814321	0.703909766	0.549038272	0.768272099	0.399305182
0.698658025	0.992561975	0.420669255	0.549243827	0.768660988	0.399489534
0.711151852	1	0.406169438	0.549900617	0.769810617	0.399908625
0.6961	1	0.436575205	0.549995679	0.77	0.400010999
0.687915432	1	0.453667055	0.549946296	0.77	0.400136714
0.66947716	1	0.493702936	0.549646914	0.769992593	0.400885866
0.694453704	1	0.4399808	0.549762963	0.77	0.400603627

0.712092593	1	0.404311757	0.55	0.77	0.4
0.645302469	0.958790617	0.485800323	0.55	0.77	0.4
0.547777778	0.999425185	0.824508452	0.54997284	0.77	0.400069139
0.537940741	0.99518716	0.849994033	0.549843827	0.769998765	0.400395398
0.536723457	1	0.863156878	0.549504321	0.769938272	0.401150532
0.539337654	1	0.85412606	0.55007284	0.769991605	0.399799353
0.520590123	1	0.920896988	0.550812346	0.769941481	0.39782902
0.541741975	0.994235432	0.835256409	0.550924074	0.77	0.397651757
0.547617284	0.997824691	0.822120522	0.54952963	0.768910247	0.399215266
0.548691358	0.999673704	0.821923544	0.548969753	0.76881284	0.400464844
0.548706173	1	0.822469018	0.548956173	0.769381605	0.401535574

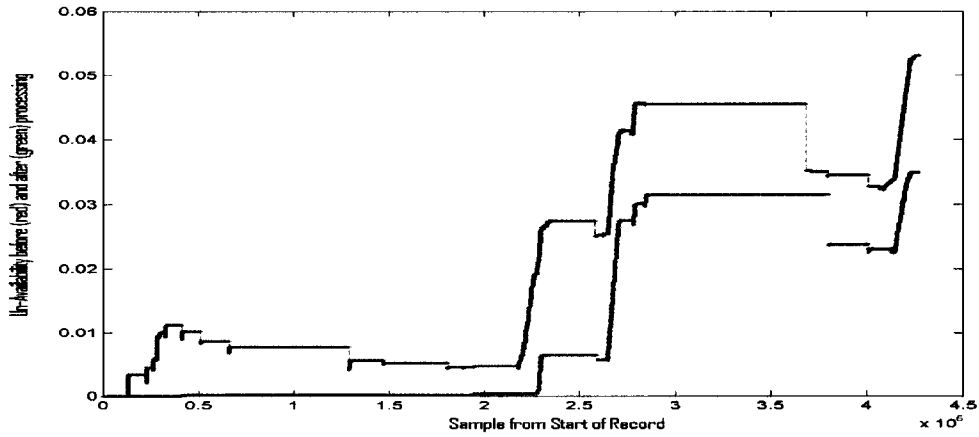


Figure 5.12 Case 1 CAT I PA Un-Availability before (red) and after (green) processing.

Table 5.2 Case 1 Un-Availability Performance comparison.

Un-Avai Before	Un-Avai After	Rela. Change	Un-Avai Before	Un-Avai After	Rela. Change
0	0	NaN	0.005071189	0.000365102	-0.92800458
0.000071303	0	-1	0.015447453	0.000542958	-0.964851309
0.003412969	0	-1	0.027044918	0.006312627	-0.766587308
0.00650164	0	-1	0.027502228	0.00640025	-0.76728247
0.011038605	0	-1	0.027502228	0.00640025	-0.76728247
0.010378936	0.000107989	-0.989595349	0.025854269	0.005987797	-0.768402009
0.009015992	0.000121004	-0.986578975	0.03757498	0.02170263	-0.422418044
0.00854104	0.00013642	-0.984027672	0.043611045	0.028734915	-0.341109225
0.00784432	0.000227114	-0.971047277	0.045588818	0.031277971	-0.313911344
0.00784432	0.000227114	-0.971047277	0.04557011	0.031487384	-0.309034276
0.00784432	0.000227114	-0.971047277	0.04557011	0.031487384	-0.309034276
0.00784432	0.000227114	-0.971047277	0.04557011	0.031487384	-0.309034276
0.00784432	0.000227114	-0.971047277	0.04557011	0.031487384	-0.309034276
0.00784432	0.000227114	-0.971047277	0.04557011	0.031487384	-0.309034276
0.00740024	0.000227114	-0.969309855	0.04557011	0.031487384	-0.309034276
0.005673047	0.000227114	-0.95996606	0.04557011	0.031487384	-0.309034276
0.005620071	0.000214706	-0.961796525	0.04557011	0.031487384	-0.309034276
0.005301434	0.000135933	-0.974359149	0.040006867	0.031487384	-0.212950516
0.005301434	0.000135933	-0.974359149	0.03485013	0.029400171	-0.156382746

0.005301434	0.000135933	-0.974359149	0.034486479	0.023748868	-0.311357124
0.005016394	0.000135933	-0.972902192	0.034486479	0.023748868	-0.311357124
0.004622827	0.000135933	-0.970595206	0.032704208	0.023170374	-0.291517053
0.004767023	0.000337256	-0.92925234	0.035358208	0.024166032	-0.316536858
0.004782475	0.000365102	-0.923658269	0.05022525	0.033629982	-0.330416834

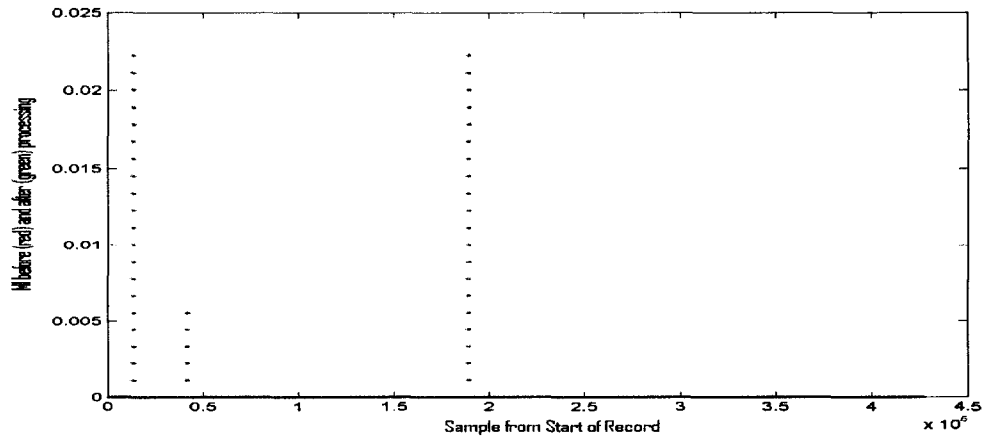


Figure 5. 13 Case 1 CAT I PA Misleading Information (MI) before (red) and after (green) processing.

Table 5. 3 Case 1 Misleading Information (MI) Performance comparison.

MI Before	MI After	Rela. Change	MI Before	MI After	Rela. Change
0	0	NaN	0	0	NaN
0	0.000440741	NaN	0	0	NaN
0	0.001783951	NaN	0	0	NaN
0	0	NaN	0	0	NaN
0	0	NaN	0	0	NaN
0	0.000556173	NaN	0	0	NaN
0	0	NaN	0	0	NaN
0	0	NaN	0	0	NaN
0	0	NaN	0	0	NaN
0	0	NaN	0	0	NaN
0	0	NaN	0	0	NaN
0	0	NaN	0	0	NaN
0	0	NaN	0	0	NaN
0	0	NaN	0	0	NaN
0	0	NaN	0	0	NaN
0	0	NaN	0	0	NaN
0	0	NaN	0	0	NaN
0	0	NaN	0	0	NaN
0	0	NaN	0	0	NaN
0	0	NaN	0	0	NaN
0	0	NaN	0	0	NaN
0	0.002175309	NaN	0	0	NaN
0	0	NaN	0	0	NaN
0	0	NaN	0	0	NaN



Case 2: Apr. 28th, 2000

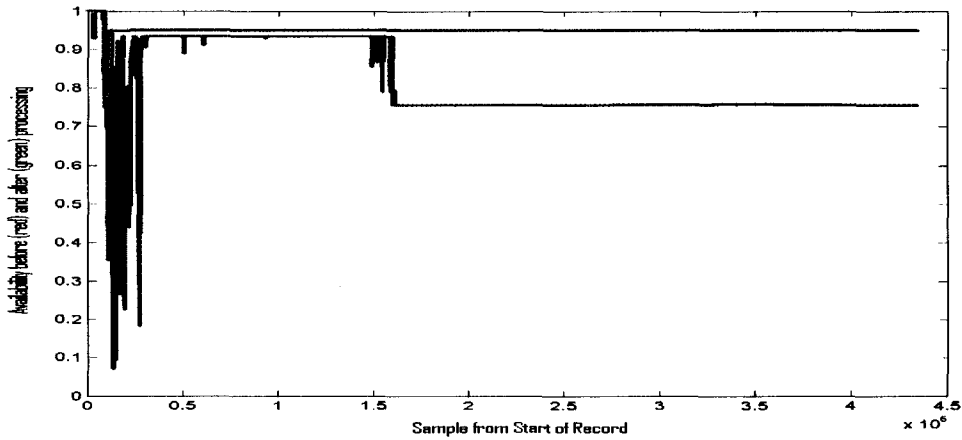


Figure 5. 15 Case 2 CAT I PA Availability before (red) and after (green) processing.

Table 5. 5 Case 2 Cat I Availability Performance comparison.

CAT I Avai Before	CAT I Avai After	Rela. Change	CAT I Avai Before	CAT I Avai After	Rela. Change
1	1	0	0.755554074	0.948886667	0.255881874
0.894822222	0.96095963	0.073911226	0.755555556	0.948888889	0.255882353
0.57270716	0.947777778	0.654908203	0.755555556	0.948888889	0.255882353
0.745559506	0.948676667	0.27243588	0.755555556	0.94888716	0.255880065
0.931216049	0.948888889	0.018978238	0.755555556	0.948888889	0.255882353
0.933333333	0.948888889	0.016666667	0.755548765	0.948885309	0.255888901
0.929945679	0.948888889	0.020370233	0.755555556	0.948888889	0.255882353
0.931639506	0.948888889	0.018515083	0.756247654	0.948884568	0.254727287
0.933333333	0.948888889	0.016666667	0.756666667	0.948888889	0.254038179
0.933333333	0.948888889	0.016666667	0.756662963	0.948888889	0.254044317
0.933333333	0.948888642	0.016666402	0.756666049	0.948888889	0.254039202
0.932937654	0.948887037	0.017095872	0.756666667	0.948888642	0.254037853
0.933333333	0.948888889	0.016666667	0.756666667	0.948888889	0.254171188
0.933333333	0.948888889	0.016666667	0.757582469	0.948888889	0.252522237
0.933333333	0.948888889	0.016666667	0.757775309	0.948888889	0.252203494
0.933333333	0.948888889	0.016666667	0.757777778	0.948888889	0.252199413
0.933333333	0.948888889	0.016666667	0.757437901	0.948878272	0.252747281
0.917397531	0.948888889	0.03432684	0.756661728	0.948888889	0.254046363
0.843115062	0.949181235	0.125802726	0.756641975	0.948888889	0.254079102
0.754520741	0.948888889	0.257604778	0.756666667	0.948888889	0.254038179
0.755544444	0.948877901	0.255886279	0.75600679	0.948872346	0.255110877
0.755546296	0.948881358	0.255887776	0.755554938	0.948888889	0.255883379
0.755530247	0.948888889	0.255924422	0.755326173	0.948888889	0.256263748
0.755555556	0.948888889	0.255882353	0.75555037	0.948888889	0.255890972
			0.75555	0.948888889	0.255891587

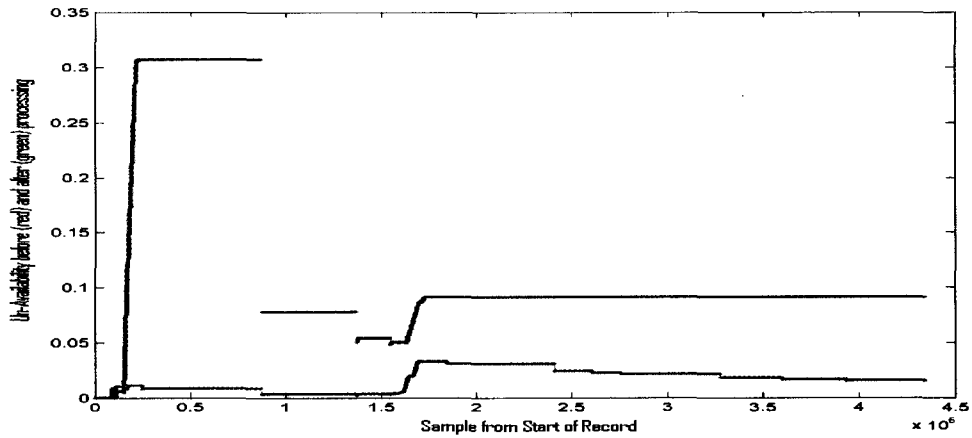


Figure 5. 16 Case 2 CAT I PA Un-Availability before (red) and after (green) processing.

Table 5. 6 Case 2 Un-Availability Performance comparison.

Un-Avai Before	Un-Avai After	Rela. Change	Un-Avai Before	Un-Avai After	Rela. Change
0	0	NaN	0.030912428	0.090932756	1.941624496
0.002134355	0.00024567	-0.884897276	0.030912428	0.090932756	1.941624496
0.010283627	0.07926888	6.708260879	0.030912428	0.090932756	1.941624496
0.010033374	0.30127053	29.02684103	0.027762394	0.090932756	2.275393213
0.008568127	0.30641049	34.76166708	0.02395428	0.090932756	2.796096468
0.008568127	0.30641049	34.76166708	0.023439149	0.090932756	2.879524692
0.008568127	0.30641049	34.76166708	0.022372155	0.090932756	3.064550616
0.008568127	0.30641049	34.76166708	0.021740894	0.090932756	3.182567401
0.008568127	0.30641049	34.76166708	0.021371986	0.090932756	3.254764043
0.008568127	0.30641049	34.76166708	0.021371986	0.090932756	3.254764043
0.005558282	0.183382171	31.99259989	0.021371986	0.090932756	3.254764043
0.002971327	0.077499714	25.08252885	0.021371986	0.090932756	3.254764043
0.002971327	0.077499714	25.08252885	0.021371986	0.090932756	3.254764043
0.002971327	0.077499714	25.08252885	0.018595505	0.090932756	3.890039575
0.002971327	0.077499714	25.08252885	0.018037172	0.090932756	4.041408591
0.002971327	0.077499714	25.08252885	0.018037172	0.090932756	4.041408591
0.003161229	0.053224794	15.83674003	0.017621971	0.090932756	4.160192219
0.003193115	0.053176382	15.65345192	0.016680894	0.090932756	4.451311882
0.005939411	0.049963786	7.412245385	0.016680894	0.090932756	4.451311882
0.026914759	0.076546623	1.844038935	0.016680894	0.090932756	4.451311882
0.03281279	0.090932756	1.771259471	0.016048799	0.090932756	4.666016164
0.031402745	0.090932756	1.895694483	0.015622063	0.090932756	4.820790381
0.030912428	0.090932756	1.941624496	0.015622063	0.090932756	4.820790381
0.030912428	0.090932756	1.941624496	0.015622063	0.090932756	4.820790381

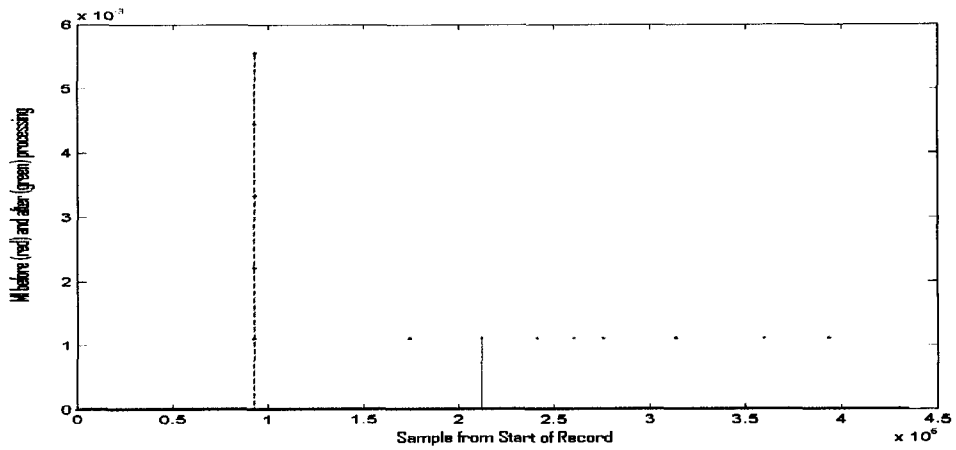


Figure 5. 17 Case 2 CAT I PA Misleading Information (MI) before (red) and after (green) processing.

Table 5. 7 Case 2 Misleading Information (MI) Performance comparison.

MI Before	MI After	Rela. Change	MI Before	MI After	Rela. Change
0	0	NaN	0.000001481	0.000002222	-0.999997778
0	0	NaN	0	0	NaN
0	0	NaN	0	0	NaN
0	0	NaN	0	0.000001728	NaN
0	0	NaN	0	0	NaN
0	0	NaN	0	0.000002963	NaN
0	0	NaN	0	0	NaN
0	0	NaN	0	0.000004321	NaN
0	0	NaN	0	0	NaN
0	0	NaN	0	0	NaN
0	0.000000247	NaN	0	0	NaN
0.000395679	0.000001852	-0.999998148	0	0.000000247	NaN
0	0	NaN	0	0	NaN
0	0	NaN	0	0	NaN
0	0	NaN	0	0	NaN
0	0	NaN	0	0	NaN
0	0	NaN	0	0.000002469	NaN
0	0	NaN	0	0	NaN
0	0	NaN	0	0	NaN
0	0	NaN	0	0	NaN
0	0.000010988	NaN	0	0.000008765	NaN
0	0	NaN	0	0	NaN
0	0	NaN	0	0	NaN
0	0	NaN	0	0	NaN
0	0	NaN	0	0	NaN



Case 3: Nov. 27th, 2000

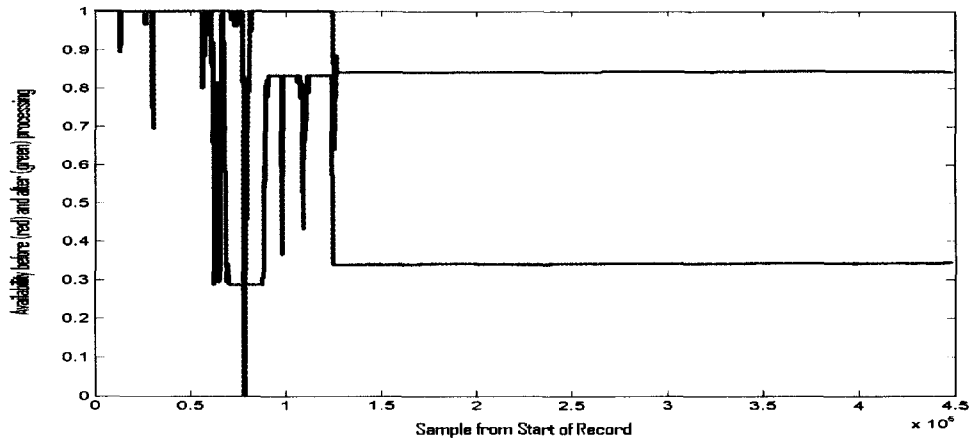


Figure 5. 19 Case 3 CAT I PA Availability before (red) and after (green) processing.

Table 5. 9 Case 3 Cat I Availability Performance comparison.

CAT I Avai Before	CAT I Avai After	Rela. Change	CAT I Avai Before	CAT I Avai After	Rela. Change
1	1	0	0.339505556	0.84111	1.477455777
0.989432716	1	0.010680144	0.339741852	0.84105321	1.475565507
1	1	0	0.341111111	0.841111111	1.465798046
0.987293827	0.969521728	-0.01800082	0.341111111	0.841111111	1.465798046
1	1	0	0.341412222	0.841470247	1.464675229
1	1	0	0.342216049	0.842222222	1.461083353
0.976654938	1	0.023903081	0.342222222	0.842222222	1.461038961
0.612639012	1	0.6322826	0.341708148	0.842222222	1.464741408
0.289430864	0.87715963	2.030636114	0.341540741	0.842222222	1.46594951
0.287777778	0.901060741	2.131099099	0.341965309	0.842222222	1.462887904
0.766593704	1	0.304471971	0.342118025	0.842222222	1.46178851
0.806055556	1	0.240609277	0.341687531	0.842041235	1.464360442
0.779080864	1	0.283563807	0.342222222	0.842142346	1.460805556
0.833333333	1	0.2	0.343025185	0.84323284	1.458224282
0.371467284	0.844653457	1.273830007	0.343298765	0.843333333	1.456558014
0.338888889	0.840670617	1.480667395	0.343333333	0.843333333	1.45631068
0.339151852	0.841111111	1.480042808	0.343333333	0.843333333	1.45631068
0.338907407	0.841111111	1.481831594	0.343333333	0.843333333	1.45631068
0.339935679	0.841111111	1.4743243	0.343333333	0.843333333	1.45631068
0.340804815	0.840965309	1.467586349	0.343042593	0.843332346	1.458389611
0.341195062	0.840328889	1.462898744	0.343333333	0.843333333	1.45631068
0.341885185	0.841096173	1.460171453	0.343333333	0.843333333	1.45631068
0.340647654	0.841093333	1.469100617	0.343035309	0.842599753	1.456306193
0.34	0.841111111	1.473856209	0.343198025	0.842222222	1.454041578
0.339916667	0.841111111	1.474462695	0.343717778	0.841835432	1.449205385

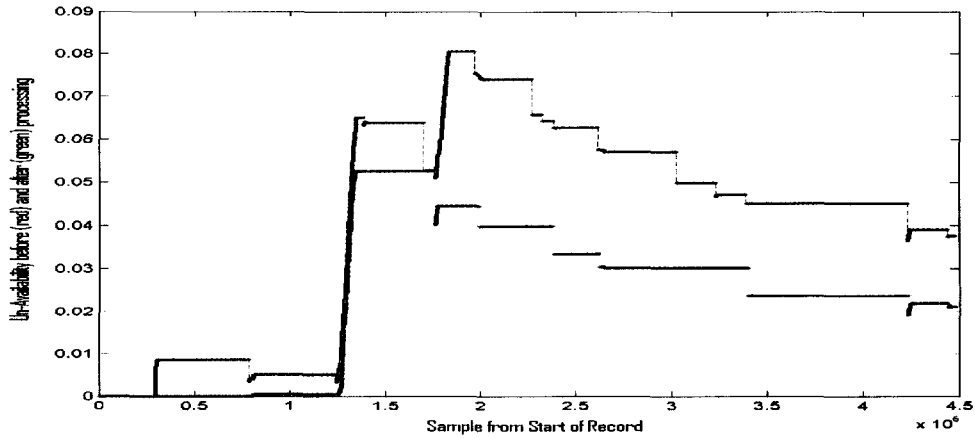


Figure 5. 20 Case 3 CAT I PA Un-Availability before (red) and after (green) processing.

Table 5. 10 Case 3 Un-Availability Performance comparison.

Un-Avai Before	Un-Avai After	Rela. Change	Un-Avai Before	Un-Avai After	Rela. Change
1	0	NaN	0.339505556	0.039821414	-0.425984745
0.989432716	0	NaN	0.339741852	0.038048735	-0.404215262
1	0	NaN	0.341111111	0.033429586	-0.466446536
0.987293827	0	-1	0.341111111	0.033429586	-0.466446536
1	0	-1	0.341412222	0.031600987	-0.464024243
1	0	-1	0.342216049	0.030142574	-0.471209823
0.976654938	0	-1	0.342222222	0.030142574	-0.471209823
0.612639012	0	-1	0.341708148	0.030142574	-0.471209823
0.289430864	0	-1	0.341540741	0.030142574	-0.462970585
0.287777778	0.000321017	-0.932955913	0.341965309	0.030142574	-0.396008996
0.766593704	0.000443088	-0.912143248	0.342118025	0.030142574	-0.396008996
0.806055556	0.000443088	-0.912143248	0.341687531	0.030142574	-0.368450246
0.779080864	0.000443088	-0.912143248	0.342222222	0.030142574	-0.358918079
0.833333333	0.000443088	-0.912143248	0.343025185	0.023980034	-0.469175429
0.371467284	0.01660538	-0.255289158	0.343298765	0.023601039	-0.477616727
0.338888889	0.052166726	-0.178349896	0.343333333	0.023601039	-0.477616727
0.339151852	0.05263197	-0.176800242	0.343333333	0.023601039	-0.477616727
0.338907407	0.05263197	-0.176800242	0.343333333	0.023601039	-0.477616727
0.339935679	0.05263197	-0.176800242	0.343333333	0.023601039	-0.477616727
0.340804815	0.051369131	-0.061352998	0.343042593	0.023601039	-0.477616727
0.341195062	0.044470955	-0.387583637	0.343333333	0.023601039	-0.477616727
0.341885185	0.044468237	-0.447201436	0.343333333	0.023601039	-0.477616727
0.340647654	0.041887423	-0.442074048	0.343035309	0.022099327	-0.454594976
0.34	0.039821414	-0.462390851	0.343198025	0.021844002	-0.44223263
0.339916667	0.039821414	-0.462390851	0.343717778	0.021530718	-0.441245768





**Case 4: May. 1st, 2001**

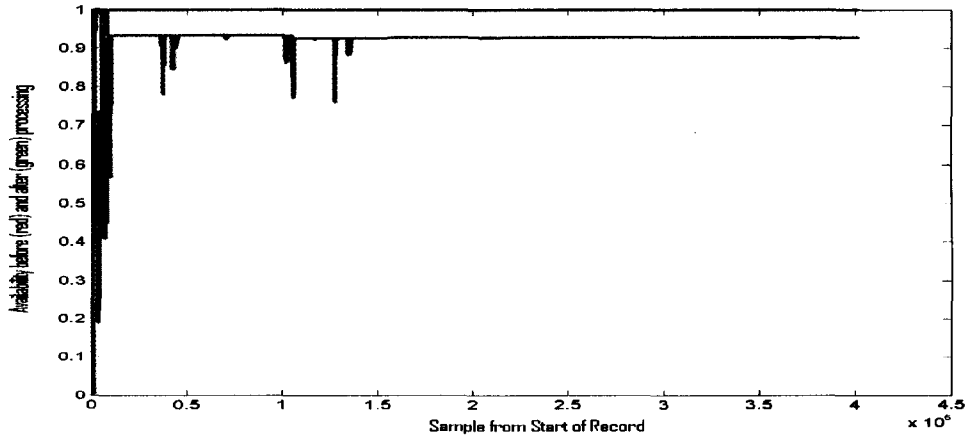


**Figure 5. 23 Case 4 CAT I PA Availability before (red) and after (green) processing.**

**Table 5. 13 Case 4 Cat I Availability Performance comparison.**

CAT I Avai Before	CAT I Avai After	Rela. Change	CAT I Avai Before	CAT I Avai After	Rela. Change
0.409457831	0.721177912	0.761299596	0.99906	0.926666667	-0.072461447
0.892427878	0.902281358	0.011041205	0.999994444	0.926666667	-0.073328185
1	0.932222222	-0.067777778	0.999930864	0.926666667	-0.073269263
0.99999321	0.932222222	-0.067771448	0.999106667	0.926666667	-0.072504771
0.999378272	0.922961481	-0.07646433	0.998888889	0.926663457	-0.072305772
0.998888889	0.927429383	-0.071538994	0.99958284	0.926666667	-0.072946603
0.999640864	0.932222222	-0.067442863	0.999983951	0.926658272	-0.073326856
1	0.932222222	-0.067777778	0.999932716	0.926666667	-0.073270979
0.999989506	0.931816049	-0.068174172	0.998971481	0.926553951	-0.07249209
0.999858642	0.932222222	-0.067645982	0.998888889	0.926666667	-0.072302558
1	0.932222222	-0.067777778	0.999197037	0.926666667	-0.072588656
0.999080741	0.926910247	-0.072236898	0.99937037	0.926666667	-0.072749509
0.999702469	0.915534198	-0.084193322	0.999868395	0.926666667	-0.073211363
0.99959321	0.925463086	-0.074160291	0.999209259	0.926666667	-0.0726
0.998888889	0.921058642	-0.077916821	0.999466667	0.926666667	-0.072838847
0.99924642	0.922857407	-0.076446621	0.99890679	0.926576914	-0.072409035
0.999957407	0.925555556	-0.074405021	0.998888889	0.926280123	-0.072689532
0.999636296	0.925891728	-0.073771399	0.999008642	0.926623951	-0.072456522
0.999924815	0.926666667	-0.073263656	0.998888889	0.926357037	-0.072612532
0.999980864	0.926590123	-0.073392145	0.999011728	0.926666667	-0.072416629
0.999990741	0.926666667	-0.073324753	0.343333333	0.843333333	1.45631068
0.999723333	0.926666667	-0.073076885	0.343333333	0.843333333	1.45631068
0.998982099	0.926592593	-0.072463267	0.343035309	0.842599753	1.456306193
0.998888889	0.926415062	-0.072554443	0.343198025	0.842222222	1.454041578
0.998888889	0.926458025	-0.072511432	0.343717778	0.841835432	1.449205385

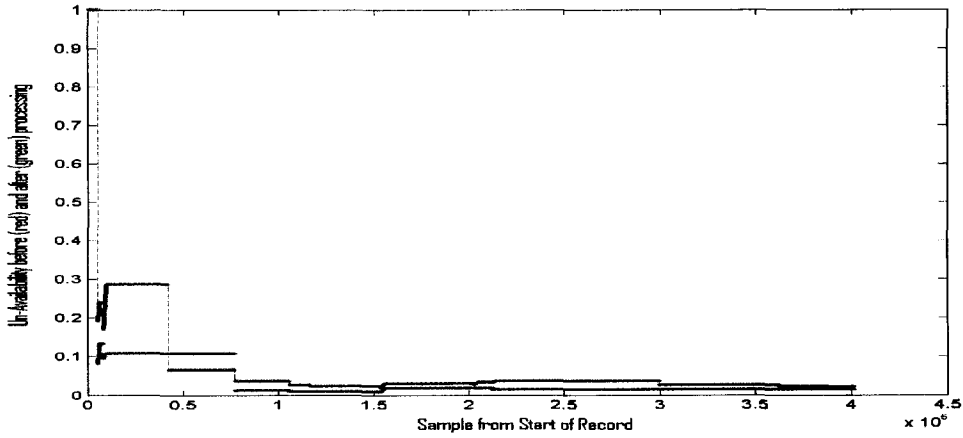


Figure 5. 24 Case 4 CAT I PA Un-Availability before (red) and after (green) processing.

Table 5. 14 Case 4 Un-Availability Performance comparison.

Un-Avai Before	Un-Avai After	Rela. Change	Un-Avai Before	Un-Avai After	Rela. Change
1	1	0	0.036904056	0.015970412	-0.567245077
0.276481225	0.133600023	-0.516784467	0.036904056	0.015970412	-0.567245077
0.286429143	0.108297583	-0.621904455	0.036904056	0.015970412	-0.567245077
0.286429143	0.108297583	-0.621904455	0.036904056	0.015970412	-0.567245077
0.286429143	0.108297583	-0.621904455	0.036904056	0.015970412	-0.567245077
0.092892453	0.108297583	0.165838339	0.036904056	0.015970412	-0.567245077
0.067634553	0.108297583	0.601216816	0.036904056	0.015970412	-0.567245077
0.067634553	0.108297583	0.601216816	0.036904056	0.015970412	-0.567245077
0.065811379	0.102538477	0.558066065	0.03420468	0.015970412	-0.533092789
0.037868454	0.013899895	-0.632942641	0.028490671	0.015970412	-0.439451187
0.037868454	0.013899895	-0.632942641	0.028490671	0.015970412	-0.439451187
0.037868454	0.013899895	-0.632942641	0.028490671	0.015970412	-0.439451187
0.029245927	0.010808347	-0.630432397	0.028490671	0.015970412	-0.439451187
0.026263971	0.009873793	-0.624055577	0.028490671	0.015970412	-0.439451187
0.025525822	0.009680351	-0.620762405	0.028490671	0.015970412	-0.439451187
0.025525822	0.009680351	-0.620762405	0.026792355	0.015970412	-0.403919068
0.025525822	0.009680351	-0.620762405	0.02405613	0.015970412	-0.336118817
0.027646888	0.013888562	-0.49764464	0.023724746	0.015970412	-0.326845824
0.032278981	0.020402137	-0.367943596	0.023309322	0.015970412	-0.31484872
0.032139373	0.020402137	-0.365198045	0.023128519	0.015970412	-0.309492677
0.032118125	0.020402137	-0.364778089	0.045179546	0.023601039	-0.477616727
0.032118125	0.020402137	-0.364778089	0.045179546	0.023601039	-0.477616727
0.031928243	0.020402137	-0.361000332	0.040519112	0.022099327	-0.454594976
0.03408043	0.020296889	-0.404441541	0.039163285	0.021844002	-0.44223263
0.036794301	0.015970258	-0.565958389	0.038533431	0.021530718	-0.441245768





Case 5: Nov. 12th, 2001

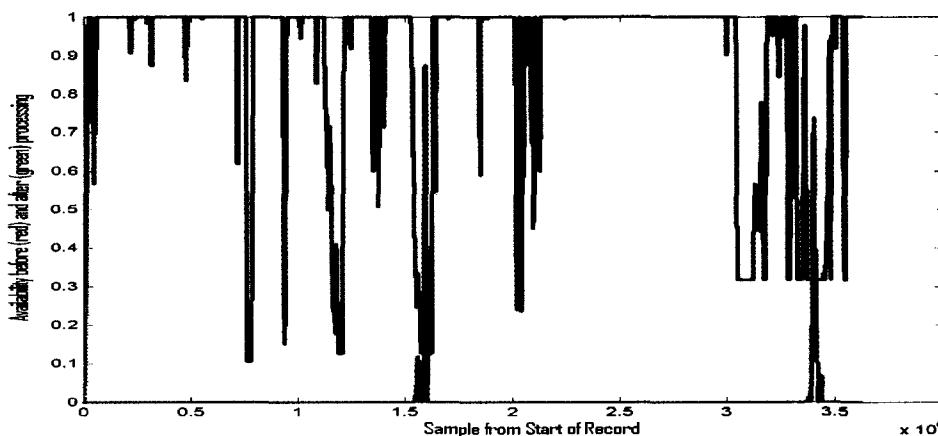


Figure 5. 27 Case 5 CAT I PA Availability before (red) and after (green) processing.

Table 5. 17 Case 5 Cat I Availability Performance comparison.

CAT I Avai Before	CAT I Avai After	Rela. Change	CAT I Avai Before	CAT I Avai After	Reia. Change
0.418901742	0	-1	0.999548765	0	-1
0.935483951	0	-1	1	0	-1
1	0	-1	1	0	-1
0.989988889	0	-1	1	0	-1
0.985662963	0	-1	1	0	-1
0.995564815	0	-1	1	0	-1
0.987672222	0	-1	1	0	-1
1	0	-1	1	0	-1
0.96567037	0	-1	0.998453086	0	-1
0.716904938	0	-1	0.675561235	0	-1
1	0	-1	0.438767284	0	-1
0.878761728	0	-1	0.946107284	0	-1
0.984917284	0	-1	0.61424642	0	-1
0.536017407	0	-1	0.36685	0.14010037	-0.618099031
0.847797407	0	-1	0.787567778	0	-1
0.91258284	0	-1	0.904274074	0	-1
0.950109753	0	-1	0.998888889	0.926280123	-0.072689532
0.858035926	0.006422593	-0.992514774	0.999008642	0.926623951	-0.072456522
0.297256667	0.131253827	-0.558449509	0.998888889	0.926357037	-0.072612532
0.999514815	0	-1	0.999011728	0.926666667	-0.072416629
1	0	-1	0.343333333	0.843333333	1.45631068
0.966157407	0	-1	0.343333333	0.843333333	1.45631068
1	0	-1	0.343035309	0.842599753	1.456306193
0.775574074	0	-1	0.343198025	0.842222222	1.454041578
0.915330247	0	-1	0.343717778	0.841835432	1.449205385

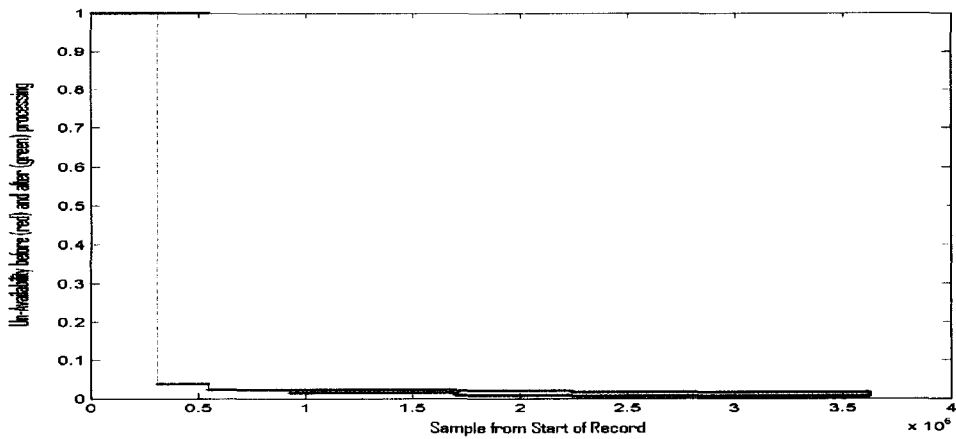


Figure 5. 28 Case 5 CAT I PA Un-Availability before (red) and after (green) processing.

Table 5. 18 Case 5 Un-Availability Performance comparison.

Un-Avai Before	Un-Avai After	Rela. Change	Un-Avai Before	Un-Avai After	Rela. Change
1	1	0	0.007423421	0.018849051	1.539132665
1	1	0	0.006537026	0.016195271	1.477467674
1	1	0	0.006537026	0.016195271	1.477467674
1	1	0	0.006537026	0.016195271	1.477467674
0.217116546	1	3.60582124	0.006537026	0.016195271	1.477467674
0.038621661	1	24.89220564	0.006537026	0.016195271	1.477467674
0.035909695	0.83232855	22.17837968	0.006537026	0.016195271	1.477467674
0.023191145	0.022011778	-0.050854186	0.006537026	0.016195271	1.477467674
0.023191145	0.022011778	-0.050854186	0.006537026	0.016195271	1.477467674
0.023191145	0.022011778	-0.050854186	0.006537026	0.016195271	1.477467674
0.023191145	0.022011778	-0.050854186	0.006537026	0.016195271	1.477467674
0.014219288	0.022011778	0.548022562	0.006537026	0.016195271	1.477467674
0.013962358	0.022011778	0.576508705	0.006537026	0.016195271	1.477467674
0.013962358	0.022011778	0.576508705	0.006537026	0.016195271	1.477467674
0.013962358	0.022011778	0.576508705	0.006537026	0.016195271	1.477467674
0.013962358	0.022011778	0.576508705	0.006537026	0.016194585	1.477362779
0.013962358	0.022011778	0.576508705	0.02405613	0.015970412	-0.336118817
0.013962358	0.022011778	0.576508705	0.023724746	0.015970412	-0.326845824
0.013962358	0.022011778	0.576508705	0.023309322	0.015970412	-0.31484872
0.011348876	0.019636383	0.730249102	0.023128519	0.015970412	-0.309492677
0.007962703	0.02045173	1.56844053	0.045179546	0.023601039	-0.477616727
0.007962703	0.02045173	1.56844053	0.045179546	0.023601039	-0.477616727
0.007962703	0.02045173	1.56844053	0.040519112	0.022099327	-0.454594976
0.007962703	0.02045173	1.56844053	0.039163285	0.021844002	-0.44223263
0.007962703	0.02045173	1.56844053	0.038533431	0.021530718	-0.441245768





**Case 6: May. 2nd, 2002**

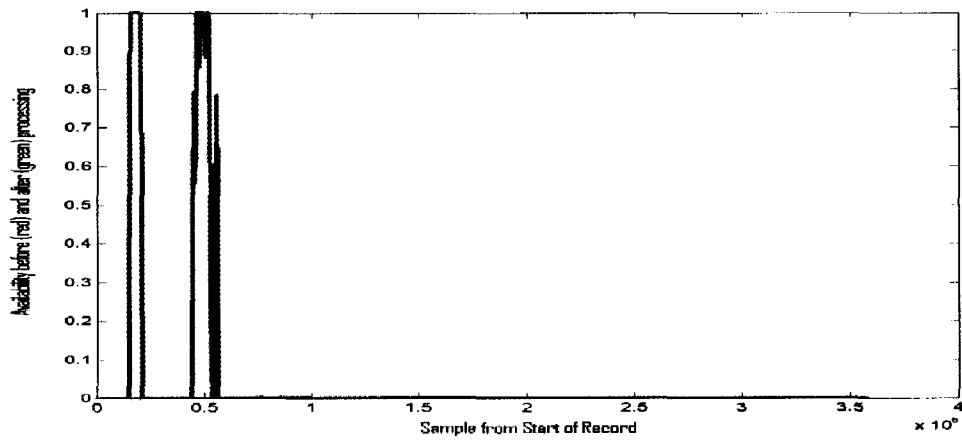


**Figure 5.31 Case 6 CAT I PA Availability before (red) and after (green) processing.**

**Table 5.21 Case 6 Cat I Availability Performance comparison.**

CAT I Avai Before	CAT I Avai After	Rela. Change	CAT I Avai Before	CAT I Avai After	Rela. Change
0	0	NaN	0	0	NaN
0	0.125387189	Inf	0	0	NaN
0	0.506277778	Inf	0	0	NaN
0	0	NaN	0	0	NaN
0	0	NaN	0	0	NaN
0	0.777144568	Inf	0	0	NaN
0	0.11904284	Inf	0	0	NaN
0	0	NaN	0	0	NaN
0	0.000224074	Inf	0	0	NaN
0	0.000301728	Inf	0	0	NaN
0	0.001060988	Inf	0	0	NaN
0	0.000162222	Inf	0	0	NaN
0	0	NaN	0	0	NaN
0	0	NaN	0	0	NaN
0	0.000018765	Inf	0	0	NaN
0	0.000611728	Inf	0.904274074	0	-1
0	0.00007716	Inf	0.998888889	0.926280123	-0.072689532
0	0	NaN	0.999008642	0.926623951	-0.072456522
0	0	NaN	0.998888889	0.926357037	-0.072612532
0	0	NaN	0.999011728	0.926666667	-0.072416629
0	0	NaN	0.343333333	0.843333333	1.45631068
0	0	NaN	0.343333333	0.843333333	1.45631068
0	0	NaN	0.343035309	0.842599753	1.456306193
0	0	NaN	0.343198025	0.842222222	1.454041578
0	0	NaN	0.343717778	0.841835432	1.449205385

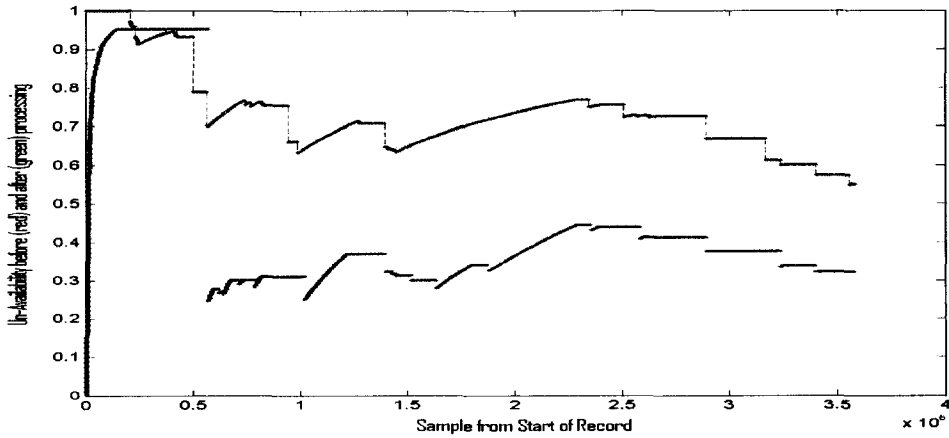


Figure 5. 32 Case 6 CAT I PA Un-Availability before (red) and after (green) processing.

Table 5. 22 Case 6 Un-Availability Performance comparison.

Un-Avai Before	Un-Avai After	Rela. Change	Un-Avai Before	Un-Avai After	Rela. Change
1	0.66967657	-0.33032343	0.766879408	0.439436765	-0.426980617
1	0.934497963	-0.065502037	0.756788635	0.439047145	-0.419854997
0.97087911	0.95053148	-0.020957944	0.755400075	0.439126563	-0.418683453
0.926477208	0.95053148	0.025963155	0.729945261	0.435211705	-0.403774874
0.940845875	0.95053148	0.010294571	0.726280627	0.41149171	-0.433426014
0.901061513	0.95053148	0.054901876	0.72667017	0.411559857	-0.433635955
0.746992253	0.638208233	-0.145629382	0.72667017	0.411559857	-0.433635955
0.738278349	0.282932975	-0.616766529	0.6889281	0.387814353	-0.437075722
0.758802507	0.298762067	-0.60627164	0.669136528	0.375362444	-0.439034594
0.756515802	0.30500703	-0.596826623	0.669136528	0.375362444	-0.439034594
0.726017765	0.309014599	-0.574370472	0.633282437	0.375362444	-0.407274823
0.647313054	0.287075414	-0.556512243	0.601578118	0.343824275	-0.428462797
0.671124928	0.306602526	-0.543151338	0.599031741	0.33665632	-0.437999196
0.695864952	0.356845038	-0.487192109	0.573139956	0.321961363	-0.438250012
0.708809711	0.369077921	-0.479299006	0.565736424	0.321961363	-0.430898649
0.688358582	0.354512155	-0.484989126	0.006537026	0.016194585	1.477362779
0.641519592	0.313485322	-0.511339442	0.02405613	0.015970412	-0.336118817
0.660092941	0.300107571	-0.545355582	0.023724746	0.015970412	-0.326845824
0.678670235	0.292810255	-0.568552973	0.023309322	0.015970412	-0.31484872
0.695321682	0.317654735	-0.54315428	0.023128519	0.015970412	-0.309492677
0.710332051	0.339832507	-0.52158641	0.045179546	0.023601039	-0.477616727
0.723932596	0.337573875	-0.533694328	0.045179546	0.023601039	-0.477616727
0.73631306	0.365936735	-0.503014744	0.040519112	0.022099327	-0.454594976
0.747630599	0.393150959	-0.474137416	0.039163285	0.021844002	-0.44223263
0.758016482	0.418124917	-0.448396008	0.038533431	0.021530718	-0.441245768





Case 7: Oct. 12th, 2002

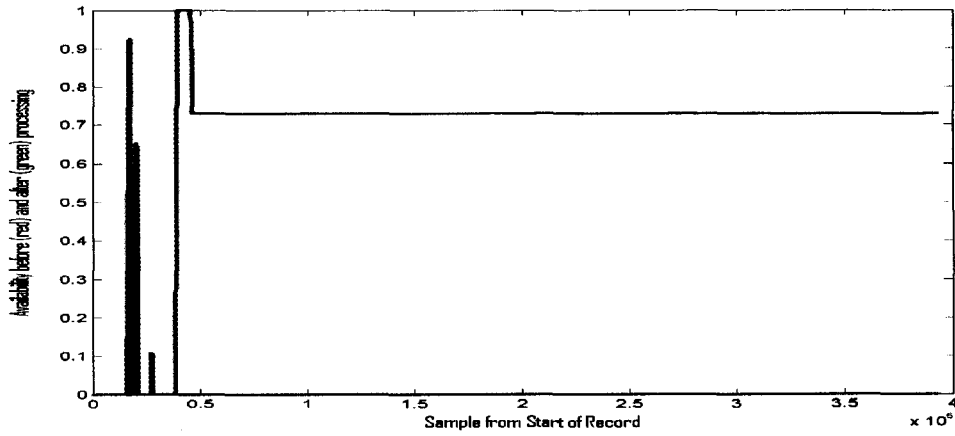


Figure 5. 35 Case 7 CAT I PA Availability before (red) and after (green) processing.

Table 5. 25 Case 7 Cat I Availability Performance comparison.

CAT I Avai Before	CAT I Avai After	Rela. Change	CAT I Avai Before	CAT I Avai After	Rela. Change
0	0	NaN	0	0.728603457	Inf
0	0	NaN	0	0.727777778	Inf
0	0.219577037	Inf	0	0.727777778	Inf
0	0.010678519	Inf	0	0.727777778	Inf
0	0.342277778	Inf	0	0.727777778	Inf
0	0.849012469	Inf	0	0.728510617	Inf
0	0.727777778	Inf	0	0.728232222	Inf
0	0.727777778	Inf	0	0.727777778	Inf
0	0.727777778	Inf	0	0.727883704	Inf
0	0.727777778	Inf	0	0.728736173	Inf
0	0.727777778	Inf	0	0.728314444	Inf
0	0.728066914	Inf	0	0.727777778	Inf
0	0.727777778	Inf	0	0.727777778	Inf
0	0.727777778	Inf	0	0.727777778	Inf
0	0.727777778	Inf	0	0.727777778	Inf
0	0.727777778	Inf	0	0.72778272	Inf
0	0.727777778	Inf	0	0.727777778	Inf
0	0.727777778	Inf	0	0.727777778	Inf
0	0.727777778	Inf	0	0.727777778	Inf
0	0.727777778	Inf	0	0.727777778	Inf
0	0.727777778	Inf	0	0.728555556	Inf
0	0.727777778	Inf	0.999011728	0.926666667	-0.072416629
0	0.728223827	Inf	0.343333333	0.843333333	1.45631068
0	0.728654815	Inf	0.343333333	0.843333333	1.45631068
0	0.727777778	Inf	0.343035309	0.842599753	1.456306193
0	0.728609877	Inf	0.343198025	0.842222222	1.454041578
0	0.728888889	Inf	0.343717778	0.841835432	1.449205385

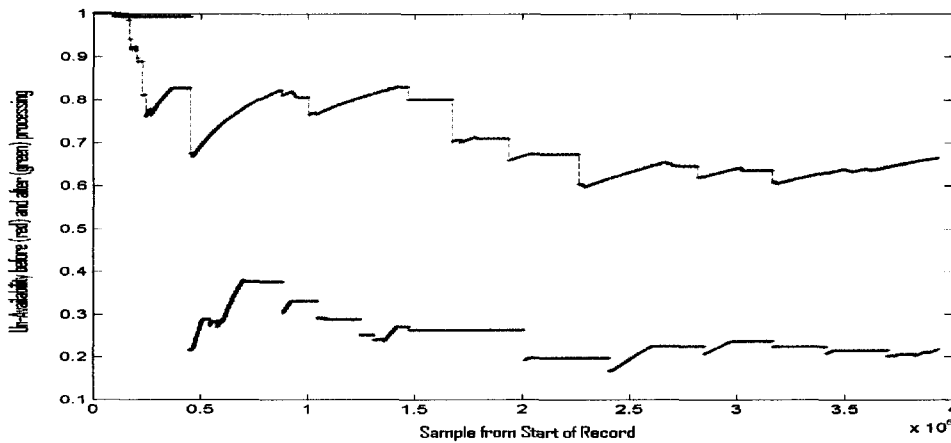


Figure 5.36 Case 7 CAT I PA Un-Availability before (red) and after (green) processing.

Table 5.26 Case 7 Un-Availability Performance comparison.

Un-Avai Before	Un-Avai After	Reia. Change	Un-Avai Before	Un-Avai After	Reia. Change
1	1	0	0.636982318	0.196733898	-0.691147002
1	0.995494665	-0.004505335	0.608665834	0.196733898	-0.676778476
0.914260821	0.992384481	0.08545008	0.623074236	0.178071728	-0.714204636
0.784946674	0.992384481	0.264269935	0.636459212	0.203561341	-0.680165928
0.823119376	0.992384481	0.205638587	0.648798657	0.224105099	-0.654584521
0.734285328	0.516544837	-0.296533899	0.647796972	0.225191264	-0.652373701
0.721827238	0.283680774	-0.606996302	0.636204693	0.225191264	-0.646039606
0.760780369	0.327880928	-0.569020257	0.627956458	0.217011878	-0.654415724
0.790152159	0.376370083	-0.523673917	0.63807207	0.235110282	-0.631530209
0.813093108	0.376130862	-0.53740739	0.636418371	0.236360826	-0.628607789
0.814930878	0.330004368	-0.595052321	0.621723964	0.229654116	-0.630617237
0.788104309	0.328427808	-0.583268605	0.613533085	0.223047834	-0.636453453
0.778783597	0.288923147	-0.629007149	0.623932648	0.223047834	-0.642512962
0.795602037	0.287678829	-0.63841366	0.632651671	0.215533258	-0.65931765
0.810042863	0.255401014	-0.68470679	0.635987887	0.214732324	-0.662364129
0.822577143	0.24684578	-0.699911696	0.638227848	0.214732324	-0.663549115
0.81992402	0.26736213	-0.673918408	0.644449752	0.207080912	-0.678670197
0.801375121	0.261195856	-0.674065429	0.65288263	0.204560412	-0.686681185
0.796418436	0.261195856	-0.672036904	0.660924738	0.210795756	-0.681059364
0.70641739	0.261195856	-0.630252794	0.023128519	0.015970412	-0.309492677
0.710028423	0.261195856	-0.632133239	0.045179546	0.023601039	-0.477616727
0.701459275	0.261195856	-0.627639315	0.045179546	0.023601039	-0.477616727
0.667774365	0.237865264	-0.643793957	0.040519112	0.022099327	-0.454594976
0.673905019	0.196733898	-0.708068804	0.039163285	0.021844002	-0.44223263
0.673905019	0.196733898	-0.708068804	0.038533431	0.021530718	-0.441245768

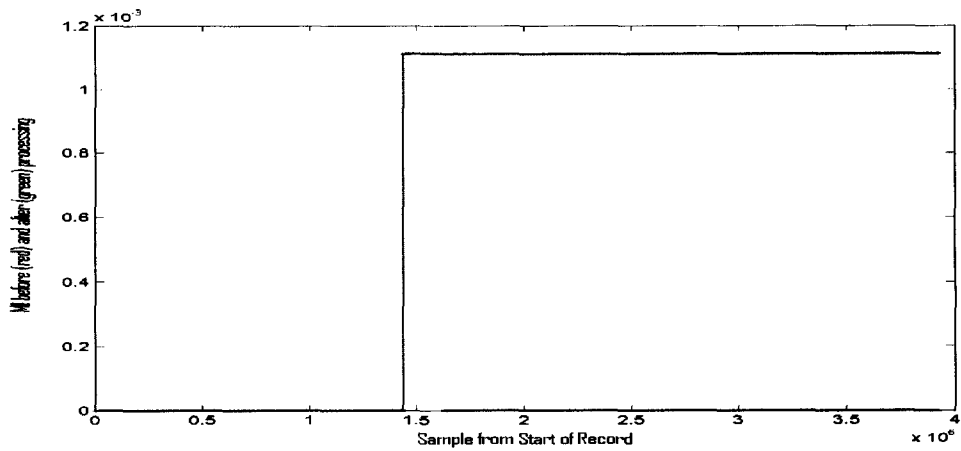


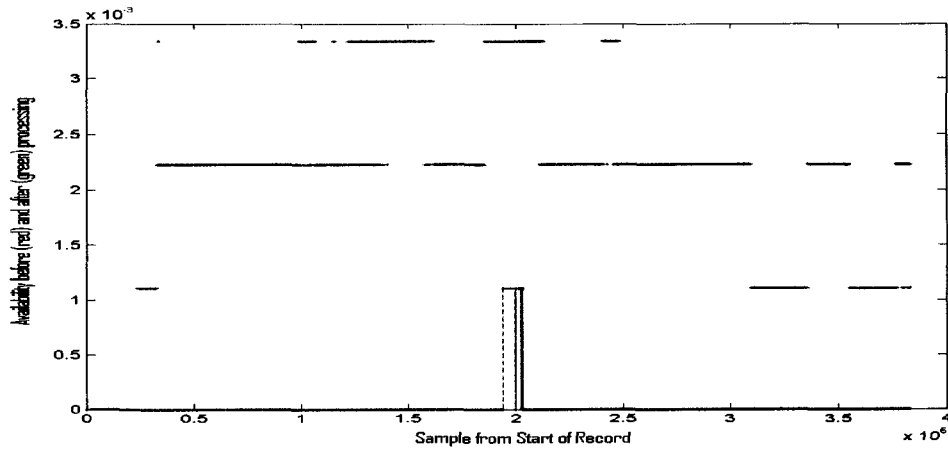
Figure 5. 37 Case 7 CAT I PA Misleading Information (MI) before (red) and after (green) processing.

Table 5. 27 Case 7 Misleading Information (MI) Performance comparison.

MI Before	MI After	Rela. Change	MI Before	MI After	Rela. Change
0	0	NaN	0.001111111	0	-1
0	0	NaN	0.001111111	0	-1
0	0	NaN	0.001111111	0	-1
0	0	NaN	0.001111111	0	-1
0	0	NaN	0.001111111	0	-1
0	0	NaN	0.001111111	0	-1
0	0	NaN	0.001111111	0	-1
0	0	NaN	0.001111111	0	-1
0	0	NaN	0.001111111	0	-1
0	0	NaN	0.001111111	0	-1
0	0	NaN	0.001111111	0	-1
0	0	NaN	0.001111111	0	-1
0	0	NaN	0.001111111	0	-1
0	0	NaN	0.001111111	0	-1
0	0	NaN	0.001111111	0	-1
0.000785185	0.000667407	-0.999332593	0.001111111	0	-1
0.001111111	0.001111111	-0.998888889	0.001111111	0	-1
0.001111111	0.000396049	-0.999603951	0.001111111	0	-1
0.001111111	0.000076049	-0.999923951	0	0	NaN
0.001111111	0	-1	0	0	NaN
0.001111111	0	-1	0	0	NaN
0.001111111	0	-1	0	0	NaN
0.001111111	0	-1	0	0	NaN
0.001111111	0	-1	0	0	NaN



**Case 8: Oct. 28th, 2002**



**Figure 5. 39 Case 8 CAT I PA Availability before (red) and after (green) processing.**

**Table 5. 29 Case 8 Cat I Availability Performance comparison.**

CAT I Avai Before	CAT I Avai After	Reia. Change	CAT I Avai Before	CAT I Avai After	Rela. Change
0	0	NaN	0	0.002222222	Inf
0	0	NaN	0	0.002222222	Inf
0	0	NaN	0	0.002871605	Inf
0	0.00097716	Inf	0	0.002227778	Inf
0	0.002091852	Inf	0	0.002222222	Inf
0	0.002222222	Inf	0	0.002222222	Inf
0	0.002222222	Inf	0	0.002222222	Inf
0	0.002222222	Inf	0	0.002222222	Inf
0	0.002222222	Inf	0	0.002222222	Inf
0	0.002222222	Inf	0	0.002222222	Inf
0	0.002222222	Inf	0	0.002013086	Inf
0	0.002222222	Inf	0	0.001111111	Inf
0	0.002771481	Inf	0	0.001111111	Inf
0	0.002518272	Inf	0	0.00140358	Inf
0	0.002289877	Inf	0	0.002222222	Inf
0	0.002920494	Inf	0	0.00209716	Inf
0	0.002925309	Inf	0	0.001111111	Inf
0	0.003326173	Inf	0	0.001111111	Inf
0	0.003333333	Inf	0	0.001772593	Inf
0	0.002484568	Inf	0	0.728555556	Inf
0	0.002222222	Inf	0.999011728	0.926666667	-0.072416629
0	0.002222222	Inf	0.343333333	0.843333333	1.45631068
0	0.00326716	Inf	0.343333333	0.843333333	1.45631068
0.001012222	0.003333333	2.293084523	0.343035309	0.842599753	1.456306193
0.00006	0.003328395	54.47325103	0.343198025	0.842222222	1.454041578
0	0.002287037	Inf	0.343717778	0.841835432	1.449205385

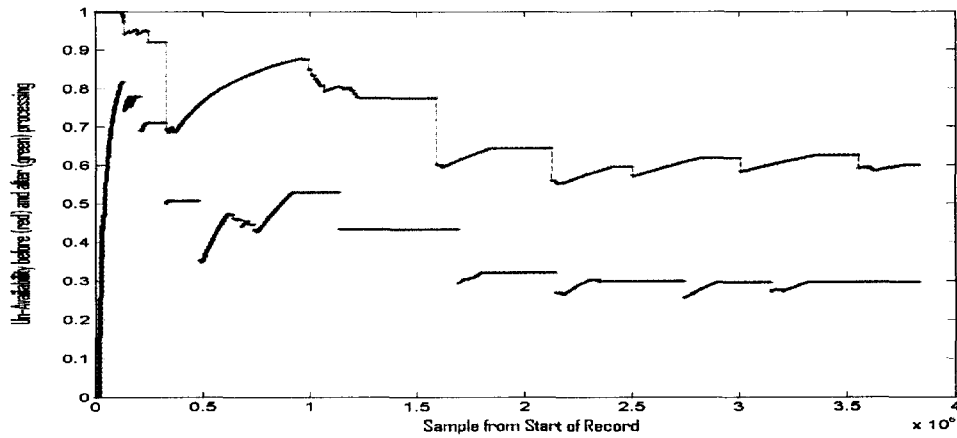


Figure 5. 40 Case 8 CAT I PA Un-Availability before (red) and after (green) processing.

Table 5. 30 Case 8 Un-Availability Performance comparison.

Un-Avai Before	Un-Avai After	Reia. Change	Un-Avai Before	Un-Avai After	Reia. Change
1	0.234859299	-0.765140701	0.566553906	0.286771938	-0.493831152
0.996221274	0.73278756	-0.264432934	0.583194205	0.298787644	-0.487670418
0.947138739	0.757470923	-0.200253467	0.593804498	0.296356667	-0.50091879
0.926206616	0.708179759	-0.235397646	0.578741206	0.296356667	-0.487928863
0.720552481	0.52728654	-0.268219104	0.586743425	0.296356667	-0.494912675
0.741650782	0.4791235	-0.353976951	0.600496246	0.293647781	-0.510991479
0.784536033	0.402196316	-0.487345005	0.613262564	0.26796195	-0.5630551
0.815190076	0.463042269	-0.431982452	0.617961889	0.289208135	-0.531996811
0.83819836	0.442167531	-0.47247865	0.611245797	0.293448041	-0.519918104
0.856106802	0.465565874	-0.456182485	0.588747925	0.293448041	-0.501572696
0.87044308	0.516215586	-0.406950784	0.600417288	0.281303211	-0.531487156
0.851914951	0.527332432	-0.381003431	0.611501471	0.279215538	-0.543393515
0.801732383	0.527332432	-0.342258785	0.621502973	0.293261307	-0.528141746
0.797520412	0.440223996	-0.448009118	0.623932746	0.293914007	-0.528933192
0.775628991	0.43186511	-0.443206591	0.620081379	0.293914007	-0.526007365
0.775459404	0.43186511	-0.443084825	0.588641881	0.293914007	-0.50069131
0.775459404	0.43186511	-0.443084825	0.590986853	0.293914007	-0.502672512
0.775459404	0.43186511	-0.443084825	0.597425225	0.293914007	-0.508032144
0.61448929	0.43186511	-0.297196686	0.660924738	0.210795756	-0.681059364
0.616567128	0.331702315	-0.462017516	0.023128519	0.015970412	-0.309492677
0.635610777	0.315458446	-0.503692421	0.045179546	0.023601039	-0.477616727
0.642923099	0.318210165	-0.50505719	0.045179546	0.023601039	-0.477616727
0.642923099	0.318210165	-0.50505719	0.040519112	0.022099327	-0.454594976
0.642923099	0.318210165	-0.50505719	0.039163285	0.021844002	-0.44223263
0.560045126	0.283215026	-0.494299632	0.038533431	0.021530718	-0.441245768

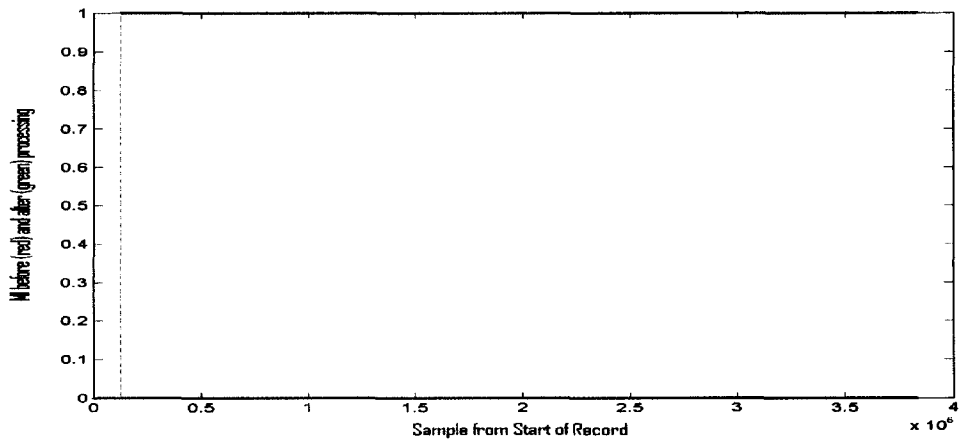


Figure 5. 41 Case 8 CAT I PA Misleading Information (MI) before (red) and after (green) processing.

Table 5. 31 Case 8 Misleading Information (MI) Performance comparison.

MI Before	MI After	Rela. Change	MI Before	MI After	Rela. Change
0	0	NaN	1	1	0
0.151888889	0	-1	1	0	-1
1	0	-1	1	0	-1
1	0	-1	1	0	-1
1	0	-1	1	0	-1
1	0	-1	1	0	-1
1	0	-1	1	0	-1
1	0	-1	1	0	-1
1	0	-1	1	0	-1
1	0	-1	1	0	-1
1	0	-1	1	0	-1
1	0	-1	1	0	-1
1	0	-1	1	0	-1
1	0	-1	1	0	-1
1	0	-1	0.001111111	0	-1
1	0	-1	0	0	NaN
1	0	-1	0	0	NaN
1	0	-1	0	0	NaN
1	0	-1	0	0	NaN
1	0	-1	0	0	NaN
1	0	-1	0	0	NaN



Case 9: Mar. 14th, 2003

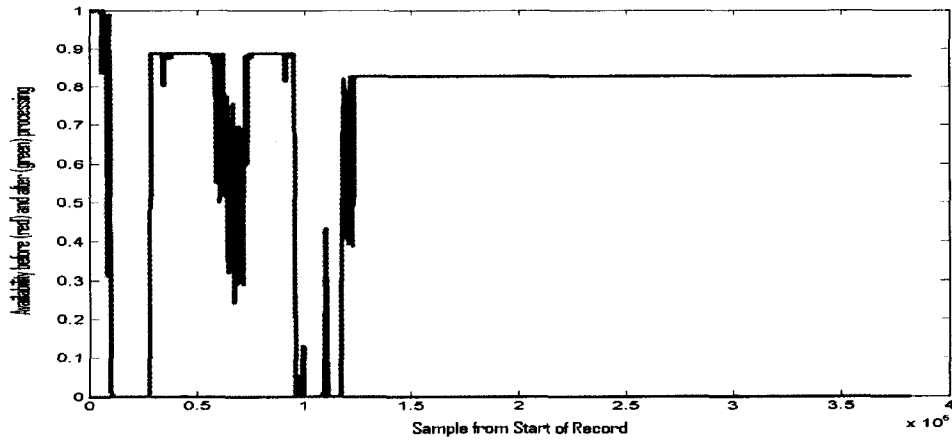


Figure 5. 43 Case 9 CAT I PA Availability before (red) and after (green) processing.

Table 5. 33 Case 9 Cat I Availability Performance comparison.

CAT I Avai Before	CAT I Avai After	Rela. Change	CAT I Avai Before	CAT I Avai After	Rela. Change
0	0.998661974	Inf	0	0.825839259	Inf
0	0.580832099	Inf	0	0.826653827	Inf
0	0	NaN	0	0.826634938	Inf
0	0.235065802	Inf	0	0.826648519	Inf
0	0.876995185	Inf	0	0.826666667	Inf
0.000182716	0.885555556	4845.621622	0	0.826666667	Inf
0	0.884086543	Inf	0	0.82588284	Inf
0	0.65458	Inf	0	0.825688025	Inf
0	0.598867778	Inf	0	0.826666667	Inf
0	0.885555556	Inf	0.0001	0.826666667	8265.666667
0	0.878920617	Inf	0	0.826405185	Inf
0	0.20754	Inf	0	0.825577654	Inf
0	0.050725802	Inf	0	0.82587	Inf
0	0.219019136	Inf	0	0.82652963	Inf
0	0.775958765	Inf	0	0.826297037	Inf
0	0.826063086	Inf	0	0.825692716	Inf
0	0.826064198	Inf	0	0.825950247	Inf
0	0.825555556	Inf	0	0.826062963	Inf
0	0.825555556	Inf	0	0.728555556	Inf
0	0.825555556	Inf	0.999011728	0.926666667	-0.072416629
0	0.826045185	Inf	0.343333333	0.843333333	1.45631068
0	0.826666667	Inf	0.343333333	0.843333333	1.45631068
0	0.826361728	Inf	0.343035309	0.842599753	1.456306193
0	0.825555556	Inf	0.343198025	0.842222222	1.454041578
0	0.825555556	Inf	0.343717778	0.841835432	1.449205385

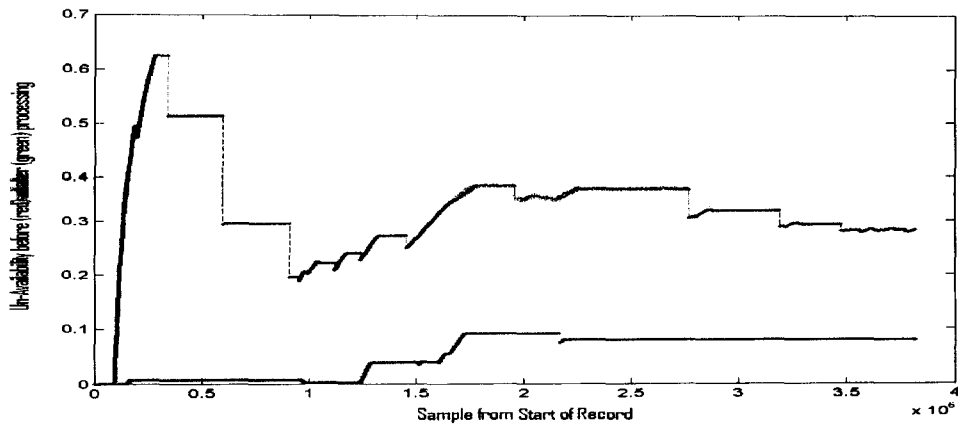


Figure 5. 44 Case 9 CAT I PA Un-Availability before (red) and after (green) processing.

Table 5. 34 Case 9 Un-Availability Performance comparison.

Un-Avai Before	Un-Avai After	Rela. Change	Un-Avai Before	Un-Avai After	Rela. Change
0	0	NaN	0.369264689	0.077359882	-0.7905029
0.052630008	0	-1	0.374741861	0.077359882	-0.793564879
0.42630576	0.004170516	-0.990217079	0.374741861	0.077359882	-0.793564879
0.59021737	0.006494317	-0.988996736	0.374741861	0.077359882	-0.793564879
0.553920225	0.006494317	-0.988275717	0.374741861	0.077359882	-0.793564879
0.512489385	0.006494317	-0.987327899	0.374741861	0.077359882	-0.793564879
0.512489385	0.006494317	-0.987327899	0.332258408	0.077359882	-0.767169529
0.342534473	0.006494317	-0.981040397	0.319533526	0.077359882	-0.757897449
0.295369357	0.006494317	-0.978012894	0.319915004	0.077359882	-0.758186141
0.295369357	0.006494317	-0.978012894	0.319915004	0.077359882	-0.758186141
0.266154302	0.006494317	-0.975599427	0.319915004	0.077359882	-0.758186141
0.203498446	0.003354043	-0.983518093	0.293123484	0.077359882	-0.736084327
0.222265618	0.001629051	-0.992670703	0.293720739	0.077359882	-0.736620975
0.231256146	0.001629051	-0.992955644	0.293211212	0.077359882	-0.73616329
0.24343922	0.015354936	-0.936924971	0.283753516	0.077359882	-0.727369434
0.271921615	0.037866935	-0.860743195	0.281706221	0.077359882	-0.725388096
0.267180249	0.037866935	-0.858271952	0.283010857	0.077359882	-0.726654014
0.278373259	0.037752292	-0.864382475	0.281420018	0.077359882	-0.725108817
0.317703143	0.044348144	-0.86041012	0.660924738	0.210795756	-1.681059364
0.353790781	0.076965603	-0.78245447	0.023128519	0.015970412	-0.309492677
0.379332542	0.090687283	-0.760929335	0.045179546	0.023601039	-0.477616727
0.381089258	0.090687283	-0.762031385	0.045179546	0.023601039	-0.477616727
0.358947888	0.090687283	-0.74735251	0.040519112	0.022099327	-0.454594976
0.351030884	0.090687283	-0.741654404	0.039163285	0.021844002	-0.44223263
0.348423346	0.085412118	-0.754861095	0.038533431	0.021530718	-0.441245768





**Case 10: May. 29th, 2003**

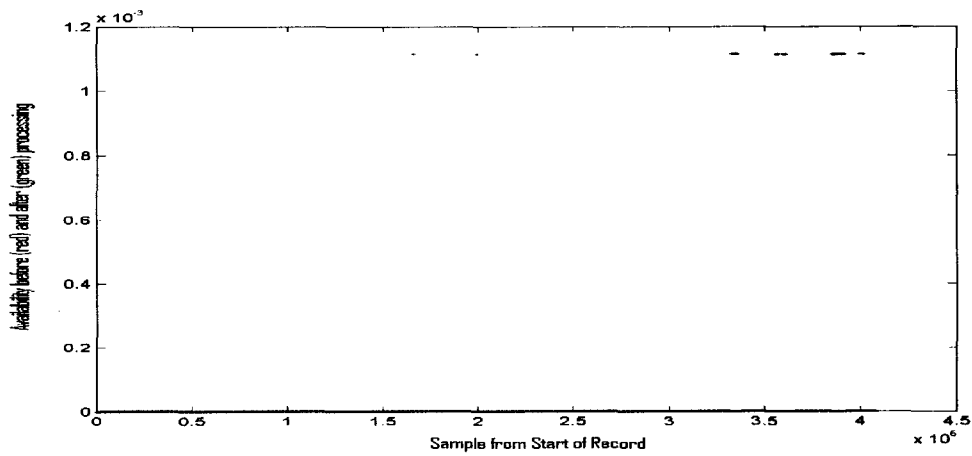


**Figure 5. 47 Case 10 CAT I PA Availability before (red) and after (green) processing.**

**Table 5. 37 Case 10 Cat I Availability Performance comparison.**

CAT I Avai Before	CAT I Avai After	Rela. Change	CAT I Avai Before	CAT I Avai After	Rela. Change
0	0	NaN	0	0	NaN
0	0	NaN	0	0	NaN
0	0	NaN	0	0	NaN
0	0	NaN	0	0	NaN
0	0	NaN	0	0	NaN
0	0	NaN	0	0	NaN
0	0	NaN	0	0	NaN
0	0	NaN	0	0	NaN
0	0	NaN	0	0	NaN
0	0	NaN	0	0	NaN
0	0	NaN	0	0	NaN
0	0	NaN	0	0	NaN
0	0	NaN	0	0	NaN
0	0	NaN	0	0	NaN
0	0	NaN	0	0.000252222	Inf
0	0	NaN	0	0.000044568	Inf
0	0	NaN	0	0	NaN
0	0	NaN	0	0.000138025	Inf
0	0	NaN	0	0	NaN
0	0	NaN	0	0	NaN
0	0	NaN	0	0.000502716	Inf
0	0.00001716	Inf	0	0.000237778	Inf
0	0	NaN	0	0.000005556	Inf
0	0	NaN	0.343333333	0.843333333	1.45631068
0	0.000000494	Inf	0.343035309	0.842599753	1.456306193
0	0	NaN	0.343198025	0.842222222	1.454041578
0	0	NaN	0.343717778	0.841835432	1.449205385

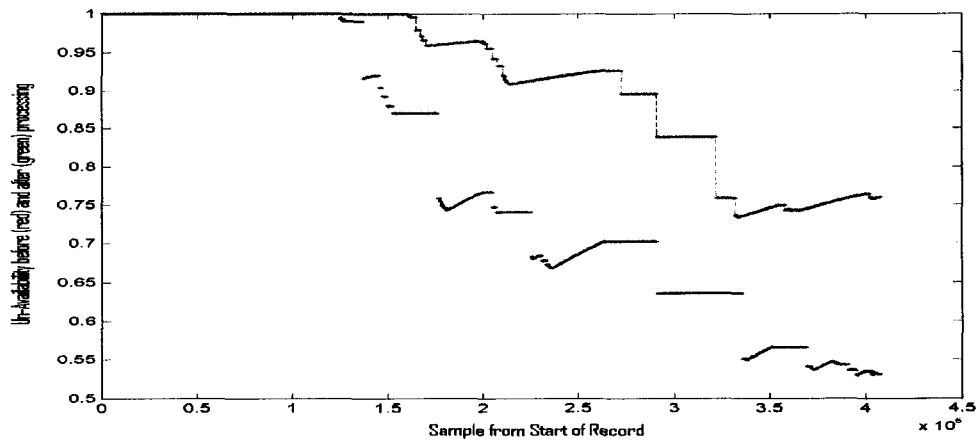


Figure 5. 48 Case 10 CAT I PA Un-Availability before (red) and after (green) processing.

Table 5. 38 Case 10 Un-Availability Performance comparison.

Un-Avai Before	Un-Avai After	Rela. Change	Un-Avai Before	Un-Avai After	Rela. Change
1	1	0	0.912079047	0.723065637	-0.207233585
1	1	0	0.915488258	0.676564686	-0.260979395
1	1	0	0.918642918	0.673676308	-0.266661403
1	1	0	0.921570514	0.685410527	-0.256258185
1	1	0	0.924294239	0.696335694	-0.246629845
1	1	0	0.924802923	0.701353757	-0.241618144
1	1	0	0.895239324	0.701353757	-0.216574007
1	1	0	0.895239387	0.701353757	-0.216574062
1	1	0	0.841452597	0.638061277	-0.241714531
1	1	0	0.83872087	0.634839007	-0.24308667
1	1	0	0.83872087	0.634839007	-0.24308667
1	1	0	0.797196666	0.634839007	-0.203660735
1	1	0	0.749569707	0.634839007	-0.153062082
1	1	0	0.738106943	0.555653809	-1.247190648
	0.996194842	-0.003805158	0.744858246	0.562460401	-1.244875916
1	0.98658297	-0.01341703	0.745699556	0.564920841	-1.242428354
1	0.916512512	-0.083487488	0.743454166	0.558766208	-1.248418754
1	0.882018144	-0.117981856	0.748939606	0.539428802	-1.279743256
0.998181092	0.869350172	-0.129065679	0.754806615	0.544051751	-1.279217033
0.967145331	0.869350172	-0.101117336	0.760405662	0.534523522	-1.297054784
0.960370439	0.78209959	-0.185627173	0.760333447	0.532293963	-1.299920363
0.962276841	0.749992558	-0.220606248	0.045179546	0.023601039	-0.477616727
0.963811224	0.76140477	-0.210006325	0.040519112	0.022099327	-0.454594976
0.945810636	0.753402601	-0.20343188	0.039163285	0.021844002	-0.44223263
0.913111803	0.73965911	-0.189957783	0.038533431	0.021530718	-0.441245768

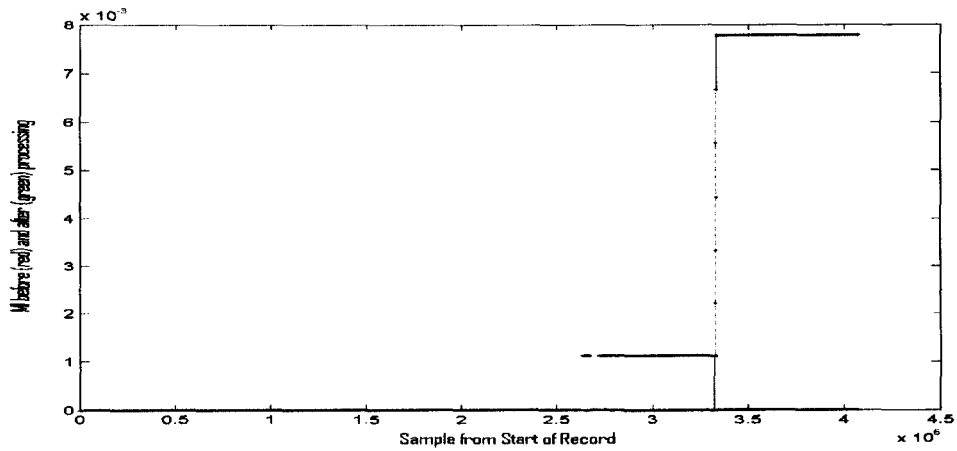


Figure 5. 49 Case 10 CAT I PA Misleading Information (MI) before (red) and after (green) processing.

Table 5. 39 Case 10 Misleading Information (MI) Performance comparison.

MI Before	MI After	Rela. Change	MI Before	MI After	Rela. Change
0	0	NaN	0	0	NaN
0	0	NaN	0	0	NaN
0	0	NaN	0	0	NaN
0	0	NaN	0	0	NaN
0	0	NaN	0	0.000020494	NaN
0	0	NaN	0	0.000508148	NaN
0	0	NaN	0	0.000883086	NaN
0	0	NaN	0	0.00103037	NaN
0	0	NaN	0	0.001111111	NaN
0	0	NaN	0	0.001111111	NaN
0	0	NaN	0	0.001111111	NaN
0	0	NaN	0	0.001111111	NaN
0	0	NaN	0	0.001111111	NaN
0	0	NaN	0.002269753	0.000858519	-0.999141481
0	0	NaN	0.007777778	0	-1
0	0	NaN	0.007777778	0	-1
0	0	NaN	0.007777778	0	-1
0	0	NaN	0.007777778	0	-1
0	0	NaN	0.007777778	0	-1
0	0	NaN	0.007777778	0	-1
0	0	NaN	0.007777778	0	-1
0	0	NaN	0.007777778	0	-1
0	0	NaN	0	0	NaN
0	0	NaN	0	0	NaN
0	0	NaN	0	0	NaN
0	0	NaN	0	0	NaN



is a significant increase. For Un-Availability, it decreases on average by around 50%, which is also very good. MI and HMI performances are not bad either, each having a couple of low spikes and not much change.

In Case 2, CAT I availability improves by a median of about 20%. This is again a good increase. The Un-Availability actually increases, which is not good. Thankfully, the increase is quite small and could most likely be tolerated. MI and HMI perform OK, each having a couple of low spikes.

In Case 3, on a good day, a significant improvement of CAT I availability of about 130% occurs. Un-Availability on average decreases by around 40%, which is also very good. MI and HMI performances are perfect.

In Case 4, CAT I availability increases sometimes and decreases at other times. Un-Availability on average decreases by around 50%. MI and HMI performances are perfect again.

In Case 5, Improvement of CAT I availability is not noticeable. Un-Availability performance is poor and increases at low levels. MI performance is also poor. Luckily the HMI performance, which is of more importance, is very good.

In Case 6, Shown in Table 5.21, CAT I availability I slightly improved. The Un-Availability on average decreases by around 50%, which is also very good. MI and HMI performances are not too bad either, varying at low levels.

In Case 7, shown in Table 5.25, we see a huge improvement of CAT I availability. The Un-Availability on average decreases by around 50%, which again is solid. MI decreases and that is very nice to have. HMI performance has good and bad moments.

In Case 8, CAT I availability improves immensely. Un-Availability decreases by around 50%, which is also very good. MI is decreased by 100% and that is great. HMI is perfect.

In Case 9, CAT I availability is again dramatically increased. The Un-Availability decreases by around 70%, which is very good. MI and HMI performances are simply perfect.

In Case 10, CAT I availability performance is just Okay because of the data type on that specific day. Un-Availability on average decreases by around 40%, which is not bad. MI wavers but does have some bursty regions where MI is decreased by 100%. HMI has a small spike.

### **5.3 Conclusions**

This research has developed a new algorithm to tighten up the overly conservative *VPL* specification. This new algorithm is called the pseudo-*VPL*. In ordinary cases, the pseudo-*VPL* reduces the *VPL* magnitude by 3dB, which is significant. This helps increase the system availability a tremendous amount. This can be shown by an example: A *VPL* at 18 meters is not good for CAT I precision approach. With a 3dB improvement, the new pseudo-*VPL* becomes less than 12 meters, good enough for CAT I precision approach. VPE filtering helps reduce invalid bias, but to a lesser reliability.

This pseudo-*VPL* algorithm alone will improve the compactness of the *VPL* data footprint. However, it doesn't improve the integrity, which is of crucial importance. As a matter of fact, the pseudo-*VPL* algorithm can potentially generate additional HMIs if no other action is taken since the new pseudo-*VPL* moves the data cluster downward

without interfering with actual system error. This can move data points above the diagonal line under it, hence creating new HMIs. My solution to this is to apply Kalman filtering to the actual altitude data so that the VPE is as small as possible, i.e. is as far away from the diagonal line as possible. This, combined with a similar fault detection and error correction mechanism similar to those in pseudo-*VPL*, delivers a higher system availability for WAAS without penalizing system integrity monitoring capability.

With the new pseudo-*VPL* algorithm, on good days, which can be expected more than 95% of the time when GPS and WAAS are up, one can improve the CAT I availability by at least 70 to 100%. Simultaneously, the Un-Availability is decreased by at least 50%. At the same time, the integrity is maintained intact, and sometimes even improved.

The performance of the pseudo-*VPL* algorithm does depend on the data type it is applied to. With a diffuse data locus (“peppered” data points), it can induce extra MI or even HMI. The good news is that this kind of hazard is not evidenced by our tables from real data. But it is still a concern. With future planned upgrades of the GPS and WAAS systems, hopefully this kind of poor data will be eliminated.

## Chapter 6

### Lessons learned and Future Research

WAAS is a well defined space based augmentation system. However, there is still a long way to go before WAAS can be utilized as a primary source for various types and stages of flight navigation, especially for precision approach.

The approach that has been taken in this dissertation is position domain based. The advantages of this approach include low computational overhead, less interference with the current messaging structure and reliable improvement on system availability. While the availability can be improved through our algorithm, the integrity has to be sacrificed to some degree due to the nature of the SIS. As demonstrated in Chapter 5, the sacrifice depends on the WAAS SIS data quality situation. On normal days when the data can be classified as good or better, the new algorithm works very well. However, when the data points are scattered, even when it is good data according to the criterion  $VPL \geq VPE$ , the algorithm performs less than perfectly. This in principle is intolerable. More information is needed than mere position-domain information to correct this shortcoming.

The easiest way to improve the new algorithm is to include the range/correction domain based solution. As demonstrated in the altitude filtering section in Chapter 4 and its results in Section 5.2, the position domain solution alone suffers from an integrity breach in certain types of data sets under some special satellite configurations. Although this will not happen in the majority of days, this is still a serious problem since it is an aviation use. It is recommended to use either range/correction information or the position

solution to identify the actual “bogus” points where cases such as those in Section 4.2 arise. A new problem will be faced with this approach. This approach requires significantly more computation than the position domain solution. To avoid this undesirable overhead, the messaging structure would have to be modified, which would require a significantly long process for approval and certification. Most likely the best approach lies somewhere between. The best solution will be some sort of combination of position domain and range/correction domain solutions. Using the new algorithm presented in this dissertation as the backbone and the range/correction domain methods as a backup to detect false alarms and correct the hard-to-detect biases could be an attractive method.

Further research needs to be carried out to learn how best to combine the position domain algorithm and the range/correction domain method. Since the range/correction domain method usually requires a lot more computation, more need to be learned to have these two approaches complement each other in an effective and efficient way.

# Appendix A:

## A new position domain algorithm to improve WAAS availability and continuity while maintaining integrity

Guangwei Mu, Joebob P. Havlicek, John Fagan, *Univ. of Oklahoma*

### BIOGRAPHY

**Guangwei Mu** is a Ph.D. candidate in the School of Electrical and Computer Engineering at the University of Oklahoma. Mu's areas of interest are GPS based navigation system, WAAS system modeling, digital signal processing and telecommunication. His contributions involved the acquisition of flight test data, data reduction, analysis, and presentation.

**Joebob P. Havlicek** is Professor of Electrical and Computer Engineering at the University of Oklahoma. Professor Havlicek's research interests include signal and image processing, multimedia communications, and intelligent transportation systems.

**John Fagan** is Professor of Electrical and Computer Engineering at the University of Oklahoma. Professor Fagan's research is in the area of data acquisition and systems test and has been working with the OU department of aviation in joint research for the past 8 years. Professor Fagan is the OU principle investigator for the flight test project and leads the instrumentation, data acquisition and data analysis portion of the current GPS WAAS/LAAS evaluation project.

### ABSTRACT

The integrity algorithms are well defined in the Wide Area Augmentation System (WAAS) Minimum Operational Performance Standards (MOPS) [1]. However, our experimental data clearly indicate that the MOPS VPL and HPL algorithms are over-conservative, at least from a practical point of view. As a result, the confidence bounds are sufficiently large to cover the correction error and hence to some extent guarantees the integrity. However, this lack of compactness from the MOPS introduces unnecessary epochs of the system being unavailable. To improve the system performance, the intuitive approach is through the range/correction domain since these factors can be observed, controlled and manipulated to improve the system performance in individual cases. However, we need a better error model and better understanding of the threat model, i.e. we need to know more about the nature of all error sources and the threats the WAAS faces, which is very difficult due to the stochastic natures of these sources, to accomplish this. Therefore, it is unlikely that a range/correction domain solution can be applied to wide range of applications while having significant improvement for the system performance. Besides, it is still subject to the hindrance that the WAAS message structure might need to be changed or adjusted to take advantage of the new development.

In this article, we present a new position domain algorithm to improve the MOPS integrity methodology in hopes of improving the overall system performance. The information needed to do this is already in the WAAS messages. Therefore, this new algorithm will not require any change of the existing correction messaging structure. We introduce pseudo-VPL and pseudo-HPL measures in this paper to facilitate the development of the new algorithm, which we will call as the pseudo-VPL algorithm for the vertical part of WAAS improvement. It is based on the currently used MOPS algorithms and improves upon them. The new VPL and HPL algorithms are developed by taking advantage of the WAAS correction error's stochastic characteristics and a 1-Dimension tracking Kalman filtering. The algorithm has been tested using real static and dynamic data collected by our Enhanced Miniature Advanced GPS Receiver (EMAGR) used in conjunction with the OU flight test program. This methodology shows significant improvement over the standardized MOPS algorithms. It improves the system availability and continuity without penalizing integrity.

### INTRODUCTION

WAAS is a GPS based navigation system developed and being tested in the United States by the Federal Aviation Administration (FAA). WAAS provides correction signals and integrity monitoring messages to aviation users equipped with a WAAS-capable GPS receiver. The WAAS correction signal improves the positioning solution by supplying more accurate GPS clock, satellite ephemeris, and delay times for the WAAS receivers as GPS signal suffers various errors as it travels. These corrections are broadcast for use by virtually all users with WAAS capability in North America via geostationary satellites. A master station and a network of monitoring ground stations are needed to collect information, generate correction messages and upload them to the geo-synchronized WAAS satellite. WAAS provides improvements in four metrics over standard GPS: accuracy, integrity, availability and continuity. From its initial conception to deployment, WAAS has been hailed as revolutionary for the navigation industry. However, the WAAS deployment effort has suffered significant delays and budget overruns. The reason for these misfortunes lies in the demanding mandates on the performance of the WAAS system, especially integrity and availability. In the long process of getting WAAS commissioned, availability has always been the metric that holds the system back from achieving the promised capability. To date WAAS performs well, but not well enough to meet its original objectives. The inherent tradeoff between integrity and availability is the major reason that the VPL and HPL algorithms need to be improved.

For applications using the satellite based navigation system such as WAAS the integrity is of the uttermost importance

since human life is involved. The requirement for the integrity has to be extremely stringent. This, however causes the achievable availability of the system suffer. For a certain type of service compromise has to be made in the middle ground. In this paper the Cat I precision approach will be used as the example to demonstrate the performance of the pseudo-PL algorithm. For this type of service the requirement for the guaranteed final position solution is that the Probability of Hazardously Misleading Information (HMI) must be less than  $10^{-7}$  per approach, while the availability requirement specifying that the system must be available at least 99.9% of the time. The current integrity algorithm is devised to achieve this goal [2].

However, according to our observation these requirements have not been met consistently. In our data collection covering almost the whole WAAS lifetime we have observed the over-conservativeness of the current WAAS integrity algorithm and concluded that the overall performance is not satisfactory. Although it is impossible to realize the probability of the HMI in the sense of strict definition, we will demonstrate that even with a loosened standard the integrity performance is still not satisfactory, i.e. there is space for improvement.

Only the vertical part of the WAAS is discussed in this paper, i.e. only the improvement of VPL performance is presented. This is simply because the vertical part and the horizontal part of the WAAS performance are similar in nature and independent of one another [3]. Doing so enables us to focus more on developing and evaluating the new algorithm.

From observation of our data collection it is obvious that there is a discrepancy between the Vertical Position Error (VPE) and Vertical Protection Level (VPL), best estimation of VPE by WAAS integrity monitoring. The difference between them behaves nonlinearly which is not ideal for filtering. The object of this paper is to reduce this discrepancy as much as possible. To achieve this goal, a transformation is introduced to linearize the envelope of this difference, so that it can be better modeled and hence reduced. This transformation generates what we call pseudo-VPL. The new metric pseudo-VPL shows better linearity and is a better pseudo-measurement for modeling and filtering for the WAAS performance improvement.

In this paper we present a new and improved position domain algorithm based on pseudo-VPL. This pseudo-VPL algorithm takes advantage of the newly found linearity of the pseudo-VPL, combined with the modeling of the discrepancy of the VPE and VPL as a 1-dimension tracking problem, and the false alarm and error prevention. After these steps and the final reverse conversion to the original VPL the new algorithm is established and the performance is compared based on the real static data collected at the University of Oklahoma.

#### DATA COLLECTION

Real WAAS data is used in developing and validating the new pseudo-VPL algorithm. The GPS research group at the University of Oklahoma has been taking observations of the WAAS signal in both static and dynamic settings. The devices used include the Rockwell EMAGR (Enhanced Miniature Aviation GPS Receiver) WAAS capable GPS receiver, the Ashtech Z12 GPS receiver, Rockwell software BBCOM and post processing software, and the Ashtech post processing software Prism. The research effort uses a second redundant EMAGR WAAS receiver to make sure that any unexpected results are not due to malfunctioning on WAAS receiver's part [3]. It was concluded that the observed errors originate from the quality of the Signal In Space (SIS) and this is a presumption in this paper.

Analysis of this research focuses on WAAS static data. Static Data is a good starting point for the ease of getting the ground truth. For moving aircraft, only small adjustments need to be made. Ground truth is obtained by performing a series of surveys to determine the true positions of a few stable sites that have good satellite visibility and relatively easy access for installation of antennae. Two antennae were installed on the roofs of buildings at the University of Oklahoma (OU). One is on building 210 of the OU north research campus, located coincidentally with Max Westheimer Airport. The other is on the Carson Engineering Center building on the main OU campus. Both antenna sites were accurately surveyed in longitude, latitude and altitude. In addition, both are maintained to ensure quality of satellite signal reception.

#### CLASSIFICATION OF DATA TYPE

This paper deals with the WAAS navigation system performance, especially integrity and availability. Therefore the navigation requirements have to be understood to do a good job of upgrading the system integrity and availability. For a navigation system to provide specific capability, which is usually set by government agency after extensive research on safety and economy, some system performance metrics are to be set as the standard. Minimum system performance has to be at least on par with the standards, i.e. the accuracy, integrity, availability and continuity needs to perform at or above a set standard. These standard can be devised in different ways, according to different agencies and different purposes. Most notably in the list above is the integrity requirement of less than  $10^{-7}$  chance of receiving HMI per approach, and the availability requirement of that the system should be usable in more than 99.9% of the time. For the requirement for Category I (CAT I) and instrument approach with vertical guidance (IPV) airplane Precision Approach (PA), the vertical standard for classification of the data points is shown in triangle charts figure 1. CAT I and IPV have Vertical Alert Limit (VAL) of 12 and 20 meters respectively. Based on the navigation requirements, the whole absolute VPL-VPE space can be broken into the 7 color-coded areas:

1.  $VPL > VPE$ ;  $VPL \leq 12$ ; Available, suit for CAT I operation.
2.  $VPL > VPE$ ;  $VPL \leq 19$ ; Available, suit for instrument approach with vertical guidance (IPV) operation.
3.  $VPL > VPE$ ;  $VPL > 19$ ; System Unavailable.
4.  $VPL < VPE$ ;  $VPL > 19$ ; Misleading Information (MI-1).
5.  $VPL < VPE$ ;  $12 < VPL < 19$ ,  $12 < VPL < 19$ ; Misleading Information (MI-2).
6.  $VPL < VPE$ ;  $VPL < 12$ ,  $VPE < 12$ ; Misleading Information (MI-3).
7.  $VPL < VPE$ ; all the remaining area; Hazardously Misleading Information (HMI).

Of these sections in the triangle charts, Case 1 represents the requirement for CAT I precision approach, with the Vertical Alert Limit (VAL) at 12 meters. Case 2 is for the requirement for IPV precision approach, with the Vertical Alert Limit (VAL) at 20 meters. Case 3 is the unavailable area where VPL is too large to support the desired navigation procedure. Case 4, 5 and 6 are the cases when the error exceeds the VPL and provides Misleading Information (MI). Operationally, these regions are not hazardous as we notice they are different from HMI region. However, in normal operation mobile users do not have access to the actual error. They are trustingly dependent on the accuracy of VPL, the VPE estimate. Therefore, this definition only makes sense in post analysis of altitude data. An unsafe region where the VPL supports the operation but the error is large enough to create Hazardously Misleading Information

(HMI), Case 7 is the part of the VPL-VPE space that we are most concerned about, since it indicates the system's failure of informing the breach of integrity and therefore can potentially cause fatal consequence. Thus all data points ideally should fall above the diagonal line in the triangle charts and concentrate at the lower left corner, i.e. the lower part of case 1.

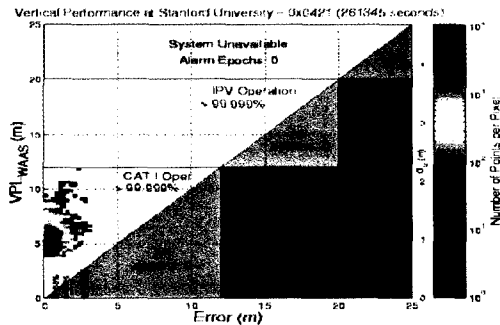


Figure 1 WAAS performance classification, vertical part [4]

#### ASSESSMENT OF OVER-CONSERVATIVENESS OF WAAS SOLUTION

A quick look at the VPL-VPE performance triangle charts shows the area we need to work on. From our data collection we use the following 2 days as example to demonstrate the development of our new algorithm. These days are representative of the normal data types we have witnessed throughout our observation and therefore will be used to demonstrate how normal day's WAAS data responds to the new algorithm. Figure 2 and 3 shows the VPE-VPL performance of these data days. Later on the results of the new algorithm will be compared with these original plots.

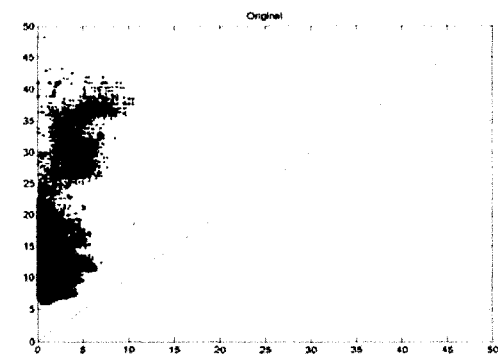


Figure 2 11/27/2000 WAAS performance

The 11/27/2000 data in figure 2 represents a good solid day with integrity monitoring working well, but the availability is not up to the WAAS initial project requirement. There is a discrepancy of about 10 meters between VPL and VPE since VPL is centered around 15 meters while VPE is limited to less than 5 meters most of time.

03/14/2003, figure 3 is an exceptional day for WAAS performance too. Things fall into the expected performance standards. Data clusters in the VPL-VPE chart are compact and not spread all over. Still, it is not good enough for the original specification for CAT I precision approach. It is a very good

WAAS day. The VPL-VPE discrepancy is about 15 meters with a higher VPL centering.

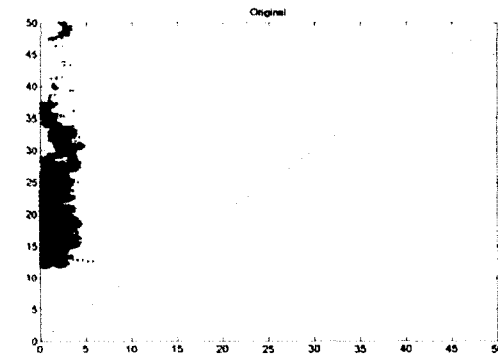


Figure 3 03/14/03 WAAS performance

To have a better insight into the temporal behavior of VPL and VPE, we plot VPL and VPE performances along the GPS time on 11/27/00 as an example, shown in figure 4. We can vaguely identify the action VPL takes when VPE has a significant turn, which shows how well the VPL algorithm is mimicking the vertical error. The consistent gap between VPL and VPE also catches our eyes. This is the potential space we can tap into to improve the tightness of the current VPL algorithm. These charts help us understand the performance of VPE and VPL better. However, there is still more to be desired. This kind of graphing doesn't help us at coming into the new VPL algorithm too much since the VPL is by far larger than VPE and basically overwhelms VPE. To have a more intuitively perceptive way of reading information from data, a new metric of VPL and VPE is needed. Obviously the relationship between VPL and VPE is not linear. Same VPE might have a varied VPL due to different circumstances. However the envelopes of the VPL and VPE are relatively consistent. Therefore when a position domain algorithm is proposed we intuitively consider to work on the envelopes of VPL and VPE.

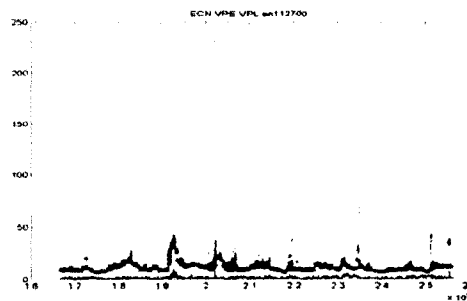


Figure 4 VPE and VPL performance over GPS time on 11/27/00

#### TRANSFORMATION TO LINEARIZE WAAS VPL-VPE PERFORMANCE ENVELOPE

By looking at the figure 2 through 4, it is hard to draw any clear-cut conclusion on how VPL and VPE relate. VPL is usually much larger than the VPE and thus makes VPE look like background noise. To see more details of the comparison one need a better way to look at them. One easy way is to zoom in around the baseline, but that leaves the bigger picture out.

Noticing the VPL and VPE have peaks of no more than tens of thousand, one wonders if using logarithmic scale would be beneficial. In the following charts from figure 5 and 6,  $\text{Log}(VPL + 1)$  vs.  $\text{Log}(VPE + 1)$  are shown along GPS time. Later in this paper these two metrics will simply be called LVPL and LVPE. This scale transformation makes even the highest VPL and VPE be converted into modest value. The constant number 1 is for avoiding the singularity at 0 which could happen for VPE, and still not being too much a factor for VPL since it is relatively small. The difference between these charts and figure 4 is very noticeable. Now we can view the details of the VPE and VPL temporal performance. The striking point off the observation is the resemblance between their envelopes. VPL envelope follows the VPE envelope quite closely with a comfortable cushion in majority of "UP" time. There are exceptions when the VPL shows spikes while VPE remains tame. These probably can be explained by the change of configuration the receiver is having. More discussion will follow.

By now we can agree on that the logarithmic scale better represents the inter-correlation between VPL and VPE and gives more insight to the solution to improve the WAAS VPL availability. After the LVPL and LVPE are processed the reverse process is necessary but trivial. We might need to pay attention to the round out error during processing due to limited storage precision while computing is carried on. It turned out it is of non-major concern in this regard.

According to the WAAS MOPS [1], the formation of WAAS integrity monitoring system is quite definitive. WAAS MOPS specifies how users combine error confidences from different sources to form a position bound. The service provider guarantees that the error at any user location is smaller than the respective bound with a sufficiently high confidence. Simple as it seems, it is deceiving to think the system is a definitive system since the WAAS is inherently a non-stationary system. WAAS relies on satellites that are constantly in motion and that may change their characteristics. Additionally, the propagation of the satellite signals varies with local conditions, thus, the system has differing properties over time and space. It is very clear that the WAAS SIS integrity is by no means a simple system [5]. From published in WAAS MOPS, the WAAS integrity algorithm currently in use is well defined. There are formulae to follow to come up with the VPL and HPL. One has to wonder though, for two or more locations in a relatively large area, the integrity will be almost the same as long as the locations are within the same grid zone defined in WAAS MOPS. This is despite of sometime significant localized difference, such as weather and multipath.

If one wishes to solve the VPL in closed form, which would have been the best thing for this space base augmentation system, he or she finds out it will cost enormous amount of energy and computing time to even get close. It quickly becomes clear that the Navigation error and VPL system can be assimilated to a Chaos system. Every open nonlinear dissipative system has some relationship to another open system and their operations will intersect, overlap and converge. If the systems are sensitive to the initial conditions as in WAAS' case, we don't know exactly in detail every little piece of information, and thus we have a potentially chaotic system. WAAS integrity and availability model has an indeterminate quality about itself and hence is unpredictable. If this system is perturbed either internally or externally, it will display chaotic behavior. And this behavior will be amplified microscopically and macroscopically. By nature we shouldn't try to solve the integrity in closed form because that can't be done for a chaotic system. We can, however, try to understand how the system

behaves under different condition and circumstance of which to take advantage and improve the overall system performance.

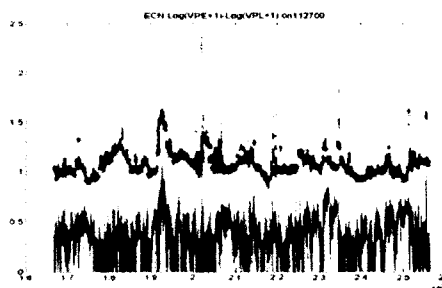


Figure 5 11/27/00 LVPE vs. LVPL

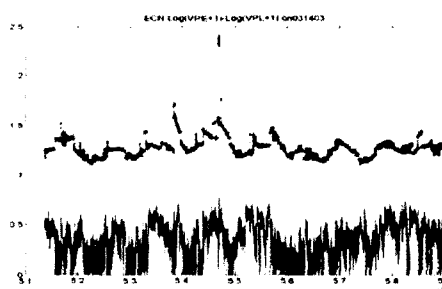


Figure 6 03/14/03 LVPE vs. LVPL

[6] describes the validation of the MOPS integrity equation. Actual data from the National Satellite Test Bed (NSTB), a prototype for WAAS, is compared side-by-side to simulated data. The difference between actual and expected performance is investigated in detail. It was shown that compared to the NSTB data, the assumptions used in the integrity equation are conservative. Integrity is perfect in both the simulated and NSTB data. The comparison of the two data sets provides insights as to the actual probability distribution of the errors in the real data and about correlations between different error components. This knowledge helps to ensure that the integrity requirements are always met. However, this can potentially hurt the availability performance. It may be possible to utilize this information to improve the availability of the system. The objective of our game is to take advantage of the over-conservativeness of the MOPS integrity algorithm. The performance of real WAAS was studied by collecting and analyzing WAAS data. Out of these observations the insight to improve the integrity algorithm is realized. As stated in the above reference paper, the stringent requirements are already met by the MOPS integrity algorithm. We need to improve the availability to improve the overall system performance.

From LVPL and LVPE performance charts in figure 5 and 6 there is certainly some inter-correlation between the two functions of LVPL and LVPE. We can write a relation between them simply as:

$$LVPL = f(LVPE) \quad (1)$$

With the chaos background in mind, and the observation made in charts in figure 5 and 6, we can linearly model the LVPL as VPE with certain stochastic noise characteristics, plus a bias, which was introduced intentionally to safe guard the integrity safety:

$$LVPL = LVPE + n_{lvpe} + bias \quad (2)$$

where  $n_{vpe}$  is the central part of this dissertation. Once one understands the way this noise characteristics works one can easily establish an algorithm to de-noise VPL to make it better mimic the VPE, hence reduce the conservativeness of the MOPS VPL algorithm, and in turn increase the system availability.

#### JUSTIFYING MULTIPLICATIVE MODELING OF VPL

Equations 1 and 2 indicate some multiplicative modeling between VPL and VPE. The most used noise model is the Gaussian Additive White Noise (AGWN) where the different contributions to the total noise are added up. It is very normal in signal processing. In this LVPL-LVPE modeling, however, one might ask, why additive? From all the articles regarding the WAAS error sources up to today, it has always been assumed that the different noise sources are combined in additive fashion [1]. It is also assumed that the additive nature makes the most conservative bound therefore suffices the requirement of integrity algorithm. This is intuitive and easy to understand. However, it is unlikely that different error sources work together to get the WAAS into trouble. In other words, the bounds based on MOPS are almost always too conservative.

The essential point of the new algorithm is the modeling LVPL as a noise stained version of LVPE. The threat model for VPE is an additive model with clock error, ephemeris error, ionospheric and tropospheric errors working in additive way. But that doesn't assimilate the relationship between the VPL and VPE. This is a whole new story. We still need to investigate through their behavior to determine what kind of nature the modeling noise works its way in, which is not necessarily additive. In the development of VPL algorithm there are different error source estimates contributing to the total error bound, which is the VPL [1] [6]. The error sources combine in a worst way, which is very unlikely in the real world. After that, VPL has to be large enough to ensure the probability of VPL being less than VPE to be extremely small. Therefore, assuming a Gaussian distribution, one can use a constant K to generate a 3-Sigma bound. This constant K has to have been over-bounded due to the steps taken before its evaluation and the use of the assumption of Gaussian Noise.

Given an initial estimate for position and an estimate for the weighting matrix, the position estimate solution is [1] [2]:

$$\Delta \hat{x} = (G^T \cdot W \cdot G)^{-1} \cdot G^T \cdot W \cdot \Delta \hat{y} \equiv K \cdot \Delta \hat{y} \quad (3)$$

where K is defined as

$$K \equiv (G^T \cdot W \cdot G)^{-1} \cdot G^T \cdot W \quad (4)$$

One step further, the VPL equations

$$VPL_{\sigma_z} \equiv \kappa(\text{Pr}) \cdot \sigma_z \quad (5)$$

along the vertical direction,

$$VPL_{\sigma_y} \equiv \kappa(\text{Pr}) \cdot \sigma_y \quad (6)$$

where

$$\sigma_y \equiv \sqrt{\left[ (G^T \cdot W \cdot G)^{-1} \right]_{3,3}} \quad (7)$$

with the requirement of the integrity of better than 99.9%, the constant K can be determined at 4.58 by the PDF integration over the tails. As mentioned before, the tail is cut off to some degree due to the fault detection and error correction mechanism implemented in the integrity algorithm. This alone certifies the over-conservativeness of the MOPS algorithm. The worst case combination rarely happens. Also the individual error models are loosely established and therefore conservative

in the first place. The Gaussian Noise assumption is not accurate at least due to the implementation of error correction and fault detection mechanism, which cut the tail part of the Gaussian curve off. Therefore, there is room for the MOPS VPL algorithm to be relaxed. This algorithm can be established through the use of real world data. If after testing the new algorithm in sufficiently diversified data types and getting satisfactory result, it can be claimed this real-data-based algorithm will work in general cases.

Figure 7 and 8 demonstrate that the LVPL minus LVPE, which is the  $(n_{lvpe} + bias)$  term, is more linear than VPL-VPE.

Indeed, a few simple tests based on the data set chosen shows this estimate is valid, we have an improvement of nonlinearity of (VPL-VPE) at 9.00821 to nonlinearity of (LVPL-LVPE) at 0.30773. In the following example in figure 7 and 8 it can be easily seen that with the nonlinearity criteria the (LVPL-LVPE) does indeed have a better linearity than the (VPL-VPE). This is very normal with all types of data sets.

These illustrations are just an example to show that the logarithmic based function of VPL and VPE is a better fit to use as the basis to improve the WAAS SIS performance. In conclusion one now can utilize the LVPL-LVPE linearity to simplify the filtering process in the De-Noising process in the followed modeling. The simplest model is a constant

$(n_{lvpe} + bias)$  model. Without more details for threat models this is also the safest model. The actual value of this constant can be determined by trial and readjustment process. Therefore this algorithm is a pseudo-heuristic algorithm. This makes good sense with the 3-Sigma K overvalued. By subtract this constant  $(n_{lvpe} + bias)$  between LVPL and LVPE, we can rid the VPL of the averaging factor in the over-estimate of error sources combination. At the same time removing constant  $(n_{lvpe} + bias)$  also works on the correcting the 3-Sigma constant K. Nice two birds with one stone.

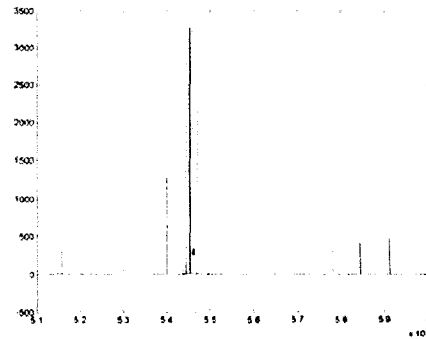


Figure 7 (11/27/00) Nonlinearity of (VPL - VPE):  
(Std(VPL - VPE)/Mean(VPL - VPE)) = 9.00821

Observation of figure 5 and 6 also shows there are plenty of spikes for both LVPL and LVPE. LVPL needs to be "smoothed out" so that it doesn't have the choppiness. Kalman Filter is our choice to achieve this. Using Kalman filtering retains the localized flavor of the WAAS performance to certain degree. Also the computing cost is limited [7].

During a span of time without violent thunderstorm, sunspot activity or some other adverse condition, one should expect the WAAS solution close to be continuous. However, as been observed, in time-VPL-VPE charts in figure 6 and 7, due to

various reasons choppy gaps do exist and generate HMIs. Since probable cause of these gaps is false alarm of the WAAS, they can be deemed as to-be-filtered-out gaps. We hope to smooth them out to reduce the probability of HMIs.

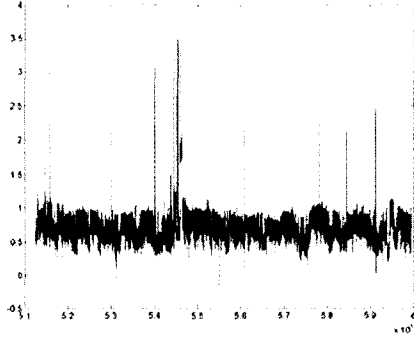


Figure 8 (11/27/00) Nonlinearity of (LVPL - LVPE):  
(Std(LVPL - LVPE)/Mean(LVPL - LVPE)) = 0.30773

### KALMAN FILTERING THE PESUDO-VPL SOLUTION

Using WAAS static data the initialization of Kalman filter can be done based on information after investigating the dynamics of the system.

$$\hat{x}_0^- = 0 \quad (8)$$

$$P_0^- = \pi_0$$

The VPL can be modeled as a random process. Therefore denote

$$i_k^c = \log_{10}(1 + VPL) \quad (9)$$

$i_k^c$  is LVPL, a random process as well. From what has been seen in the preceding sections  $i_k^c$  can be easily seen as a random 1-Dimension tracking target, and hence this becomes a 1-D tracking problem of LVPL. A simple yet fitting model would be  $\alpha$  &  $\beta$  tracking filter.  $\alpha$  &  $\beta$  tracking filter is a simplified version of Kalman filter, i.e. a special case of Kalman filter. Basically saying, it is a least square root solution of the problem given the statistic measurements.

To simplify, we assume a constant velocity from frame to frame. This is close to truth from observation of the data. And deviation from that can be modeled by a white noise. Since there are 5 samples a second in WAAS signal, there are 5 frames per second. The position of target at frame  $k+1$  can be written as

$$i_{k+1}^c = i_k^c + \Delta v_k \quad (10)$$

where  $\Delta$  is the frame time, 0.2 seconds in this case, and  $v_k$  is the velocity. As stated above, it is unlikely that over a long period of time the velocity remain truly constant. Hence, a small "velocity drift" from frame to frame will now be allowed

$$v_{k+1} = v_k + u_k \quad (11)$$

where  $u_k$  is modeled as a white "velocity drift" noise with the statistics of

$$E[u_k] = 0 \quad (12)$$

$$E[u_k u_l] = \sigma_u^2 \delta_{k-l}$$

For the measurement noise the symbol  $n_k$  will be used and

$n_k$  is also a white noise process, with

$$E[n_k] = 0 \quad (13)$$

$$E[n_k n_l] = \sigma_n^2 \delta_{k-l}$$

and  $E[u_k n_l] = 0$ . The observation is then given by

$$z_k = i_k^c + n_k \quad (14)$$

By combining the above equations the system model can be written in matrix form:

$$\begin{pmatrix} i_{k+1}^c \\ v_{k+1} \end{pmatrix} = \begin{pmatrix} 1 & \Delta \\ 0 & 1 \end{pmatrix} \begin{pmatrix} i_k^c \\ v_k \end{pmatrix} + \begin{pmatrix} 0 \\ 1 \end{pmatrix} u_k \quad (15)$$

$$z_k = \begin{pmatrix} 0 & 1 \end{pmatrix} \begin{pmatrix} i_k^c \\ v_k \end{pmatrix} + n_k \quad (16)$$

To initialize, at  $k = -2$ , measurement

$$z_{-2} = i_{-2}^c + n_{-2} \quad (17)$$

And at  $k = -1$ ,

$$z_{-1} = i_{-1}^c + n_{-1} \quad (18)$$

Taking  $\hat{i}_{-1}^c = z_{-1}$ , and  $\hat{v}_{-1} = \frac{z_{-1} - z_{-2}}{\Delta}$  leads to

$$x_{-1} = \begin{pmatrix} \hat{i}_{-1}^c \\ \hat{v}_{-1} \end{pmatrix} = \begin{pmatrix} z_{-1} \\ \frac{z_{-1} - z_{-2}}{\Delta} \end{pmatrix} \quad (19)$$

and then

$$\begin{aligned} P_{-1} &= E[e_{-1} e_{-1}^T] = E\{[(x_{-1} - \hat{x}_{-1})(x_{-1} - \hat{x}_{-1})^T]\} \\ &= E\left\{ \begin{pmatrix} i_{-1}^c - \hat{i}_{-1}^c \\ v_{-1} - \hat{v}_{-1} \end{pmatrix} \begin{pmatrix} i_{-1}^c - \hat{i}_{-1}^c \\ v_{-1} - \hat{v}_{-1} \end{pmatrix}^T \right\} \end{aligned} \quad (20)$$

Now,

$$i_{-1}^c - \hat{i}_{-1}^c = i_{-1}^c - z_{-1} = i_{-1}^c - (i_{-1}^c + n_{-1}) = -n_{-1} \quad (21)$$

$$v_{-1} - \hat{v}_{-1} = v_{-1} - \frac{z_{-1} - z_{-2}}{\Delta} = u_{-2} - \frac{n_{-1} - n_{-2}}{\Delta} \quad (22)$$

To compute  $P_{-1}$  the following quantities are needed:

$$E[(i_{-1}^c - \hat{i}_{-1}^c)^2] = E[(-n_{-1})^2] = \sigma_n^2 \quad (23)$$

and

$$\begin{aligned} &E[(i_{-1}^c - \hat{i}_{-1}^c)(v_{-1} - \hat{v}_{-1})] \\ &= E[(-n_{-1})(u_{-2} - \frac{n_{-1} - n_{-2}}{\Delta})] = \frac{\sigma_n^2}{\Delta} \end{aligned} \quad (24)$$

Using symmetry the following is shown:

$$E[(v_{-1}^c - \hat{v}_{-1}^c)(i_{-1}^c - \hat{i}_{-1}^c)] \\ = E[(i_{-1}^c - \hat{i}_{-1}^c)(v_{-1}^c - \hat{v}_{-1}^c)] = \frac{\sigma_n^2}{\Delta}$$

The last term in  $P_{-1}$  is

$$E[(v_{-1}^c - \hat{v}_{-1}^c)^2] = E[(u_{-2} - \frac{n_{-1} - n_{-2}}{\Delta})^2] \\ = (1 + \frac{2}{\Delta^2})\sigma_v^2 \quad (26)$$

Combine all four components,

$$P_{-1} = \begin{pmatrix} \sigma_n^2 & \frac{\sigma_n^2}{\Delta} \\ \frac{\sigma_n^2}{\Delta} & (1 + \frac{2}{\Delta^2})\sigma_v^2 \end{pmatrix} \quad (27)$$

Now one can have the iteration initial condition:

$$\hat{x}_0^- = \phi_{-1} \hat{x}_{-1} = \begin{pmatrix} 1 & \Delta \\ 0 & 1 \end{pmatrix} \begin{pmatrix} \hat{i}_{-1}^c \\ \hat{v}_{-1}^c \end{pmatrix} \quad (28)$$

and

$$P_0^- = \phi_{-1} P_{-1} \phi_{-1}^T + Q_{-1} = \begin{pmatrix} 5\sigma_n^2 + \Delta^2 \sigma_v^2 & \frac{3\sigma_n^2 + \Delta \sigma_v^2}{\Delta} \\ \frac{3\sigma_n^2 + \Delta \sigma_v^2}{\Delta} & 2(\frac{\sigma_n^2}{\Delta^2} + \sigma_v^2) \end{pmatrix} \quad (29)$$

With these initial conditions we can start the iteration of the specialized Kalman filter,  $\alpha - \beta$  filter.

Use the Kalman filter notations the following is produced

$$\phi_k = \begin{pmatrix} 1 & \Delta \\ 0 & 1 \end{pmatrix}, \quad x_k = \begin{pmatrix} i_k^c \\ v_k \end{pmatrix} \quad (30)$$

$$H_k = \begin{pmatrix} 0 & 1 \end{pmatrix} \quad (31)$$

$$Q_k = \begin{pmatrix} 0 & 0 \\ 0 & \sigma_v^2 \delta_{i-k} \end{pmatrix} \quad (32)$$

$$R_k = E[n_k n_i] = \sigma_n^2 \delta_{i-k} \quad (33)$$

Compare to the general Kalman filter derivation [7] the implementation of the Kalman filter is then reduced to processing the observations  $z_k$ , which in my research comes with the observed VPL over time. Subject to the initial conditions:

$$\begin{cases} \hat{i}_{-1}^c = z_{-1} \\ \hat{v}_{-1}^c = \frac{z_{-1} - z_{-2}}{\Delta} \end{cases} \Rightarrow \hat{x}_{-1} = \begin{pmatrix} z_{-1} \\ \frac{z_{-1} - z_{-2}}{\Delta} \end{pmatrix} \quad (34)$$

$$\hat{x}_0^- = \phi_{-1} \hat{x}_{-1} = \begin{pmatrix} 1 & \Delta \\ 0 & 1 \end{pmatrix} \begin{pmatrix} \hat{i}_{-1}^c \\ \hat{v}_{-1}^c \end{pmatrix}$$

The Kalman gains

$$\begin{pmatrix} \alpha_k \\ \beta_k \end{pmatrix} = K_k = F_k^T H_k^T (H_k F_k H_k^T + R_k)^{-1} \\ = \begin{pmatrix} P_k(1,1) & P_k(1,2) \\ P_k(2,1) & P_k(2,2) \end{pmatrix} \begin{pmatrix} 1 \\ 0 \end{pmatrix} \left( (1 \ 0) \begin{pmatrix} P_k(1,1) & P_k(1,2) \\ P_k(2,1) & P_k(2,2) \end{pmatrix} \begin{pmatrix} 1 \\ 0 \end{pmatrix} + \sigma_n^2 \right)^{-1} \\ = \begin{pmatrix} \frac{P_k(1,1)}{P_k(1,1) + \sigma_n^2} \\ \frac{P_k(2,1)}{P_k(1,1) + \sigma_n^2} \end{pmatrix} \quad (35)$$

Filtered state vector error covariance matrix:

$$P_k^- = (I - K_k H_k) P_k^- \\ = \begin{pmatrix} (1 - \alpha_k) P_k^-(1,1) & (1 - \alpha_k) P_k^-(1,2) \\ (1 - \alpha_k) P_k^-(1,2) & P_k^-(2,2) - \beta_k P_k^-(1,2) \end{pmatrix} \quad (36)$$

And the filtered state vector error covariance matrix

$$P_{k+1}^- = \phi_k P_k \phi_k^T + Q_k \quad (37)$$

Hence

$$\begin{cases} P_{k+1}^-(1,1) = P_k(1,1) + 2\Delta P_k(1,2) + \Delta^2 P_k(2,2) \\ P_{k+1}^-(1,2) = P_k(1,2) + \Delta P_k(2,2) \\ P_{k+1}^-(2,1) = P_k(2,1) + \Delta P_k(2,2) = P_k(1,2) + \Delta P_k(2,2) \\ P_{k+1}^-(2,2) = P_k(2,2) + \sigma_v^2 \end{cases} \quad (38)$$

The pre-computation of Kalman gains now can be calculated in the following iteration:

- 1) Begin with  $P_0^-$  as given;  $k = 0$ ;
- 2) Compute  $\alpha_k$  and  $\beta_k$  using (35);
- 3) Compute  $P_k$  using (36);
- 4) Compute  $P_{k+1}^-$  using (37) and (38)
- 5) Let  $k = k+1$
- 6) Go loop back to step 3.

Typically the Kalman gains converge to asymptotic values. From what has been observed from my Kalman filter implementation on the pseudo-VPL, this is certainly true. The overall Kalman iteration is shown below:

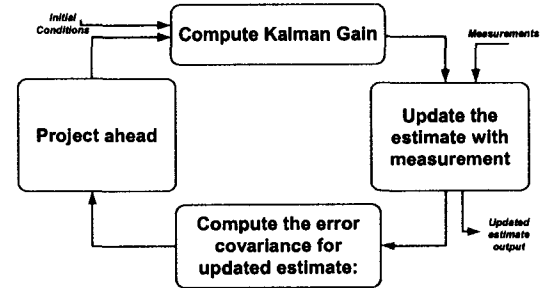


Figure 9 Kalman filtering recursion.

## FALSE ALARMS AND ERROR PREVENTION

It has been suggested that the improvement of WAAS integrity, availability and continuity need to be done on range/correction domain [5] [8]. There are merits in the suggestions. We have noticed there are mysterious spikes in WAAS position solution. Through further study most of them are associated with change of SV used by the receiver. In order to improve the system performance, a better error model and better understanding of the threat model is needed, i.e. we need to know more about the nature of all error sources and the threats the WAAS faces, which is very difficult due to the stochastic natures of these sources. Luckily when it comes to false alarm and error prevention, the position-domain solution shows its advantage and can be used to improve the system availability. It is known that the HMI requirement is specified in the position domain, yet WAAS broadcasts values in the range/correction domain. The uses of WAAS receivers combine the corrections and confidences with their geometry to form the position solution and protection level. Depending on individual circumstance, each receiver determines which corrections and satellites are used, with WAAS SIS having no direct input. Therefore, how the position error depends on the residual errors, and is known only to the users. This can cause unpredictable jump in the position solution. In [5] example for specific user geometry by using Stanford's Matlab Algorithm Availability Simulation Tool (MAAST) [9], one can see the positioning solution can vary significantly when a seemingly insignificant SV drops out of the view sight. It is so serious that it can move a cluster of perfectly performing data points into the HMI area. Without detail of the cause of this sort of incidents, the best we can do is to use a simple low-pass filter to filter the VPE solution to reduce the abrupt change of the position solution. This helps remove false alarms and hence reduces false HMIs. Combine this into the pseudo-VPL algorithm helps improve or maintain the integrity performance.

The more important part of the false alarm and error prevention lies in the PL processing. We introduce the SV factor into the Kalman filtered position solution. The LVPL is coasted for a period of time every time a suspect solution appears, which means the altitude jumps by more than a pre-set threshold and the corresponding number of SV changes. This is especially true when either the before or after of the SV number change is the minimum 4 satellites. Again determining of the threshold and the period of time are trial and readjustment process. This method helps increase the availability.

#### SUMMARY AND RESULTS OF THE PSEUDO-VPL ALGORITHM

Combine the preceding sections we can summarize the new pseudo-VPL algorithm as followed:

1. Use transformation of LVPL to transform the VPL envelope to linearly mimic VPE envelope.
2. Kalman filtering LVPL.
3. False alarm and error prevention.
4. Translate LVPL by 3 dB. This is a trial and adjustment process. 3 dB proves to be a safe value for various type of data set.
5. Reverse step 1.

To show how the new algorithm works on the real data, the previously used two data sets are demonstrated. Since it is impossible to show strictly defined availability and integrity, we use moving past 3-minutes average on available/unavailable data points over total points ratio as the availability/Un-availability. Table 1.1 and 1.2 shows the availability and Un-availability performance comparison with the current VPL algorithm and the pseudo-VPL algorithm on the 11/27/2000 data set. Table 2.1 and 2.2 are for 03/14/2003 data set.

#### Case 1: 11/27/2000: Before and after the filtering

Most data points are squeezed into the lower part of the upper half of the triangle chart and there is no HMI present before and after the algorithm is applied. The system availability is improved and yet the integrity is not compromised.

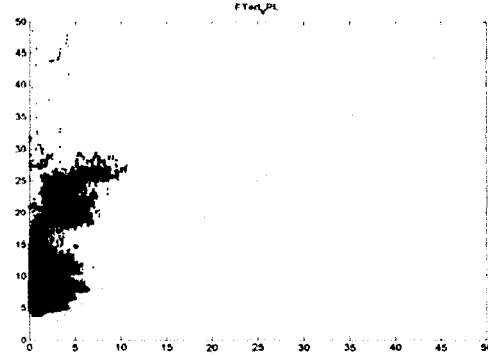


Figure 10 11/27/2000: Before and after the filtering

In Case 3, CAT I availability increase sometime and decrease on other time, but mostly improving. Un-Availability it on average decreases by around 50. MI and HMI performances are perfect again.

Table 1- 1 Case 1 Cat I Availability Performance comparison for 11/27/2000 Data.

CAT I Avail Before	CAT I Avail After	Rela. Change	CAT I Avail Before	CAT I Avail After	Rela. Change
1	1	0	0.339505556	0.84111	1.477455777
0.989432716	1	0.010890144	0.339741852	0.84105321	1.475865507
1	1	0	0.341111111	0.841111111	1.485798046
0.987283827	0.989521728	-0.01800082	0.341111111	0.841111111	1.485798046
1	1	0	0.341412222	0.841470247	1.484875229
1	1	0	0.342218049	0.842222222	1.481083353
0.976854938	1	0.023803081	0.342222222	0.842222222	1.481083961
0.612639012	1	0.6322828	0.341708148	0.842222222	1.484741408
0.289430884	0.87715983	2.030638114	0.341540741	0.842222222	1.48584951
0.287777778	0.901060741	2.131099099	0.341985309	0.842222222	1.482887904
0.786593704	1	0.304471971	0.342118025	0.842222222	1.48178851
0.806055556	1	0.240809277	0.341887531	0.842041235	1.484380442
0.779080884	1	0.283683807	0.342222222	0.842142346	1.480805556
0.833333333	1	0.2	0.343025186	0.84323284	1.458224282
0.371487284	0.844653457	1.273830007	0.343288765	0.843333333	1.458558014
0.338888889	0.840870617	1.480687395	0.343333333	0.843333333	1.45831088
0.339151852	0.841111111	1.490042808	0.343333333	0.843333333	1.45831088
0.338607407	0.841111111	1.481831594	0.343333333	0.843333333	1.45831088
0.339635879	0.841111111	1.4743243	0.343333333	0.843333333	1.45831088
0.340804815	0.840985309	1.487588349	0.343042593	0.843332346	1.458389611
0.341195062	0.840328889	1.482898744	0.343333333	0.843333333	1.45831088
0.341885185	0.841098173	1.480171453	0.343333333	0.843333333	1.45831088
0.340647854	0.841093333	1.488100617	0.343035309	0.842599753	1.458306193
0.34	0.841111111	1.473856209	0.343198025	0.842222222	1.454041878
0.339918687	0.841111111	1.474462895	0.343171778	0.841836432	1.449205385

**Table 1- 2 Case 2 Un-Availability Performance comparison for 11/27/2000 Data.**

Un-Aval Before	Un-Aval After	Rela. Change	Un-Aval Before	Un-Aval After	Rela. Change
1	0	NaN	0.339505556	0.039821414	-0.425984745
0.989432716	0	NaN	0.339741852	0.038048735	-0.404215282
1	0	NaN	0.341111111	0.033429586	-0.466446536
0.987293827	0	-1	0.341111111	0.033429586	-0.466446536
1	0	-1	0.341412222	0.031600887	-0.464024243
1	0	-1	0.342218049	0.030142574	-0.471208823
0.978854938	0	-1	0.342222222	0.030142574	-0.471209823
0.812639012	0	-1	0.341708146	0.030142574	-0.471208823
0.288430864	0	-1	0.341540741	0.030142574	-0.462870585
0.287777778	0.000321017	-0.932955913	0.341965309	0.030142574	-0.398008996
0.786893704	0.000443088	-0.912143248	0.342118025	0.030142574	-0.398008996
0.806055556	0.000443088	-0.912143248	0.341887531	0.030142574	-0.388450246
0.779080884	0.000443088	-0.912143248	0.342222222	0.030142574	-0.358918079
0.833333333	0.000443088	-0.912143248	0.343025185	0.023980034	-0.489175429
0.371467284	0.01680538	-0.255289156	0.343298785	0.023601039	-0.477816727
0.338888889	0.052166726	-0.178349896	0.343333333	0.023601039	-0.477816727
0.339151852	0.05263197	-0.178800242	0.343333333	0.023601039	-0.477816727
0.338907407	0.05263197	-0.178800242	0.343333333	0.023601039	-0.477816727
0.339635678	0.05263197	-0.178800242	0.343333333	0.023601039	-0.477816727
0.340804615	0.051369131	-0.081352898	0.343042593	0.023601039	-0.477816727
0.341195062	0.044470955	-0.387583837	0.343333333	0.023601039	-0.477816727
0.341885185	0.044468237	-0.447201436	0.343333333	0.023601039	-0.477816727
0.340847854	0.041887423	-0.442074048	0.343035309	0.022099327	-0.454949478
0.34	0.038821414	-0.482380851	0.343198025	0.021844002	-0.442232863
0.338918667	0.038821414	-0.482380851	0.343717778	0.021530718	-0.441245789

**Case 2: 03/14/2003: Before and after the filtering**  
 On a good quality day in figure 5.1.9 one has quality results again. Now it can be concluded that the pseudo-VPL-VPE algorithm performs quite consistently on normal days. Its correction capability, however, is at best a suspect.

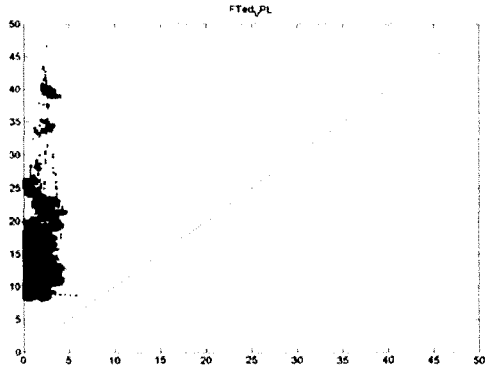


**Figure 11 03/14/2003: Before and after the filtering**

**Table 2- 1 Case 2 Cat I Availability Performance comparison for 03/14/2003 Data.**

CAT I Aval Before	CAT I Aval After	Rela. Change	CAT I Aval Before	CAT I Aval After	Rela. Change
0	0	NaN	0.369264869	0.077359882	-0.7905029
0.052830006	0	-1	0.374741861	0.077359882	-0.793584879
0.42830576	0.004170516	-0.980217079	0.374741861	0.077359882	-0.793584879
0.59021737	0.008494317	-0.988998738	0.374741861	0.077359882	-0.793584879
0.553820225	0.008494317	-0.888275717	0.374741861	0.077359882	-0.793584879
0.512488385	0.008494317	-0.987327899	0.374741861	0.077359882	-0.793584879
0.512488385	0.008494317	-0.987327899	0.332258408	0.077359882	-0.787189529
0.342534473	0.008494317	-0.981040387	0.319533526	0.077359882	-0.757897449
0.295389357	0.008494317	-0.978012894	0.319915004	0.077359882	-0.758186141
0.295389357	0.008494317	-0.978012894	0.319915004	0.077359882	-0.758186141
0.288154302	0.008494317	-0.975599427	0.319915004	0.077359882	-0.758186141
0.203498446	0.003354043	-0.983518093	0.293123484	0.077359882	-0.738084327
0.222286818	0.001829051	-0.992670703	0.293720739	0.077359882	-0.736820875
0.231258148	0.001829051	-0.992955644	0.283211212	0.077359882	-0.73818329
0.24343922	0.015354936	-0.936924971	0.283753516	0.077359882	-0.727389434
0.271921615	0.037868935	-0.860743195	0.281708221	0.077359882	-0.725388986
0.287180249	0.037868935	-0.858271952	0.283010857	0.077359882	-0.72684014
0.278373259	0.037752292	-0.864382475	0.281420018	0.077359882	-0.725108817
0.317703143	0.044348144	-0.86041012	0.868092478	0.210795756	-1.881059384

0	0.988681974	Inf	0	0.825838259	Inf
0	0.580832069	Inf	0	0.826653827	Inf
0	0	NaN	0	0.828634938	Inf
0	0.235085802	Inf	0	0.828648519	Inf
0	0.878995185	Inf	0	0.826686667	Inf
0.000182716	0.885555556	4845.821622	0	0.828686667	Inf
0	0.884088543	Inf	0	0.82558284	Inf
0	0.85458	Inf	0	0.825688025	Inf
0	0.598867778	Inf	0	0.828686667	Inf
0	0.885555556	Inf	0.0001	0.828686667	8285.866667
0	0.878920617	Inf	0	0.828405185	Inf
0	0.20754	Inf	0	0.825577854	Inf
0	0.050725802	Inf	0	0.82587	Inf
0	0.219019138	Inf	0	0.82852963	Inf
0	0.775958785	Inf	0	0.828297037	Inf
0	0.828683086	Inf	0	0.825892716	Inf
0	0.828694198	Inf	0	0.825950247	Inf
0	0.825555556	Inf	0	0.828682963	Inf
0	0.825555556	Inf	0	0.728555556	Inf
0	0.825555556	Inf	0.999011728	0.928686667	-0.072418829
0	0.8286045185	Inf	0.343333333	0.843333333	1.45631088
0	0.828686667	Inf	0.343333333	0.843333333	1.45631088
0	0.828381728	Inf	0.343035309	0.842599753	1.458306193
0	0.825555556	Inf	0.343180025	0.842222222	1.45041578
0	0.825555556	Inf	0.343717778	0.841835432	1.449205385

**Table 2- 2 Case 1 Un-Availability Performance comparison for 03/14/2003 Data.**

Un-Aval Before	Un-Aval After	Rela. Change	Un-Aval Before	Un-Aval After	Rela. Change
0	0	NaN	0.369264869	0.077359882	-0.7905029
0.052830006	0	-1	0.374741861	0.077359882	-0.793584879
0.42830576	0.004170516	-0.980217079	0.374741861	0.077359882	-0.793584879
0.59021737	0.008494317	-0.988998738	0.374741861	0.077359882	-0.793584879
0.553820225	0.008494317	-0.888275717	0.374741861	0.077359882	-0.793584879
0.512488385	0.008494317	-0.987327899	0.374741861	0.077359882	-0.793584879
0.512488385	0.008494317	-0.987327899	0.332258408	0.077359882	-0.787189529
0.342534473	0.008494317	-0.981040387	0.319533526	0.077359882	-0.757897449
0.295389357	0.008494317	-0.978012894	0.319915004	0.077359882	-0.758186141
0.295389357	0.008494317	-0.978012894	0.319915004	0.077359882	-0.758186141
0.288154302	0.008494317	-0.975599427	0.319915004	0.077359882	-0.758186141
0.203498446	0.003354043	-0.983518093	0.293123484	0.077359882	-0.738084327
0.222286818	0.001829051	-0.992670703	0.293720739	0.077359882	-0.736820875
0.231258148	0.001829051	-0.992955644	0.283211212	0.077359882	-0.73818329
0.24343922	0.015354936	-0.936924971	0.283753516	0.077359882	-0.727389434
0.271921615	0.037868935	-0.860743195	0.281708221	0.077359882	-0.725388986
0.287180249	0.037868935	-0.858271952	0.283010857	0.077359882	-0.72684014
0.278373259	0.037752292	-0.864382475	0.281420018	0.077359882	-0.725108817
0.317703143	0.044348144	-0.86041012	0.868092478	0.210795756	-1.881059384

0.353790761	0.0769685603	-0.78245447	0.023128519	0.015970412	-0.309492677
0.378332542	0.090687283	-0.780829335	0.045179546	0.023801039	-0.477816727
0.381089258	0.090687283	-0.782031385	0.045179546	0.023801039	-0.477816727
0.358947886	0.090687283	-0.74735251	0.040519112	0.022099327	-0.454594978
0.351030884	0.090687283	-0.741654404	0.039163285	0.021844002	-0.44223263
0.348423348	0.085412118	-0.754861095	0.038533431	0.021530718	-0.441245788

In Case 2, CAT I availability has a huge increase again. Un-Availability decreases by around 70%, which is very good. MI and HMI performances are also perfect.

## CONCLUSIONS

This research has developed a new algorithm to tighten up the VPL looseness. This new algorithm is called the pseudo-VPL-VPE. In ordinary cases the pseudo-VPL reduces the LVPL magnitude by 3dB, which is significant. This helps increase the system availability a tremendous amount. This can be shown by an example: A VPL at 18 meters is not good for CAT I precision approach. With a 3dB improvement, the new pseudo-VPL becomes less than 12 meters, good enough for CAT I precision approach. VPE filtering helps reduce invalid bias, but to a lesser reliability.

This pseudo-VPL-VPE algorithm alone will improve the compactness of the VPL structure. However, it doesn't improve the integrity, which is of crucial importance. As a matter of fact, the pseudo-VPL algorithm can potentially generate additional HMIs if no other action is taken since the new pseudo-VPL moves the data cluster downward without interfering with actual system error. This can move data points above the diagonal line under it, hence create new HMIs. Our solution to this is to Kalman filtering the actual altitude so that the VPE is as small as possible, i.e. as far away from the diagonal line as possible. This, combined with a similar fault detection and error correction mechanism similar to those in pseudo-VPL, A higher system availability for WAAS has been achieved without penalizing system integrity monitoring capability.

With the new pseudo-VPL-VPE algorithm, on good days, which can be expected from more than 95% of time when GPS and WAAS are up, can improve the CAT I Availability by at least 70 to 100%. Decrease the Un-Availability by at least 50%.

At the same time keeps the integrity intact, sometime even improving the integrity.

The performance of the pseudo-VPL-VPE algorithm does depend on the data type it is applied to. With peppered around data points it can induce extra MI or even HMI. Good news is that this kind of hazard is not evidenced by our tables from real data. But it is still a concern. With the upgrade on GPS and WAAS system, chances of this kind of poor data appearing will be reduced or eliminated.

## REFERENCES

- [1] RTCA/DO-229B, "Minimum Operational Performance Standards (MOPS) for Global Positioning System/Wide Area Augmentation System Airborne Equipment". Washington, October 6, 1999.
- [2] Walter, T., Enge, P., Hansen, A., "Integrity Equations for WAAS MOPS", Selected Papers on Satellite Based Augmentation Systems (SBASs): Volume VI, The Institute of Navigation, 1999.
- [3] Darne, E., "A static and dynamic analysis of the operational GPS WAAS", Master dissertation, University of Oklahoma 2000.
- [4] Andrew Hansen, "WAAS Precision Approach Metrics: Accuracy, Integrity, Continuity and Availability", <http://waas.stanford.edu/~www/walter/WAAS/metrics.htm>
- [5] Walter, T., Enge, P. and DeCleene, B, "Integrity lessons learned from the WAAS Integrity Performance Panel (WIPP)", 2004 ION NTM.
- [6] Walter, "Validation of the WAAS MOPS Integrity Equation", in ION Annual Meeting 1999.
- [7] Brown, R.G, Hwang, P. Y.C. "Introduction to Random Signals and Applied Kalman filtering : With MATLAB Exercises and Solutions", New York : John Wiley & Sons, Inc., c1997.
- [8] Walter, T., Hansen, A. and Enge, P., "Message Type 28", ION NTM 2001.
- [9] Jan, S., Chan, W., Walter, T., and Enge, P., "Matlab Simulation Toolset for SBAS Availability Analysis," in Proceeding of ION GPS-2001, Salt Lake City, UT, September 2001.

## Appendix B:

### Acronyms Frequently used in Navigation Research

#### ACRONYM MEANING

AAAE	American Association of Airports Executives
ABAS	Aircraft Based Augmentation System
AC	Advisory Circular
ADO	Airport District Office
ADS-B	Automation Dependent Surveillance – Broadcast
AEE	Office of Environmental and Energy
AFIS	Automated Flight Inspection System
AFS	FAA Flight Standards Service
AGC	Automatic Gain Control
AIP	Airport Improvement Program
ALAs	Approach-and-landing accidents
ALP	Airport Layout Plan (5-20 Years out)
ALPA	Air Line Pilots Association's
AMASS	Airport Movement Area Safety System
AMD	Airport Master Plan (5-20 Years out)
AMM	Airborne Multipath Model
ANC	Air Navigation Commission (An ICAO organization)
ANP	Actual Navigation Performance.
AOA	FAA Office of the Administrator
AOA	Airport Operations Area
APV	Approach with Vertical Guidance
ARINC 424	The defined standard for aeronautical navigation data
ARSA	Airport Radar Surveillance Area (Class C airspace)
ARSR-4	Air Route Surveillance Radar, Model 4
ARTC	Air Route Traffic Control Center
ASDE	Airport Surface Detection Equipment
ASDE-X	Airport Surface Detection Equipment, Model X
A-SMGCS	Advanced Surface Movement Guidance & Control System
ASOS	Automated Surface Observing System
ASR	Area Surveillance Radar
ATA	Airline Transport Association
ATCBI	Air Traffic Control Beacon Interrogator
ATCSCC	Air Traffic Control System Command Center
ATCT	Airport Traffic Control Tower
ATCU	Air Traffic Control Unit
ATIDS	Airport Traffic Identification Systems
ATIS	Automatic Terminal Information Service
ATM	Air Traffic Management

<b>ACRONYM</b>	<b>MEANING</b>
ATOP	Advanced Technology and Oceanic Procedures
ATPAC	Air Traffic Procedures Advisory Committee
AVN	Aviation System Standards
AVS	Additional VDB Sub-System
AWO	All Weather Ops guys
AWOHWG	All Weather Operations Harmonization Working Group
AWOS	Automated Weather Observing System
BFOT	Backfill Overtime
BMNs	Baseline Management Notices
B-Spec	Prime Item Development Specification
CA Code	Course Acquisition Code
CAA	Cargo Airlines Association
CAASD	Center for Advanced Aviation Systems Development
CAPA	Coalition of Airline Pilots Association
CASA	Civil Aviation Safety Authority
CBA	Cost Benefits Analysis
CCB	Configuration Control Board
CDI	Course Deviation Indicator
CDR	Critical Design Review
CDRL	Contract Data Requirements List
CDTI	Cockpit Display of Traffic Information
CE	categorical exclusions
CF	Course to Fix
CF/MOS	Cost Functions/Measure of Success
CFIT	controlled flight into terrain
CGSIC	Civil GPS Service Interface Committee
CI	Configuration Items
CMN	Control Motion Noise
CNS	Communications, Navigation and Surveillance
CNS/ATM	Communications, Navigation and Surveillance/ Air Traffic Management
CPDLC	Controller pilot data link communications
CRAF	Civil Reserve Air Fleet
CRC	Cycle Redundancy Check
CRDA	Converging Runway Display Aid
CSCIs	Computer Software Configuration Items
CSER	Contractor Site Engineering Report
CSPA	Closely Spaced Parallel Approaches
CTAF	Common Traffic Advisory Frequency
CW	Continuous Wave
DA	Decision Altitude
DCIA	Dependent Converging Instrument Approaches
DER	Departure End Of Runway
DF	Direct to Fix
DGPS	Differential Global Positioning System
DH	Decision Height. Old term. See DA above.

<b>ACRONYM</b>	<b>MEANING</b>
DH/DA	Decision Height/Decision Altitude
DME	Distance Measuring Equipment
DO-178B	Software Consideration in Airborne Systems and Equipment Certification
DO-236	RNP RNAV MASPS
DO-245	LAAS MASPS
DO-246	RTCA LAAS Interface Control Document (ICD)
DO-253A	MOPS for GPS LAAS Airborne Equipment
DP	Departure Procedure
DRVSM	Domestic Reduced Vertical Separation Minima
DTED	Digital Terrain Elevation Data
DTG	Distance To Go
DTOP	Displaced Threshold Operations
EA	environmental assessments
EAP	Environmental Protection Agency
ECAC	European Civil Aviation Conference
EDR	Eddy Dissipation Rate (Wind Sheer/Turbulence Term)
EGNOS	European Geo-stationary Navigation Overlay Service
EGPWS	Enhanced Ground Proximity Warning System
EHSI	Electronic Horizontal Situation Indicator
EIS	Environmental Impact Statement
EPU	Estimated Position Uncertainty
ERP	Effective Radiate Power
EUROCAE	European Organization for Civil Aviation Equipment
F&E	Facilities and Equipment
FANS	Future Air Navigation Systems
FBO	Fixed Base Operations or Fixed Base Operator
FCA	Functional Configuration Audit
FD	Fault Detection
FD	Fault Detection. Done in WAAS airborne receiver
FDE	Fault Detection and Exclusion. Done in WAAS airborne receiver
FHA	Functional Hazard Assessment
FHA	Functional Hazards Assessment/Analysis
FMS	Flight Management System
FONSI	findings of no significant impact
FPAP	Flight Path Alignment Point
FRAC	Final Review and Comment
FSD	Full Scale Development
FSF	Flight Safety Foundation
FTP	Fictitious Threshold Point
GA	General Aviation
GAD	Ground Accuracy Designator (C-Curve)
GBAS	Ground Based Augmentation System
GDP	Ground Delay Program
GEOS	Geo-stationary Earth Orbit Satellite

## **ACRONYM MEANING**

GES	Ground Earth Station
GLS	Global Navigation Satellite System (GNSS) or GPS Landing System
GMA	Guided Missed Approaches
GNAS	General National Airspace System
GNDIR	General Nav Direct
GNSS	Global Navigation Satellite Systems (Such as GPS DGPS WAAS/LAAS)
GNSSP	Global Navigation Satellite System – Panel
GNSSP	Global Navigation Satellite System Panel
GNSSU	Global Navigation Satellite Sensor Unit
GOIWG	GNSS Operational Integration Working Group
GOTS	GPS Outage Terminal Simulator
GPA	Glide Path Angle
GPWS	Ground-Proximity Warning System
GQS	GS Qualification Surface
GRAS	Ground Based Regional Augmentation System
GRAS	Ground Based Regional Augmentation System
HAL	Horizontal Alert Limit
HMI	Human Machine Interface
HPL	Horizontal Protection Limit
HPOL	Horizontal Polarization
HSI	Horizontal Situation Indicator
IAPA	Instrument Approach Procedures Automation
IAPs	Instrument Approach Procedures
IATA	International Air Transport Association
ICAO	International Civil Aviation Organization
IDR	Integrity Design Review/Report
IGEB	Interagency GPS Executive Board
ILS	Frequency Range 108 – 112 MHz
IMC	Instrument Meteorological Conditions
IMLA	Integrated Multipath Limiting Antennas
INAS	International and National Airspace
INAS	International Airspace System
INMARSAT	International Maritime Satellite Service Provider
IOD	GPS Issue of Data
ION	Institute of Navigation
IOT&E	Independent Operational Test & Evaluation ATQ
IRS	Inertial Reference System
ISO	International Standards Organization
JAA	Joint Aviation Authorities
JPALS	Joint Precision Approach Landing System
JPO	Joint Planning and Development Office
JPO	Joint Planning Office (FAA)
JPO	Joint Program Office (Military)
JRC	Joint Resources Council

<b>ACRONYM</b>	<b>MEANING</b>
JTIDS	Joint Tactical Information Distribution System
KTA	Key Technical Advisors
L1	1575.42 Mhz
L2	1227.60 Mhz
L5	1176.45 MHz
LAAS	Local Area Augmentation System
LAHSO	Land and Hold Short Operations
LAL	Lateral Alert Limit
LDA	Localizer-type Directional Aid
LEAP	LAAS Equipage and Avionics Pathfinder
LGF	LAAAS Ground Facility
LIP	LAAS Integrity Panel (may be replaced by IDR)
LIP	LAAS Integrity Panel (Group of Program Office Personnel)
LLWAS	Low Level Wind Shear Advisory System
LNAV	Lateral Navigation
LOCA	LGF Object Clearance Area
LPV	Localizer Performance with Vertical guidance
LRIP	Low Rate Initial Production
LRR	Long Range Radar
LSP	Local Status Panel
LTP	LAAS Test Prototype
LTP	Landing Threshold Point
LTP	Landing Threshold Points
MALSR	Medium Intensity Approach Light System with RAIL
MASPS	Minimum Aviation System Performance Standards
MDE	Minimum Detectable Error
MDT	Maintenance Data Terminal
MFD	Multi-Functional Display
MI	Misleading Information
MIB	Management Information Base
MIDS	Multifunctional Information Distribution System
MIL-STD-882	System Safety Requirement
MLA	Multipath Limiting Antenna
MMS	Maintenance Management System
MOI	Maintenance Operations Inspectors
MOPS	Minimum Operational Performance Standards
MPAP	Multiple Parallel Approach Program
MVA	Minimum Vectoring Altitude
MVMC	Marginal VMC
NAAT	North American Aviation Trilateral
NAATS	National Association of Air Traffic Specialists
NAPT	National Airspace Procedure Team
NAR	National Airspace Redesign (1997)
NASPAC	NAS Performance Analysis Capability
NATCA	National Air Traffic Controllers Association

<b>ACRONYM</b>	<b>MEANING</b>
NCP	NAS Change Proposal
NDGPS	Nationwide Differential GPS
NEPA	National Environmental Policy Act
NEXTOR	National Center of Excellence for Aviation Operations Research
NFDC	National Flight Data Center
NFPO	National Flight Procedures Office
NGS	National Geodetic Service (Work for NOAA)
NIMS	NAS Infrastructure Mgt System
NIMS	NAS Infrastructure Management System
NMI	Nautical Mile
NOTAMS	Notice to Airman
NPA	Non-Precision Approach
NSE	Navigation Sensor Error
NTAP	Notices to Airmen Publication
NTE	Not To Exceed
NTZ	No-Transgression Zone
OBE	Overcome By Events
OCP	Obstacle Clearance Panel
ODP	Obstacle Departure Procedures
OEP	Operational Evolution Plan
OFA	Object Free Areas
OFZ	Obstacle Free Zones
OIT	Operational Integration Team
OK City	FAA's Mike Monroney Aeronautical Center in Oklahoma City, OK.
PACS	Primary Airport Control Stations
PANS-OPS	Procedures for Air Navigation Services-Operations
PAPI	Precision Approach Path Indicator
PARC	Performance Based Aviation Rulemaking Committee
PART 121	Major Carriers and Cargo Carriers
Part 129	Foreign Aircarriers and Foreign Operator flying US registered aircraft
PART 135	9 Passengers or less plus air taxi flights
PART 150	Part 150, Airport Noise Compatibility Planning
PART 91	General Aviation
PAT	Product Acceptance Team
PBARC	Performance Based Rule Making Committee (Replace TAOARC)
PCA	Physical Configuration Audit
PCA	Positive Controlled Airspace (Class A airspace)
PCHs	Phase Center Heights
PCR	Pseudorange Correction Rate
PDA	Preferred Departure Route
PDR	Preliminary Design Review
PES	Primary Equipment Shelter
PFAF	Precision Final Approach Fix
PFE	Path Following Error
PHA	Preliminary Hazard Analysis

## **ACRONYM MEANING**

PIP	Product Integration Plan
PIP	Product Integration Plan
POI	Principal Operations Inspectors
PRC —	Pseudorange Correction
PRN	Pseudorandom Number
PVS	Primary VDB Sub-System
Q Routes	US and Canada use the term Q to refer to RNAV routes
RAA	Regional Airline Association
RAAS	Remote altimeter setting sources
RAAS	Remote Alternate Altimeter Setting
RAIL	Runway Alignment Indicator Lights
RAIM	Receiver autonomous integrity monitoring (RAIM) is the satellite-based navigation community's term for fault detection (FD).
RAPT	Regional Airspace Procedure Team
RF	Radius to Fix
RFO	Responsible Federal Official
RIPS	Runway Incursion Prevention System (NASA) Program
RIRP	Runway Incursion Reduction Program
RNAV	Area Navigation (Free Flight)
RNP	Required Navigation Performance
ROD	Record of Decision
RPAT	RNP Parallel Approach Transition
RPDS	Reference Path Data Selector
RPI	Reference Path Indicator
RR	Reference Receiver
RRA	Reference Receiver Antenna
RRS	Reference Receiver Station
RSA	Runway Safety Areas
RSP	Remote Status Panel
RTA	Required Time of Arrival
RTCA	Radio Technical Commission for Aeronautics, Inc.
RVSM	Reduced Vertical Separation Minimums (aircraft)
SA	Selective Availability
SAARS	Special Aircraft And Aircrew Authorization Required
SACS	Secondary Airport Control Stations
SARPS	Standard and Recommended Practices (ICAO Term)
SBAS	Satellite Based Augmentation System
SCAP	Security Certification & Authorization Package
SCAT-1	Special Category. Sometimes shown as SCAT 1 Approaches
SCIA	Simultaneous Converging Instrument Approaches
SDP	Software Development Plan
SDP	Software Development Plan
SIAP	Standard Instrument Approach Procedure
SID	Standard Instrument Departure
SIS	Signal-in-Space

## **ACRONYM MEANING**

SMGCS	Surface Movement Guidance and Control System (See A-SMGCS)
SNAPIT	SatNav Automated Program Integration Tool
SNI	Simultaneous non-interfering
SNMP	Simple Network Management Protocol
SOIA	Simultaneous Offset Instrument Approach
SOIR	Simultaneous Operations on Intersecting Runways
SPS	Standard Positioning Service. GPS provides a SPS
SQM	Signal Quality Manager
SRGPS	Ship Relative GPS
SRR	System Requirements Report
SSPP	System Safety Program Plan
SSR	Secondary Surveillance Radar
SSS	System Segment Specification
STAR	Standard Terminal Arrivals
STAR	Standard Terminal Arrival Route
STAR	Standard Instrument Arrival Route
STARS	Standard Terminal Automated Radar System
STC	Supplemental Type Certification
SWG	Siting Working Group for LAAS
TAAM	Total Airspace & Airport Modeler
TACAN	Tactical Air Navigation
TAOA	Terminal Area Operational Applications
TAOARC	Terminal Area Operations Aviation Rulemaking Committee
TAP	Terminal Area Path
TARGETS	Terminal Area Route Generation, Evaluation and Traffic Simulation
TAWS	Terrain Awareness and Warning System
TBD	To Be Determined
TBD	To Be Determined
TCA	Terminal Controlled Airspace (Class B airspace)
TCAS	Traffic Collision and Avoidance System
TCH	Threshold Crossing Height
TDMA	Time Division Multiple Access
TECH Center	The FAA William J. Hughes Technical Center
TERPS	Terminal Area Procedure or Terminal Instrument Procedures
TF	Track to Fix
TIS	Traffic Information Services
TLS	Transponder Landing System
TNIFR	Terminal NAV IFR
TOR	Technical Onsite Representative
TRACON	Terminal Radar Approach Control
TSO	Technical Standard Order
TSO C-145A	Airborne Nav Sensors using WAAS
TSO-146A	Stand alone Nav Equip using WAAS
TSPI	Time Space Position Information System
TTA	Time To Alarm

**ACRONYM MEANING**

TWG	Technical Working Group
UDRE	User's Differential Range Error
UNICOM	Uniform Communications: A non-government communication facility which may provide airport information at certain airports.
UTC	Coordinated Universal Time
VAL	Vertical Alert Limit (See VPL below)
VDB	VHF Data Broadcaster
VDI	Vertical Display Indicator
VMC	Visual Meteorological Conditions
VNAV	Vertical Navigation
VPL	Vertical Protection Limit (See VAL above)
VPOL	Vertical Polarization
VRTM	Verification Requirements Test Matrix
VSWR	Voltage Standing Wave Ratio
WGS-84	World Geodetic Survey 1984
Wx	Weather

## Bibliography

- [1]. Loh, R., Wullschleger, V., Elrod, B., Lage, M., and Haas, F., "The U.S. Wide-Area Augmentation System (WAAS)", NAVIGATION, Vol. 42, No. 3, pp. 435-466, Fall 1995.
- [2]. Enge, P., "Wide Area Augmentation of the Global Positioning System," Proceedings of the IEEE, 84(8): pp.1063-1088, August 1996.
- [3]. RTCA/DO-229B, "Minimum Operational Performance Standards (MOPS) for Global Positioning System/Wide Area Augmentation System Airborne Equipment". RTCA Inc. Document No. RTCA/DO-229B, Washington, October 1999.
- [4]. The White House, Office of the Press Secretary, "Statement by the president regarding the United States' decision to stop degrading Global Positioning System accuracy", May 1, 2000.
- [5]. RTCA Special Committee 159 Working Group 2, "Wide Area Augmentation Signal Specification ", September, 1995.
- [6]. [http://www.ngs.noaa.gov/FGCS/info/sans\\_SA/](http://www.ngs.noaa.gov/FGCS/info/sans_SA/), April 1<sup>st</sup>, 2004.
- [7]. <http://gps.faa.gov/GPSbasics/index.htm>, March 10th, 2003.
- [8]. Richard Fuller, "Aviation Utilization of Geostationary satellites for the augmentation to GPS: Ranging and Datalink", Ph.D. Dissertation, Stanford University, 2000.
- [9]. Darne, E., "A static and dynamic analysis of the operational GPS WAAS", Master Thesis, University of Oklahoma 2000.
- [10]. ICAO, "Navstar GPS Space Segment/User Interfaces, IRN-200C-002", Navstar GPS JPO, 25 September 1997.
- [11]. Tsai, Y., Chao, Y.C., Walter, T., Kee, C., Powell, D., Enge, P., Parkinson, B., "Evaluation of Orbit and Clock Models for Real-Time WAAS", Proceedings of the National Technical Meeting, 1999, pp. 539-547, The Institute of Navigation, Anaheim, California, 1995.
- [12]. Dai, D., Walter, T., Enge, P., Powell, J.D., "Satellite-Based Augmentation System Signal-In-Space Integrity Performance Analysis, Experience and Perspectives", Proceedings of ION GPS-99, pp. 159-170, The Institute of Navigation, Nashville, TN, September 1999.

- [13]. Klobuchar, J., "Design and Characteristics of the GPS Ionospheric Time Delay Algorithm for Single-Frequency Users." Proceedings of the PLANS-86 conference, pp. 280-286, Las Vegas, NV, Nov 1986.
- [14]. Parkinson, B.W., Spilker, J.J., Axelrad, P., Enge, P., "Global Positioning System: Theory and Applications, Volumes I and II, Progress in Astroautics and Aeronautics", American Institute of Aeronautics and Astronautics, 1996.
- [15]. "Global Positioning System Standard Positioning Service Signal Specification", November 5, 1993, published by the US Department of Defense.
- [16]. Saunders, S.R., "Antenas and Propagation for Wireless Communication Systems", Chichester, UK: John Wiley & Sons, Inc., c1999.
- [17]. Fan Liu, "RTCA LAAS-MOPS, Analysis of integrity monitoring for the Local Area Augmentation System using the Global navigation satellite system", Ph.D. Dissertation, Ohio University, 1998.
- [18]. <http://gps.faa.gov/programs/index.htm>, March, 2003.
- [19]. T. Walter, P. Enge, F. Van Grass, "Integrity for the Wide Area Augmentation System," Proceedings of DSNS-95, Vol II, No. 38. Bergen, Norway, April, 1995.
- [20]. K. Sam Shanmugan, Arthur M. Breipohl. "Random signals: detection, estimation, and data analysis", New York: Wiley, c1988.
- [21]. Walter, T., Enge, P., and Hansen, A., "A Proposed Integrity Equation for WAAS MOPS," in proceedings of ION GPS-97, pp. 475-484, Kansas City, MO, September 1997.
- [22]. Hayes M. H., "Statistical Digital Signal Processing and Modeling", John Wiley & Sons; New York, March 1996.
- [23]. Axelrad, P. and Brown, R.G., "GPS navigaton Algorithms, Chapter 9 in Global Positioning System: Theory and applications", Washington D.C., published by AIAA, 1996.
- [24]. Brown, R.G, Hwang, P. Y.C. "Introduction to Random Signals and Applied Kalman filtering : With MATLAB Excercises and Solutions", New York : John Wiley & Sons, Inc., c1997.
- [25]. Papoulis, A., "Probability, Random Variables, and Stochastic Processes", Singapore, McGraw-Hill Book Co., 1984.

- [26]. Enge, P., "WAAS Messaging System: Data Rate, Capacity, and Forward Error Correction", Navigation, Vol. 44, No. 1, pp. 63-76, Spring 1997.
- [27]. Andrew Hansen, "WAAS Precision Approach Metrics: Accuracy, Integrity, Continuity and Availability",  
<http://waas.stanford.edu/~wwu/walter/WAAS/metrics.html> , January, 2004.
- [28]. Walter, "Validation of the WAAS MOPS Integrity Equation", in Proceeding of ION GPS 1999, pp. 217-226, Institute of Navigation, Nashville, TN, Sep. 1999.
- [29]. "FAA Commissions WAAS", GPS World, pp. 10-13, August 2003.
- [30]. Walter, T., Hansen, A. and Enge, P., "Message Type 28", Proceeding of ION NTM 2001, pp. 522-532, Long Beach, CA, January 2001.
- [31]. Blanch, Juan, Walter, T., and Enge, P., "Adapting Kriging to the WAAS MOPS inonspheric Grid", Proceeding of ION NTM 2003, pp. 848-853, Anaheim, CA. January 2003.
- [32]. Walter, T., Enge, P. and DeCleene, B, "Integrity lessons learned from the WAAS Integrity Performance Panel (WIPP)", Proceeding of ION NTM 2003, pp. 183-194, Anaheim, CA, January 2003.
- [33]. Kapitaniak, Tomasz, "Chaos for engineers: theory, applications, and control", Berlin; New York: Springer, c2000.
- [34]. Jan, S., Chan, W., Walter, T., and Enge, P., "Matlab Simulation Toolset for SBAS Availability Analysis," in Proceeding of ION GPS-2001, pp. 2366-2375, Salt Lake City, UT, September 2001.
- [35]. Cabler, H. and DeCleene, B., "LPV: New, Improved WAAS Instrument Approach," in Proceedings of ION GPS-2002, pp. 1013-1021, Portland, OR, September 2002.
- [36]. Kalman, R. E. 1960. "A New Approach to Linear Filtering and Prediction Problems," Transaction of the ASME--Journal of Basic Engineering, pp. 35-45, March 1960.
- [37]. Walter, T. "WAAS MOPS: Practical Examples", Proceeding of ION NTM 1999, pp. 283-294, Institute of Navigation, San Diego, California, January 1999.